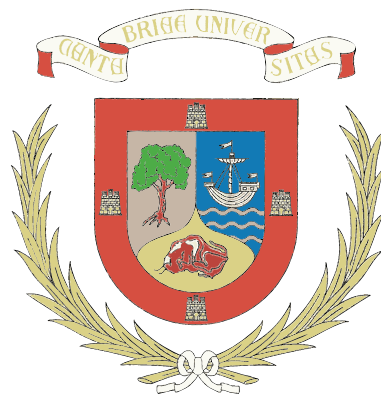


**UNIVERSIDAD DE CANTABRIA**

**DEPARTAMENTO DE  
INGENIERÍA DE COMUNICACIONES**



**TESIS DOCTORAL**

**MEDIDA, CARACTERIZACIÓN Y EMULACIÓN  
DE CANALES MIMO BANDA ANCHA**

**Autor: Jesús Gutiérrez Terán**  
**Directores: Jesús Ibáñez Díaz**  
**Jesús Pérez Arriaga**

**2013**

**UNIVERSITY OF CANTABRIA**

**DEPARTMENT OF  
COMMUNICATIONS ENGINEERING**



**PhD Dissertation**

**MEASUREMENT, CHARACTERIZATION  
AND EMULATION OF WIDEBAND  
MIMO CHANNELS**

**Author: Jesús Gutiérrez Terán**  
**Supervisors: Jesús Ibáñez Díaz**  
**Jesús Pérez Arriaga**

**2013**

# **Medida, caracterización y emulación de canales MIMO banda ancha**

Tesis que se presenta para optar al título de  
Doctor por la Universidad de Cantabria

**Autor:** Jesús Gutiérrez Terán  
**Directores:** Jesús Ibáñez Díaz  
Jesús Pérez Arriaga

Programa Oficial de Posgrado en Tecnologías de la Información y Comunicaciones en Sistemas  
de Telecomunicación

Grupo de Tratamiento Avanzado de Señal

Departamento de Ingeniería de Comunicaciones

Escuela Técnica Superior de Ingenieros Industriales y de Telecomunicación

Universidad de Cantabria

2013



Autor: Jesús Gutiérrez Terán  
Directores: Jesús Ibáñez Díaz  
Jesús Pérez Arriaga

El tribunal nombrado para juzgar la tesis doctoral citada, compuesto por los señores

Presidente:

Vocales:

Secretario:

Acuerda otorgarle la calificación de

Santander, a de de 2013



The difference between measurements and simulations  
is that nobody believes in simulations, except the one who did them,  
but everybody believes in measurements, except the one who did them.

## **Affiliations**

Advanced Signal Processing Group  
Department of Communications Engineering  
University of Cantabria, Spain

The research leading to this work has received funding from the Ministerio de Economía y Competitividad under grant agreement FPI BES-2008-002085.



# Acknowledgements

Me gustaría comenzar los agradecimientos por mis directores de tesis, Jesús Ibáñez y Jesús Pérez, a quienes debo gran parte de las ideas y consejos. Además, por toda su dedicación y paciencia a la hora de afrontar los diferentes retos que la tesis ha supuesto. Gracias Jesús Ibáñez por contagiarme tu optimismo en los momentos difíciles. Gracias Jesús Pérez por tu exigencia y disposición a la hora de analizar y entender cómo funcionaban las cosas. Me gustaría extender el agradecimiento a Ignacio Santamaría, cabeza visible del Grupo de Tratamiento Avanzado de Señal (GTAS), por su confianza desde primer momento; allá por el 2007 cuando realicé mi proyecto de fin de carrera bajo su tutela. Por su comprensión y por estar siempre disponible para cualquier cuestión, a él también va el agradecimiento.

Quiero destacar también la ayuda, apoyo y colaboración de David Ramírez y Óscar González. Unos auténticos apasionados de nuestro trabajo, que tan generosamente me han aportado su conocimiento para la realización de esta tesis. Al primero por su apoyo constante, además de ser un gran amigo y confidente. Agradecer enormemente a Óscar el haber compartido conmigo casi dos años de trabajo y multitud de fructíferas charlas. Gracias también a él esta tesis doctoral ha sido posible.

Me gustaría agradecer a todo el GTAS su generosidad a la hora de resolver cualquier duda. A los miembros actuales: Steven Van Vaerenbergh, Javier Vía, Luis Vielva, Christian Lameiro, Julio Manco y Álvaro Gonzalo; así como a los antiguos miembros: Víctor Elvira, Fouad Gholam, Gabriel García, Darío García, Fernando Moreno, Alfredo Nazábal, Martín Otí, etc. En especial al primero de ellos, Víctor, bien sabe él que le tengo un aprecio especial y que los años que hemos compartido en el despacho (y fuera de él) han sido realmente un placer.

A mis compañeros de promoción, en especial Lino Osorio, David Ramírez, Jesús Rubio, Darío García, Alfonso Real, Pablo Alonso, Lucía López, Jose María Álvarez, Alberto Salas, Moisés Arce, Javier Valiño, Fernando Moreno, Ignacio Ahedo, Raúl Pérez, Enrique Venero, Noe Ortega, Juan María Rivas, Martina Fuentevilla, Juan Ramón Santana, Óscar Fernández, etc. por haber hecho estos años de Universidad muy llevaderos y divertidos. Extendiendo además el agradecimiento al resto de compañeros.

Me gustaría destacar también la oportunidad que el Profesor Markus Rupp de la Universidad Técnica de Viena me brindó, posibilitando mi estancia en dicha universidad durante cuatro meses. Agradecer su confianza y trato, así como el de los compañeros y amigos que tengo en esa magnífica ciudad: Elena Recas, Javier Moreno, Josep Colom, Michal Simko, Qi Wang, Philipp Gentner, Aamir Habib, Bujar Krasniqi, Christoph Mecklenbräuker; así como al resto de amigos que compartieron conmigo esos cuatro meses: Alexandra Martínez, Marta Castaño, David Fernández, Celia y Jose, David Vargas, Alex Camatx, Amalia Lorca, Edu Muñoz, Emilio Muñoz, Miriam y Nacho, Germán, Manfred, etc.

Agradecer cómo no la comprensión y confianza depositada por mis actuales jefes: Rolf Kraemer, Milos Krstic y Eckhard Grass; además del resto de compañeros de IHP (que siempre

me preguntaban cuándo iba a depositar y presentar la tesis): Nikola, Arjun, Markus Günther, Mariana, Pedro, Iria, Despoina, Miroslav, Miljana, Goran, etc.

A Lino Osorio, Carmen Solar y María Osorio. Quién le iba a decir a Lino que acabaría haciendo la Tesis en la UC; ambos queríamos conocer mundo cuando acabáramos. Por desgracia no pudimos hacer muchos viajes. Esta Tesis se la dedico a él y me encantaría poder celebrarla por todo lo alto estando él aquí.

A mis amigos, algunos de los cuales ya he nombrado. En especial a Óscar Fernández, Óscar López, José Tordesillas, Susana Correas, Jesús Rubio, Pelayo Villanueva, Mikel Maeztu, Darío García, Alfonso Real, José María Álvarez, Eloisa Tapia, Pablo Varillas, Pablo Alonso, Lucía López, Alicia Ramos, Alberto González, Luis Ángel Fernández, Guillermo Rodríguez, Marina García, Laura Fernández, Blanca Fuentes, Cristina Ysart, Mónica Puig-Pey, Pilar Badiola, Rebeca Celada, Inés Mosquera, etc. También agradecer el apoyo de mis amigos de Riente y alrededores: Isabel Rábago, Yolanda Rábago, Alberto Polanco, Fernando Díaz, Manuel Herrero, Marcos Díaz, Jesús de la Cueva, Sira Rivero, Elsa González, Sara González, Vanessa González, Mariano Puente, Jorge Rodríguez, etc.

A mis primos, tíos y demás familia.

A mi padre y a mi madre, Jesús Gutiérrez y Julia Terán. Por su paciencia, comprensión y ánimo. Que han permitido que, desde que comenzase esta aventura en el mundo de las telecomunicaciones allá por el año 2001, no me faltara de nada. Nunca he tenido palabras, quizás sea parco en ellas en multitud de ocasiones, para agradecer todo cuanto han hecho por mí. A ellos se la dedico. Recordar también a mis abuelos, que ya no están con nosotros.

Jesús

Santander, 31 de julio de 2013

# Abstract

Indoor multipath propagation and its impact on multiple-input multiple-output (MIMO) systems have been of continued interest, particularly for the design and evaluation of wireless local area networks (WLAN). The characteristics of indoor MIMO channels, such as temporal and spatial correlation, time variation, etc. impact the performance of those systems. Due to this, it is of paramount importance to have a deep channel knowledge.

The radio channel in indoor environments can be represented by multiple paths with certain gains and delays. It is common to use mathematical models for describing the channel, which can be done from either a deterministic or a statistical viewpoint. On one hand, we may use classical propagation theory and a knowledge of the physical indoor environment to deterministically predict the behavior of the channel. This results time consuming for a high number of multipath components. On the other hand, it is possible to statistically model the channel. This approach needs extensive measurement data and do not provide site-specific information.

Measuring the MIMO channel has become the best way to complement the models. Channel measurements offer information of variations in time, correlation among the signals at both transmit and receive array, etc. In an effort to gain a better understanding of the multipath signals, the wireless research community has been carrying out experimental measurements to determine the multipath characteristics. The unpredictable channel variations can not be modeled, hence measuring the MIMO channel results indispensable when tracking these changes.

In the first part of this work, we present the hardware of the nodes in which the Advanced Signal Processing Group (GTAS) MIMO testbed is based. This equipment consist of digital processing units (DPUs), digital-to-analog conversion(DAC) and analog-to-digital conversion (ADC) capabilities, allowing real-time processing due to the use of Field Programmable Gate Arrays (FPGAs). As the main contribution, the GTAS group has provided the testbed with a web-based interface, allowing fully interaction with the testbed and offering universal access. This interface is characterized the ease of deployment, updatability, and controllability. Moreover, it serves as a powerful tool for testing wireless devices and MIMO algorithms over real channels. As an example of its utilization, a MIMO channel estimation procedure is described within the context of an European Union funded project within the 7th Framework Programme called Advanced MIMO systems for maximum reliability and performance (MIMAX).

In the second part of this work, we consider the problem of measuring the wideband MIMO channel. The unaffordable costs of the channel sounders led us to think up of a channel measurement methodology to be implemented in our MIMO testbed. This technique involves the transmission of complex exponentials over a specific frequency band. At the receiver, the amplitudes of the exponentials (which are affected by the channel) are estimated, and from them the channel is readily estimated. One of the key features of this method is that, due to the use of complex exponentials, difficult tasks such as synchronization or symbol detection

are avoided during channel sounding. Moreover, it is computationally very simple and can get the channel measures very fast. The proper operation and the validation of the results were verified by commercial hardware. The channel measures along time corroborates the fact that the indoor channel, in a static environment, can be considered deterministic.

However, today's wireless communication devices are tested under different and variable conditions, if it is possible, controllable and repeatable. The assessment of those devices under controlled channels is one of the requirements of commercial channel emulators. Finally, in the same way, we decided to make the most of testbed capabilities to design and implement a channel emulation methodology. It is based on the transmission/reception scheme of the channel measuring methodology, taking advantage of its synchronization procedure. The emulation itself is based on a linear processing combination at the receiver, based on the MIMAX beamforming scheme. It is able to reproduce any channel realization from the actual channel and the channel to emulate. Furthermore, it is able to emulate Rayleigh and Rician channel with certain spatial correlation properties. Its implementation on the MIMO testbed provides the whole system the possibility of testing MIMO algorithms in the lab, even over outdoor channels.

In summary, this dissertation tackles the problem of measuring, characterizing and emulating MIMO channels in indoor environments, using a conventional MIMO testbed. The performance of these implementations is far away to be competitive with commercial equipment. However, for academic purposes and small research laboratories, it results of high importance when testing MIMO devices and assessing MIMO algorithms. Also, the remote capabilities of the testbed will encourage future developments along these lines within the GTAS group and the whole wireless research community.

# Resumen y Conclusiones

El estudio de la propagación multicamino (del inglés *multipath propagation*) ha sido, en los últimos años, una de los tópicos más relevantes en lo que al canal inalámbrico se refiere. El diseño y la evaluación de sistemas de redes de área local inalámbricas (*Wireless Local Area Networks* o WLAN) depende, en gran medida, de las características del canal inalámbrico. Éste se puede modelar de manera determinista, considerando un canal en concreto; o de forma estocástica, modelado más flexible utilizando variables aleatorias. De las aproximaciones estocásticas para modelar el canal en interiores destacan los modelos *Rayleigh* y *Rician*. El primero asume que las amplitudes de las infinitas componentes multitrayecto se pueden modelar como una variable aleatoria normal, representando un modelo sin visión directa (*non-line of sight* o NLOS). En el segundo caso se asume la existencia de visión directa entre el transmisor y receptor (*line of sight* o LOS).

Existen situaciones en las que, debido a las características adversas del entorno de propagación, la tasa de transmisión se ve reducida. Dado que las aplicaciones futuras demandan un incremento de tasa que no consiguen las técnicas tradicionales, en los últimos quince años se ha llevado a cabo una intensa investigación de los sistemas de múltiples entradas y múltiples salidas (*Multiple-Input Multiple-Output* o MIMO), lo que en sistemas inalámbricos equivale a múltiples antenas en transmisión y recepción. A partir del trabajo pionero realizado por Foschini y Telatar, los sistemas MIMO han sido utilizados para mejorar drásticamente el rendimiento de los sistemas de comunicaciones inalámbricas. El desarrollo de estos sistemas pasa por disponer de modelos teóricos que tengan en cuenta los principales mecanismos de propagación en los distintos tipos de entornos. Como ejemplo, diferentes modelos de canal MIMO han sido desarrollados para diferentes entornos. Estos modelos de propagación pueden proceder bien del análisis de los datos recogidos en campañas de medidas, o bien de modelos más complejos que resuelven el problema electromagnético desde un punto de vista teórico. Sin embargo, numerosas técnicas MIMO no han sido suficientemente testeadas bajo condiciones de propagación reales, de ahí que se requiera aún más trabajo experimental para caracterizar dichos canales inalámbricos.

Esta tesis se divide en tres partes. En la primera parte se aborda el estudio de plataformas MIMO hardware, las cuales se vienen utilizando en los últimos años para testear algoritmos y dispositivos MIMO. En concreto se presenta la plataforma MIMO del GTAS, describiendo sus características, limitaciones y posibles usos. La principal aportación de esta parte consiste en dotar a la plataforma de una interfaz de control basada en *webservices* mediante la cual se pueden controlar todas sus funcionalidades de una manera sencilla y eficaz. En segunda parte se describe el diseño e implementación de una metodología para la medida del canal MIMO banda ancha basada en el envío de exponenciales complejas. Finalmente, se diseña e implementa una técnica para el testeo de dispositivos y/o algoritmos por el aire (del inglés *over the air* o OTA) mediante la emulación de canales MIMO basada en la combinación lineal de matrices pesos variantes en el tiempo. Esta técnica ha dado lugar a dos formas diferentes de emular el canal: una que reproduce realizaciones de canal de modelos conocidos

o medidas de canal previas, y otra que emula características espaciales y temporales de canales con distribuciones determinadas. Todo el trabajo realizado tiene como finalidad su implementación en la plataforma MIMO del GTAS.

En el Capítulo 2, a modo de introducción, se analiza el estudio de la propagación inalámbrica en canales MIMO en interiores para posteriormente adentrarse en el desarrollo de tres partes.

## Plataforma MIMO del GTAS

En el Capítulo 3 se presenta la plataforma MIMO de comunicaciones del GTAS. Está compuesta por tres nodos constituidos por módulos de fácil conexión (*Commercial off-the-shelf* o COTS). Cada nodo basa su funcionamiento en una serie de funciones a bajo nivel proporcionadas por el fabricante, las cuales permiten un control independiente de los mismos. Ésto no satisface las necesidades de una plataforma en la que la comunicación entre nodos es primordial.

El trabajo en este punto consiste en dotar a la plataforma de un control basado en el uso de *webservices*. Éste permite el manejo de la plataforma desde cualquier lugar del mundo haciendo uso de aplicaciones web o software como Matlab. Esta nueva arquitectura hardware/software supone un antes y un después a la hora de realizar experimentos de comunicaciones, testar dispositivos o algoritmos MIMO. Entre sus ventajas, permite implementar comunicaciones multiusuario, *cooperative communications*, etc. Y lo que es más, facilita enormemente la realización de experimentos relacionadas con otras aportaciones presentadas en esta tesis.

En el momento en el que se adquiere la plataforma, el GTAS se integra en el proyecto MIMAX, el cual aboga por la reducción de complejidad y coste de los sistemas MIMO mediante la utilización de un sistema de múltiples antenas con *beamforming* analógico. La disponibilidad de dos nodos de la plataforma posibilita que diversas partes del proyecto se puedan testar en la misma. El cálculo de los *beamformers* óptimos requiere de una estima de canal MIMO. Para ello se diseña una estrategia basada en la aplicación de pesos en banda base utilizando tramas 802.11a modificadas para, posteriormente, ser implementada en la plataforma MIMO. Con el paso del tiempo, MIMAX requiere de medidas de canal para testear algoritmos banda base. La no disponibilidad de equipamiento dedicado para la medida de canal nos lleva a idear una metodología para la medida de canal con la plataforma GTAS. Esta metodología, descrita a continuación, posibilita la evaluación de algoritmos MIMO sobre canales reales. A su vez, diversos problemas que surgen a la hora de implementar el esquema de *beamforming* analógico, hacen que éste se deba llevar a cabo en banda base en nuestra plataforma.

## Medida de canal MIMO

En esta segunda parte se idea un método de medida de canal MIMO banda ancha basado en la transmisión y adquisición de exponenciales complejas. Además de la sencillez y simplicidad del método propuesto, este algoritmo proporciona gran precisión en la estima de la respuesta del canal a las respectivas frecuencias de las exponenciales. La metodología resulta muy versátil y flexible a la hora de medir el canal, dado que es posible considerar cualquier ancho de banda y separación entre exponenciales.

La metodología propuesta puede ser implementada en cualquier hardware compuesto por módulos de radiofrecuencia y unidades de procesamiento digital banda base. En este caso se implementa sobre la plataforma MIMO del GTAS, la cual impone las restricciones de ancho

de banda de medida, resolución frecuencial, entre otros parámetros. Hay que destacar que el uso de esta metodología evita la necesidad de emplear dispositivos de sincronización entre nodos (cables, GPS, etc...), ya que el algoritmo empleado en recepción se encarga de esta tarea. Dicho algoritmo, el (Iterative Weighted Phase Averager o IWPA), ha sido adaptado y aplicado por vez primera a la estima de canal y, a su vez, se ha modificado con el fin de trabajar con exponenciales complejas.

La señal a transmitir,  $s[n]$ , consiste en un conjunto de  $M$  exponenciales complejas:

$$s[n] = \sum_{i=1}^M A_i \exp(j(\omega_i n + \phi_i)), \quad (1)$$

donde  $A_i$  son los coeficientes de predistorsión obtenidos en el proceso de calibración y  $\omega_i$  un conjunto de frecuencias que muestrean adecuadamente el ancho de banda de interés. Por otra parte,  $\phi_i$  representa las fases necesarias para hacer frente al principal problema de las señales multitono: la relación potencia pico potencia media (*Peak-to-average power ratio* o PAPR).

El envío de las señales transmitidas se basa en un esquema de multiplexación en el tiempo, con el fin de medir todas las posibles combinaciones del canal MIMO. El transmisor conmuta las antenas de forma rápida, de manera que se transmita por todas las antenas al menos una vez en el tiempo de coherencia del canal. De este modo, las antenas receptoras adquieren una especie de trama con  $M$  transmisiones, cada una de las cuales corresponde a un transmisor diferente.

Tras atravesar el canal, la señal recibida puede denotarse como sigue

$$r[n] = \sum_{i=1}^M A'_i \exp(j(\omega'_i n + \phi'_i)), \quad (2)$$

donde  $A'_i$ ,  $\omega'_i$  y  $\phi'_i$  se corresponden con los parámetros  $A_i$ ,  $\omega_i$  y  $\phi_i$  respectivamente, tras haberse visto afectados por la transmisión a través del canal.

Para la estima de los parámetros  $A'_i$ ,  $\omega'_i$  y  $\phi'_i$ , se utiliza el algoritmo IWPA. El algoritmo IWPA es un método de estimación frecuencial no paramétrico basado en la transformada rápida de Fourier (Fast Fourier Transform o FFT), capaz de proporcionar una estimación precisa.

La técnica de estima de canal del proyecto MIMAX que se presenta en el Capítulo 3, comentada anteriormente, valida esta metodología de acuerdo a diferentes medidas de canal realizadas con ambas. En dichas medidas se demuestra que, en un entorno estático en interiores, el canal es prácticamente invariable e, incluso, se puede considerar determinista.

Un aspecto positivo a destacar del uso de esta metodología es que resulta un solución de bajo coste, en el sentido de que no requiere modificaciones hardware en la plataforma, ni gastos adicionales. En resumen, su implementación en una plataforma MIMO resulta una alternativa económica a los *channel sounders* comerciales. Lógicamente, las prestaciones de estos últimos mejoran holgadamente las de nuestro sistema.

Hasta el momento se plantea la cuestión de que el canal MIMO en interiores es invariable en el tiempo si el entorno permanece estacionario. Estos canales deterministas pueden ser útiles para testear algoritmos o dispositivos sobre un canal concreto. Sin embargo, los sistemas de comunicación inalámbricos de hoy en día suelen evaluarse en condiciones variantes, lo que limita el número y la variedad de experimentos a realizar.

## Emulación de canal MIMO

La tercera parte de la tesis aborda el diseño e implementación de una metodología para la emulación del canal MIMO. Para ello se hace uso de la plataforma del GTAS junto con el esquema de medida de canal presentada en el Capítulo 4 y la aplicación de pesos variantes en el tiempo utilizada en MIMAX (Capítulo 3) para emular el canal MIMO. En el Capítulo 5 se presenta una solución para la emulación de canales MIMO banda estrecha de manera flexible, precisa y fácilmente escalable. Esta metodología se puede utilizar de dos maneras: una de ellas permite la carga de realizaciones de canal provenientes de campañas de medidas previas o de modelos conocidos (por ejemplo WINNER); la segunda permite emular canales *Rician* con unas determinadas características espaciales y temporales.

En primer lugar, se mide el canal MIMO utilizando, por ejemplo, la metodología presentada en el Capítulo 4. El canal resultante será el medido entre el nodo transmisor y el receptor. Las señales transmitidas se combinan linealmente con el fin de emular el canal deseado. Los coeficientes (o pesos) de la combinación lineal se calculan en función del canal MIMO medido y del que se quiere emular. Estos pesos se pueden aplicar muestra a muestra, lo que requiere un volcado previo a memoria de los mismos así como de las las señales transmitidas. La rapidez con la que se apliquen los pesos será por tanto controlada por la frecuencia de muestreo, y es adecuada para la emulación de canales altamente variantes en el tiempo. Sin embargo, los canales típicos en interiores se consideran *block fading*, con lo que la actualización de los pesos a aplicar no está sujeta a cambios rápidos. Ésta es la opción utilizada para la presentación de los resultados, así como de las aplicaciones futuras de la metodología.

En resumen, la metodología para la emulación de canal MIMO resulta una herramienta precisa y flexible que se puede implementar en sistemas con posibilidad de ejecución en tiempo real. Dicha metodología es integrable en una plataforma de comunicaciones para emular canales MIMO. Este hecho abre una multitud de posibilidades prácticas; por ejemplo, es posible testear algoritmos posicionando la plataforma en entornos interiores y, a su vez, cargando en ella realizaciones de canal en exteriores.

## Conclusiones

En este trabajo se proponen una serie de técnicas para la medida y emulación del canal MIMO utilizando una plataforma MIMO convencional. Para ello, esta última ha sido dotada con un interfaz web basado en *webservices* que permite aprovechar sus funcionalidades y prestaciones de una forma más simple y eficaz. Las ventajas de disponer de una manera económica y sencilla de medir y emular el canal MIMO son numerosas, puesto que permiten conocer entornos reales de propagación que son muy difíciles de caracterizar por otros medios o requieren de un equipamiento específico que suele resultar costoso. El resultado es una solución económica para pequeños centros de investigación y universidades que permite conocer el canal de comunicaciones, así como emular características del mismo. Es importante resaltar que el hecho de utilizar la plataforma para medir y emular el canal MIMO, acarrea las consiguientes limitaciones en términos de prestaciones frente al equipamiento comercial dedicado.

En la primera parte de la tesis se presenta la plataforma del GTAS. La principal aportación en este apartado consiste proveer a la misma de un interfaz web basado en *webservices* que permite controlar los nodos de manera remota y facilita la comunicación entre ellos.



En la segunda parte de la tesis se presenta una metodología para la medida de canal MIMO basada en el envío de señales multifrecuencia. Dicha metodología es muy versátil y flexible a la hora de medir el canal, dado que se puede considerar cualquier ancho de banda y separación entre señales. El uso de esta metodología evita la necesidad de emplear dispositivos de sincronización entre nodos (cables, GPS, etc...) ya que el algoritmo empleado en recepción se encarga de esta tarea. Dicho algoritmo, el IWPA, ha sido adaptado y aplicado por vez primera a la estima de canal y ha sido modificado para poder trabajar con exponenciales complejas. La metodología puede ser implementada en cualquier hardware compuesto por módulos de RF y unidades de procesamiento digital banda base. En esta tesis, se ha implementado en nuestra plataforma, la cual impone las restricciones de ancho de banda de medida, resolución frecuencial, etc.

Finalmente, se presenta una técnica para la emulación del canal MIMO banda estrecha basada en la combinación lineal de las señales banda base en el transmisor. La metodología permite la emulación de cualquier realización de canal equivalente banda base. Se presentan expresiones cerradas para el cálculo de los coeficientes de dicha combinación a partir de la medida del canal físico entre los nodos de la plataforma y del canal deseado. La metodología se implementa en la plataforma GTAS, en la cual se ha testeado con excelentes resultados.



# Notation and Acronyms

## Notation

$a$	Scalar
$\text{Re}\{\cdot\}, \text{Im}\{\cdot\}$	Real and imaginary parts.
$\mathbf{a}$	Column vector
$\mathbf{A}$	Matrix
$\mathbf{I}$	Identity matrix. A subscript can be used to indicate the dimension.
$\mathcal{R}$	Toeplitz Matrix
$\hat{(\cdot)}$	Matrix, vector, scalar estimate
$\mathbf{I}_n$	Identity matrix of dimension $n$
$\mathbf{0}$	All-zeros matrix (or vector) of adequate dimensions
$E[\cdot]$	Expectation operator
$\mathbf{x} \sim \mathcal{CN}(\boldsymbol{\mu}, \mathbf{R})$	$\mathbf{x}$ is a complex random circularly Gaussian vector of $\boldsymbol{\mu}$ mean and covariance matrix $\mathbf{C}$
$\otimes$	Kronecker product
$\odot$	Hadamard product
$\mathcal{F}(\cdot)$	Discrete-time Fourier Transform
$\det(\mathbf{A})$	Determinant of matrix $\mathbf{A}$
$\text{tr}(\mathbf{A})$	Trace of matrix $\mathbf{A}$
$\text{cov}(\mathbf{A})$	Covariance of matrix $\mathbf{A}$
$E[\cdot]$	Statistical expectation. A subscript can be used to indicate the random variable considered for the expectation.
$\text{diag}(\mathbf{A})$	diagonal matrix with the diagonal elements of matrix $\mathbf{A}$
$(\cdot)^T$	transpose function
$(\cdot)^H$	hermitic function
$\triangleq$	Defined as
$\text{vec}(\cdot)$	vec-operator: if $\mathbf{X} = [\mathbf{x}_1 \dots \mathbf{x}_n]$ , then $\text{vec}(\mathbf{X}) = [\mathbf{x}_1^T \dots \mathbf{x}_n^T]^T$ .
$*$	Convolution
$\sim$	Distributed according to.
$\mathbf{x} \sim \mathcal{CN}(\mathbf{m}, \mathbf{C})$	$\mathbf{x}$ is a complex circularly symmetric Gaussian vector distribution with mean $m$ and covariance matrix $\mathbf{C}$ .

## Acronyms

AC	Anechoic Chamber
ACF	Autocorrelation Function
ADC	Analog to Digital Conversion
AFE	Analog Front-End
AGC	Automatic Gain Control
API	Application Programming Interface
AR	Autoregressive [stochastic process]
ASIC	Application-Specific Integrated Circuits
BB	Baseband
BC	Broadcast Channel
BER	Bit Error Rate
CFO	Carrier Frequency Offset
CIR	Channel Impulse Response
COTS	Commercial Off- The-Shelf
CPLD	Complex Programmable Logic Devices
CR	Cognitive radio
CSI	Channel State Information
CW	Continuous Wave
DAC	Digital to Analog Conversion
DC	Direct Current
DFT	Discrete Fourier Transform
DLL	Dynamical-Link Library
DPU	Digital Processing Unit
DSP	Digital Signal Processor
DUT	Device Under Test
ED	Energy Detector
FFT	Fast Fourier Transform
FIR	Finite Impulse Response [filter]
FPGA	Field Programmable Gate Array
GPIO	General Purpose Input/Output
GPS	Global Positioning System
GSCM	Geometry-based Stochastic Channel Model
GTAS	Advanced Signal Processing Group
GTEC	Group of Electronic Technology and Communications
GUI	Graphical User Interface
IEEE	Institute of Electrical and Electronics Engineers
IF	Intermediate Frequency
i.i.d.	Independent and Identically Distributed
IMD	Intermodulation Distortion
I/O	Input/Output
I/Q	In-phase and Quadrature
IWPA	Iterative Weighted Phase Averager
LNA	Low-Noise Amplifier
LO	Local Oscillator

---

LOS	Line-Of-Sight
LS	Least Squares [estimation]
LTE	Long Term Evolution [Standard]
LTI	Linear Time Invariant
LTV	Linear Time Variant
MA	Moving Average [stochastic process]
MAC	Multiple Access Channel
MBps	Mega Bytes per second
MF	Matched Filter
MIMAX	Advanced MIMO systems for MAXimum reliability and performance
MIMO	Multiple-Input Multiple-Output
MISO	Multiple-Input Single-Output
ML	Maximum Likelihood [estimator]
MPC	Multipath Component
MS	Mobile Station
MS/s	Megasamples per second
MSE	Mean Square Error
NLOS	Non Line-Of-Sight
OFDM	Orthogonal Frequency Domain Multiplexing
OTA	Over The Air
PA	Power Amplifier
PAPR	Peak to Average Power Ratio
PC	Personal Computer
PCI	Peripheral Component Interconnect
pdf	Probability Density Function
PDP	Power Delay Profile
PN	Pseudo Noise
PNA	Programmable Network Analyzer [instrumentation]
PRBS	Pseudo-Random Binary Signals
PRNS	Pseudo-Random Noise Signals
PSD	Power Spectral Density
RAM	Random Access Memory
RC	Reverberation Chamber
RF	Radio frequency
RMS	Root Mean Square
RX	Receiver
SDR	Software Defined Radio
SDRAM	Synchronous Dynamic Random Access Memory
SIMO	Single-Input Multiple-Output
SINR	Signal to Interference plus Noise Ratio
SISO	Single-Input Single-Output
SNR	Signal to Noise Ratio
SPI	Serial Peripheral Interface
TBMCE	Testbed-based MIMO Channel Emulation
TCP	Transmission Control Protocol
TDMA	Time Division Multiple Access
TX	Transmitter
UDC	Universidade da Coruña

VCO	Voltage-Controlled Oscillator
VGA	Variable Gain Amplifier
VNA	Vector Network Analyzer
w/ and w/o	With and without, respectively
WCDMA	Wideband Code Division Multiple Access
WiMAX	Worldwide Interoperability for Microwave Access
WS	Web Services
WSS	Wide-Sense Stationary [process]
WSSUS	Wide-Sense Stationary Uncorrelated Scattering
XPC	Cross Polarization Coupling
XPD	Cross-Polarization Discrimination

# Contents

<b>Acknowledgements</b>	<b>ix</b>
<b>Abstract</b>	<b>xi</b>
<b>Resumen y Conclusiones (Spanish Summary)</b>	<b>xiii</b>
<b>Notation and Acronyms</b>	<b>xix</b>
<b>Contents</b>	<b>xxv</b>
<b>1 Introduction</b>	<b>3</b>
1.1 Goal of the Thesis . . . . .	3
1.2 Outline and contributions . . . . .	7
<b>2 Multi-antenna indoor wireless channels</b>	<b>9</b>
2.1 Multipath propagation . . . . .	10
2.1.1 Deterministic multipath channel . . . . .	11
2.1.2 Stochastic modeling . . . . .	14
2.1.3 Rayleigh and Rician channels . . . . .	17
2.1.4 Complex-Baseband Equivalent Channel . . . . .	18
2.2 Multi-antenna wireless channel . . . . .	19
2.2.1 Spatial correlation . . . . .	20
2.3 Indoor channel characterization . . . . .	21
2.4 Conclusions . . . . .	22
<b>3 MIMO testbedding</b>	<b>23</b>
3.1 Prototyping for MIMO systems: MIMO testbeds . . . . .	24
3.1.1 MIMO Testbed Requirements . . . . .	25
3.1.2 COTS Modules . . . . .	27
3.1.3 Testbed applications . . . . .	27
3.2 Testbeds review . . . . .	28
3.2.1 Future of the Testbeds . . . . .	28
3.3 Lyrtech MIMO nodes . . . . .	29
3.3.1 VHS BB boards . . . . .	29
3.3.2 Analog Front End (AFE) . . . . .	30
3.3.3 Host PC and node control . . . . .	34
3.4 GTAS MIMO testbed . . . . .	37
3.4.1 Real-time processing . . . . .	38
3.4.2 Local testbed interface . . . . .	38
3.4.3 Remote control PC . . . . .	40
3.5 Remote testbed interface . . . . .	41
3.5.1 Multi-Node capabilities . . . . .	43
3.5.2 Example with the interface . . . . .	43
3.5.3 Success stories . . . . .	46
3.6 Control PC . . . . .	46

3.6.1	Synchronization . . . . .	47
3.6.2	Automatic Gain Control (AGC) . . . . .	47
3.6.3	Typical utilization procedure . . . . .	48
3.7	Real-time processing . . . . .	49
3.7.1	FPGA: interface, control, user DSP . . . . .	49
3.7.2	Work flow: Tools . . . . .	50
3.7.3	Work flow followed with the GTAS MIMO testbed . . . . .	52
3.7.4	How to control the FPGA . . . . .	53
3.8	General example . . . . .	55
3.9	Example of GTAS Testbed utilization: MIMAX project . . . . .	57
3.9.1	Beamforming in MIMAX . . . . .	58
3.9.2	MIMAX baseband implementation . . . . .	59
3.9.3	MIMAX channel estimation . . . . .	60
3.10	Conclusions . . . . .	61
<b>4</b>	<b>Multifrequency methodology for measuring MIMO channels</b>	<b>63</b>
4.1	Measuring the MIMO channel . . . . .	64
4.1.1	State of the art and background . . . . .	64
4.2	Proposed scheme . . . . .	67
4.3	SIMO channel measurement procedure . . . . .	68
4.3.1	Transmit signal design . . . . .	69
4.3.2	Signal processing at the receiver side. IWPA algorithm . . . . .	73
4.4	Extension to MIMO channels . . . . .	75
4.4.1	Multiplexing technique . . . . .	75
4.4.2	Transmitter identification . . . . .	76
4.5	Implementation in GTAS MIMO testbed . . . . .	77
4.5.1	Description of Measurement Setup . . . . .	78
4.5.2	System calibration . . . . .	79
4.5.3	System validation . . . . .	80
4.6	Comparison with other channel sounders . . . . .	84
4.7	Experimental results . . . . .	84
4.7.1	Description of Measurements Scenarios . . . . .	85
4.7.2	Low-mobility measurements . . . . .	86
4.7.3	Nomadic measurements . . . . .	86
4.8	Verification of the MIMAX channel estimation procedure . . . . .	90
4.9	Success stories . . . . .	91
4.10	Conclusions . . . . .	92
<b>5</b>	<b>Testbed-based MIMO channel emulation</b>	<b>95</b>
5.1	MIMO channel emulation review . . . . .	96
5.1.1	Conducted (or wired) testing solutions . . . . .	97
5.1.2	OTA solutions . . . . .	100
5.2	MIMO channel emulation using a conventional testbed . . . . .	102
5.3	Emulation of channel realizations . . . . .	103
5.3.1	Emulation of MISO channel realizations . . . . .	104
5.3.2	Emulation of MIMO channel realizations . . . . .	105
5.4	Emulation of spatial correlation . . . . .	106
5.4.1	Emulation of MISO channels . . . . .	106
5.4.2	Emulation of MIMO channels . . . . .	107
5.4.3	Emulation of MIMO channels based on dual-polarized antennas . . . . .	108
5.5	Emulation of time-varying MIMO channels . . . . .	109
5.6	Why not apply the linear processing at the receive side? . . . . .	110
5.7	Implementation and measurement setup . . . . .	111
5.7.1	Implementation setup . . . . .	112



5.7.2	Weighting block . . . . .	113
5.7.3	Weights application . . . . .	115
5.8	Validation of the emulation of MIMO channel realizations . . . . .	115
5.9	Validation of statistical channel emulation . . . . .	118
5.10	Comparison between TBMCE and other OTA emulation methods . . . . .	122
5.11	Successful stories . . . . .	124
5.12	Conclusions . . . . .	124
<b>6</b>	<b>Conclusions and Future Lines</b>	<b>127</b>
6.1	Conclusions . . . . .	127
6.2	Future lines . . . . .	128
6.2.1	Wideband MIMO channel emulation . . . . .	128
6.2.2	Scope of application . . . . .	129
6.2.3	Straightforward improvements . . . . .	129
<b>A</b>	<b>MIMO channel measurement features (Section 4.6)</b>	<b>131</b>
A.1	SISO measurement time . . . . .	131
A.2	Doppler Calculation . . . . .	132
A.3	Maximum scatterer velocity . . . . .	133
<b>B</b>	<b>Publications</b>	<b>135</b>
B.1	Publications derived from the dissertation . . . . .	135
B.1.1	Journal publications . . . . .	135
B.1.2	International Conferences . . . . .	135
B.2	Other Publications . . . . .	136
B.2.1	International Conferences . . . . .	136
	<b>List of Figures</b>	<b>139</b>
	<b>List of Tables</b>	<b>141</b>
	<b>List of Algorithms</b>	<b>143</b>
	<b>Bibliography</b>	<b>145</b>







# Chapter 1

## Introduction

### 1.1 Goal of the Thesis

A major requisite in the evaluation of any wireless device is an adequate characterization of the radio channel. Indoor radio channels suffer from multipath propagation, i.e. the transmitted wave interacts with obstructions and surface irregularities creating a continuum of scattered paths. Therefore, the received signal is the superposition of many copies of the original transmitted signal with different time delays, amplitudes and phases. This phenomenon gives rise to a complex, time varying multipath transmission channel which depends on the specific properties of the transmission environment.

With the advent of multiple-input multiple-output (MIMO) systems and, consequently, their associated channels, the study of multipath propagation becomes indispensable. The use of MIMO systems has received a great deal of interest from the research community as well as from the wireless communications industry in recent years. Existing and emerging standards for wireless communications such as IEEE 802.16 (WiMAX) [IEEE, 2006, IEEE 802.16, 2004] or 3GPP UMTS LTE [3GPP, 2013] support multiple antenna transmissions in their high-performance profiles.

The propagation characteristics of indoor MIMO channels may change due to modifications in the environment, scatterers or people moving around, etc. Due to this, it is of high importance to have equipment that thoroughly measures (or sounds) the channel. Experimental evaluation of MIMO technologies in real-world scenarios is necessary to assess how these MIMO technologies perform over realistic, imperfect wireless channels. This fact has become an essential tool in every educational institution or even companies and allows a better understanding of the channel itself, along with the properties that describe its behavior. Up to now, there exist many publications devoted to channel measuring [Howard and Pahlavan, 1990, Wirnitzer et al., 2001, Wallace et al., 2003], and the typical propagation parameters can be extracted from the resulting channel measures [Kyritsi et al., 2003].

The experimental assessment of wireless communications systems not only takes into account the real multipath propagation in wireless channels, but also the implementation impairments so often ignored during the simulations. The evaluation of MIMO radio communications, as depicted in Figure 1.1, in terms of realism and effort, grows from the theoretical point of view towards the final product, passing by different stages. But, testbed development and the evaluation of algorithms and systems on it entail great effort for an acceptable realism level. The cost associated to this hardware setups explains why the experimental evaluation of MIMO techniques in MIMO laboratories is still not spread enough.

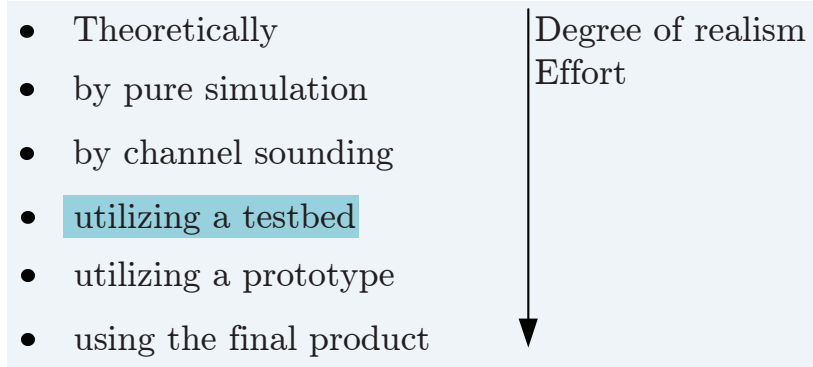


**Figure 1.1:** Evaluating MIMO radio communication.

The need of characterizing and testing MIMO devices over real channels led the Advanced Signal Processing Group (GTAS) to acquire a conventional MIMO testbed. The flexibility that a testbed provides when testing communication schemes and algorithms led us to opt for this hardware. These platforms stand out by their flexibility, being enough powerful to provide the user with real time processing, great storage capacity as well as offline post-processing [Caban et al., 2006, i. Fábregas et al., 2006, Vielva et al., 2010, García-Naya et al., 2010]. The importance of assessing MIMO algorithms over real channels is unpayable. The fundamental role that testbeds play in bridging the gap between theory and real operation, makes them indispensable in MIMO system evaluations. Regarding implementation issues, in this dissertation we show several possibilities that a commercial MIMO testbed can offer. The fact that it consists of digital processing units (DPUs) with field programmable gate arrays (FPGAs) as well as analog front-ends (AFEs), presents multiple capabilities and configurations and can stand alongside the prototypes or dedicated hardware.

Our first goal is to provide the GTAS MIMO testbed with a simple and universal way of controlling its functionalities from any place with internet connection. Such a control brings along the definition of the platform to be used, security issues, as well as the applications that support it. This research led to the development of a web platform that allows dealing with these requirements in a flexible way. Its architecture allows handling the testbed centralized to a unique computer, which facilitates each experiment to be carried out with it.

At the time that the testbed is available, GTAS is immersed in the European project Advanced MIMO systems for maximum reliability and performance (MIMAX) [MIMAX, 2008, Eickhoff et al., 2008], which advocates for the complexity and cost reduction of MIMO systems by utilizing a MIMO analog beamforming scheme. Unlike conventional MIMO systems, which usually need as many parallel operating receiving (RX) or transmitting (TX) paths as antennas are used for communication (if the signal processing is performed in the digital baseband (BB)), MIMAX shifts this paradigm to the analogue RF domain and reduces the number of RX and TX paths to a single one. Therefore, the hardware overhead consists only of additional antennas and a modified RF front-end compared to a single-input single-output (SISO) system.

As time goes by, MIMAX starts to demand a huge amount of real MIMO channel measurements for developing its BB algorithms. The lack of dedicated equipment to perform these measurements and the huge expense it involves, lead us to think up a methodology for measuring the MIMO channel using our MIMO testbed. The implementation of this method-

ology results in a powerful tool that becomes essential in the first steps of MIMAX as well as in other research projects. The channel estimation that is carried out in MIMAX (the same as performed in 802.11a) validates the proper behavior of this methodology. MIMAX also requires using the testbed to test those BB algorithms (and the whole system) in real conditions. The analog beamforming scheme it suggests is delayed due to diverse technological problems that emerge in its implementation by one of the project partners. Thus, to validate the MIMAX concept, the emulation of analog beamforming has to be carried out in BB using our MIMO testbed.

The measurement campaigns carried out with both methodologies indicate that the indoor channel is time invariant if there is no movement of people, scatterers, etc. To obtain statistically representative measures, we were forced to move the testbed nodes provoking channel fluctuations. Other option involved buying automatic positioning tables. But the use of this equipment does not assure control of the channel realizations. Making the most of MIMAX implementation, a digital BB beamformer that changes with time is then implemented within the FPGA of the TX node. This scheme allows varying the channel in a controllable way.

Finally, the combination of all the previous ideas gives rise to a methodology for emulating MIMO channels implemented in BB using the GTAS MIMO testbed. The signals at the TX are linearly combined in order to emulate the desired MIMO channel. The coefficients of the linear combination are calculated as functions of the actual channel in the laboratory and of the channel to emulate.

The advantages of having an economic and simple way to characterize MIMO channel are numerous, since it allows understanding real propagation environments which are quite difficult to characterize by other means, or require specific equipment. As an example, there exist dedicated commercial hardware to perform this task, as the well known channel sounders. However, its acquisition entails a great expense, which leads us to think up of a channel measurement methodology to be implemented in the GTAS MIMO testbed. The proposed technique involves the transmission of complex exponentials over a specific frequency band. At the receiver, the amplitudes of the exponentials (which are affected by the channel) are estimated and, from them, the channel is readily estimated. One of the key features of this method is that, due to the use of complex exponentials, difficult tasks such as synchronization or symbol detection are avoided during channel sounding. Moreover, it is computationally very simple and can get the channel measures very fast. The proper operation and the validation of the results were verified by commercial hardware.

These kind of channels could be interesting for testing algorithms or devices under a certain fixed channel. However, today's wireless communication devices are tested under different and variable conditions, if possible, controllable and repeatable. The assessment of those devices under controlled channels is one of the requirements of commercial channel emulators. As happened with channel sounders, this kind of equipment offers high performance, at a high cost.

In the same way, we decided to make the most of testbed capabilities to design and implement a channel emulation methodology. Moreover, it is based on the transmission/reception scheme of the channel measuring methodology, taking advantage of its synchronization procedure. The idea of the emulation itself emerges from the MIMAX beamforming scheme; in this case only used at the transmit side. This methodology offers a flexible and accurate solution for the emulation of any channel realization that could come from MIMO channel models or even previous channel measurement campaigns. Its implementation over the GTAS

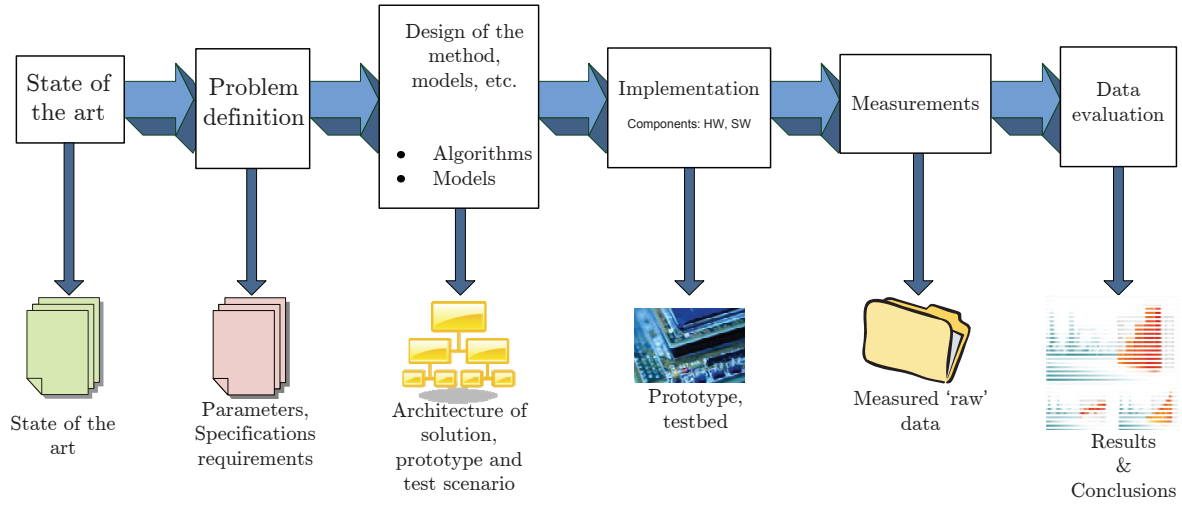


**Figure 1.2:** General methodology followed during thesis and type of result from each step.

MIMO testbed provides the whole system the possibility of testing MIMO algorithms in the lab, or even emulate outdoor channels inside it.

In summary, this dissertation tackles the problem of measuring, characterizing and emulating MIMO channels in indoor environments, using a conventional MIMO testbed. To that end, a series of steps including channel estimation, synchronization, beamforming design, real-time implementation, etc. have been followed. The two paradigmatic examples are channel sounding and channel emulation, although the door is opened to other functionalities as well. The performance of these implementations is far away to be competitive with commercial equipment. However, for academic purposes and small laboratories, it results of high importance when testing MIMO devices. The flexibility of the GTAS MIMO testbed will encourage future developments in the GTAS group.

In general, all the lines of work have followed the same methodology, with some light variations according to the work carried out in each one:

- Study of the state of the art.
- Problem definition and the different aspects to work on.
- System design: algorithms, models.
- System implementation and the subsequent evaluation.
- System validation, measurement campaigns and data analysis.

Figure 1.2 represents graphically the methodology that has been followed throughout the thesis.



## 1.2 Outline and contributions

The rest of this document is organized as follows:

- Chapter 2 overviews the basic modeling of single-antenna wireless channels, focusing on indoor channels. The extension to MIMO channels and the features they include are of study, e.g. spatial correlation. A brief study of the typical parameters of indoor wireless channels is also included.
- Chapter 3 reviews the state of the art as in hardware implementation is concerned. The MIMO testbed available in the GTAS group is addressed along with its features, impairments and control. We focus on the developed web-platform that easily allows its control. Finally, one of the first developments within the MIMO testbed, regarding the MIMAX project, is presented.

The results presented in this chapter have given place to the following publications:

- L. Vielva, J. Vía, J. Gutiérrez, Ó. González, J. Ibáñez y I. Santamaría. “Building a Web Platform for Learning Advanced Digital Communications using a MIMO Testbed”. *IEEE International Conference on Acoustics, Speech and Signal Processing (ICASSP 2010)*, Dallas, USA, March 2010.
- Ó. González, J. Gutiérrez, J. Ibáñez, L. Vielva y R. Eickhoff. “Experimental evaluation of an RF-MIMO transceiver for 802.11a WLAN”. *Future Network and Mobile Summit 2010*, Florence, Italy, June 2010.
- Chapter 4 presents a novel methodology for measuring the wideband MIMO channel making use of the GTAS MIMO testbed. It offers high accuracy and does not require synchronization between nodes using cables.

The results presented in this chapter have given place to the following publications:

- J. Gutiérrez, Ó. González, J. Pérez, D. Ramírez, L. Vielva, J. Ibáñez and I. Santamaría. “Frequency-Domain Methodology for Measuring MIMO Channels Using a Generic Test Bed”. *IEEE Transactions on Instrumentation and Measurement*, vol.60, no.3, pp.827-838, March 2011.
- In Chapter 5, we analyze the problem of testing devices or algorithms over-the-air (OTA) using channel emulation. We present a methodology that linearly combines the transmit signals to emulate MIMO channels, whether they are imported from channel models or generated from certain distributions and spatial and temporal characteristics. These techniques have been implemented in the GTAS MIMO testbed and their performance and accuracy are analyzed.

The publications that have contributed to this chapter are the following: <sup>1</sup>

- J. Gutiérrez, J. Ibáñez and J. Pérez. “MIMO OTA Testing Based on Transmit Signal Processing”. *Hindawi International Journal of Antennas and Propagation (Special Issue on Antenna Measurement Systems and Antenna Technology for Next Wireless Generation (NEXT))*, vol. 2013, June 2013.

---

<sup>1</sup>Note that some publications belong to more than one chapter.

- J. Gutiérrez, J. Ibáñez and J. Pérez. “Spatial correlation beamforming scheme for MISO channel emulation”. *International Symposium on Wireless Communication Systems (ISWCS)*, Paris, France, August 2012.
- J. Gutiérrez, J. Ibáñez and J. Pérez. “Beamforming-based emulation of spatial and temporal correlated MISO channels”. *International Symposium on Signals, Systems and Electronics (ISSSE)*, Potsdam, Germany, September 2012.
- Finally, Chapter 6 summarizes the results and concluding remarks, and proposes some future research topics.

### Other contributions not presented in this dissertation

- M. Morales, J. Gutiérrez and A. G. Armada. “Achievable Throughput with Block Diagonalization on OFDM Indoor Demonstrator”. *European Signal Processing Conference (EUSIPCO 2013)*, Marrakech, Morocco, September 2013.
- J. Gutiérrez, A. Habib and M. Rupp. “Selection Schemes for Orthogonal Tripole Antennas”. *European Conference on Antennas and Propagation (EUCAP 2013)*, Gothenburg, Sweden, April 2013.
- J. Gutiérrez, A. Habib and M. Rupp. “Indoor measurements by dual tripole antennas”. *Loughborough Antennas & Propagation Conference (LAPC 2012)*, Loughborough, UK, November 2012.
- J. Manco Vásquez, J. Gutiérrez, J. Pérez, J. Ibáñez and I. Santamaría. “Experimental Evaluation of Multiantenna Spectrum Sensing Detectors using a Cognitive Radio Testbed”. *International Symposium on Signals, Systems and Electronics (ISSSE)*, Potsdam, Germany, October 2012.
- J. Pérez, J. Gutiérrez y L. Vielva. “Performance Analysis of Transmit Antenna Selection in Broadcast MISO Channels”, *IEEE International Symposium on Broadband Multimedia Systems and Broadcasting*, Bilbao, Spain, May 2009.

### Participation in European and National Projects

- Advanced MIMO systems for maximum reliability and performance (MIMAX) Project

<http://www.ict-mimax.eu/>

- COMONSENS, <http://www.comonsens.org/>
- COSIMA, <http://www.cosimaproject.es/>

# Multi-antenna indoor wireless channels

Radio propagation typically consists of several distinct multipath components (MPCs) departing from the transmitter (TX) and arriving at the receiver (RX) with specific directions and delays. This fact is due to reflections and diffractions in the surrounding environment. It is common practice in the design and evaluation studies of wireless communication systems to use mathematical models for describing the channel. Whilst deterministic modeling is valid for specific scenarios, stochastic models serve well when the channel in question is fairly generic [Durgin, 2002].

At present, wireless technologies such as long term evolution (LTE) and Worldwide Interoperability for Microwave Access (WiMAX), bring along high throughput communications. Their underlying radio technology, which allows enhancing the overall performance of radio transmitters and receivers, is based on multiple-input multiple-output (MIMO) systems. A MIMO system [Foschini, 1996] is a wireless communication system that is equipped with multiple antennas at both ends of the link. The performance of these systems is directly related to the propagation environment in which the device is operating, which is denoted as the MIMO channel. MIMO channel modeling is of paramount importance in the design of such systems.

This chapter reviews the MIMO multipath channel characterization. Firstly, it describes the SISO deterministic multipath modeling, where channel parameters as delay spread and coherence are introduced. Secondly, the multipath channel is modeled as a multi-dependent random wide/sense stationary (WSS) process. Correlation functions and power spectral densities (PSDs) are defined. Later, the MIMO channel and its intrinsic characteristics are reviewed. Popular models as MIMO Rayleigh and Rician channels are presented.

This chapter does not claim to be a rigorous and complete revision of wireless channel modeling. The objective is to revisit some concepts related to channel modeling that will be treated through the next chapters. Thereby, we try to make this dissertation as self-contained as possible.

This chapter is organized as follows: Section 2.1 presents multipath channel modeling, highlighting the most important parameters to be considered throughout this dissertation. In Section 2.2 we extend the channel modeling to MIMO systems, focusing on their spatial properties. Section 2.3 studies the parameters presented in previous section, particularized for indoor scenarios. Finally, in Section 2.4, the main conclusions are summarized.

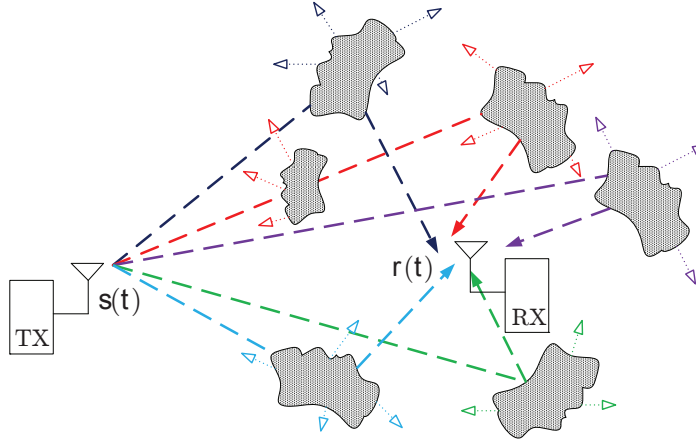


**Figure 2.1:** Different path lengths not only derive in different component amplitudes but their phases, that can provoke destructive interferences.

## 2.1 Multipath propagation

The importance of properly knowing and characterizing the wireless channel is undeniable. This allows a better design and optimization of systems and algorithms, taking into account the characteristics of multipath propagation and delay, frequency dependence, temporal fading, etc. It is well-known that wireless propagation environment entails certain limitations on communication systems. The propagation path between the TX and the RX may consist of a single path, line-of-sight (LOS). In a multipath environment, the transmitted signals reach the receiver through different propagation paths, non line-of-sight (NLOS) (see Figure 2.1). The signal phase deviation and the attenuation at different frequencies depends on the length of each path. Therefore, received signal fading depends on frequency due to constructive or destructive effects of the individual components.

Three main propagation mechanisms determine how electromagnetic waves propagate through the environment: *reflection*, *scattering*, and *diffraction* [Rappaport, 2001].

A defining characteristic of the mobile wireless channel is the variations of the channel strength over time and frequency. In a broad sense, the channel can be modeled in two different ways, large-scale propagation model and small-scale propagation model [Rappaport, 2001]. Propagation models that predict the mean signal strength for any TX/RX separation become useful in estimating the transmitter coverage area. This is generally termed as large-scale propagation models. Propagation models that characterize rapid fluctuations of the received signal within few wavelengths (short distances) are called small-scale propagation models. These fluctuations are caused by changing phases of superposing multipath components. In this chapter we will focus on small-scale propagation models and the effects that rise according to different phenomena caused by multipath fading.

Figure 2.2 represents an overview of fading channel manifestations [Sklar, 1997], distinguishing these two categories.

The impulse response of such channels is typically characterized by time-variations and time-spreading. Time variations are due to the relative motion between the TX and the RX and temporal variations of the propagation environment. Time-spreading is due to the fact that the emitted electromagnetic wave arrives at the receiver having undergone reflections, diffraction and scattering from various objects along the way, at different delay times.

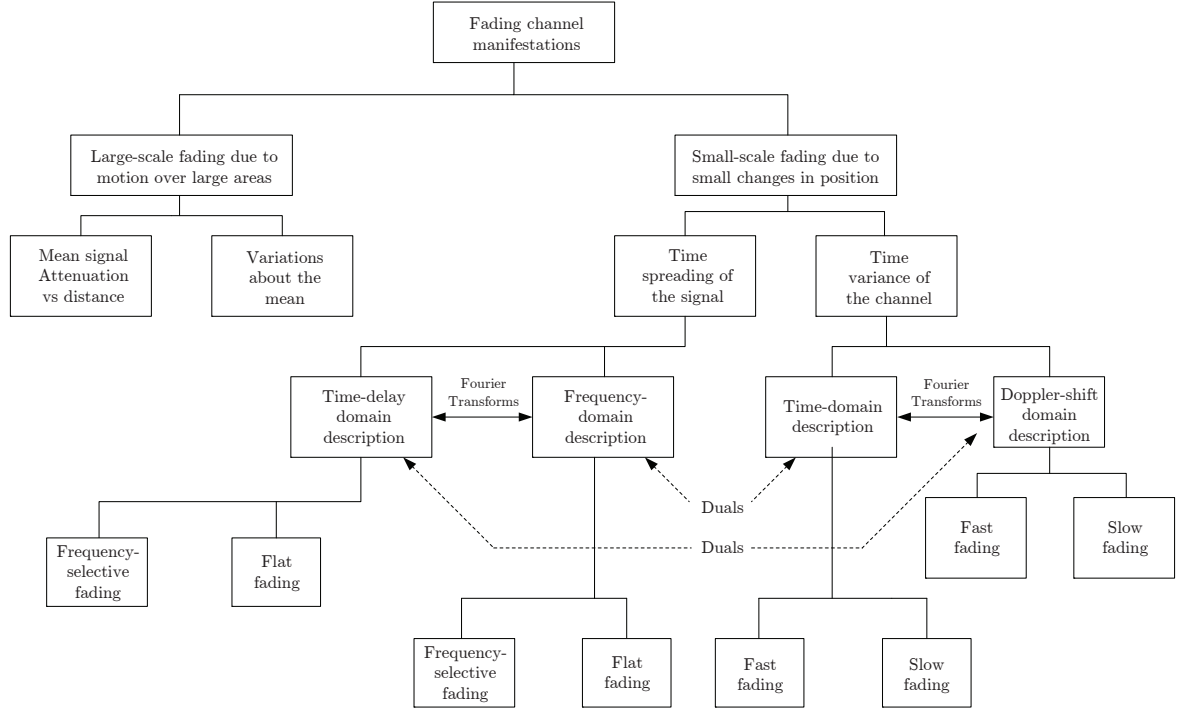


Figure 2.2: Fading channel manifestations.

These signal fluctuations, called multipath fading, are responsible for the degradation of the communication system performance.

### 2.1.1 Deterministic multipath channel

Consider a SISO multipath channel. Each signal path has its own individual path length,  $d_i$ , and gain (or attenuation),  $a_i$ . The resultant signal at the receive antenna,  $r(t)$ , is a superposition of the multipath signals. The TX and the RX bandpass signals are  $s(t)$  and  $r(t)$ , respectively.

The multipath channel can be viewed as a linear time invariant (LTI) system or as a linear time variant (LTV) system. The former is valid when the TX, RX and the propagation environment are stationary during the transmission of  $s(t)$ .

#### Time-invariant channel

In a time-invariant channel,  $r(t)$  can be written as

$$r(t) = \sum_i a_i s(t - \tau_i), \quad (2.1)$$

where  $a_i$  and  $\tau_i$  are the real amplitudes and delays, respectively, of the  $i$ th multipath component. The delays are given by  $\tau_i = d_i/c$ , where  $c$  is the speed of light and  $d_i$  is length of each path. The channel impulse response,  $h(\tau)$ , will be

$$h(\tau) = \sum_i a_i \delta(t - \tau_i), \quad (2.2)$$

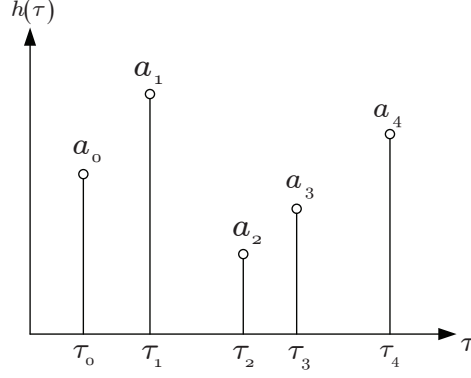


**Figure 2.3:** An example of the discrete channel impulse response for a 5-path radio channel.

In practice, we have infinite multipath components, so  $h(\tau)$  is a continuous function.

The *delay spread* is defined as the difference between the time of arrival of the earliest significant multipath component (typically the LOS component, if it exists) and the time of arrival of the latest multipath component.

$$\Delta\tau_{max} = \tau_{max} - \tau_0. \quad (2.3)$$

It is typically of the order of microseconds. Figure 2.3 depicts a 5-path channel impulse response. Therefore, the delay spread will be  $\Delta\tau_{max} = \tau_4 - \tau_0$ .

This model assumes that the amplitudes,  $a_i$ , and delays,  $\tau_i$ , are frequency independent in the band of interest. The received signal,  $r(t)$ , can be described in terms of the transmitted signal,  $s(t)$ , and the channel impulse response as

$$r(t) = s(t) * h(t) = \sum_i a_i \delta(t - \tau_i), \quad (2.4)$$

Analogously, in the frequency domain, the channel frequency response,  $h(f)$ , will be

$$h(f) = \sum_i a_i \exp(-j2\pi f \tau_i), \quad (2.5)$$

and the received signal in the frequency domain,  $r(f)$ , will be

$$r(f) = s(f)h(f) = s(f) \sum_i a_i \exp(-j2\pi f \tau_i) \quad (2.6)$$

Let  $f_c$  denote the carrier frequency. The channel response at frequency  $f = f_c + \Delta f$  will be

$$\begin{aligned} h(f_c + \Delta f) &= \sum_i \exp(-j2\pi f_c \tau_i) \exp(-j2\pi \Delta f \tau_i) \\ &= \exp(-j2\pi \Delta f \tau_0) \left[ \sum_i \exp(-j2\pi f_c \tau_i) \exp(-j2\pi \Delta f (\tau_i - \tau_0)) \right], \end{aligned} \quad (2.7)$$

and the channel response at  $f = f_c$  will be

$$h(f_c) = \sum_i \exp(-j2\pi f_c \tau_i), \quad (2.8)$$

Comparing (2.7) and (2.8), there might be significative changes in  $|h(f)|$  when

$$2\pi\Delta f(\tau_i - \tau_0) \geq \pi/2 \quad \Rightarrow \quad \Delta f \geq \frac{1}{4\Delta\tau_{max}} = B_c. \quad (2.9)$$

where  $B_c$  is usually called coherence bandwidth of the channel. In practical systems,  $B_c$  is of the order of *unit MHz*.

If the bandwidth of  $s(t)$ , denoted as  $B$ , is less than the coherence bandwidth,  $B_c$ , then the fading is flat about the carrier frequency. This kind of channels are denoted as narrowband. On the contrary, if  $B > B_c$  the channel is considered frequency-selective. From (2.7). Taking modulus in (2.7)

$$|h(f_c + \Delta f)| = \left| \sum_i a_i \exp(-j2\pi f_c \tau_i) \exp(-j2\pi \Delta f(\tau_i - \tau_0)) \right|. \quad (2.10)$$

If  $\Delta f \Delta\tau_{max} < 1/4$ , then

$$|h(f_c + \Delta f)| \approx \left| \sum_i \exp(-j2\pi f_c \tau_i) \right| = |h(f_c)| = |h|, \quad (2.11)$$

which does not depend on  $\Delta f$ .

### Time-variant channel

In a mobile communication system, the channel changes with time due to the motion of the TX, RX, and/or objects, within the propagation scenario. The channel variation in time provokes temporal variations in both amplitudes and delays,  $a_i(t) = \alpha_i/d_i(t)$ ,  $\tau_i = d_i(t)/c$ , where  $d_i(t)$  are the distances traveled from TX to RX by the paths. The time variations of both the amplitudes,  $a_i(t)$ , and delays,  $\tau_i(t)$ , of each multipath component, are slow compared with the delay spread. Hence, we can consider the channel as a LTI channel with time-varying channel response.

Assuming linear variation in time for each path,  $d_i(t) = v_i t + d_{0,i} \rightarrow \tau_i(t) = \frac{d_i(t)}{c} = \frac{v_i}{c}t + \frac{d_{0,i}}{c}$ , then the impulse response can be written as

$$h(t, f) = \sum_i a_i(t) \exp\left(-j2\pi f \frac{d_{0,i}}{c}\right) \underbrace{\exp\left(-j2\pi f \frac{v_i}{c}t\right)}_{\text{temporal dependence}}. \quad (2.12)$$

where  $f_i^D = -f \frac{v_i}{c}$  is the so called Doppler frequency deviation of the  $i$ -th path. Maximum Doppler deviations in outdoor environments are typically of the order of 100 MHz. In indoor environments, the Doppler frequency used to be almost zero, or even zero in static environments.

According to (2.12) the channel response at  $t = t_0 + \Delta t$ , will be

$$h(t_0 + \Delta t, f) = \sum_i a_i(t_0 + \Delta t) \exp\left(-j2\pi f \frac{d_{0,i}}{c}\right) \exp(j2\pi f_i^D t_0) \exp(j2\pi f_i^D \Delta t) \quad (2.13)$$

whereas at  $t = t_0$  the channel response is

$$h(t_0, f) = \sum_i a_i t_0 \exp\left(-j2\pi f \frac{d_{0,i}}{c}\right) \exp(j2\pi f_i^D t_0) \quad (2.14)$$

Comparing (2.13) and (2.14), there will be significant changes in  $|h(t, f)|$  with  $t$  when

$$2\pi f_{max}^D \Delta t \geq \pi/2 \quad \Rightarrow \quad \Delta t \geq \frac{1}{4\Delta f_{max}^D} = T_c. \quad (2.15)$$

In practical systems,  $T_c$  is of the order of milliseconds to few seconds in indoor environments due the movement of people [Keshavarzian et al., 2007]. This means that it usually exceeds multiple frame transmission times. It is called coherence time of the channel. If the time that takes transmitting  $s(t)$  is lower than  $T_c$ , the channel can be considered time-invariant.

The channel response also depends on the location of the TX and the RX. Therefore, we can write the channel response as a function of both spatial dependencies, along with time and frequency:  $h(\mathbf{r}_R, \mathbf{r}_T, t, f)$ .

$$h(\mathbf{r}_R, \mathbf{r}_T, t, \tau) = \sum_i a_i(\mathbf{r}_R, \mathbf{r}_T, t) \delta(\tau - \tau_i(\mathbf{r}_R, \mathbf{r}_T, t)) \quad (2.16)$$

$$h(\mathbf{r}_R, \mathbf{r}_T, t, f) = \sum_i a_i(\mathbf{r}_R, \mathbf{r}_T, t) \exp(-j2\pi f \tau_i(\mathbf{r}_R, \mathbf{r}_T, t)) \quad (2.17)$$

The coherence distance of the channel is defined at both the TX and the RX side. The coherence distance at the TX side,  $D_{c,T}$ , is defined as the maximum spatial displacement,  $\Delta \mathbf{r}_T$ , so  $|h(\mathbf{r}_T)| \approx |h(\mathbf{r}_T + \Delta \mathbf{r}_T)|$ . In the same way, the coherence distance at the RX side,  $D_{c,R}$ , is defined as the maximum spatial displacement,  $\Delta \mathbf{r}_R$ , so  $|h(\mathbf{r}_R)| \approx |h(\mathbf{r}_R + \Delta \mathbf{r}_R)|$ . Typically, if  $\Delta \mathbf{r} < \lambda/2$ , the channel is spatially invariant, where  $\lambda$  is the wavelength that corresponds to the maximum frequency of  $s(t)$ .

As an example, Figure 2.4 depicts several channel measures where these three dependencies are appreciable. We assume a fixed TX position, fixed  $\mathbf{r}_T$ , and four different RX positions. We have 11 curves for each RX position.

First, it is appreciable that the curves do not follow the same trend, which means that the separation between the receive antennas is larger than the coherence distance. One can also notice that the curves vary in frequency, some vary more than others. This fact reflects that the coherence bandwidth gets higher with the flatness of these curves. Finally, the variations in time is negligible. The 11 curves are almost perfectly overlapping, thus the channel can be considered static with  $T_c$  higher than the transmission duration.

Hereafter, for the sake of notation simplicity, we will consider a single spatial depending,  $\mathbf{r}$ , where  $\mathbf{r}$  can denote the TX location of a fixed RX location and vice versa.

### 2.1.2 Stochastic modeling

A complete deterministic characterization of wireless channels is infeasible due to their complexity. Even if such a characterization were possible, it would only apply to a specific environment, whereas wireless systems need to be designed for a wide variety of operating conditions. This motivates stochastic characterizations, which consider the channel as a wide-sense stationary (WSS) random process



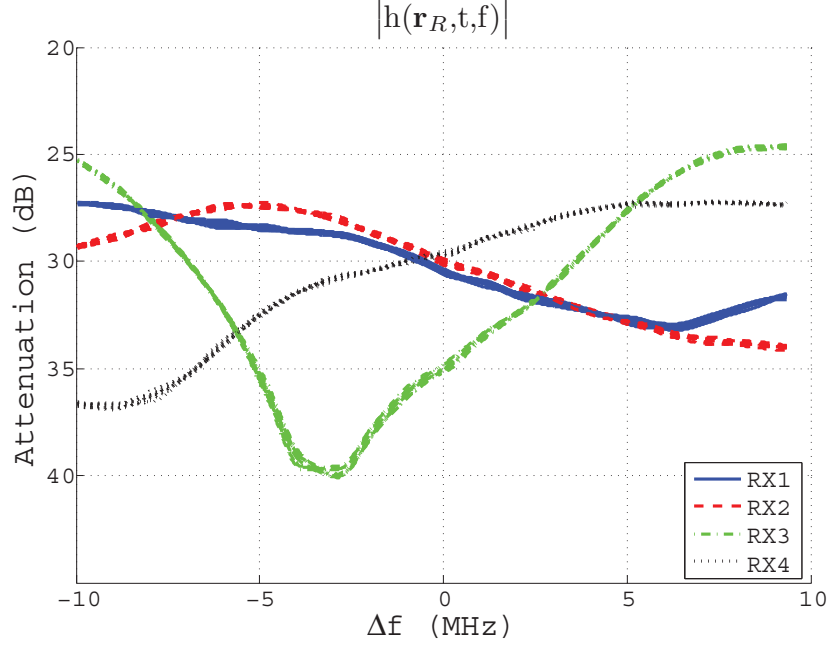


**Figure 2.4:** Multipath propagation causing fading in time, frequency and space.

$$h(\mathbf{r}, t, f) = \sum_i a_i(\mathbf{r}, t) \exp(-j2\pi f\tau_i(\mathbf{r}, t)) \quad (2.18)$$

where  $a_i$  and  $\tau_i$  are stochastic processes in  $\mathbf{r}$  and  $t$ .

A statistical description of the channel is given by the correlation functions in space, time and frequency

$$R_h(\Delta\mathbf{r}, t_0, f_0) = E\{h(\mathbf{r}, t_0, f_0)h^*(\mathbf{r} - \Delta\mathbf{r}, t_0, f_0)\} \quad (2.19)$$

$$R_h(\mathbf{r}_0, \Delta t, f_0) = E\{h(\mathbf{r}_0, t, f_0)h^*(\mathbf{r}_0, t - \Delta t, f_0)\} \quad (2.20)$$

$$R_h(\mathbf{r}_0, t_0, \Delta f) = E\{h(\mathbf{r}_0, t_0, f)h^*(\mathbf{r}_0, t_0, f - \Delta f)\} \quad (2.21)$$

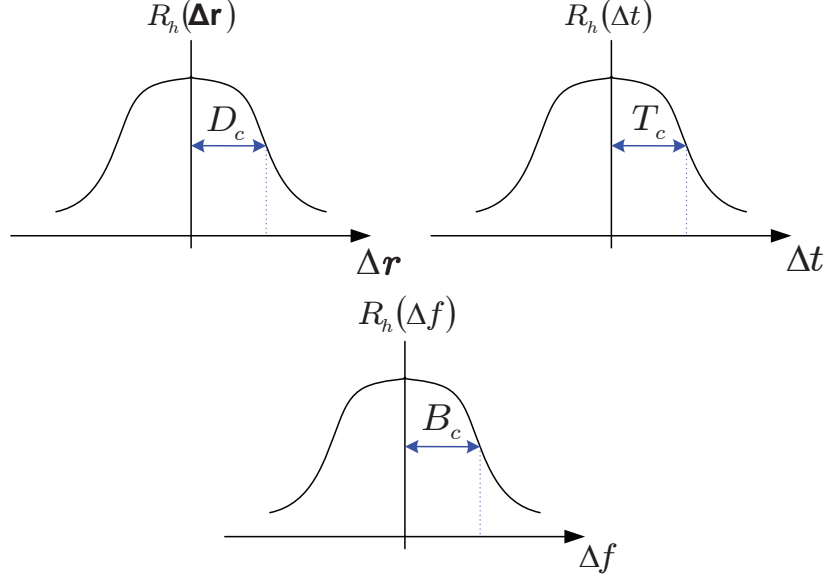
These ACFs, defined for the channel as a function of space, time, and frequency, allow calculating the corresponding coherence parameters:  $D_c$ ,  $T_c$  and  $B_c$ , respectively. They are defined as the width for which the corresponding ACF is above a certain level. Remember that  $\Delta\mathbf{r}$  can denote RX displacement for a fixed  $\mathbf{r}_T$  or TX displacement for a fixed  $\mathbf{r}_R$ . Then,  $R_h(\Delta\mathbf{r})$  can be the spatial correlation function at the RX or at the TX. Accordingly, we distinguish between coherence distance at the RX,  $D_{cR}$ , and at the TX,  $D_{cT}$ .

Table 2.1 shows the corresponding power density spectrums.

They are the Doppler PSD, or Doppler Spectrum, the delay PSD, or Power Delay Profile (PDP), and the wavenumber PSD, or wavenumber spectrum.

The width of these PSD functions provide insight into the coherence of a channel. As the PSD widens, its autocorrelation becomes narrower and coherence decreases. The most common parameter of the PSD width is the root-mean-square (RMS) width. It is the normalized second centered moment of the corresponding spectrum.

The RMS delay spread is



**Figure 2.5:** Stochastic definition of coherence distance,  $D_c$ , coherence time,  $T_c$ , and coherence bandwidth,  $B_c$ .

Autocorrelation	Power spectral densities (PSDs)
$R_h(\Delta \mathbf{r}) = \frac{1}{2\pi} \int_{-\infty}^{\infty} S_h(k) \exp(jk\Delta \mathbf{r}) dk$	$S_h(k) = \int_{-\infty}^{\infty} R_h(\Delta \mathbf{r}) \exp(-jk\Delta \mathbf{r}) d\Delta \mathbf{r}$
$R_h(\Delta t) = \frac{1}{2\pi} \int_{-\infty}^{\infty} S_h(\omega) \exp(j\omega\Delta t) d\omega$	$S_h(\omega) = \int_{-\infty}^{\infty} R_h(\Delta t) \exp(-j\omega\Delta t) d\Delta t$
$R_h(\Delta f) = \frac{1}{2\pi} \int_{-\infty}^{\infty} S_h(\tau) \exp(-j2\pi\tau\Delta f) d\tau$	$S_h(\tau) = \int_{-\infty}^{\infty} R_h(\Delta f) \exp(j2\pi\tau\Delta f) d\Delta f$

**Table 2.1:** Relevant autocorrelation-spectrum relationships.

$$\sigma_\tau = \overline{\tau^2} - (\overline{\tau})^2, \quad \text{where } \overline{\tau^n} = \frac{\int_{-\infty}^{+\infty} \tau^n S_h(\tau) d\tau}{\int_{-\infty}^{+\infty} S_h(\tau) d\tau}. \quad (2.22)$$

A larger delay spread implies increased frequency selectivity and a smaller coherence bandwidth. Many wireless engineers calculate the coherence bandwidth using the rule of thumb,  $B_c \approx \frac{1}{5\sigma_\tau}$ .

The RMS Doppler spread is

$$\sigma_\omega = \overline{\omega^2} - (\overline{\omega})^2, \quad \text{where } \overline{\omega^n} = \frac{\int_{-\infty}^{+\infty} \omega^n S_h(\omega) d\omega}{\int_{-\infty}^{+\infty} S_h(\omega) d\omega}. \quad (2.23)$$

An increased Doppler spread implies a channel with faster temporal fluctuations and a smaller coherence time.  $T_c$  is inversely proportional to  $\sigma_\omega$ .

### 2.1.3 Rayleigh and Rician channels

In practise, it is difficult to model  $a_i$  and  $\tau_i$  as stochastic processes. Many times,  $a_i$  and  $\tau_i$  are modeled just as random variables with a certain distribution. Therefore

$$h(f) = \sum_i a_i \exp(-j2\pi f \tau_i) \quad (2.24)$$

In these models we lose information about temporal and spatial correlation of  $h$ .  
Let consider the modulus of the channel response at  $f = f_c + \Delta f$

$$|h(f_c + \Delta f)| = \left| \sum_i^N a_i \exp(-j\phi_i) \right|, \quad (2.25)$$

where  $\phi_i = 2\pi(f_c + \Delta f)\tau_i$ . The channel behaves as a Rayleigh fading channel when the following three conditions are fulfilled

1. There exist a large number of multipath components,  $N \gg 1$ .
2.  $\phi_i = 2\pi(f_c + \Delta f)\tau_i = 2\pi(\lambda_c + \Delta\lambda)d_i \sim \mathcal{U}(0, 2\pi)$ , and they are independent, where  $\lambda_c = c/f_c$  is the wavelength of the carrier frequency.

Since  $d_i \gg \lambda_c$ , small (random) changes in  $d_i$  produces high fluctuations in  $\phi_i$  so  $\phi_i$  can be modeled as a uniform distributed random phase.

3. There is not a dominant  $a_i$ .

On the basis of the central limit theorem [Papoulis and Pillai, 2002]

$$h(f_c + \Delta f) = \sum_i^N a_i \exp(-j\phi_i) \sim \mathcal{CN}(0, \sigma^2), \quad \sigma^2 = \sum_i a_i^2 \quad (2.26)$$

Therefore, the envelope of the channel frequency response will be Rayleigh distributed. If there is a LOS component  $i = 0$ ,

$$|h(f_c + \Delta f)| = \left| a_0 + \sum_{i \neq 0} a_i \exp(-j(\phi_i - \phi_0)) \right|. \quad (2.27)$$

Since

$$a_0 + \sum_{i \neq 0} a_i \exp(-j(\phi_i - \phi_0)) \sim \mathcal{CN}(a_0, \sigma^2), \quad \sigma^2 = \sum_{i \neq 0} a_i^2, \quad (2.28)$$

$|h|$  will be Rician distributed with Rician factor given by

$$K = \frac{a_0^2}{\sigma^2}. \quad (2.29)$$

In (2.29), when  $K = 0$ , we have a Rayleigh fading channel. On other hand, if  $K = \infty$ , we have a free space channel.

Under condition 2, the frequency ACF will be

$$R_h(\Delta f) = E[h(f_c)h^*(f_c - \Delta f)] = \sum_i a_i^2 \exp(-j2\pi\Delta f \tau_i). \quad (2.30)$$

Then, from Table 2.1, the PDP can be expressed as

$$S_h(\tau) = \sum_i a_i^2 \delta(\tau - \tau_i), \quad (2.31)$$

and (2.22), the delay spread will be

$$\sigma_\tau = \frac{\sum_i a_i^2 \tau_i - (\sum_i a_i^2 \tau_i)^2}{\sum_i a_i^2}. \quad (2.32)$$

In the LOS case, the mean of the envelope is  $E[|h(f_c + \Delta f)|] = a_0$ ,  $\forall \Delta f$ . The autocovariance  $\mathcal{C}_h(\Delta f) = R_h(\Delta f) - a_0^2$  where,  $R_h(\Delta f)$  is the one in (2.30) without the term  $i = 0$ .

#### 2.1.4 Complex-Baseband Equivalent Channel

Up to now, we have modeled the bandpass channel. In (2.4),  $s(t)$  is a bandpass signal centered in  $f_c$ , with a bandwidth of  $2B$ . Therefore,  $r(t)$  also results a bandpass signal.

Let  $s_b(t)$  and  $r_b(t)$  be their baseband equivalent representations. The relation between the baseband and bandpass representations in the frequency domain is given by

$$S_b(f) = \begin{cases} S(f + f_c), & -B \leq f \leq B \\ 0 & \text{otherwise} \end{cases}, \quad (2.33)$$

whilst in the temporal domain is

$$s(t) = \text{Re}\{s_b(t) \exp(j2\pi f_c t)\}. \quad (2.34)$$

These relationships also apply to  $r(t)$ .

Then, the baseband input/output relationship is given by

$$r_b(t) = s_b(t) * h_b(\tau) \quad (2.35)$$

$$r_b(f) = \frac{1}{2} s_b(f) h_b(f), \quad (2.36)$$

where  $h_b(\tau)$  is the equivalent baseband representation of  $h(\tau)$ , centered in  $f_c$

$$h_b(f) = h(f + f_c), \quad -B \leq f \leq B. \quad (2.37)$$

Outside this frequency band, it does not matter how  $h_b(f)$  behaves, since  $s_b(t)$  is a baseband signal of bandwidth  $B$ .

Therefore, the bandpass/baseband relationship of the multipath channel model will be

$$h(f) = \sum_i a_i \exp(-j2\pi f \tau_i) \Rightarrow h_b(f) = \sum_i \exp(-j2\pi f \tau_i) a_i \exp(-j2\pi f_c \tau_i). \quad (2.38)$$

The baseband representation can be written as

$$h_b(f) = \sum_i a_i^c \exp(-j2\pi f \tau_i), \quad a_i^c = a_i \exp(-j2\pi f_c \tau_i). \quad (2.39)$$

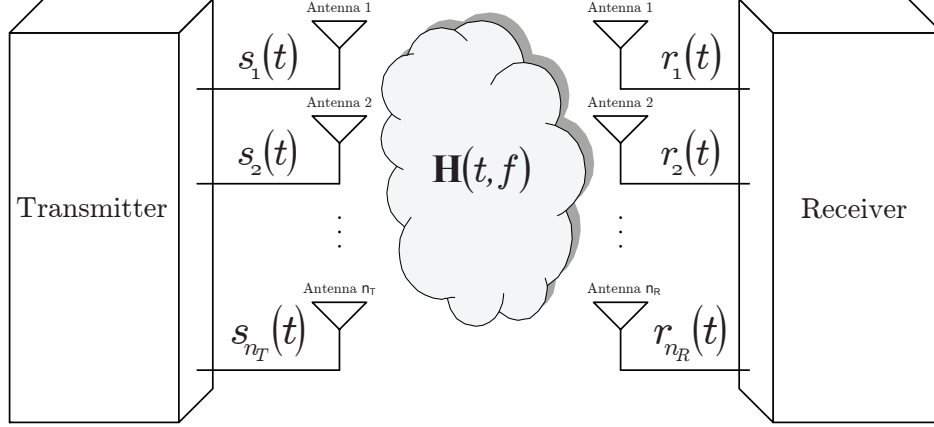


**Figure 2.6:** Baseband equivalent MIMO channel.

Finally, the impulse channel response of the baseband equivalent channel will be given by the inverse Fourier Transform of (2.39)

$$h_b(\tau) = \sum_i a_i^c \delta(\tau - \tau_i) \quad (2.40)$$

As can be seen, the difference with respect to the bandpass representation is the  $a_i^c$  complex term, instead of  $a_i$ . What has been found out so far for the bandpass, also apply to the equivalent baseband.

Hereafter we will consider the baseband representation. For the sake of notation simplicity. We will omit the subscript  $b$ , so,  $h$  will denote the baseband equivalent channel and, similarly,  $s(t)$  and  $r(t)$  will denote baseband equivalent signals.

## 2.2 Multi-antenna wireless channel

Usually, a MIMO channel is represented as a matrix with  $n_R$  rows and  $n_T$  columns, being  $n_R$  and  $n_T$  the number of TX and RX antennas, respectively. Each entry corresponds to a SISO channel modeled as described in Section 2.1. In general, they vary with time and frequency, being dependent on TX-RX antenna positions,  $(\mathbf{r}_R^j, \mathbf{r}_T^i)$ , where  $j = 1 \dots n_R$  and  $i = 1, \dots, n_T$ . Then, the MIMO channel matrix can be written as

$$\mathbf{H}(t, f) = \begin{bmatrix} h(\mathbf{r}_R^1, \mathbf{r}_T^1, t, f) & h(\mathbf{r}_R^1, \mathbf{r}_T^2, t, f) & \cdots & h(\mathbf{r}_R^1, \mathbf{r}_T^{n_T}, t, f) \\ h(\mathbf{r}_R^2, \mathbf{r}_T^1, t, f) & h(\mathbf{r}_R^2, \mathbf{r}_T^2, t, f) & \cdots & h(\mathbf{r}_R^2, \mathbf{r}_T^{n_T}, t, f) \\ \vdots & \vdots & \ddots & \vdots \\ h(\mathbf{r}_R^{n_R}, \mathbf{r}_T^1, t, f) & h(\mathbf{r}_R^{n_R}, \mathbf{r}_T^2, t, f) & \cdots & h(\mathbf{r}_R^{n_R}, \mathbf{r}_T^{n_T}, t, f) \end{bmatrix} \quad (2.41)$$

In Figure 2.6, the conventional MIMO scheme is depicted, where  $s_i(t)$  is the signal transmitted by the  $i$ -th TX antenna and  $r_j(t)$  is the signal received by the  $j$ -th RX antenna.

In (2.41) we introduce the concept of spatially sampled channels. Space variables  $\mathbf{r}_R$  and  $\mathbf{r}_T$  are sampled at the locations of the  $n_R$  receive and  $n_T$  TX antennas. The channel between TX antenna  $i$  and RX antenna  $j$  can be denoted as

$$h(\mathbf{r}_R^j, \mathbf{r}_T^i, t, f) \equiv h_{ji}(t, f) \quad (2.42)$$

If the channel response is time invariant, or the duration of the transmit frame is less than  $T_c$ , for all TX-RX antenna pairs, the channel matrix is only frequency dependent,  $\mathbf{H}(f)$ . On the other hand, if the channel response is frequency flat, or the transmit signal bandwidth is less than the channel coherence bandwidth ( $B < B_c$ ) for all TX-RX antenna pairs, the channel response will be constant with frequency,  $\mathbf{H}(t)$ . If the channel is time and frequency invariant,  $\mathbf{H}$  will be a conventional matrix with scalar entries.

In this case the signal model will be

$$\mathbf{r}(t) = \mathbf{H}\mathbf{s}(t) + \mathbf{n}(t), \quad (2.43)$$

where  $\mathbf{s}(t) = [s_1(t) \dots s_{n_T}(t)]^T$ ,  $\mathbf{r}(t) = [r_1(t) \dots r_{n_R}(t)]^T$  and  $\mathbf{n}(t) = [n_1(t) \dots n_{n_R}(t)]^T$  comprises the baseband equivalent noise processes at the RX branches.

The i.i.d. Rayleigh fading stochastic channel is the most common channel model for MIMO systems. In this case, according to (2.26),

$$\mathbf{H} \sim \mathcal{CN}(0, \sigma^2 \mathbf{I}) \quad (2.44)$$

Hereafter, this channel model will be denoted by  $\mathbf{H}_w$ .

### 2.2.1 Spatial correlation

In MIMO systems, the spatial correlation properties of the channel are of paramount importance in their performance. In general, the spatial correlation matrix of the MIMO channel is defined as the following  $n_T n_R \times n_T n_R$  matrix

$$\mathbf{R} = E[\mathbf{H}\mathbf{H}^H]. \quad (2.45)$$

The channel is said spatially white or spatially uncorrelated if  $\mathbf{R}$  is diagonal. This is the case of MIMO systems where the TX and RX antennas are placed far from each other, with respect to  $D_{cT}$  and  $D_{cR}$ , and there are not mutual coupling effects.

In general, for a given TX antenna  $i$ , there will be a receive spatial correlation matrix

$$\mathbf{R}_R^i = E[\mathbf{h}_R^i (\mathbf{h}_R^i)^H], \quad \mathbf{h}_R^i = [h_{1i}, h_{2i}, \dots, h_{n_R, i}]^T \quad (2.46)$$

Similarly, for a given RX antenna  $j$ , there will be a transmit spatial correlation matrix

$$\mathbf{R}_T^j = E[\mathbf{h}_T^j (\mathbf{h}_T^j)^H], \quad \mathbf{h}_T^j = [h_{j,1}, h_{j,2}, \dots, h_{j, n_T}]^T \quad (2.47)$$

Note that all entries of the transmit and receive correlation matrices are in  $\mathbf{R}$ .

If the receive correlation matrices are identical for all transmit antennas, and the transmit correlation matrices are identical for all receive antennas, i.e.

$$\mathbf{R}_R^i = \mathbf{R}_R, \forall i \quad (2.48)$$

$$\mathbf{R}_T^j = \mathbf{R}_T, \forall j, \quad (2.49)$$

then

$$\mathbf{R} = \mathbf{R}_T \otimes \mathbf{R}_R, \quad (2.50)$$

where  $\otimes$  denotes Kronecker product. This is the so-called Kronecker model for the spatial correlation in MIMO channel [Kermoal et al., 2002]. The Kronecker model has gained many supporters and also detractors [Weichselberger et al., 2006]. The model has been proven to be accurate enough for indoor scenarios.

Realizations of a spatially correlated MIMO Rayleigh channel can be obtained from

$$\text{vec}(\mathbf{H}) = \mathbf{R}^{1/2} \mathbf{H}_w. \quad (2.51)$$

Moreover, assuming the Kronecker model

$$\mathbf{H} = \mathbf{R}_R^{1/2} \mathbf{H}_w \mathbf{R}_T^{1/2}. \quad (2.52)$$

For a Rician channel, the MIMO channel matrix,  $\mathbf{H}$  can be split in two parts  $\mathbf{H} = \mathbf{H}_d + \mathbf{H}_s$ , where  $\mathbf{H}_s$  coincides with  $\mathbf{H}$  in (2.51), and  $\mathbf{H}_d$  is the deterministic component (LOS component).

The Rician K-factor plays an important role in wireless communication and determines the type of fading environment. It is essentially the ratio between the power in the estimated LOS component and the power in all the other components. In principle, the Rician factor can be associated with each of the TX/RX antenna elements. However, in practice, people assume a certain K-factor for the channel. The channel matrix can be calculated from the Rician factor as

$$\mathbf{H} = \sqrt{\frac{K}{K+1}} \mathbf{H}_d + \sqrt{\frac{1}{K+1}} \mathbf{H}_s. \quad (2.53)$$

## 2.3 Indoor channel characterization

Indoor radio propagation is characterized by the same propagation mechanisms as outdoor propagation. But the situation is more complex for indoor environments, where numerous objects may act as scatterers close to the antennas. The smaller distances may lead to smaller delay dispersions, dense multipath propagation with a higher number of multipath components.

### Channel distribution

Analysis of SISO channels corroborates that the magnitude (envelope) of the channel response is often well described by a complex normal distribution [Svantesson and Wallace, 2002]: Rician for LOS environments, and Rayleigh for NLOS environments. Also, the phase can be well approximated with a uniform distribution. These assumptions can be also applied to MIMO channels.

In indoor channels, from different measurement campaigns, the typical values of the Rician K-factor result  $\approx 8$  dB [Svantesson and Wallace, 2002, Jagannatham and Erceg, 2004].

### Temporal variations of the channel

Indoor experiments have shown that the channel is WSS, only if data is collected over short intervals of time [Bultitude, 1987, Bultitude et al., 1988]. Typical coherence time values are on the order of few seconds, which is reasonable for residential buildings or office environments in which one does not expect a large degree of movement [Hashemi, 1993b].

### Delay spread

In indoor environments, the RMS delay spread,  $\sigma_\tau$  values are typically between 10 and 50 ns, with a mean value in the 20 – 30 ns range [Hashemi, 1993a]. The RMS delay spread typically increases with distance [Tse and Viswanath, 2005]. This increase is due to the fact that at larger distances, multipath with large delays have strengths comparable to the LOS path, contributing to  $\sigma_\tau$ .

### Correlation properties of MIMO channels

For isotropic Rayleigh fading, where the multipath components reaches the RX from all angles equiprobably, the coherence distance,  $D_{cR} \approx 0.1\lambda_c$ , where  $\lambda_c$  is the wavelength of  $f_c$ . In practice, several factors determine the degree of spatial correlation, such as array element spacing [Lee, 1982], transmitter-receiver separation [Kyritsi et al., 2003], etc. Spatial correlation and coherence distance also depend on  $f_c$  and the signal bandwidth,  $B$ , as described in [Malik, 2008].

Measurements corroborate [Svantesson and Wallace, 2002] that the NLOS part should exhibits a low  $D_c$  since there are many multipath contributions that change rapidly with distance [Jagannatham and Erceg, 2004]. For the LOS positions, a longer coherence distance is expected since there exist a stable LOS component.

## 2.4 Conclusions

Throughout this chapter, we have reviewed the modeling principles of wireless multipath SISO channels. Both the deterministic and the stochastic modeling were described. We defined parameters such as delay spread, and channel coherence as function of antenna location, time and frequency. The deterministic approach has been generalized for random channel variations by stochastic modeling. Popular channel models as Rayleigh and Rician were described as particular cases of multipath channels. The extension to MIMO channels has been also described, highlighting the differences with respect to SISO. Among MIMO channel features, we have highlighted the spatial correlation properties and their characterization. Finally, we have briefly summarized the values of some channel model parameters obtained from measurement campaigns in indoor environments.



# 3

Chapter

## MIMO testbedding

The proper development and testing of multiple-input multiple-output (MIMO) systems lie in a detailed channel knowledge. As stated in Chapter 2, multipath propagation in indoor environments may be modeled theoretically, in a deterministic or stochastic way. These models can truly reflect real propagation, but still lack of experimental work to support and complement the channel modeling process [Almers et al., 2007]. Because of this, the assessment of MIMO devices in real indoor channels is of paramount importance. To that end, the acquisition of equipment for evaluating devices and MIMO techniques under real conditions is the starting point of experimental evaluation and characterization.

In the past years, MIMO wireless testbeds and prototypes have received much interest from research community [Caban et al., 2006, i. Fábregas et al., 2006, Vielva et al., 2010, García-Naya et al., 2010]. A MIMO testbed is specially suitable for research and educational purposes since allows carrying out multiple MIMO tests and measurements in a simple way. They usually serve as a intermediate testing of final products, aiming at evaluating different components separately. Their flexibility allow themselves to fulfill the requirements of most of the current wireless standards.

The need to assess wireless devices or algorithms, whether they are related or not test them under real channels, led us to acquire a commercial MIMO testbed. The Advanced Signal Processing Group (GTAS in spanish) testbed does not represent a novelty in MIMO context, but its novelty lies in the flexibility and the multifunctionality it can offer. At first it was thought to serve as a solution for evaluating MIMO algorithms over real channels. Then, as soon as its capabilities were discovered, new algorithms and functionalities have been developed and implemented. This fact and the expense it entailed become an incentive to make the most of it for our research purposes.

The testbed has been fitted with a remote control software based on web services (WS). Hence, all these functionalities are accessible in a remote manner from any place with internet connection, being its use opened to any research group. This fact has turned out to be a significant improvement and it is considered in this chapter as one of the main achievements regarding this MIMO testbed development.

As an example of its utilization, a methodology for measuring MIMO channels within the European Union funded project: Advanced MIMO systems for maximum reliability and performance (MIMAX) (FP7/2007-2013 no 213952) [MIMAX, 2008], is presented.

This chapter is organized as follows: Section 3.1 presents the different questions that come up when deciding to deal with practical equipments, mainly focusing on testbeds, and their features and applications. In Section 3.2 we review the state of the art in MIMO testbedding. In Section 3.3 we detail the structure and properties of the nodes acquired from Lyrtech.

Section 3.4 highlights the GTAS testbed, built from Lyrtech nodes and provided with an interface. The web-based remote control interface is presented in Section 3.5, which allows making the most of the testbed when carrying out experiments. The procedure for controlling the testbed from a remote control PC is detailed in Section 3.6. Section 3.7 focuses on real-time processing within GTAS testbed. A basic example combining all the ideas presented so far is summarized in Section 3.8. In Section 3.9 we present, as an example, a MIMO channel measurement technique that was implemented on the GTAS MIMO testbed, as part of MIMAX project. Finally, in Section 3.10, the main conclusions are put forward.

### 3.1 Prototyping for MIMO systems: MIMO testbeds

The implementation of wireless communications systems for testing and prototyping purpose can be divided into three groups [Naya, 2010, Burg and Rupp, 2004, Mehlführer et al., 2006]. First, the so-called *demonstrators*, which are utilized to show specific technologies to prospective customers. Because of this, they are not meant to be flexible and scalable but they require little time for their design and implementation. The second group is formed by *prototypes*. A prototype is a first full-scale and usually functional realization of a research concept. It often constitutes a preliminary stage where the system is debugged and subsequently implemented as a consumer product. Finally, the third group includes *testbeds*. A testbed provides convenient means for assessing theoretical findings through practical implementations and measurements, offering real-time transmission capabilities.

There exist many aspects to be considered when facing up with this kind of hardware for testing MIMO systems:

- *Type of environment which the system is intended for*: indoor or outdoors, stationary or dynamic.
- *Wireless standard* (if any is considered), which entails a carrier frequency,  $f_c$ , bandwidth,  $B$ , and modulation.
- *Operational basis*: *real-time* or *offline*, burst-like or continuous processing.
- *Level of implementation*: measurement device, demonstrator, prototype, commercial product.
- *Hardware* (software radio platform): digital signal processing (DSP) boards, field programmable gate arrays (FPGAs), application-specific integrated circuits (ASICs), etc.
- *Number of antennas at both transmission and reception*:  $n_T$  and  $n_R$  respectively.
- *Feedback*: available at the transmitter (TX) or not.
- *Type of scenario*: single-user or multiuser.
- *Unidirectional or bidirectional data traffic*: simplex, semiduplex or full duplex.

From now on all we will refer to testbeds and their features in the MIMO context. Based on the presented testbed concept, a wireless MIMO testbed is able to operate in two well-differentiated modes:

The first mode is the so-called *offline* mode, where preprocessed digital data (signals) are transmitted from memory, and received data is stored into memory. This mode is especially reasonable for algorithm testing on logged real data and also for system debugging purposes. Nevertheless, this mode is a rather convenient starting point for development and is a favorable way to analyze nonidealities like radiofrequency (RF) impairments (see Section 3.3.2).

In the second mode, the so-called *real-time* mode (*online mode*), the whole processing is performed in real-time, so it will allow us, as an example, to study the system behavior in multiuser scenarios where cooperation among multiple users require real-time processing.

The sum of real-time capabilities, along with the subsequent offline processing, make a testbed a very powerful method for evaluating algorithms using realistic over-the-air (OTA) transmissions. It is particularly easy to measure the relative difference between two types of receivers because:

- The same stored receive data can be evaluated, thus making the comparison fair.
- Debugging is also made easier, because the received data remains equal.
- Low number of required channel realizations.

Both types of testbed have their pros and cons. Depending on the research goal, a real-time or an offline testbed might be better suited. For instance, it is easier and faster to evaluate the performance of new detection algorithms or to compare between different synchronization methods on an offline testbed. On the other hand, a real-time testbed is better suited for the evaluation of MIMO multi-user scenarios including wireless feedback links. An offline testbed would probably be too slow and the acquired channel state information would already be outdated before they are actually used. Also, live demonstrations, as for instance video streaming, are only possible on a real-time testbed. However, most of the times these modes are combined. Some parts of the TX or the receiver (RX) are implemented in real-time while others are developed offline.

### 3.1.1 MIMO Testbed Requirements

The decision of whether or not to acquire a MIMO testbed arises from two questions:

- Why is a testbed needed and how can the associated expenditure of time, money, and resources be justified?
- What elements and components are needed to make the testbed and the subsequent research successful?

The design and development of a testbed is guided by a number of parameters derived from the specific research goal and the available funding. While the research goal itself may range from simple transmit/receive experiments to more complex implementation of algorithms, other parameters such as desired performance, cost, configurability, mobility and development time, are equally relevant. Testbeds are often used to check if a new algorithm, the physical layer of a communications standard, or even a complete standard system that has been proven useful by simulations, is also valid in realistic wireless scenarios (indoor, outdoor or a combination of both). Also, this real hardware presents certain particularities that must be taken into account when performing these evaluations.

As shown in Figure 3.1, testbed hardware components can be classified in four groups, according to their functionality: host personal computer (PC), digital processing units (DPUs), digital-to-analog and analog-to-digital conversion (DAC/ADC) stages and the RF analog front-end (AFE or RFFE). The PC is where we allocate one or more boards containing the digital section of the testbed hardware and the hard disk arrays for data storage, graphics processing units to speed up signal processing operations, etc. The DPUs includes the digital hardware components, e.g. non general purpose processors such as DSPs or FPGAs. In the DAC/ADC stages, the conversion between the digital and the analog domain and vice versa, is performed. Finally, the AFE up/down converts to the carrier frequency,  $f_c$ , or to

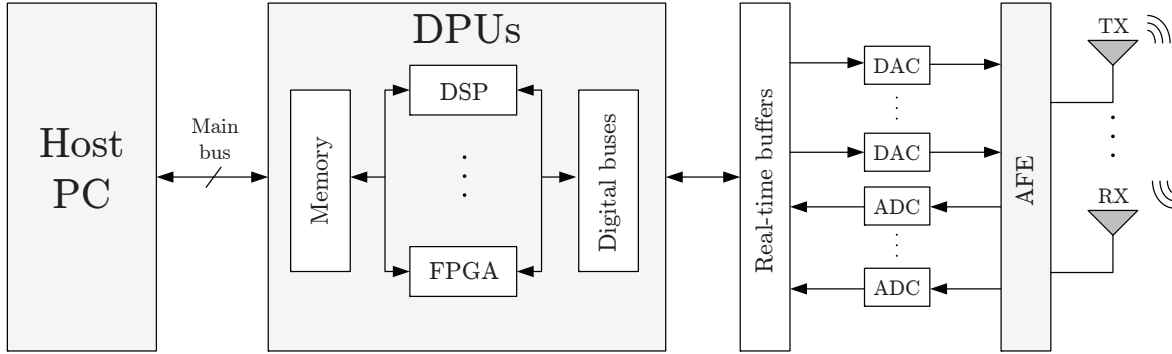


**Figure 3.1:** Block diagram of testbed hardware components including DSPs, FPGAs, DAC/ADC stages, and RF transceivers.

baseband (BB), the signals that come from the digital or the ones that are sent through the air, respectively.

With this basic configuration at the TX side, it is possible to send samples coming directly from the main bus, convert them into the analog domain using the DACs and up convert them to the desired carrier RF using the AFE. At the RX side, the signals are down converted by the AFE, converted to the digital domain by the ADCs, and then sent to the host through the main bus.

Not so long ago, testbeds had to be created 'from scratch' for supporting the development of a specific wireless transceiver. Then, the building process required large budgets for paying the combined work of electronic designers, RF engineers and software developers [Caban et al., 2006]. Ad-hoc solutions require time, money and manpower along with and test equipment for the RF hardware.

At present, the situation has changed drastically since generic testbeds can be made up faster and cheaper than ever, thanks to the use of commercial off-the-shelf (COTS) modules, that can be combined to create systems compliant with almost any wireless transceiver specification. Moreover, software development to handle such modules is not a tough task with the help of rapid prototyping software tools. Nevertheless, setting up a testbed for wireless MIMO measurements can not still be considered a straightforward task.

Testbeds present the following advantages from the wireless communications research point of view:

- **Flexibility.** Testbed hardware is often meant to be used for *offline* processing since, apparently, only the signals are sent and acquired through the air. This is by far not true, even though they are equipped with DSPs/FPGAs that are in charge of signaling control, interface, or even real-time processing (if it is required).
- **Modularity.** The minimum modularity that a testbed should have is the separation between the DPUs, DAC/ADC stages, and the AFE. Anyway, the digital hardware can be split into different modules. For the RF section it is possible to find custom ad hoc solutions or commercial products, allowing operation at/in different bands.
- **Scalability.** When developing ad-hoc MIMO testbeds, one can start testing the system with a reduced number of antennas. In a later step, the testbed is scaled to support a greater number of antennas, thus only requiring more hardware instead of replacing it

entirely. All the evolutions should be carried out from the existing hardware, minimizing the new hardware needs and making use of acquired know-how.

### 3.1.2 COTS Modules

COTS Modules [Naya, 2010] enable rapid algorithm development from conception to hardware implementation and testing. Concretely, the advantage of using these modules is that they are prefabricated and tested and can be connected together easily to form an entire system. In addition they can operate over a large range of frequencies, rates, etc., providing the testbed with a lot of flexibility. The GTAS MIMO testbed was designed on the basis of COTS modules due to the lack of previous experience in building similar solutions; time, money and manpower required for an ad-hoc solution; and the lack of test equipment required for the RF hardware.

Among the testbeds reported in the literature some are designed on the basis of COTS modules found in the market. Some companies selling COTS modules are Ettus [Ettus, 2013], GE Fanuc [GE, 2013], Hunt Engineering [HUNT, 2012], Innovative Integration [Innovative, 2013], Lyrtech (Nutaq) [Nutaq, 2012], National Instruments [National Instruments, 2012], Pentek [Pentek, 2013], and Sundance Multiprocessor [Sundance, 2013]. Some of these are focused on real-time hardware (e.g. Nallatech), whilst some offer an extreme modular solution in which even the digital section is divided into different modules containing distinct hardware elements (e.g. Nallatech or Sundance). Companies such as Sundance or Nutaq offer both BB modules as well as RF front-ends.

### 3.1.3 Testbed applications

Although testbeds are primarily meant for testing devices or techniques over real channels, they can be used in a great variety of situations and environments. In general, the following applications stand out.

#### Real-Time Development

A methodology development process, from simulations executed offline to real-time implementations, involves a complete understanding of the problem as well as deep knowledge of the hardware. One proposed methodology is the so-called rapid prototyping [Kaiser et al., 2004, Mehlführer et al., 2006]. The testbed can be used to explore the performance impact of a specific functionality in a real-time system without requiring the availability of the real-time implementation. For example, it can be used to evaluate the impact on the system throughput of a new channel estimator or a new channel code. In short, the flexibility provided by the testbed is utilized to speed up the implementation of real-time prototypes as well as to improve the techniques used to test them.

#### Educational Environments

Society demands access to high capacity wireless communications and to the services that can be provided on top of them. To satisfy these demands, engineers are constantly developing new technologies. The student has to be familiar not only with the basic theory and techniques, but also with those of the more advanced techniques that provide a more profound insight. Usually, testbeds are being developed at public research groups that often belong to

different universities. A MIMO testbed hosted by an academic institution should be obviously of educational value in order to inspire scientific novices, foster teamwork, and improve communication skills. The overall goal is the development of flexible and modular MIMO testbeds satisfying the following major needs: offline/online implementations, easy-to-use interfaces.

There exist several contributions emphasizing the benefits of a tool like a testbed for education [Rao et al., 2004]. As an example, in [Vielva et al., 2010], the GTAS group show how to build a web platform for learning advanced digital communications, which is described in Section 3.4.

## 3.2 Testbeds review

In recent times, many researchers have been working on their own MIMO hardware equipment to test new techniques and algorithms. This equipment can be classified into two main groups. The first group comprises MIMO testbeds for implementing any standard or specification, while the second group can be considered as general-purpose. Examples of testbeds of the first type are the narrowband MIMO prototype in [Wolniansky et al., 1998], the MIMO WCDMA for 3G telephone systems in [Adjoudani et al., 2003], a MIMO 3G prototype for high-speed downlink packet access reception [Garrett et al., 2004], or a MIMO orthogonal frequency domain multiplexing (OFDM) testbed for 4G telephone systems developed by ETRI [Won et al., 2003]. This kind of platforms usually exhibits good technical characteristics but they are extremely expensive and barely flexible.

The MIMO testbed presented in this chapter belongs to the second group. Other examples of this type of platforms can be found in [Nieto et al., 2006, Caban et al., 2006, Wallace et al., 2004, Aschbacher et al., 2004, Borkowski et al., 2006, Morawski et al., 2003, Murphy et al., 2003, i. Fábregas et al., 2006, Lang et al., 2004, Chiurtu et al., 2005, Weijun Zhu, 2005]. These MIMO platforms can be compared with each other according to several performance measures

- **Number of transmit/receive antennas:**  $2 \times 2$  [Bialkowski et al., 2007, i. Fábregas et al., 2006],  $4 \times 4$  [Caban et al., 2006, Azami et al., 2008, Nieto et al., 2006][Wallace et al., 2004, Borkowski et al., 2006, Morawski et al., 2003][Weijun Zhu, 2005].
- **Carrier frequency:** 2.4 GHz band [Caban et al., 2006, Wallace et al., 2004, Morawski et al., 2003] [Murphy et al., 2003, Chiurtu et al., 2005, Weijun Zhu, 2005][Azami et al., 2008], 5 GHz band [Nieto et al., 2006, Borkowski et al., 2006, i. Fábregas et al., 2006, Lang et al., 2004].
- **Bandwidth:** 20 MHz [Caban et al., 2006, Dowle et al., 2006, i. Fábregas et al., 2006][Wilzeck et al., 2006, Weijun Zhu, 2005, Garcia-Naya et al., 2007], 40 MHz [Nieto et al., 2006].
- **Memory storage capacity and speed:** If only the transmission is performed in real-time, both the available memory amount and the access speed constitute the main limitation for the experiments to be carried out with a testbed.
- **Real-time units:** DSPs [Wallace et al., 2004, Weijun Zhu, 2005] or field programmable gate arrays (FPGAs) [Nieto et al., 2006, Caban et al., 2006, Murphy et al., 2003, Chiurtu et al., 2005, Weijun Zhu, 2005] implementations.

- **Transfer speed between the processing, storage, generation and acquisition units:** resolution varying from 12 [Wallace et al., 2004] to 16 bits, [Nieto et al., 2006, Lang et al., 2004, Wilzeck et al., 2006], and speeds up to 500 MS/s.

### 3.2.1 Future of the Testbeds

Nowadays, one of the main drawbacks of MIMO testbedding is the lack of flexible and tunable RF front-ends, hence limiting the flexibility of testbeds. Although recently new products have released in the market, they are constrained to the ISM bands and are not highly linear devices. What is more, the digital processing units of the testbeds are still very expensive and even unaffordable for small research groups. Investing more than 50K in hardware along with the costs of test equipment, e.g. oscilloscopes, spectrum analyzers, etc., becomes a luxury that only a few could attain. That is without counting the required engineers skilled enough to successfully set up the testbed. After all these expenses, valuable results must be published with the testbed and, therefore, justify the investment.

With the advent of GNU Radio [GNU Radio, 2012], a revolution in the software-defined radio technologies (SDR) is foreseen that it will greatly reduce development costs in terms of hardware, money and manpower. GNU Radio is a free and open software toolkit for the development of software-defined radio systems (e.g. testbeds). It provides the signal processing blocks for implementing reconfigurable software radios using the Universal Software Radio Peripheral (USRP). The USRP (and its successor, the USRP2) is a low-cost external device manufactured by Ettus Research LLC [Ettus, 2013] and containing the digital hardware as well as pluggable RF front-ends named daughterboards. The available set of daughterboards covers a wide range of RF bands (from 50 MHz to 2.9 GHz, and from 4.9 GHz to 5.85 GHz).

The MIMO capabilities of the URSP are very limited in the number of TX and RX antennas as well as in the maximum available bandwidth (8 MHz) shared among all TX/RX antennas). Currently, the USRP2 extends this bandwidth to 25 MHz. Moreover, multiple USRP2 systems can be connected together to form fully coherent multiple antenna systems for MIMO with as many as 8 antennas.

## 3.3 Lyrtech MIMO nodes

In 2008, the GTAS group decided to buy one MIMO node from Lyrtech, which are built taking advantage of the latest rapid prototyping technologies, and they are designed on the basis of COTS modules.

Each node has semi-duplex communication capabilities. It is equipped with a pair of transmit/receive VHS-BB boards, which integrate the DPUs and the DACs/ADCs; and an AFE, which performs the up/down conversion to BB. In Figure 3.2 we show the block diagram of one Lyrtech node. It is capable of targeting both the 2.4 GHz and 5 GHz industrial, scientific and medical (ISM) bands, being able to transmit and receive complex BB data samples on up to 4 antennas. These nodes are intended for wideband applications, such as OFDM, supporting up to 40 MHz bandpass channel bandwidth (20 MHz at BB).

This testing equipment makes use of FPGA technology for fast processing of the BB signals. Each VHS-BB board consist of a FPGA and a synchronous dynamic random access memory (SDRAM). The FPGA in the transmit side is interfaced with a DAC board made up of eight 14 bit DACs. The FPGA at the receiver is interfaced with an ADC board made up of eight 14 bit ADCs.

However, Lyrtech nodes present certain limitations:

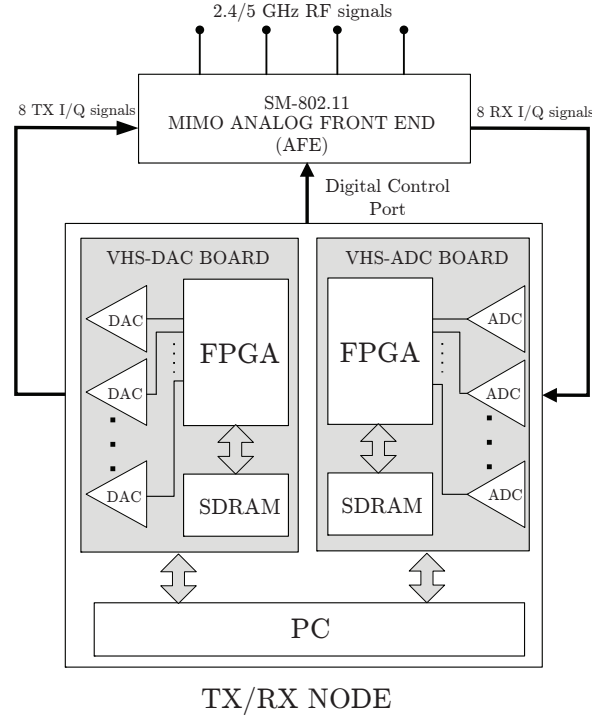


**Figure 3.2:** Block diagram of a Lyrtech node.

- Number of transceivers, limited to 4 per node (possible up to 8).
- Acquisition/transmission clock source limited to 52 and 104 MHz. However, interpolation and decimation can be performed within the FPGA (see Section 3.7), or an external clock can be used.
- The SDRAM rate is limited to 450 MBps = 225 MS/s. Hence, the node is able to sample simultaneously eight channels at 26 MS/s.

So far, we have described the general node features. From now on, we detail the different parts of the node as well as their characteristics. Each node consists of three well-distinguished parts:

### 3.3.1 VHS BB boards

The VHS BB boards were fabricated by Lyrtech, and are mounted on a 3U or 6U Eurocard-based industrial computer via a compact peripheral component interconnect (cPCI) interface. They are connected through a passive PCI backplane. Each testbed node has its own playback module (VHS-DAC board) and recording module (VHS-ADC board), consisting of Xilinx Virtex IV FPGAs for real-time processing (Xilinx Virtex IV XC4VSX55-10 FF1148). FPGAs are increasingly used in real-time signal processing since they offer very high performance (parallel processing). Each board has 8 channels and they can be upgraded to 16 channels by adding an optional add-on module. The boards provide internal clock and also offer the possibility of using an external clock.

The VHS-DAC board (see Figure 3.3) has 8 synchronous DACs (DAC5687) with a programmable sampling frequency  $f_s \leq 120$  MS/s. The internal clock can work at 52 MHz or at 104 MHz. The DACs have 14 bit resolution and an output range of  $-0.632$  V to  $+0.632$  V.



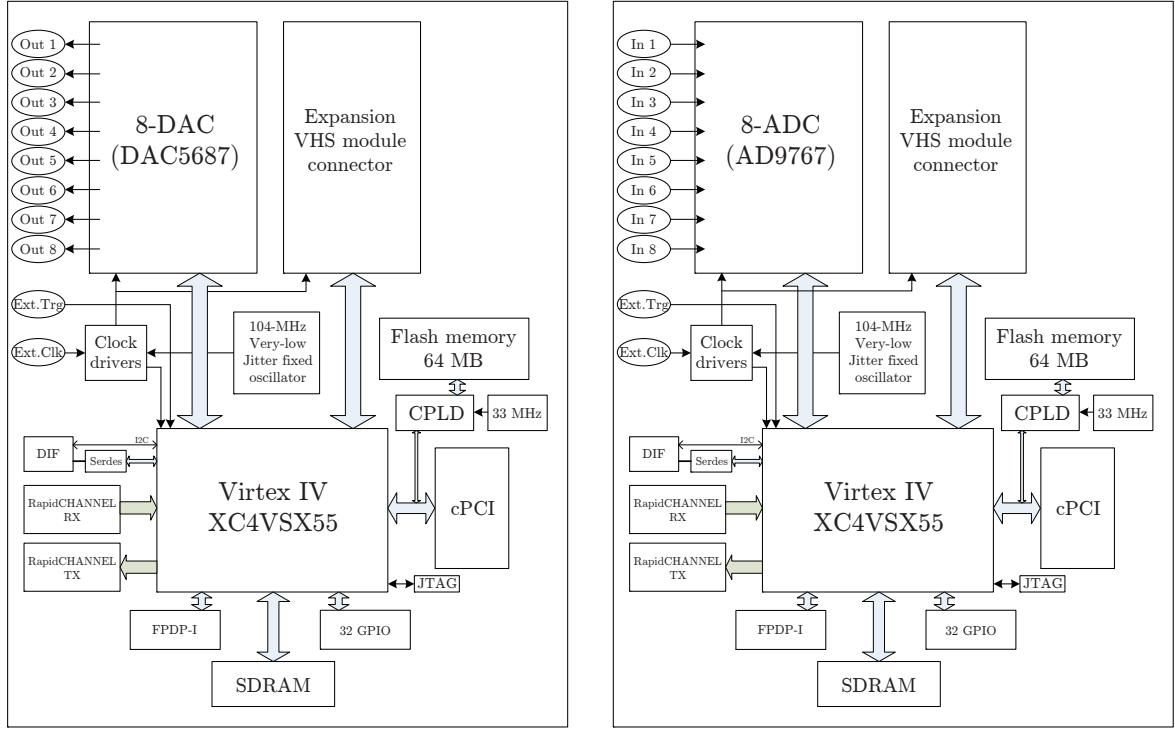


**Figure 3.3:** Lyrtech Virtex IV-based BB boards. Left: VHS-DAC board, right: VHS-ADC board.

Their gain can be programmable with 24dB range. It consists of a 128 MByte on-board SDRAM for data recording with a bandwidth of 450 Mbytes/s (225 Msps).

The VHS-ADC board (see Figure 3.3) has 8 synchronous ADCs (AD9767) with a programmable sampling frequency  $30 \text{ Msps} \leq f_s \leq 105 \text{ MS/s}$ . The internal clock can work at 52 MHz or at 104 MHz. A maximum sampling rate of 105 Msps is guaranteed (14 bit resolution) and the input range is  $-1.2 \text{ V}$  to  $+1.2 \text{ V}$ . Their gain cannot be programmable. It also consists of a 128 MByte on-board SDRAM for data recording with a bandwidth of 450 Mbytes/s (225 Msps).

### 3.3.2 Analog Front End (AFE)

The BB boards are the interfacing components between the analog and the digital domain. Each testbed node consists of an AFE fabricated by Comlab [Comlab, 2013] (known as Quad Dual Band RF Transceiver) which can be connected (controlled) from one of the VHS-BB boards.

The AFE, depicted in Figure 3.4, consists of four independent receive/transmit channels with an adjustable output power from  $-9 \text{ dBm}$  to  $21 \text{ dBm}$  (@ 1 dB compression). The RF bandwidth is 40 MHz and it can radiate among the ranges  $f_c \in [2.4, 2.5] \cup [4.9, 5.875] \text{ GHz}$ . It is entirely based on the MAX2829 single chip RF transceiver [MAX2828/MAX2829, 2013], which has been designed specifically for OFDM 802.11 WLAN applications (see block diagram in Figure 3.5). The MAX2829 integrates all the circuitry required to implement the RF transceiver function, providing a fully integrated receive path, transmit path, voltage-controlled oscillator (VCO), frequency synthesizer, and BB control serial interface. It is



**Figure 3.4:** Quad Dual-Band AFE from Lyrtech, Inc.

based on a zero-IF architecture, shown in Figure 3.3. It can be observed from the figure that the architecture is dual band, since the RF chain is duplicated (RX low noise amplifier (LNA) + mixer, TX LNA + mixer). The mixer translates the RF frequency directly to BB. A local oscillator (LO) signal, tuned to the same frequency as the desired RF signal, is injected into the mixer.

The AFE is also equipped with four dual-band SkyCross printed antennas [Skycross, 2013]. These are suitable for 802.11b/g (from 2.4 to 2.5 GHz) and 802.11a (from 4.9 to 5.85 GHz) applications. They have linear polarization and the pattern is omnidirectional.

The AFE, along with Maxim MAX2829, constitutes a mid-performance commercial solution, offering a performance similar to that of general consumer devices such as laptops, or mobile phones. Therefore, the performance offered by the AFE as well as the impairments introduced are of a magnitude similar to that of conventional devices, thus making the testbed suitable for predicting the actual performance of typical inexpensive commercial equipment.

In real-world systems, signals are affected by non-idealities and imperfections. There exist some problems that arise when dealing with the RF part. In a wireless AFE the major sources of non-linearities in the transmitter are the DAC and the power amplifier (PA). Non-linearities lead to harmonic and intermodulation distortions and can have a considerable impact on the transmitter performance. Especially in OFDM-based systems, non-linearities are no longer negligible due to the high peak-to-average power ratio (PAPR) of the time-domain signal [Schenk, 2008].

In general, among others, three major RF impairments of a wireless AFE are distinguished in literature [Schenk, 2008]: Phase noise, I/Q imbalance, and nonlinearities. However, we also describe some other impairments derived from the RF part: carrier leakage and frequency offset.

### Phase noise

Imperfections in the oscillator lead to random frequency fluctuations of its output. These fluctuations are commonly referred to as phase noise in frequency-domain or as clock jitter in time-domain. Phase noise and clock jitter are just two different ways to look at the same phenomenon [Smith, 2004]. The sources for jitter are manifold: there are system level aspects (e.g., crosstalk, dispersion effects, and impedance mismatch), data-dependent phenomena, and random noise phenomena (e.g., thermal noise).

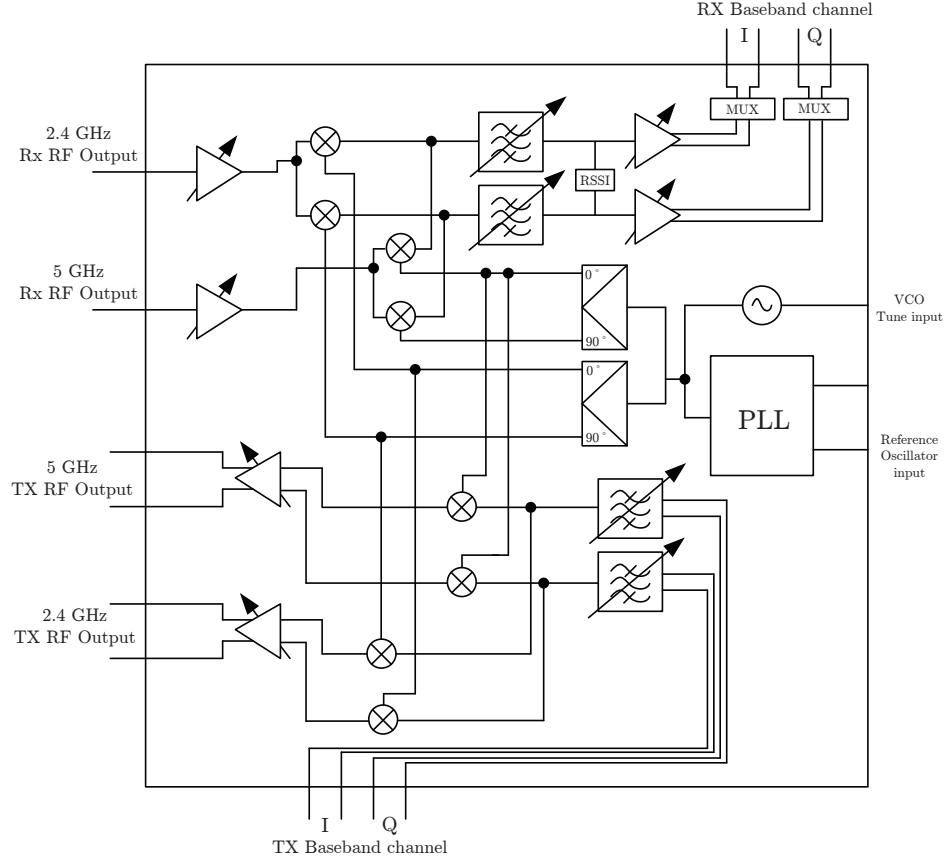


**Figure 3.5:** Zero-IF AFE architecture based on MAX2829 chip (Comlab).

Lyrtech does not provide ways to compensate the phase noise, according to MAX2829 chip it is of about  $-95$  dBc/Hz.

### I/Q imbalance

The phase and amplitude imbalance existing in the I/Q modulator/demodulator besides I/Q branches imbalances introduced by filtering, amplifications and D/A and A/D conversions are considered as an effect called I/Q imbalance. It can be characterized by two parameters: the amplitude imbalance,  $\Delta G$ , between the I and Q branches and the phase orthogonality mismatch,  $\Delta P$ . Figure 3.6 depicts an I/Q modulator with I/Q imbalance. It would also occur the same with the I/Q demodulator.

We denote  $s'[n]$  as the signal  $s[n]$  when it is affected by I/Q imbalance, that can be written [Tubbax et al., 2004] as

$$s'[n] = \alpha s[n] + j\beta s^*[n], \quad (3.1)$$

where  $*$  denotes complex conjugate and

$$\alpha = \cos \Delta P + j\Delta G \sin \Delta P \quad (3.2)$$

$$\beta = \Delta G \cos \Delta P - j \sin \Delta P. \quad (3.3)$$

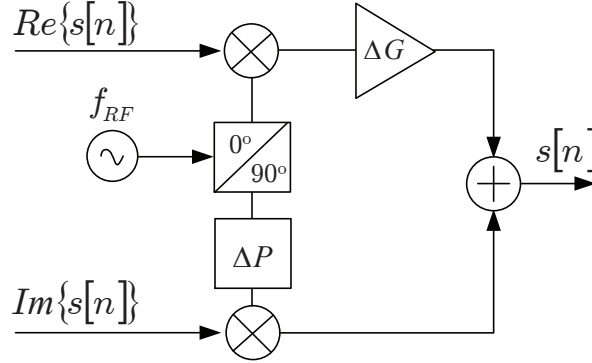


**Figure 3.6:** I/Q modulator imbalance.

Thus, the I/Q imbalance frequency domain effect,

$$S'[k] = \alpha S[k] + j\beta S^*[-k], \quad (3.4)$$

consists in a mirror frequency regrowth, producing crosstalk between symmetrical exponential pairs (regarding the LO frequency).

In Lyrtech equipment the transmitter I/Q modulator suffers from gain and phase imbalance that require to be canceled by appropriate signal processing techniques at BB. The I/Q gain and phase error is compensated in the DSP by introducing opposite value of the errors. Chapter 4 proposes a way to easily eliminate this effect.

### Nonlinearities

The PA is the main source of nonlinearities within the AFE. PAs usually operate as a linear device under small signal conditions and become more nonlinear and distorting with increasing the power level. Driving the power amplifier above the linear region results in nonlinear distortion effects, which makes it more difficult to receive the signal and generates harmonic and intermodulation signals outside of the intended frequency band.

In our case, we need to be careful to make it functioning on the linear region. The output power range is 30 dB, stepping from 0 to 63 (in steps of 1/2 dB). The PA is able to offer powers ranging from  $-7$  dBm to 9.6 dBm within the linear region.

### Carrier Leakage

The presence of a spectral component at the carrier frequency is called LO leakage. The main contributors are the offset from the baseband filter and the offset from the mixer. At the output of a direct conversion mixer, such a spectral component can often be observed. It results from a DC current offset at the input of the mixer or is generated due to imperfections in the mixer itself (e.g., transistor mismatch). The offset can be compensated by adding or subtracting a DC current offset to the BB signals.

In Lyrtech's AFE the carrier leakage without DC offset cancelation is  $-27$  dBc. The transceiver unit features TX/RX calibration modes to detect transmit LO leakage.

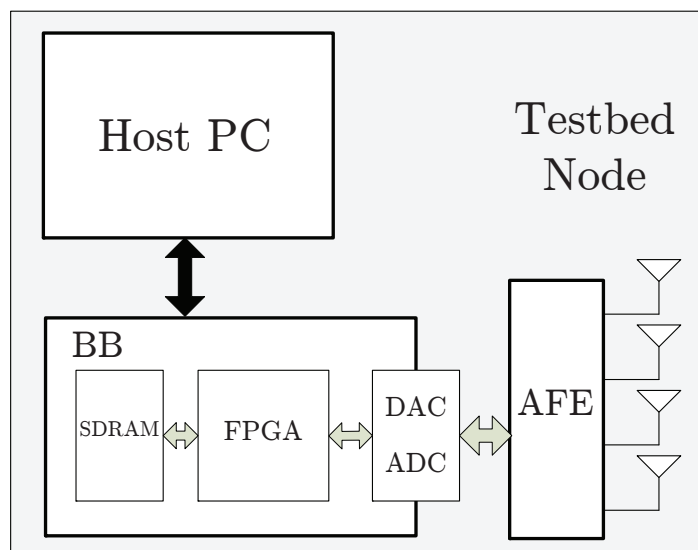


**Figure 3.7:** Block diagram of a Lyrtech node.

### Frequency Offset

Accurate frequency offset compensation is fundamental in channel sounding applications of testbeds. In these cases, the transmissions rarely have provisions for running synchronization algorithms at the receiver. Therefore, the frequency offset must be measured between all transmitter receiver branch pairs prior to the field measurement campaign. Chapter 4 describes a methodology to easily correct this fact.

#### 3.3.3 Host PC and node control

So far, we have described the hardware of Lyrtech MIMO nodes, its features and impairments, and which part of the node is in charge of its control. The ability to interface with the nodes needs to be verified sending and receiving data as well as sending configuration commands.

The host personal computer (PC) is defined as the device that configures and controls the VHS-BB boards. The host PC may be a standard computer or a CPU board, in our case it consists in a CPU board also connected to the PCI backplane. The host PC runs Microsoft Windows operating System.

Figure 3.7 depicts a general block diagram of the connections within the node. In the figure, one VHS-BB board consisting of its SDRAM and FPGA is depicted for the sake of clarity. It is possible to access all the configurable aspects of each BB board from the host PC, who communicates to the FPGA and through the V360 PCI local bus bridge, running at a speed of 33 MHz.

One can develop applications on the host PC for controlling VHS-ADC/DAC boards through the use of an application programming interface (API). Concretely, Lyrtech provides a static library (LIB) and a header file that implement an API to develop programs using C as programming language. The API comprises protocols and functions necessary to build software applications that allows interacting with the elements of the node. Then, the nodes can be controlled from C programs running on the host PC.

Lyrtech also provides a utility named VHS control utility (see Figure 3.8), which allows the user to control the VHS-BB boards with ease. This utility communicates directly with

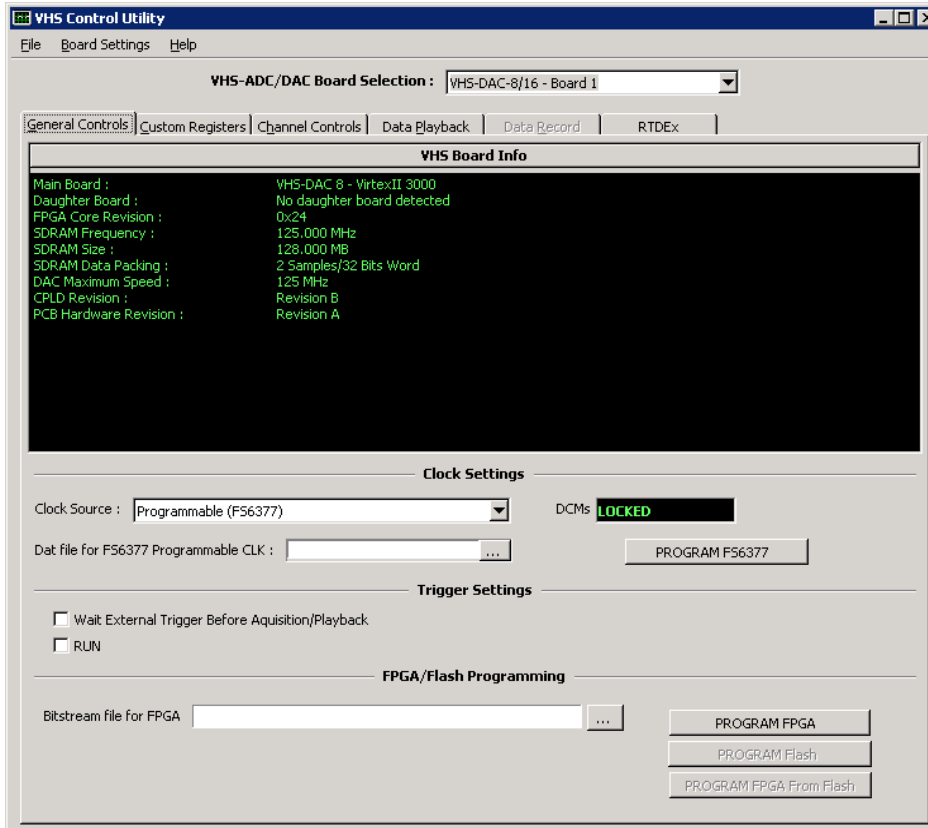


**Figure 3.8:** VHS control utility General Controls tab.

the VHS-ADC/DAC boards, thus it must run on the cPCI chassis that contains the VHS-BB boards. Through this interface, the VHS control utility allows:

- Detecting and initializing all the VHS-BB boards in the cPCI chassis.
- Setting the clock, trigger and gain values.
- Loading FPGA designs (.bit files).
- Accessing the four custom registers.
- Activating the acquisition and transmission of all the detected boards (if the FPGA designs contain the proper modules).

The first experiments with the node were carried out using the utility, uploading and downloading data for playback and acquisition. However, this kind of control of the node constrained us to simple experiments. Thus, we tried to understand how the utility works to be able to develop our own functions and design a new control method for the VHS-BB boards. Unfortunately, the C code of the utility was not available so we decided to start from the beginning, grouping the low-level functions to develop a new way of controlling the node (see Section 3.4).

Also, Lyrtech provides an AFE console application allowing the control the AFE through the VHS BB boards. It is basically a Win32 console built with the AFE high-level API. The program communicates directly with the board driver, thus it must run on the host PC. Figure 3.9 depicts a an example of the block diagram of the communication path between

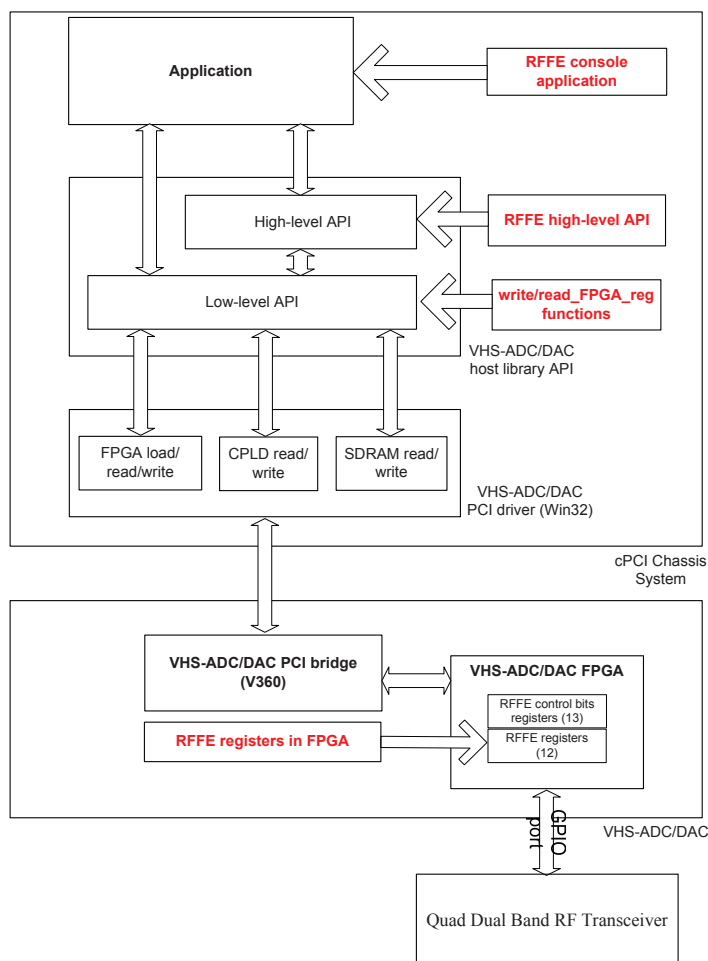


**Figure 3.9:** Communication path between host CPU application and AFE through VHS-DAC/ADC boards.

a host application and the AFE. This console allows controlling the AFE and setting the following features:

- **Mode:** Configure the AFE in TX or RX mode.
- **Gain:** Modify the TX gain (PA gain) or the RX gain (LNA and VGA gain).
- **Communication channel:** sets the communication channel for both the 2.4 GHz and 5 GHz bands.
- **PA enable:** Enabling/disabling the PA.

It is important to point out that, to handle the functions inside the API, the FPGA of the BB board in use must be programmed. Also, if our aim is also to control the AFE, one of the boards must be physically connected to it. Thus, the VHS-DAC board and the VHS-ADC board are able to handle the AFE respectively.

In summary, the node control is limited so far. We are able to control the VHS-DAC/ADC boards and the AFE in a separately manner. Figure 3.10 completes the Lyrtech node block diagram by adding the possible ways to control all its components. So far, the work with the node rely on checking its proper behavior and try to understand how the VHS utility and the AFE behaves.

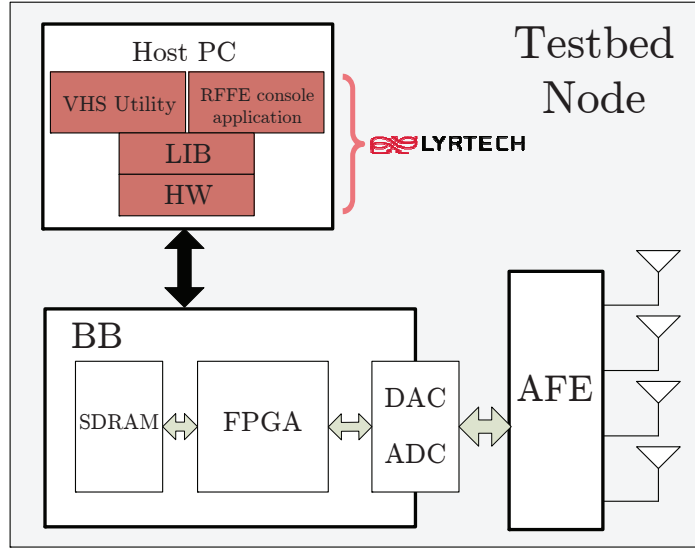


**Figure 3.10:** Lyrtech node control possibilities.

From now on, everything related to node control was developed by our own, which has resulted a tough work but, as presented along the following sections and chapters, we finally get our reward.

### 3.4 GTAS MIMO testbed

The advent of two more Lyrtech nodes motivated the GTAS group to design a centralized way of controlling nodes' functionalities, as well as transmitting/receiving data among them. Concretely, our aim was to be able to control them separately from their respective host PCs. From now on, the GTAS MIMO testbed refers to the three Lyrtech nodes along with the functionalities derived from the development of new testbed interfaces.

This kind of testbed is very strongly coupled with Matlab and can be run directly with a Matlab interface. Therefore, the next step involved providing access to external applications, like Matlab, running on each host PC to control the whole node. A detailed description of the next steps is described in Section 3.5.

A typical block diagram of the communication between two of the nodes is depicted in Figure 3.11.

#### 3.4.1 Real-time processing

As stated in Section 3.3.1, the Lyrtech nodes contains VHS-BB boards that use Xilinx FPGAs. So far the FPGA has been a mere interface between the Host PC and the BB boards and the AFE. Figure 3.12 depicts the FPGA interfaces with the rest of the components of the node.

The custom logic module is intended to contain logic that the user designs. This module provides the testbed with extra real-time capabilities that, in combination with the availability of three Lyrtech nodes, turn the testbed into a powerful tool for testing algorithms and devices. There exist many available interfaces in this module that allow external applications, e.g. running on Matlab or Simulink, deploying user logic on this module more rapidly and efficiently than through a traditional VHDL-based approach.



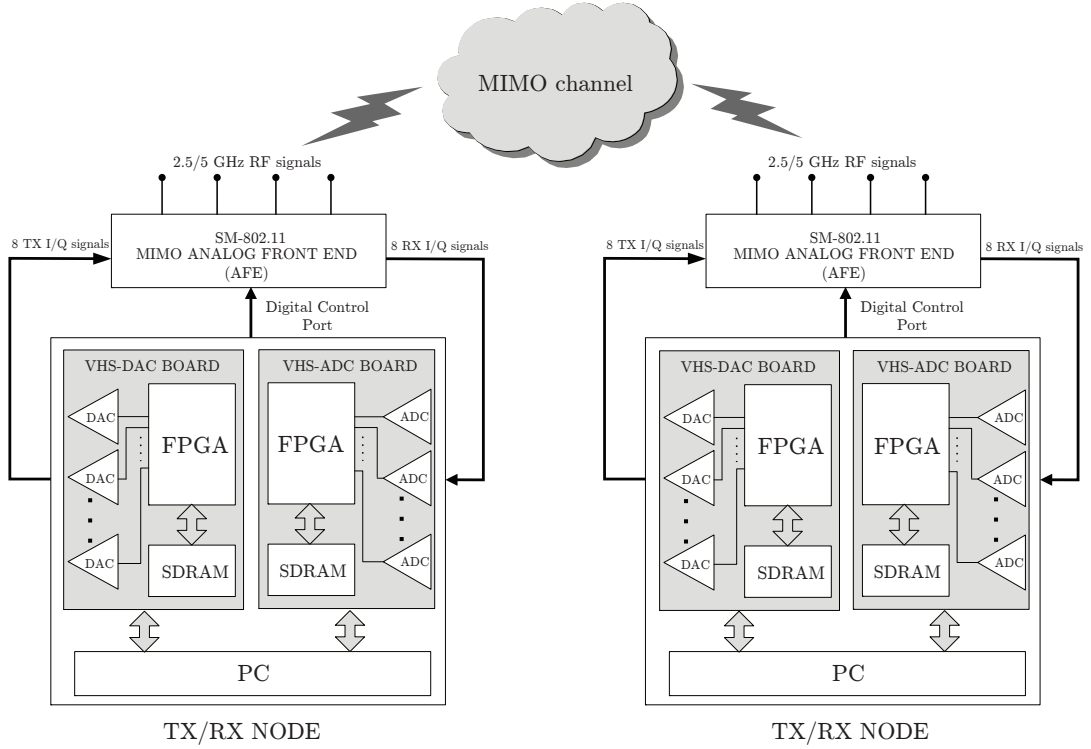


**Figure 3.11:** Block diagram of two of the nodes of the  $4 \times 4$  GTAS MIMO testbed.

As an example, Lyrtech provides a model-based design kit (MBDK), which is a collection of blocks that communicate with the various inputs and outputs of the FPGA in the VHS-BB boards. Also, Xilinx provides several tools for the design, synthesis and validation of programmable logic for DSP applications. Among them, System Generator for DSP [Sysgen, 2012] has emerged as a powerful tool to implement blocks within the custom logic in the FPGA. In summary, Lyrtech and Xilinx System Generator blocks can be easily connected in a Simulink environment to make up the user custom logic. More details are provided in Section 3.7.

### 3.4.2 Local testbed interface

The new context, three Lyrtech nodes controlled by their respective host PC, motivated us to develop a common and general controlling strategy. We decided then to combine the low-level functions described in the Lyrtech Host API Guide to imitate the behavior of the utility. Also, aided by the executable that controls the AFE, the combination of both kind of functions would lead us to control the nodes as a whole.

We first defined which functions were necessary to, at least, being able to playback and acquire signals with the BB boards, as well as transmit/receive with the AFE. These functions (we call them 'user level functions') would be a compendium of the low-level functions provided in Lyrtech's LIB. Users may access two levels of libraries (functions) to control and communicate with VHS boards:

- The first level - the low-level API - is mainly used to read and write directly to the FPGA registers of the VHS boards.

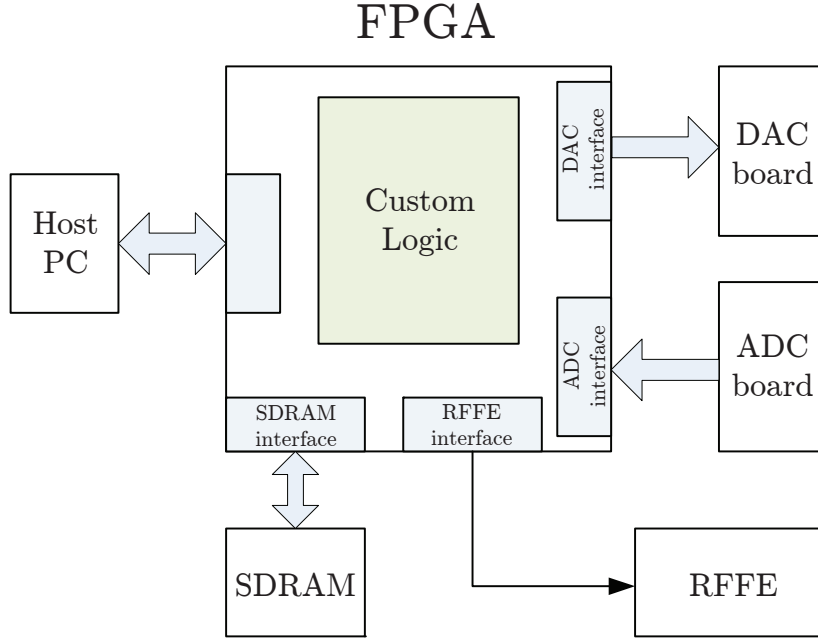


**Figure 3.12:** Block diagram approach of the FPGA interfaces.

- The second level contains high-level libraries - the high-level API - and is mainly used to perform specific actions such as programming the carrier frequencies or configuring the AFE in RX or TX.

So, we gathered the necessary functions of the LIB to form these user level functions. We then developed a C++ dynamic link library (DLL) that encapsulated the LIB and integrates the new functions. This DLL allows external applications (e.g. Matlab) running on the node's PC to control the hardware, as shown in Figure 3.13.

At this point, we were able to use Matlab in all the stages of the MIMO communication process: to prepare the data to be transmitted, send the data to the transmission node, control the sending and receiving process, get the data from the receiving node, analyze the data, and display the results. This solution offers low versatility but the way to control the nodes was really useful in the initial development steps. Our next aim was to control the node from a new PC different from the host PC. This is described in Section 3.5.

Our experience over the years has shown that it takes a considerable amount of time and manpower to get even the most basic demo programs to work. Among the reasons, the following stand out. First, researchers must deal with missing, misleading, or carelessly written and not updated manuals and sample programs. In our case, the documentation was really poor and there were no explanation of how to combine the low-level functions to get the things work. Then, there exist a lack of support from the companies and rarely they offer code in order to develop the functions rapidly. Finally, there exist some problems derived from fabrication that often occurs when plugging/unplugging cables, etc.

### 3.4.3 Remote control PC

In spite of the great functional advance obtained by just dynamically linking the nodes with Matlab, it was not close to be a good environment because of three main problems:

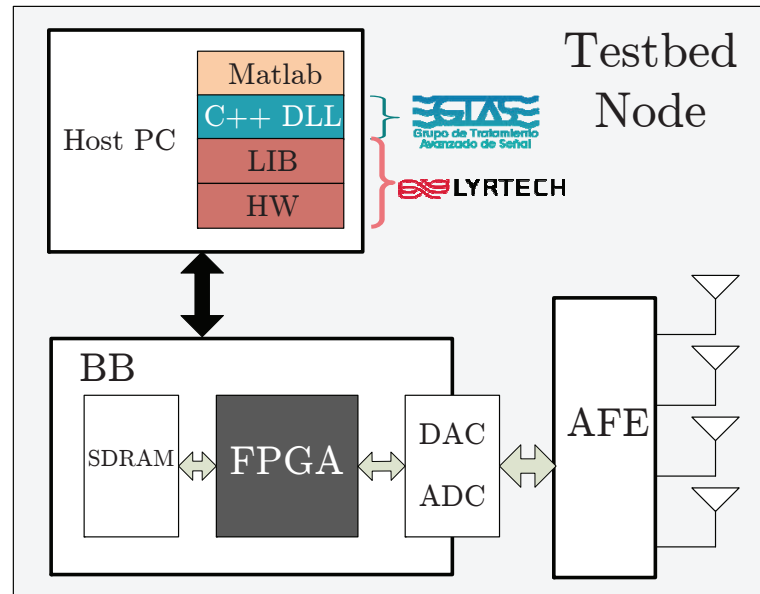


**Figure 3.13:** New interface within the Lyrtech node.

1. The new configuration required Matlab to be installed and running on each of the testbed host PCs.
2. The new configuration limits the experiments to local interaction.
3. The need of offering limited access to all the testbed functionalities.

The local interaction could be relaxed by using PNET (see Figure 3.14), a Matlab toolbox that allows a Matlab in a control PC to control that of the host PC. Logically, from the host PC of one node we can interact with other node using PNET. This toolbox relies on the use of sockets to establish the communications, with a combination of an IP address and a port number. However, this remote access technology was far from ideal and all the other caveats remained. This toolbox is quite efficient but extremely unsafe, it does not fulfill the aforementioned third problem. Therefore, all the functionalities are still accessible, but in this case from a remote Matlab.

### 3.5 Remote testbed interface

The current way to control the testbed was really useful in the initial development steps, when testing that signal transmissions could be carried out among the nodes. However, our aim was to control the three nodes from a remote control PC using high level languages. Before making any decision, we first identified a set of requirements that this interface should provide:

- Well defined interface so that the applications have access to the required functionality and have no chance to damage the node.
- Isolate the communications interface from the application program, e.g. Matlab.
- Maximize interoperability with other programs and third party tools.

A remote control software based on WS has been developed in order to handle the testbed [Vielva et al., 2010]. This remote control offers an interface to access all basic functionalities,

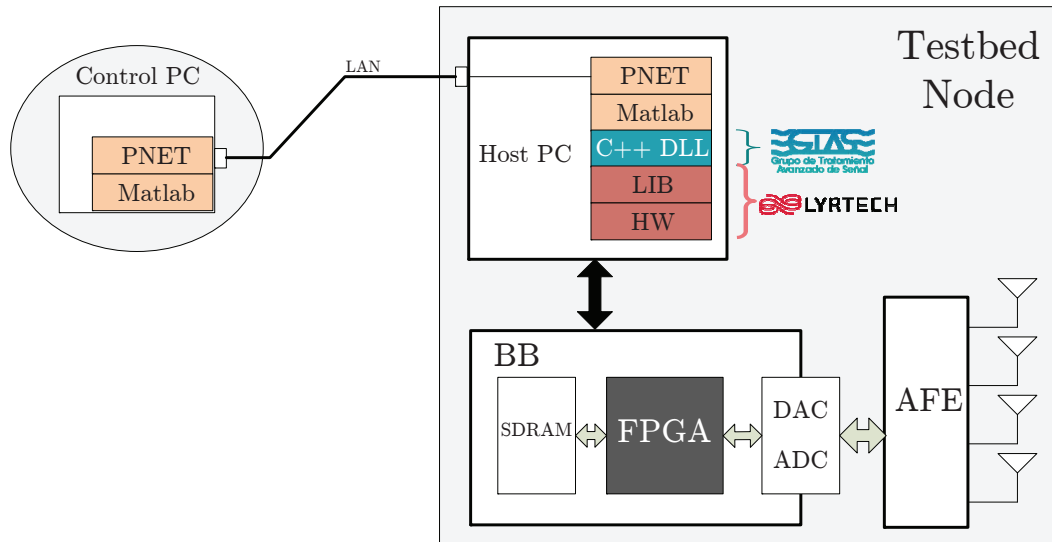


**Figure 3.14:** The first step consisted of providing access to external applications, like Matlab, running on the node PC to control the testbed. By using PNET, access was given to remote Matlab instances.

such as programming the FPGA, adjusting TX/RX gains, sampling frequencies, etc. and can be accessed and tested through the following link: <http://www.gtas.unican.es/testbed/>. This architecture allows testbed handling in a simple way, centralized to a unique PC.

Concretely, the proposed solution was to develop a C# library that encapsulates Lyrtech's DLL. For the WS layer we developed a Simple Object Access Protocol (SOAP) interface, which is a World Wide Web Consortium (W3C) recommendation [Lafon and Mitra, 2007] that allows third party applications, including Matlab, to transparently and safely interact with our nodes through the provided interface. This WS is accessible from almost every software application like Matlab, web applications or even desktop applications.

The objective was to provide an interface to the Lyrtech devices being

- Versatile: can be used by computers in a network and by different application programs.
- Efficient: minimize the payload of the data.
- Secure: the interface provides only a well-defined set of actions.

With this last evolution, we get lower efficiency than the PNET solution (WS instead of sockets) but high security (predefined and limited interface) and high versatility (any application capable of interface with SOAP WS is a full-fledge client).

Figure 3.15 depicts the architecture of the web platform interface, showing a control PC accessing through the internet for controlling the three testbed nodes. From the stack represented in each node, the ascending layers correspond to hardware, manufacturer's LIB, C++ wrapper DLL to gain access from managed code, C# classes that implement the nodes as objects and provide dual interface, the web server and the interface provided in SOAP. At the top, an external control PC represents a remote Matlab application that interfaces with the MIMO testbed through the SOAP interface.

The GTAS MIMO testbed uses the following key technologies and standards: Hypertext Markup Language (HTML) for the textual user interface like buttons, lists and text;

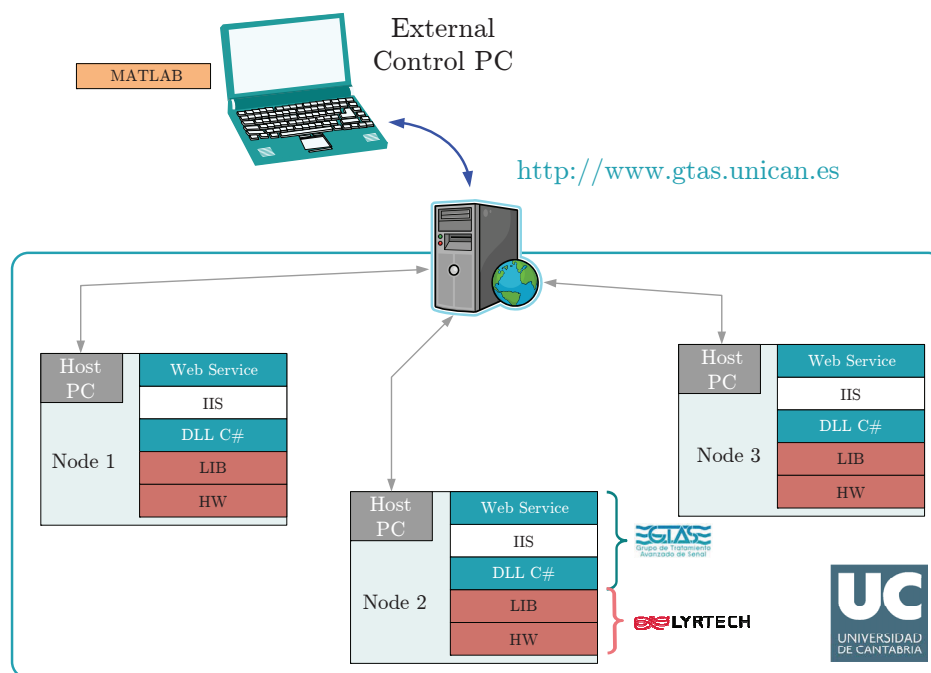


**Figure 3.15:** Architecture of the web platform.

JavaScript as the programming language that runs natively on the web browsers and modifies dynamically the user interface; Scalable Vector Graphics (SVG), and Asynchronous JavaScript and XML (Ajax). In summary, a set of technologies to implement communication between the browser and the web server.

The interface to control the testbed results quite important to carry out experiments with the testbed, and to control all the current functionalities: the ones proposed in this theses and the forthcoming developments. Moreover, the proposed web-based interface is quite important for both academic and research purposes.

In summary, this section is the starting point of MIMO experiments using the GTAS testbed. Other functionalities such as MIMO channel measuring methodologies (see Chapter 4), allow extracting MIMO channel estimates for its characterization in indoor environments. The final example will be the emulation of MIMO channels, as presented in Chapter 5.

### 3.5.1 Multi-Node capabilities

Thanks to this web-based architecture we are able to build a multinode testbed by joining two or more testbed nodes. Figure 3.16 depicts the different network scenarios that we can develop with our MIMO testbed nodes. This approach is very interesting because it makes it possible for two or more research groups to construct a multiuser testbed without the need of replicating the testbed hardware. However, if the software design of each testbed has not been carried out carefully, the integration will involve a complete redesign and implementation of the new multiuser testbed. Consequently, a more intelligent and cheaper solution consists in properly designing the software for each testbed, taking into account the scalability and flexibility requisites.

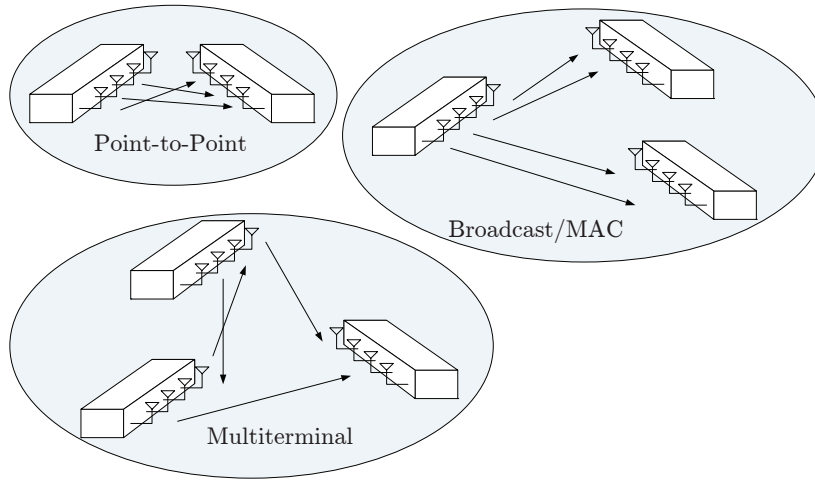


**Figure 3.16:** MIMO network scenarios.

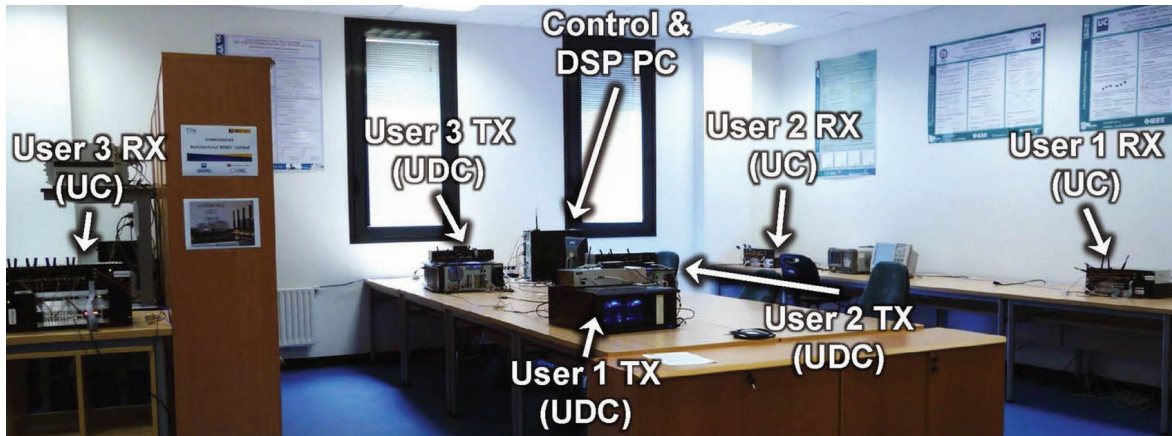


**Figure 3.17:** Panoramic picture of the multi-user testbed constructed with the two nodes of the GTAS MIMO Testbed plus two nodes of the testbed developed at the University of La Coruña.

Figure 3.17 shows a photograph of a demonstration of a multiuser testbed with four nodes with four antennas each. Two nodes are from the GTAS MIMO testbed whereas the other two are from the testbed developed by the GTEC at the University of La Coruña. In such setup, a broadcast channel with one TX node and three RX nodes was measured.

### 3.5.2 Example with the interface

Once described the web-base interface, we present an example of how interact between the control PC and one or several nodes of the MIMO testbed. Moreover, we summarize which are the calls that trigger the low-level functions of the C# DLL (Lyrtech LIB).

First, to be able to handle the GTAS testbed from Matlab in a remote PC we must download the Matlab Wrapper from the GTAS webpage:

<http://www.gtas.unican.es/testbed/downloads/wsLyrtechGTAS.zip>

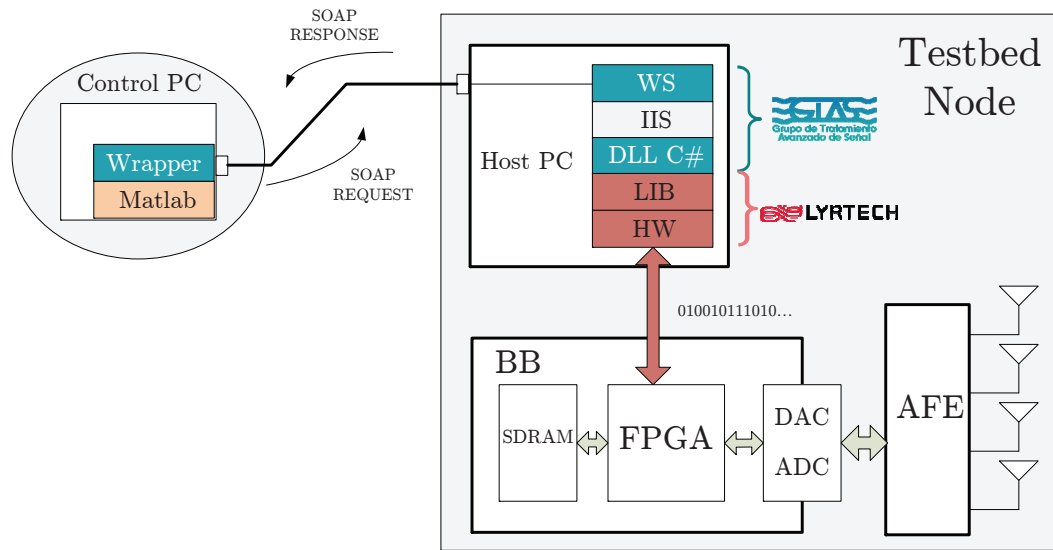


**Figure 3.18:** Final interface architecture: communication procedure between a remote PC and one of the testbed nodes.

This Wrapper can be considered as a remote interpretation of the functions that can be accessed from the node. It is in charge of interpreting the function parameters and communicate with the node using SOAP requests and SOAP responses (see Figure 3.18). The communication relies on text transfer and allows the pass of parameters: integers, boolean, etc. and even text between the control PC and the host PC. The wrapper contains all the functions that can be executed within the host PC. Let assume that a remote PC wants to communicate with one of our testbed nodes

Once the Wrapper is stored in the control PC we can create local node objects that act as a link between the control PC and the node. To create an object from the control PC we need to execute the wrapper with the IP address of the node. For example

```
tx = wsLyrtechGTAS('http://193.144.201.116/wsLyrtech.asmx');
```

In the example we have created the object *tx*, which will be used to access to the functionalities of the node through the *tx* identifier. This identifier is linked to a determined IP address. Any number of nodes can be controlled from the control PC, each with their own identifier (different from the others). We assume that the FPGA has already been programmed.

Let suppose we want to change the PA gain of the transceiver 1 in the AFE, which belongs to the object node identified as *tx* from the control PC (according to Figure 3.18). The following Matlab code details the steps to follow to adjust the transceiver gain (only for TX).

#### Matlab commands for setting the TX power

```
transceiver = 1;
PA_GAIN = 0;
pa_gain_set = rffe_TxGain(tx, PA_GAIN, transceiver);
```



We have defined the input parameters of the function that allows changing the gain: the transceiver number and the PA gain. The functions follow the following syntax. The node component: *dac*, *adc* or *rffe*; the function name, and the parameters are explicitly shown.

[destination]\_[function name](parameters)

Its execution initiates a SOAP request from the control PC to the host PC. From the request we can identify that the parameters are included as text.

#### SOAP Request (Setting TX Power)

```
<?xml version="1.0" encoding="utf-8"?>
<soap12:Envelope xmlns:xsi="http://www.w3.org/2001/XMLSchema-instance"
  xmlns:xsd="http://www.w3.org/2001/XMLSchema" xmlns:soap12="http
    ://www.w3.org/2003/05/soap-envelope">
  <soap12:Body>
    <rffe_TxGain xmlns="http://www.gtas.dicom.unican.es/">
      <PA_Gain>30</PA_Gain>
      <Transceiver>1</Transceiver>
    </rffe_TxGain>
  </soap12:Body>
</soap12:Envelope>
```

Automatically, the WS at the Host PC confirms the request with a SOAP response: true if everything was OK and false if there exist errors. As occurs with the SOAP request, it involves sending text with an explicit response (true in this case).

#### SOAP response

```
<?xml version="1.0" encoding="utf-8"?>
<soap12:Envelope xmlns:xsi="http://www.w3.org/2001/XMLSchema-instance"
  xmlns:xsd="http://www.w3.org/2001/XMLSchema" xmlns:soap12="http
    ://www.w3.org/2003/05/soap-envelope">
  <soap12:Body>
    <rffe_TxGainResponse xmlns="http://www.gtas.dicom.unican.es/">
      <rffe_TxGainResult>true</rffe_TxGainResult>
    </rffe_TxGainResponse>
  </soap12:Body>
</soap12:Envelope>%\end{small}
```

These are the commands which are sent between the control PC and the host PC. However, these instructions give place to low-level ones, making up Lyrtech LIB. Concretely, the function to be executed within the C# DLL (corresponding to the the high level functions) will access the library and identify the API function associated with it. Then, the commands in binary are transmitted to the FPGA which, through one of the VHS-BB boards (the one that controls the AFE), conveys the information to the AFE and set the desired gain.

With this receiving/sending procedure we are able to send values as well as concatenated functions in text format. These are embedded as text so they can also be exchanged and interpreted correctly.

### 3.5.3 Success stories

The design and development of the GTAS MIMO web-based interface has led to a quite useful tool to evaluate MIMO schemes in real environments as well implementing parts of standards



in real-time. So far, multiple universities and research institutes have taken advantage of the testbed capabilities from either spanish and foreign research groups. We can highlight the following success stories:

- MIMAX consortium. As an example, Section 3.9 presents an example of GTAS Testbed utilization in the context of MIMAX project.
- Joint work with Universidad de la Coruña (UDC): interference alignment (IA) and cooperative beamforming techniques.
- Joint work with Universidad Carlos III de Madrid (UC3M): Achievable throughput with Block Diagonalization on OFDM indoor demonstrator (BD) [Céspedes et al., 2013].

## 3.6 Control PC

We now focus on the role that the control PC (external client) plays on this new web-based interface. As depicted in Figure 3.15 and making use of the communication protocol described in Section 3.5.2, we are now able to summarize the steps that the control PC has to follow to handle a TX/RX communication among the nodes.

The migration of an algorithm from a simulation environment to a testbed involves cumbersome low-level programming to access the hardware as well as a very detailed knowledge of the hardware. Unlike simulations, the experimental evaluation of wireless communications systems means having to deal with frequently ignored problems, as for example time and frequency synchronization. All these issues make it more difficult to assess new MIMO communications systems in a testbed. For this reason, it is desirable to make the testbed accessible to researchers at a reasonable level of abstraction. This goal represents an important challenge due to the large number of heterogeneous technologies and development environments that have to be integrated together. However, if this challenge is met, the final result is a very attractive product for the user, who can focus on the development of new transmission techniques that can easily be translated to the testbed and later evaluated in realistic scenarios. The user must not be involved in this kind of low-level signal processing tasks (e.g. synchronization).

We must provide the means to synchronize the testbed nodes. The developed synchronization schemes are described in Section 3.6.1. We also describe a typical utilization procedure that centralize in the control PC the handling of the whole GTAS MIMO testbed (see Section 3.6.3).

### 3.6.1 Synchronization

Synchronization is one of the most important tasks in a MIMO testbed. The efficiency of the measurement process is also reduced due to the lack of an external hardware device or software method to assist in the time synchronization process. It involves the frame start detection (i.e., time synchronization) and the estimation and compensation of the frequency offset between transmitter and receiver. Without proper synchronization, it is not possible to successfully perform MIMO detection.

As there is, in general, no cable connection between the TX and the RX node, some sort of synchronization is needed to ensure that the blocks of data are transmitted and received at the proper time. Furthermore, it is possible to synchronize the frequency of the internal clocks of the TX node to those of the RX node.

Regarding software synchronization alternatives, we have used two different algorithms avoiding the use of cables and other devices.

- Well-known Pseudo Noise (PN) sequences: The use of special training sequences prior to the transmitted data, which may only be possible in static scenarios, is a simple but effective well-known synchronization strategy.
- Iterative Weighted Phase Averager (IWPA) method: high-accuracy non-parametric frequency estimation method based on the fast Fourier transform (FFT), which will be presented in Chapter 4.

There exist other ways for testbed synchronization, e.g. the two ends of the measurement system can be synchronized in frequency and phase thanks to the external reference generated by rubidium oscillators and disciplined by a global positioning system (GPS). However, these kind of synchronization methods are so far discarded due to the expense they imply, and they do not work in indoor environments (e.g. GPS).

### 3.6.2 Automatic Gain Control (AGC)

When dealing with more than one nodes in different scenarios it is desirable sometimes a gain control at the receiver. An AGC can be used in our testbed, since it can be implemented between the FPGA and the RF part, using a closed loop to control the gain of the AFE. However, most of the experiments that are performed in our laboratory do not require AGC, since the measurements are usually performed in static environments and the channel is known. Therefore, we rely on a manual gain selection for a particular gain setting within a certain range variation. The high dynamic range of the DACs and ADCs also facilitates the manual gain selection.

### 3.6.3 Typical utilization procedure

As an example, a typical procedure of how to handle the nodes from the control PC when carrying out measurements is described. The web-based architecture is able to control all these parameters. In the rest of this section we assume the following:

1. The testbed consists of two nodes, the TX and the RX.
2. It does not matter whether the testbed operates outdoors, indoors, outdoor to indoor or vice-versa. We assume that a network connection can always be established between the testbed nodes and the control PC.
3. The host PCs uses a standard operating system supporting remote operation from another PC attached to the network (e.g. the control PC).

Then, we develop a procedure that can be customized according to the requirements of the evaluation to be carried out. Before starting a new measurement, the following parameters must be defined in the template:

- Number of transmit and receive antennas,  $n_T$  and  $n_R$  respectively.
- The set of RF carriers. In order to generate different channel realizations, we take advantage of the frequency agile capabilities of the AFE.
- The set of TX power values.
- The necessary signaling parameters, e.g. number of samples per symbol, etc.

- Sampling frequency of the DACs and the ADCs, or the size of the buffers at both TX and RX sides.

The overall operation of the system can be summarized as follows: the Matlab program of the control PC generates the data to be transmitted (BB signal), which depend on the purpose to be covered (channel sounding, algorithm testing, etc.). A certain data structure should be followed: IEEE 802.11a frames, PN sequences plus data, etc. The generated signals are transmitted from the control PC to the TX node, where the signal is first stored, and after that transmitted. Since the storage capabilities in the BB are limited, and the transmission rate from BB to the RF is very high, in order to get a continuous transmission the same data are repeated until new data are stored in the SDRAM. The signals are analog converted, and then upconverted from BB to RF. After being transmitted by the antenna module, the signals undergo the channel propagation effects, and the resulting signals are received by the RX node. The reverse operations are carried out in the RX modules: the received signal is down-converted to BB and then sampled and digitally converted. Finally, the digital data are BB converted and stored in the SDRAM, from where the information is sent to the user application in order to be off-line post processed. As can be noticed, this scheme includes some modules that operate in an offline basis (generation and preprocessing of signal, and the final postprocessing of signal), although some others work in real-time (DSP-FPGA processing: up- and down-conversion, filtering, etc.). Therefore, the system is not meant to show a fully real-time operation.

## 3.7 Real-time processing

Current FPGAs possess sufficient performance and logic capacity to implement a number of DSP algorithms effectively. This is accomplished by exploiting parallelism as well as mapping techniques such as distributed arithmetic. Apart from being the interface among the rest of the parts each Lyrtech node, the FPGA also includes custom logic where the user can conceive a model-based design in Simulink and Matlab, as has been briefly described in Section 3.4. In this section, the different FPGA interfaces and the way it communicates with the rest of the node components are detailed, along with the way of control it as well as the work flow and the tools that allow its control.

### 3.7.1 FPGA: interface, control, user DSP

Figure 3.19 depicts the block diagram approach of the FPGA interfaces. These interfaces allow communication with Simulink models developed within the custom logic through I/O blocks. The figure also depicts the System Generator interface wrapper. The specific functionality contained in a wrapper depends on the board, but it usually includes such functions as control of the SDRAM and other I/O interfaces. It is a level of programming that separates the user from board-level logic.

The Lyrtech I/O blocks allow logic to communicate with the System Generator wrapper. They are based on Xilinx System Generator for DSP blocks. Since System Generator is integrated in MATLAB/Simulink environment, the blocks are available once we start Matlab or Simulink. Lyrtech blocks provide a transformation path between the typical Simulink blocks for simulating the model and System Generator for DSP blocks. When the model is compiled in an FPGA *bitstream* (.bit file), the Lyrtech blocks allows controlling the VHS-BB boards: FPGA peripherals and resources. More details are outlined in Section 3.7.2.

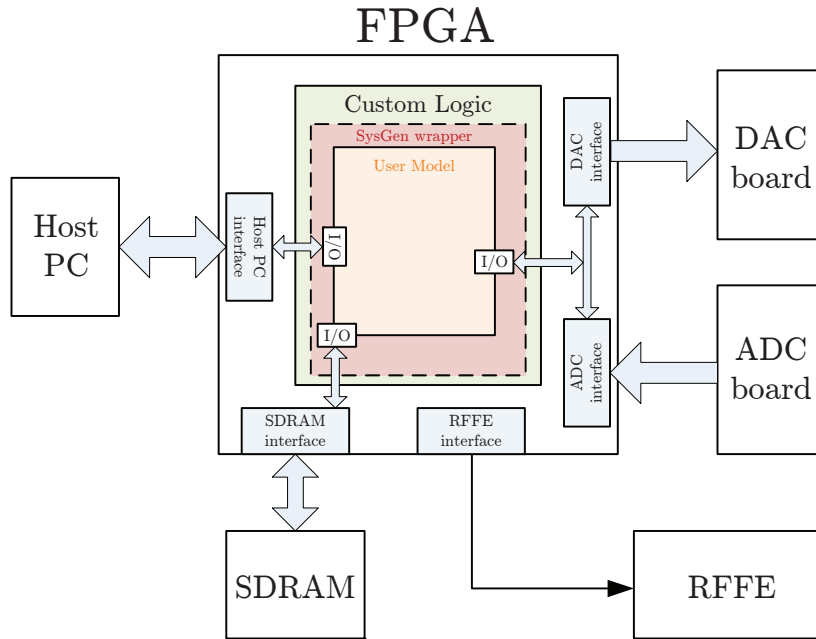


**Figure 3.19:** FPGA interfaces and custom logic.

### FPGA Host PC control

The host interface allows accessing all the configurable aspects of the board. The host PC is connected to the FPGA through the V363 PCI local bus bridge. This bus bridge uses one of its memory spaces to access the FPGA.

### FPGA SDRAM control

The FPGA SDRAM interface acts as an interface between the onboard FPGA and the SDRAM. The VHS-BB boards support one read and one write port, then it is possible to simultaneously transact larger amounts of data to and from the SDRAM of the FPGA. On one hand, it is able to acquire data and save it to the onboard SDRAM in real-time. Then, the data can be uploaded to the host PC for analysis. On the other hand, the FPGA is able to generate signals from the data downloaded to the SDRAM. The requirement here is that the memories must be accessible in real-time by the DAC or ADC, respectively.

The SDRAM can be controlled with the low-level functions available in the API. There exist functions to initialize and configure the SDRAM through FPGA registers as well as functions to read/write pages from it. The registers can be accessed through the host computer of the cPCI chassis where the VHS-BB boards are connected.

### AFE control

The AFE control interface is a software-base structure used to interface the FPGA user design and the General Purpose Input/Output (GPIO) port of the VHS-BB boards, through which these boards are connected to it. The FPGA within the boards contains a local copy of the AFE registers, related control registers, and registers for the GPIO-connected AFE control signals.

To control the AFE, users must instantiate a series of registers. These registers handle Serial Peripheral Interface (SPI) communications and all the other protocols necessary to drive the AFE input. Each set of SPI registers corresponds to each of 4 transceivers available in the AFE.

In addition to the SPI register, Lyrtech offers another set of registers to control each AFE I/O. These registers are common for the whole AFE. The most important ones are

- Address: in this register the user is able to select up to the 4 AFE transceivers.
- Parallel gain: TX and RX gain configuration.
- PABS DSW OSCS: PA switch, antenna to be selected (two options: A or B) and frequency band.

### 3.7.2 Work flow: Tools

FPGAs are programmable digital logic chips, which means that you can program them to do almost any digital function. The general workflow when working with FPGAs is the following:

1. Use of a PC to describe a certain logic function. It might be obtained either through drawing a schematic, or through creating a text file describing the function.
2. The logic function is compiled using a software provided by the FPGA vendor. That creates a binary file (*bitstream* or BIT file) that can be downloaded into the FPGA.
3. Connect a cable from the PC to the FPGA, and download the *bitstream*.

Then, the FPGA behaves according to the logic function that has been created. It is possible to download *bitstreams* into FPGAs as many times as necessary, with different functionalities. If there exists a mistake in your design, the only step to follow is to fix the logic function; re-compile and re-download it.

Of course, this is a general description, the following lines describe the different options to handle the FPGA and to create the *bitstream*. On one hand we might have written our design in VHDL code and we want to generate a *bitstream* from this code. On the other hand, for users with no VHDL experience, it is possible to generate the *bitstream* from a model-based design.

#### VHDL-based workflow

ISE Foundation suite is an integrated graphical environment that provides a design, synthesis, implementation, and programming interface for Xilinx logic designs. The Xilinx ISE tools allow the design to be entered several ways including graphical schematics, and Very High Speed Integrated Circuit Hardware Description Language (VHDL), among others.

1. Writing the VHDL model.
2. Checking the VHDL syntax.
3. Simulate the behavioral of the model: With ModelSim, it is possible to apply stimulus to a VHDL design, run the simulation, and analyze the results.
4. The input and output signals are assigned to the I/O pins on the FPGA by the compiler. Compilation is a multi-step process. In Xilinx, a VHDL design must go through the following stages: Synthesize, Translate, Map, Place & Route, and finally Program File Generation (the generation of the *bitstream*).

This overall procedure requires skills related to VHDL programming, which does not occur in our case. Moreover, we avoid the generation of traditional testbenches and extensive ModelSim simulations. Therefore, our aim is to obtain the BIT file for programming the FPGA by means of a user-friendly tool.

### System Generator-based workflow

System Generator for DSP is a Xilinx toolbox of graphical simulation blocks for simulating and generating VHDL designs. It automatically translates DSP systems developed using Matlab and Simulink into highly optimized VHDL and Intellectual Property (IP) cores for Xilinx FPGAs. Simulink is built on top of Matlab allowing the use of the full Matlab language for input signal generation and output analysis.

Before you can begin working on your model, you need to ensure that the Matlab environment is aware of System Generator and that System Generator is configured to work with Matlab. This program allows us to create some blocks and simulate their behavior:

- Feeding their inputs with Matlab signals or Simulink blocks and analyzing their outputs in Matlab. Therefore, the behavior of a System Generator-based design can be compared with its equivalent Matlab algorithm.
- These blocks can be synthesized to produce VHDL code and netlist files. This code can be integrated into a common Xilinx ISE project to get a final FPGA implementation that will run in real-time within the FPGA of the node

Such models have two principal sections:

- **Configuration section:** The configuration in an FPGA model is very straightforward since there are no special scripts to run or configurations to modify. The only requirement is for the model to contain the System Generator block from Xilinx and the FPGA board configuration block.
- **Processing section:** The processing section of an FPGA model is where users place blocks to design an algorithm. FPGA process data as fixed-point data, but Simulink uses a double data type. This is why a Gateway out block is used to convert the Xilinx data type to the Simulink data type to display data in Simulink scope.

### Other options

Using System Generator, the user is able to compile the design to NGC netlist files that can be added to an existing ISE project. These files provide the instances to Xilinx blocksets (which are directly synthesizable), interconnections, and some attributes of the blocksets. Finally, we can form a new project by merging the generated netlist files into the existing ISE project.

### 3.7.3 Work flow followed with the GTAS MIMO testbed

The model-based design kit (MBDK) for the VHS-ADC/DAC is a collection of blocks that communicate with the various inputs and outputs of the VHS-BB FPGAs. It also includes a compilation add-in for System Generator for DSP from Xilinx. There is a close relationship between this blockset and the System Generator block.

Regarding the configuration section, we use the FPGA configuration block from Lyrtech. These blocks are used to configure the building information of the FPGA model. The System

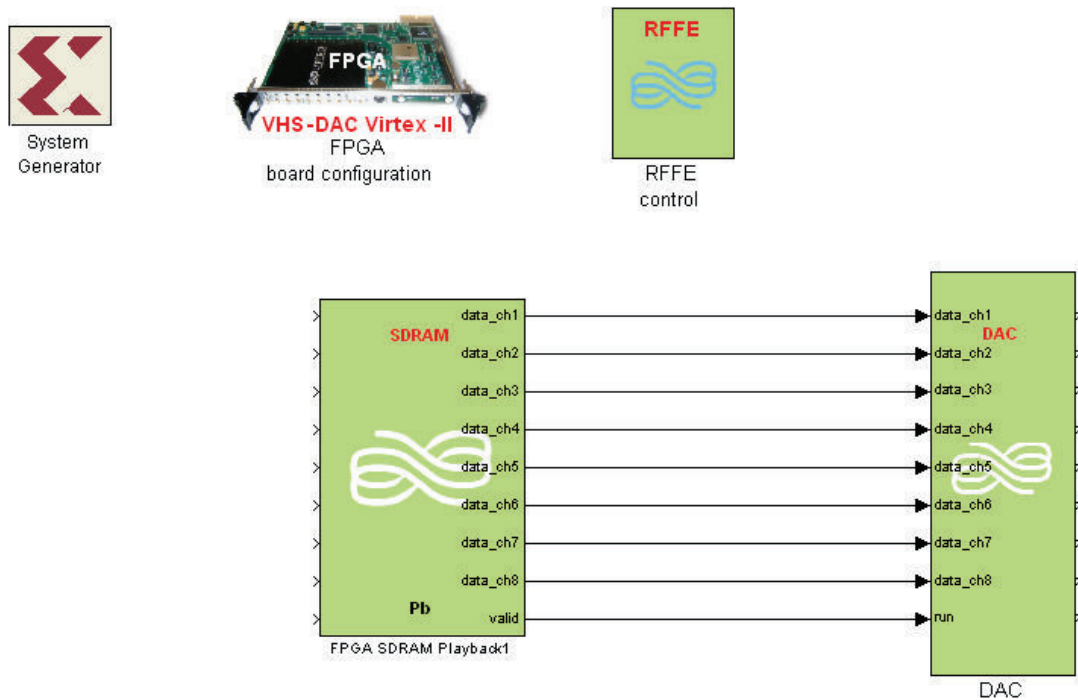


**Figure 3.20:** Typical MBDK FPGA model.

Generator block instructs Simulink to use the System Generator for DSP compilation flow, while the FPGA board configuration block instructs System Generator for DSP to use the Lyrtech compilation flow. Also it is desirable to include the RFFE control to be able to use the AFE.

The processing section is composed of Xilinx blocks, Lyrtech I/O blocks, and Simulink blocks. Xilinx blocks are the actual processing part of the FPGA model. These blocks are located in the Xilinx blocksets. The Lyrtech I/O blocks have two purposes. First, when you simulate the FPGA model, the blocks interface Xilinx processing blocks with Simulink I/O blocks. In the model, Lyrtech blocks provide a transformation path between the Simulink blocks and System Generator for DSP blocks that compose the model. When the model is compiled as an FPGA *bitstream*, the FPGA blocks allow you to access the FPGA peripherals and resources of your board.

Figure 3.20 illustrates a typical model-based FPGA model. In this case the simplest model is depicted, which is able to control the DAC board, transferring data from the FPGA, being able also to control the RFFE. This model does not include custom logic, since the only blocks that are used are the SDRAM and DAC

Every System Generator based model requires that at least one System Generator token is placed on the diagram. This block is not connected to anything but serves to drive the FPGA implementation process. System Generator works with standard Simulink models. Figure 3.21 presents the main parameters that must be configured in the System Generator block.

Here you must specify the targeted system on this list, the type of FPGA of your VHS-ADC/DAC, the target directory where the compiler writes its temporary files when building in this text box, and the FPGA clock period and the Simulink system period. The clock period and the Simulink system period are necessary to inform System Generator for DSP

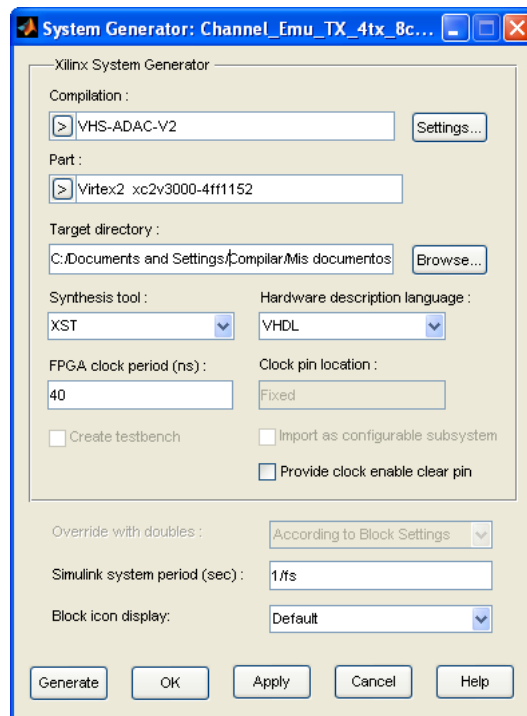


**Figure 3.21:** System Generator block dialog box for the VHS-ADC/DAC.

about the timing constraints of the FPGA design. More specifically, these parameters inform System Generator for DSP at what frequency each block in the FPGA model is running. System Generator for DSP uses this information during the place and route phase of the *bitstream* generation process (performed by ISE Foundation).

- **FPGA clock period:** Informs System Generator for DSP of the time period that corresponds to the real-time clock driving your design. Specify a value within an approximate safety margin of 5% relative to the real-time clock value that you intend to use.
- **Simulink system period:** This parameter informs System Generator for DSP of the sample period related to the real-time clock value. It also relates each Xilinx and Lyrtech FPGA blocks' sample periods to the real-time clock.

When you simulate the FPGA model, the blocks interface the Xilinx processing block with Simulink I/O blocks. This is necessary because Simulink and Xilinx processing blocks do not use the same data format. Simulink blocks mainly use floating-point precision data types, while System Generator for DSP blocks use fixed-point data format. The Lyrtech MBDK FPGA I/O blocks perform this conversion by encapsulating the Xilinx Gateway In and Gateway Out blocks, in the Xilinx blockset.

### 3.7.4 How to control the FPGA

Once we have reviewed the different interfaces that allow controlling Lyrtech nodes, we focus on the diverse ways for controlling the FPGA. Also, the procedure for accessing the memory and registers is treated.



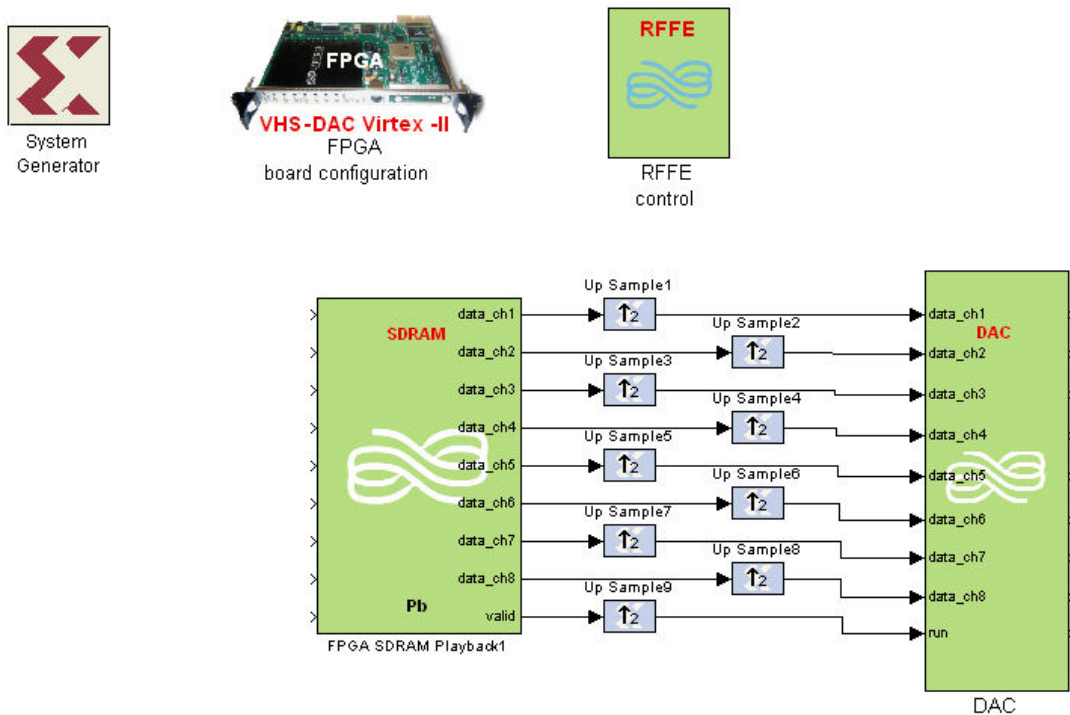


**Figure 3.22:** Simulink scheme.

The FPGA can be controlled at the time it is programmed with a BIT file. This file dictates the FPGA behavior and the parts of the testbed that it will be capable to handle. This can be done with one of the following alternatives:

- Using the VHS utility. The utility allows loading .bit files and program the FPGA
- Using low level *C* functions.
- using the WS in Matlab environment: downloading the wrapper from the GTAS webpage and executing the following command:
- From the webpage [http://www.gtas.unican.es/testbed/acquisition\\_steps](http://www.gtas.unican.es/testbed/acquisition_steps)

The following options allow accessing the FPGA registers for writing/reading:

- Using the VHS utility. Once the FPGA has been programmed, the user is able to read and write custom FPGA registers.
- Using low level *C* functions.
- Using the WS in Matlab environment: downloading the wrapper from the GTAS webpage.
- From the webpage [http://www.gtas.unican.es/testbed/acquisition\\_steps](http://www.gtas.unican.es/testbed/acquisition_steps).

As an example, at this time of FPGA model development, we are able to generate FPGA *bitstreams* of the model including decimators and interpolators from the Xilinx library, for being able to provide the acquisition/transmission clock source with flexibility (see Figure 3.22).

In this example we use interpolators for being able to reproduce signals through the 8 channels. There exist a constraint on the bandwidth (in *Mbytes/s* or *Msp/s*) to be transferred

between the SDRAM and the FPGA. This interpolation will allow us overcome this drawback using a clock of 26 MHz (instead of 52 MHz).

Once we have finished our design we can simulate it in Simulink and generate a *bitstream*. This BIT file can then be loaded into the FPGA using the API, WS, etc., reproducing the behavior of the current user logic.

### 3.8 General example

In this section we combine all what we have learnt so far in this chapter, and we present and analyze a typical TX Matlab example, explaining in detail its particularities. Let suppose we have two nodes of the testbed and we want to transmit certain signals to the other. These nodes are controlled from the Matlab of a control PC somewhere in the world. To be able to control the parts of the node, we must have previously added the wrapper to Matlab path.

First of all, if we aim at controlling one of the nodes, e.g. node 1, we need to create the object from the WS as

#### Object node creation

```
tx = wsLyrtechGTAS(['http://www.gtas.unican.es/testbed/' node '/'
wsLyrtech.asmx']);
```

We make use of the *bitstream* obtained from the model depicted in 3.22, for example. Thus the sampling frequency of the DACs will be  $f_s = 26$  MHz. The *bitstream* is defined as

#### Bitstream file definition

```
bit_file = 'DAC_Virtex4_8_channels_RFFE_interpolate_2.bit';
```

Then, to program the FPGA with this *bitstream* we need to call the function contained in the wrapper.

#### DAC board programming

```
programmed_dac = dac_FPGAConf(tx,bit_file)
```

We want to generate a sine and a cosine wave of 1 MHz through channels 1 to 2.

#### Main BB parameters

```
f = 1;
channels = [1 2];
transceivers = unique(fix((channels-1)/2)+1);

sampling_freq_TX = 52;
w_0 = f/sampling_freq_TX;

[N,D] = rat(1/w_0);

num_samples = N*D*1000;

t = 2*pi*f/sampling_freq_TX*(0:num_samples-1);
t2 = 2*t;
v1 = sin(t);
v2 = cos(t);
v_DAC = -v*(2^(13)-1);
```

The last line fits the sine and the cosine to the range of the DACs (14 bits).

We initialize the front end at a certain frequency with a certain low pass filter and we configure the PA gain of the first transceiver.

#### AFE configuration

```
fc = 24;
f_RF = 5600;
rffe_initialized = rffe_Init(tx,fc,f_RF);
antenna = 1;
PA_GAIN = 30;
pa_gain_set = rffe_TxGain(tx,30,tr);
```

FPGA frequency configuration and the samples of the two channels are written to the SDRAM. Then, channels 1 and 2 of the DACs are activated.

#### Frequency & Channels

```
freq_set = dac_SamplingFreq(tx,sampling_freq_TX);
num_samples = dac_SDRAMWrite(tx,v_DAC);
channels_configured = dac_ChannelConf(tx,sum(2.^(channels-1)),
    length(v_DAC))
```

We set the DAC channel gains,

#### BB channels' gains

```
DAC_gain = 255*dac_v2+15*(1-dac_v2);
channel_gains_set = dac_ChannelGains(tx,DAC_gain*ones(1,8));
```

and, finally, we initialize the playback.

#### Playback the signals

```
playback_started = dac_Play(tx)
```

There exist two modes for playing back the signals, one that continuously reproduce them and the other that just reproduce once the stored samples. We commonly use the first one and only the second one if we are sure that the frame can be received correctly.

At this time, the DACs are reproducing the samples through channels 1 and 2 which, in turn, are connected to the AFE which upconverts the signals and transmit them through the antenna. To acquire the signals from the other node, its object has to be created, its FPGA programmed, the AFE initialized and the receiving gain configured. Then, the sampling frequency, channel configuration and number of samples have to be defined in order to acquire the signals. Once the signals are stored as a variable in Matlab, they can be analyzed and plotted using the multiple resources that Matlab has.

### 3.9 Example of GTAS Testbed utilization: MIMAX project

In this section, we present the utilization of the GTAS MIMO testbed to implement and verify certain parts of a project in which the GTAS group was involved. This supposed one of the first challenges after the testbed and the interface to control it were ready. Moreover, some of the ideas that arose from this project, were put in practice along the following chapters of this dissertation.

MIMAX is an European Union funded project within the 7th Framework Programme that develops smart radio access in wireless communication networks [MIMAX, 2008]. Its architecture is based on an analog antenna combining architecture. Unlike conventional MIMO systems<sup>1</sup>, MIMAX shifts the spatial processing of the signals to the AFE [Eickhoff et al., 2008], involving a reduction of the number of transmit and receive chains to a single one, thus dealing with an equivalent single-input single-output (SISO) channel. The BB architecture of the MIMAX transceiver is based on the WLAN IEEE 802.11a standard [IEEE, 2013]. Therefore, the developed schemes must be specific for orthogonal frequency division multiplexing (OFDM) modulations.

MIMAX started in 2008, just at the time two complete Lyrtech testbed nodes were available at the GTAS laboratory. At that moment, meanwhile the MIMAX partners were developing their corresponding parts, the GTAS group was responsible of the development of the necessary changes at the BB processor in order to allow the calculation and application of weights (beamformers) at the RF part. To that end, it was necessary to develop a MIMO channel estimation scheme. The MIMAX concept has been tested in our  $4 \times 4$  MIMO testbed, integrating the BB processor along with the necessary blocks into the real-time modules of the testbed. The main challenge of the MIMAX BB processor is the proper calculation of those weights to be applied in RF [Via et al., 2010]. This results in reaching high SNR in the communication link, hence higher throughput, better reliability and a larger coverage can be obtained. Figure 3.23 depicts the MIMAX BB processor.

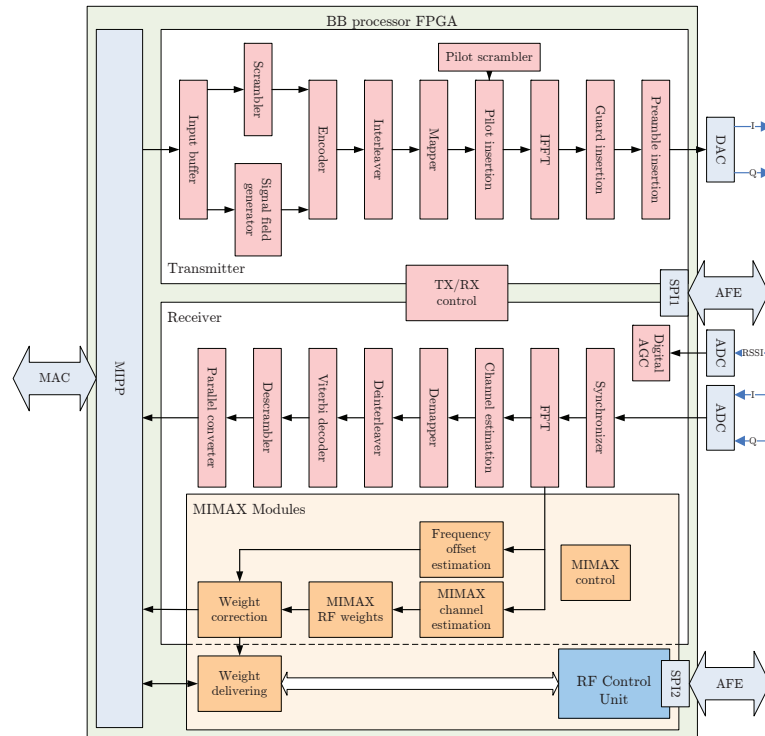


**Figure 3.23:** Block diagram of the MIMAX BB processor architecture. The blocks in orange allow MIMAX weights calculation and application.

<sup>1</sup>MIMO transmitters/receivers need parallel spatial baseband chains at both transmit and receive sides as the number of antennas used for communication increases, entailing higher power consumption and costs.

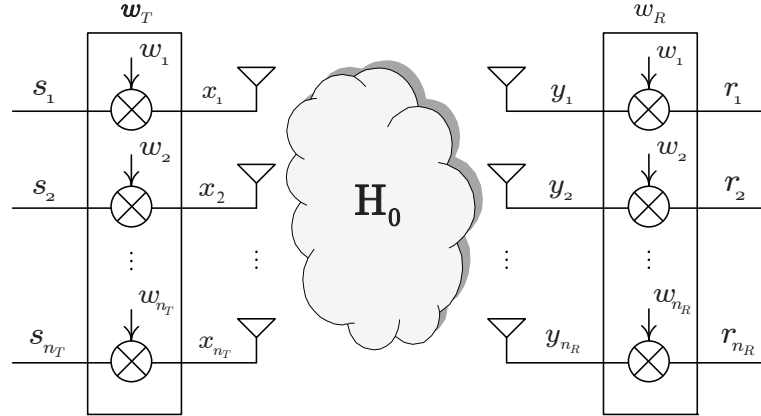


Figure 3.24: Spatial MIMO beamforming.

### 3.9.1 Beamforming in MIMAX

Beamforming is a signal processing technique which is aimed at steering the transmission energy in the desired direction through the use of antenna arrays and weights application. There exist different goals when using beamforming, whether it is applied at the transmit or at the receive side.

Figure 3.24 depicts a typical spatial MIMO beamforming for a MIMO scheme. The beamforming weight vectors can be applied both at the transmit side,  $\mathbf{w}_T$ , and at the receive side,  $\mathbf{w}_R$ . The weights at both transmit and receive sides multiply the signals according to

$$x_i = s_i w_i \quad i = 1, \dots, n_T \quad (3.5)$$

$$r_j = y_j w_j \quad j = 1, \dots, n_R \quad (3.6)$$

We assume, as we did in (2.43), that the MIMO channel is non-selective in both frequency and time. The weight vectors, although they have been presented independent of time, they can also vary with time, so we can add a temporal dependence as  $\mathbf{w}_T[n]$  and  $\mathbf{w}_R[n]$ .

MIMAX is based on the application of transmit and receive beamforming in RF, as depicted in Figure 3.25. The weights are calculated within the BB processor and applied at RF. However, this is a further step to carry out since the components that apply the weights (vector modulators) are of great complexity.

### 3.9.2 MIMAX baseband implementation

A simplified version, therefore, involves the application of the weights in BB, which leads to digital beamforming. This MIMAX emulation includes a digital beamformer for both transmit and receive sides in a  $4 \times 4$  scheme. Figure 3.26 depicts the block diagram for the application of the weights at both sides of the link. Moreover, this block diagram is the design to follow when measuring the  $4 \times 4$  MIMO channel, i.e. in the TX and RX nodes of the GTAS MIMO testbed presented in Section 3.9.3

For each transmit/receive antenna, the  $I$  and  $Q$  transmit/receive signals were multiplied by the suitable weights for each part of the frame. The digital beamformers implemented in the FPGA of each node are based on digital complex multipliers that use prestored weights quantized using 16 bits. These weights can be applied in a symbol by symbol basis (i.e. a

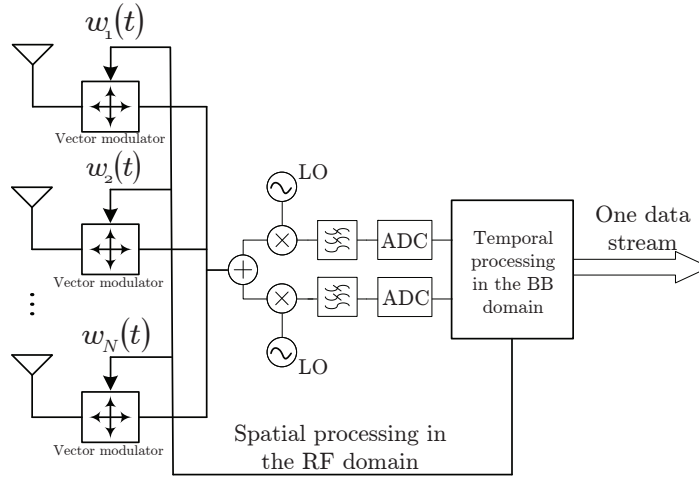


**Figure 3.25:** Analog antenna combining in the RF path for MIMO communications systems. The weights,  $w_i(t)$  are applied in RF.

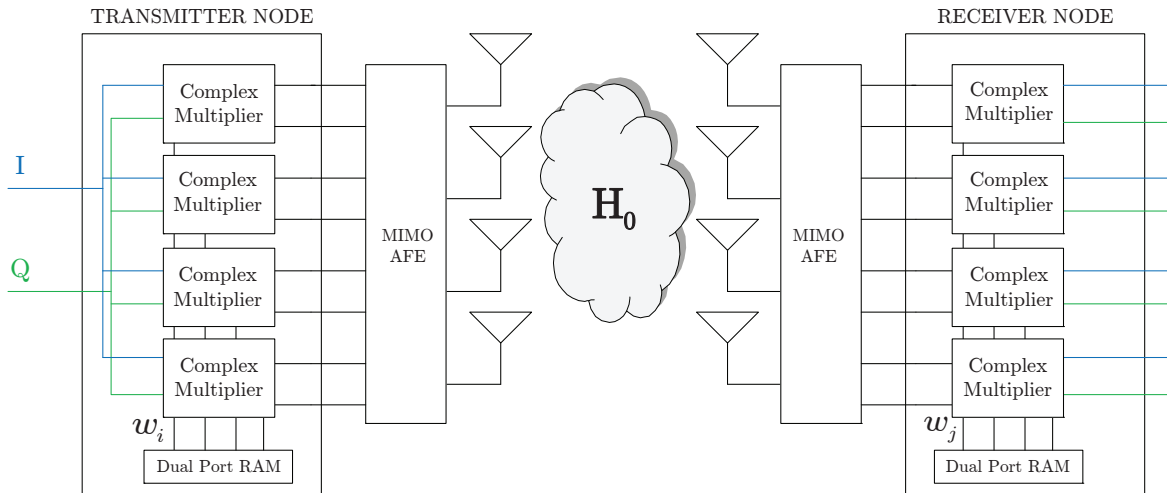


**Figure 3.26:** BB weight application.

specific weight during each OFDM baseband symbol) or even in a sample by sample basis (i.e. different weights for every baseband sample). Figure ?? depicts the complex multiplier scheme.

At the same moment that MIMAX procedure was being defined, the GTAS group started to design a methodology for measuring the frequency response of the wideband MIMO channel, using multifrequency signals (see Chapter 4). The need of measuring the MIMO channel in MIMAX led us to develop a channel estimation methodology using 802.11a frames. This procedure is presented in Section 3.9.3 and the comparison results with the methodology presented in Chapter 4 are put forward.

### 3.9.3 MIMAX channel estimation

The weights values depend on the channel state knowledge at both sides (see Section 3.9.3). Due to this, one substantial part of the BB work has focused on the study and development of

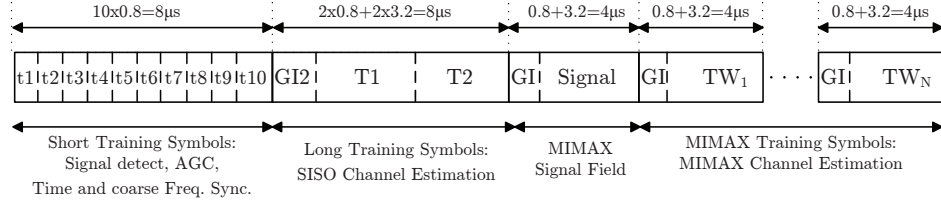


Figure 3.27: MIMAX training frame.

Transmit weights	2	1	1	0	0	0
	2	1	0	1	0	0
	2	1	0	0	1	0
	2	1	0	0	0	1
Receive weights	1	1	1	0	0	0
	1	1	0	1	0	0
	1	1	0	0	1	0
	1	1	0	0	0	1

Figure 3.28: Weight values for a  $4 \times 4$  MIMAX training frame.

the most appropriate techniques for MIMO channel estimation. Among the different options, least squares (LS) channel estimation (the one that is carried out in 802.11a) has been chosen.

The problem arises when estimating the MIMO channel using 802.11a frames, i.e. the  $4 \times 4$  MIMO channel has to be estimated from the transmission/reception of a single frame under different transmit-receive beamformers. Therefore, an 802.11a training frame called *MIMAX training frame* was created to allow the estimation of the MIMO channels (see Figure 3.27).

It includes 16 training symbols, each multiplied by different beamforming vectors. The MIMAX channel estimation block measures the  $4 \times 4$  MIMO channel based on the 16 OFDM training symbols of the received MIMAX II frame. The MIMAX training symbols (TWx) are transmitted affected by the 16 weights in order to estimate the 16 SISO equivalent channels for the 52 active subcarriers. Concretely, Figure 3.28 depicts the necessary set of transmit/receive weights to estimate a  $4 \times 4$  MIMO channel.

A typical experimental procedure involves the transmission/reception of a MIMAX training frame using two nodes of the GTAS MIMO testbed, as depicted in Figure 3.29.

The resulting  $4 \times 4$  channel estimates are depicted in Figure 3.30.

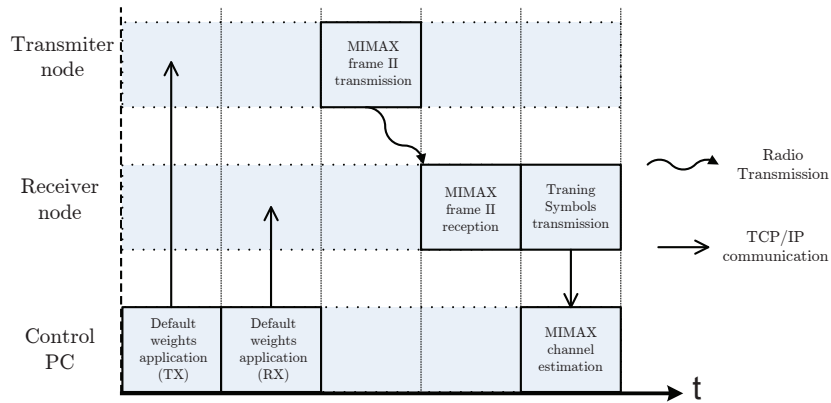
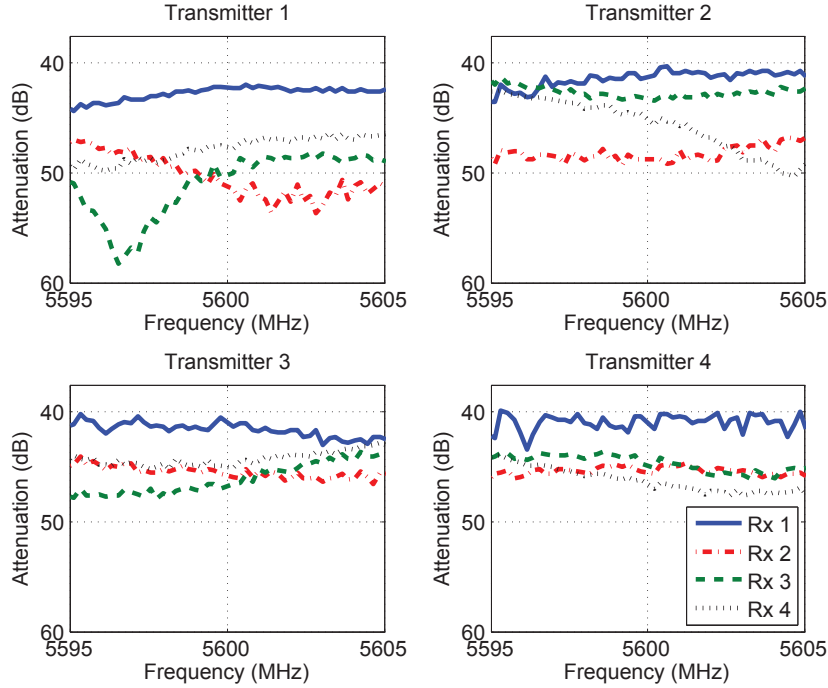


Figure 3.29: MIMAX channel measuring procedure.



**Figure 3.30:** LS MIMAX  $4 \times 4$  channel estimation results.

A large amount of measure have been carried out with MIMAX channel estimation procedure. The obtained results confirm that the channel, in static environments, does not change and can be considered deterministic [Hashemi, 1993b].

### 3.10 Conclusions

In this chapter we focused on the experimental evaluation of MIMO systems. Concretely, we briefly defined the MIMO testbed concept in the context of wireless communications research, outlining the flexibility and potential they offer, summarizing their capabilities and features.

We also introduced the COTS-based Lyrtech nodes. The idea of acquiring MIMO nodes based on COTS modules is justified by the savings in time, manpower and the amount of a priori required knowledge and time. The hardware of the nodes is described, along with the particularities and impairments that this kind of equipment imply. The performance of these nodes is similar to that offered by typical commercial devices, thus being suitable for evaluating the performance of wireless communications systems in realistic wireless scenarios.

As the main contribution of this chapter, we present a novel software method to control Lyrtech nodes, which is based on a web-based architecture. We then can refer to our GTAS MIMO testbed as a powerful and flexible tool consisting of three Lyrtech nodes, to test MIMO devices and algorithms provided with remote control handling. The new hardware/software architecture involves a huge improvement when testing MIMO algorithms or devices, since it allows multiuser schemes, cooperative communications, etc. Moreover, it allows offering its capabilities to the whole wireless research community.

Finally, as an example, the MIMAX project has been introduced, and a MIMO channel estimation methodology based on time-varying beamforming is described. The experience



gained working in this project was of paramount importance for the next chapters of this dissertation.



# Multifrequency methodology for measuring MIMO channels

This chapter arises from the need of measuring and characterizing multiple-input multiple-output (MIMO) channels, as we did, for example, in Chapter 3 within the MIMAX project. Two main objectives turn up. First, the need of assessing MIMO algorithms using realistic channel models, i.e. WINNER [WINNER II, 2006], or, even better, with realistic MIMO channel measures. The second involves validating the MIMAX channel estimation procedure, presented in Chapter 3.

Our main concern relies on how to measure the MIMO channel. The GTAS group does not have dedicated equipment, e.g. channel sounders, or alternative solutions which will imply a great expense. Nevertheless, thanks to the availability of the GTAS MIMO testbed and the flexibility it offers, we are able to accomplish this task without extra equipment.

We propose a methodology for measuring MIMO channels in the frequency-domain using the GTAS MIMO testbed. It involves the transmission of a set of frequency- and phase-optimized complex exponentials within the bandwidth of interest. Subsequently, these signals are acquired through the receive antennas for, subsequently, being estimated offline using a frequency estimation algorithm. Concretely, in this final stage, the amplitude, phase and frequency of the received complex exponentials are estimated by means of a high-accuracy non-parametric frequency estimation method based on the fast Fourier transform (FFT), which is referred to as the iterative weighted phase averager (IWPA) [Santamaría et al., 2000] algorithm. The use of this algorithm avoids the need of additional circuitry or cables to synchronize transmitter (TX) and receiver (RX) setup. Moreover, in presence of signal changes caused by movement, this algorithm is able to estimate the doppler frequency. The methodology requires minimum real time signal processing provided by the FPGA, involving interpolation and decimation. These simplifications do not avoid a thorough calibration at both TX and RX sides.

Its implementation in GTAS MIMO testbed exhibits good performance which characteristics are compared with some other equipment. Moreover the proper behavior is verified since the measurement results are compared with those measured by specific channel measurement instrumentation, e.g. vector network analyzer (VNA). Subsequently, an exhaustive analysis of the most important parameters derived from the measured MIMO channels is carried out.

The proposed methodology is presented in two steps. The first one involves measuring single-input single-output (SIMO) channels, comprising the generation and conditioning of the excitation signals as well as the offline estimation technique. The second one extends the

method to a MIMO scheme by implementing a switching-in-time transmission that allows TX identification at the RX side.

This chapter is organized as follows: Section 4.1 introduces the problem of MIMO channel measuring, describing the required signals, techniques and instrumentation to carry out this task. Section 4.3 presents the design steps for carrying out a SIMO channel characterization, from the generation of the signals to the estimation algorithm at the receiver side, including all kind of signal processing performed at the TX. In Section 4.4 we present the multiplexing and identification techniques to be able to extend the SIMO estimation procedure to MIMO. In Section 4.5, the implementation in our MIMO testbed is described. Also, we present the calibration steps and the optimal ranges and proper behavior of our MIMO estimation methodology. Moreover, the main features of the measurement campaign are described. Section 4.7 presents an example of the obtained MIMO channel measures and the possible parameters that can be extracted from that measures. Finally, in Section 4.10, the main conclusions are summarized.

## 4.1 Measuring the MIMO channel

Although theoretical studies may be of interest for channel characterization and system design, measurements in real scenarios are required in order to properly characterize the wireless channel and to validate the proposed channel models and/or algorithms [3GPP, 2013, Correia, 2006, WINNER, 2006, WINNER II, 2006]. During the last fifteen years, there has been a growing effort by the international community to study the wireless channels. Regarding MIMO systems, various equipments for measuring the MIMO channel have been developed and, as a result, substantial number of measurement campaigns have been carried out.

Different purposes may be devised in a measurement campaign, which also set the type of measurement system or testbed. Also, multiple features must be considered in the setup of a measurement campaign, such as type and number of antennas, polarization, frequency of operation, bandwidth or environment [Wallace et al., 2003]. The initial measurements for MIMO systems reported in the literature were aimed to characterize the radio channel: PDP, K factor for LOS situations, multipath characterization, etc., including multi-antenna and double-directional features as the spatial correlation [Weichselberger et al., 2006, Kermaol et al., 2000], for both narrowband and wideband cases. Some of these measurements were used to validate MIMO channel models or for the test of proposed algorithms and transceiver schemes. Finally, in recent years some system prototypes including MIMO features have been developed or are under development [i. Fábregas et al., 2006, Caban et al., 2006]. The evaluation of these prototypes provides the more complete but also the more complex system characterization, and is of great interest from the point of view of manufacturers and system designers.

Channel characteristics are fundamental in various respects: first, standards development must obey them to result in justified radio transmission technologies. Then, system design must be based on channel parameters that compactly describe the channel especially for channel simulation. Finally, performance assessment of candidate system prototypes again relies on valid channel parameters and realistic channel simulation. Therefore, a reliable channel characterization can be based only on appropriate channel measurements.

### 4.1.1 State of the art and background

The evolution of communications systems has dramatically increased the demand for wide-band measurements. In this section, we present different equipment along with a brief description of several techniques for measuring the MIMO channel.

To perform MIMO channel measurements there exist dedicated hardware such as channel sounders [RUSK, 2012, Kivinen et al., 1999b, Maharaj et al., 2008]. An outstanding example of this equipment is the RUSK system which allows measuring a maximum bandwidth of 240 MHz, which produces a 3.12 ns resolution. The system captures the signal with an eight bit 640 MHz analog to digital converter (ADC). It is capable of recording at a rate of 320 MB/s using four disk arrays in parallel controlled by a proprietary interface.

Commercial channel sounders still face up with several disadvantages:

- The rubidium clocks of the two units of the channel sounder are synchronized at the beginning of the measurements. However, after some time, the two rubidium clocks starts to diverge and the synchronization is lost. This will create a shift in the absolute delay of the measured impulse response.
- Multi-antenna channel sounders are bulky. This makes the practical organization of the measurement campaign difficult: trolleys must be used to move the channel sounder, narrow doors should be avoided, etc.

VNAs [Howard and Pahlavan, 1990, Molina-Garcia-Pardo et al., 2008], see Figure 4.1, can also be utilized for performing MIMO channel measurements. A vector network analyzer (VNA) is used to measure the transfer function of the radio channel in the frequency domain. The start frequency, stop frequency and the frequency steps can be adjusted. Using a VNA, we can measure the magnitude and phase of the forward transmission gain  $S_{21}$  as if we were exciting a test circuit (in this case the RF channel) with a single sine wave. This is repeated for a number of equally spaced frequencies within the bandwidth of interest. The advantage of using VNAs for channel sounding is that the measurement is very accurate, and that wide bandwidths can be measured. The disadvantage is that cables have to be used from the VNA to the TX antenna(s) and from the VNA to the RX antenna(s), which limits the range of the measurements. Also, due to the power loss over the cables, the dynamic range of the measurement setup is reduced.

Frequency domain channel sounding using VNAs has two major drawbacks. First, stepping a synthesizer over a large bandwidth in small steps is time consuming, and secondly, it is impossible to make mobile measurements due mainly in part to the strict timing reference requirements, which can be accomplished only through a wired system.

In summary, both channel sounders and VNAs are expensive equipment that are not usually available in research/development laboratories, mainly in signal processing ones where we carry out other experiments. The parameters that can be used for the measurement are more restrictive for a channel sounder than for a VNA.

Also, as presented in Chapter 3, the interest in MIMO techniques has led to a prolific work in MIMO equipment for measuring the wireless channel, often making use of testbeds. These testbeds [i. Fábregas et al., 2006, Caban et al., 2006, Ramírez et al., 2008] allow wireless transmissions, online processing and data storage.

MIMO channel sounding techniques [Thomä et al., 2005] can be classified in accordance with two criteria: the excitation signals that determine the characterization domain (time or frequency) and the multiplexing technique that allows for TX antenna identification.

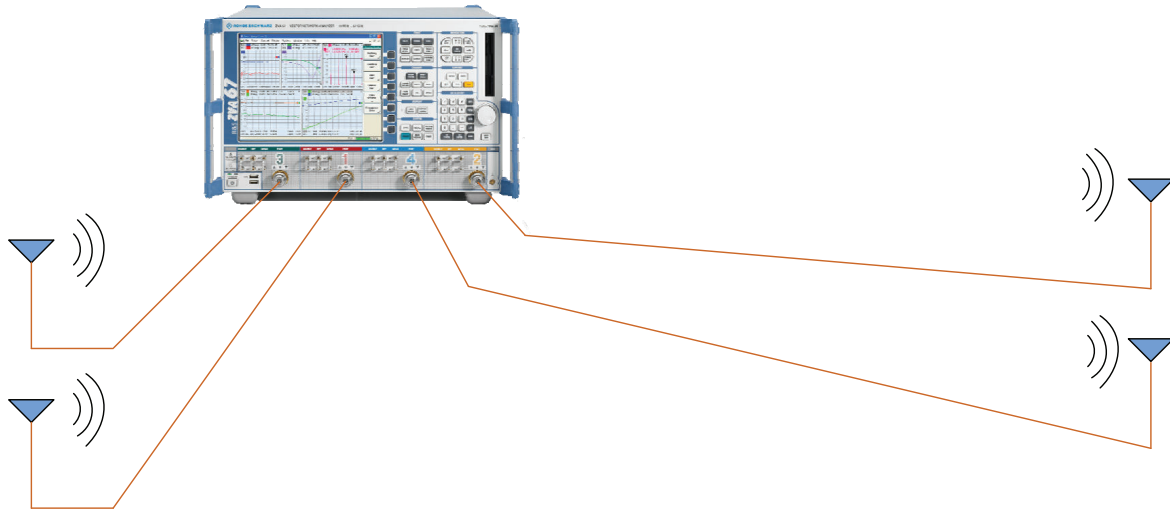


**Figure 4.1:** Vector Network Analyzer (VNA).

### Excitation signals

The excitation signal choice is a key aspect in channel sounding since it determines the following signal processing to be applied and has implications on the hardware. The first sounding experiments were carried out by using single-tone continuous wave (CW) signals. In this technique, the tones are stepped across a band of frequencies to measure the channel frequency transfer function. Large variations are then observed in the amplitude and phase of the received signal, these variations are a result of the random phase additions of signals arriving over many scattered paths. Through the years, models like Jakes [Jakes, 1994] have shown reasonable agreement with single tone measurements of the fading envelope.

As one can imagine, the tone stepping method is too slow for mobile channels. A faster alternative would be to perform a real-time frequency domain channel measurement by exciting all frequencies simultaneously and attempting to process and/or record the reception in real-time. There are two techniques available. The first one uses a swept frequency (chirp) signal instead of single tone stepping, but the frequency sounding is still sequential. The other uses a multi-tone signal and, at this time, the RUSK [RUSK, 2012] channel sounder is the best representative of this technique, which is also known as frequency domain correlation processing. For both techniques to work in mobile channels, they require at least real-time recording of baseband complex symbols.

This was sufficient as long as only the narrowband channel behavior was of interest. In order to achieve high delay resolution, sequential sounding [Baum et al., 2000] at a number of different frequencies was developed. Among the drawbacks, first, stepping a synthesizer over a large bandwidth in small steps is time consuming and, secondly, it is impossible to make mobile measurements due mainly in part to the strict timing reference requirements, which can be accomplished only through auxiliary wires (devoted to synchronization). On the other hand, it provides the best multipath resolution and very small storage requirements.

The pulse compression approach is well known from spread spectrum technology and makes these signals very useful for real-time identification of time-delay systems since all frequencies are instantaneously excited and a considerable signal-to-noise ratio (SNR) processing gain is achieved in the time domain by correlation. An example of these excitation signals are the periodic pseudo random binary sequences (PRBS) [Kivinen et al., 2001] or

pseudo random noise sequences (PRNS) [Peigang et al., 2004, Kivinen et al., 1999b]. They can be generated easily and they serve as broadband excitation signals. This is applied in the classical swept time-delay cross-correlation sounder implementation [Parsons, 2000]. The disadvantage of this principle, working sequentially, is again the long measurement time which prohibits real-time operations. Pulse compression using the chirp technique [Kemp and Bryant, 2004, Chung et al., 2005, Salous and Razavi-Ghods, 2004] has proven to be a powerful method for measuring the channel response since it avoids transmitter peak power limitations and offers excellent interference rejection capabilities. In general, the application of chirp signals for mobile radio channel characterization has always been limited by the capabilities of modern digital technology.

Finally, a flexible concept of excitation signals for measuring channel frequency response are multi-frequency signals [Thoma et al., 2000, Maharaj et al., 2005, Sakaguchi et al., 2002, Wirnitzer et al., 2001]. This approach is well known from frequency-domain system identification in measurement engineering. The advantage of this kind of signals is that channel frequency response can be measured at desired frequencies. These signals present high PAPR levels which can be reduced by numerical optimization. The difference in comparison to PRBS is that phases and magnitudes of Fourier coefficients can be arbitrarily chosen in order to optimize the system performance.

### Multiplexing techniques

A MIMO channel sounder measures the channel response matrix between all  $n_T$  antennas at the TX side and all  $n_R$  antennas at the RX side. This could be carried out by applying a parallel multiple-channel TX and RX. However, truly parallel systems are not only extremely expensive, but also inflexible (when considering changing the number of antenna channels) and susceptible to phase drift errors.

The resolution and capability of a channel sounder is determined by the choice of the hardware architecture and multiplexing strategy. There are three multiplexing schemes for MIMO channel measuring [Sakaguchi et al., 2002]: time division multiplexing (TDM), code division multiplexing (CDM) and frequency division multiplexing (FDM).

The aim of MIMO TDM is to distinguish the TX antennas as well as reducing complexity and cost. Multiple sequentially switched antenna arrays at both ends, denoted as fully-switched systems [Wirnitzer et al., 2001, Kivinen et al., 1999b], make use of a multiplexing unit that is used to step a single RF chain through all TX/RX antenna elements sequentially in time. In a semi-switched system [Peigang et al., 2004, Salous et al., 2005, Salous and Razavi-Ghods, 2004], receivers operate in parallel whereas a switching scheme is implemented at the TX. The use of parallel receive channels allows high resolution measurements of the radio environment without further reducing the effective sampling rate of the channel. This scheme is not suitable for real-time channel measurement and has some major drawbacks such as the requirement of precise synchronization between TX and RX and accuracy reduction during switching time. Figure 4.2 shows the switching time frame of a sequential MIMO sounder using antenna arrays at both sides of the link [Parsons, 2000]. Each rectangular block in the figure represents one period of the TX/RX signal. Synchronous switching at the receiver and TX is required in order to clearly assign the received signal periods to any input-output combination of the channel matrix.

Switching can be avoided using parallel transmitters and parallel receivers [Takada et al., 2001]. Clearly, the more elements that are used, the greater the requirement for using parallelism within the system. Moreover, the snapshot time (i.e. the time over all

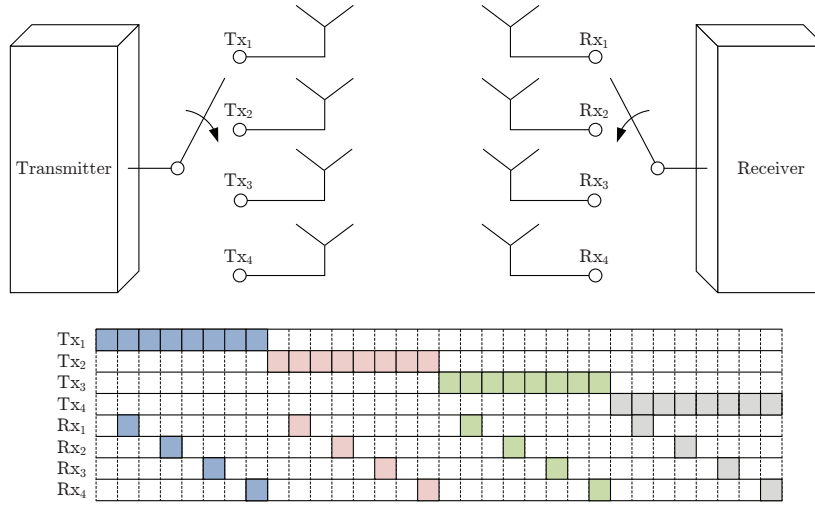


**Figure 4.2:** Fully-switched scheme.

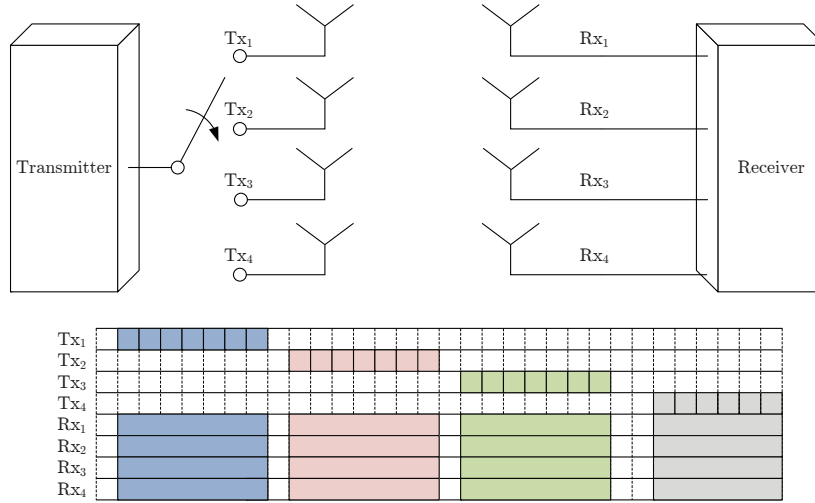


**Figure 4.3:** Semi-switched scheme.

temporal multiplexed channels) is significantly reduced if we compare with a fully-switched scheme. This approach supports FDM and CDM, each with different advantages/drawbacks. With FDM, a subset of the spanned frequencies are assigned to each antenna, thus they do not all characterize the channel at exactly the same frequencies. CDM will give excellent discrimination between antenna elements provided that a low correlation between codes is maintained within the channel being sounded. Unfortunately, as the channel is a multipath one, the cross-correlation between codes at non-zero delays is important.

## 4.2 Proposed scheme

Once we have gathered information regarding the different techniques and methodologies for measuring the MIMO channel we can decide which strategy to put in practise according to the available hardware. Given that we have a MIMO testbed in our laboratory and we can



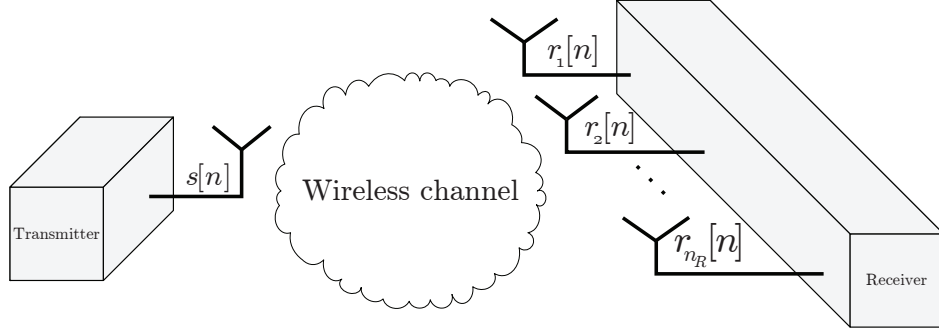


**Figure 4.4:** Measurement scheme for SISO channels.

not afford the expenses that acquiring commercial equipment entails, we use the testbed to measure the MIMO channel.

Our proposal involves the design of a semi-switched strategy, switching at the transmitter and parallel reception, regarding the multiplexing technique. For the excitation signals, we opt for frequency-domain system identification using multi-frequency signals. Concretely, complex exponentials are used.

The next section presents the SISO case and, subsequently, it will be extended to MIMO.

### 4.3 SISO channel measurement procedure

This section describes the procedure for measuring a SISO channel (see Figure 4.4). Firstly, we need to generate a robust signal with the objective of mitigating common issues such as local oscillator (LO) leakage, in-phase and quadrature (I/Q) imbalance and frequency offset. The signal generation and its optimization is presented in Subsection 4.3.1. After that, the received signal is stored and processed at the receiver applying the algorithm described in Subsection 4.3.2.

#### 4.3.1 Transmit signal design

Among the feasible signals to transmit in order to measure the MIMO channel, multifrequency probing signals are chosen due to their spectral flexibility, i.e. they allow any choice of test spectrum. The following lines describe the signal design in detail as well as the necessary steps to choose the right excitation parameters focusing the minimization of hardware effects.

From Figure 4.4 we define  $s[n]$  as a discrete signal of length  $N$  samples which consists of  $M$  complex exponentials placed at certain equally spaced frequencies,  $f_i$ :

$$s[n] = \sum_{i=1}^M A_i e^{j(\omega_i n + \phi_i)} \quad n = 0, \dots, N-1, \quad (4.1)$$

where  $\phi_i$  are the phases,  $A_i$  are the amplitudes and  $\omega_i$  are the frequencies

$$\omega_i = \frac{2\pi f_i}{f_s}, \quad (4.2)$$

where  $f_s$  is the sampling frequency.

The frequency domain representation of  $s[n]$ , i.e. the output of the  $N_{FFT}$  point discrete Fourier transform (DFT), can be written as

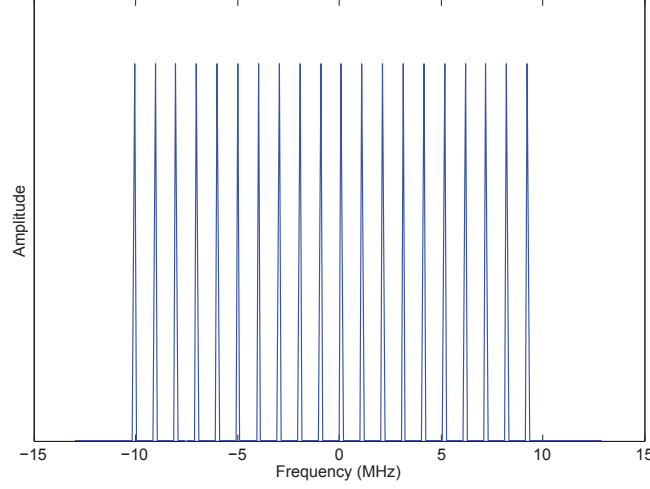


**Figure 4.5:** Example of exponential signals spectra,  $M = 20$ .

$$S[k] = A[k]e^{j\phi[k]} \quad k = \left[ -\frac{N_{FFT}}{2}, \dots, \frac{N_{FFT}}{2} - 1 \right]. \quad (4.3)$$

Figure 4.5 depicts an example of the spectra, for  $M = 20$  complex exponentials,  $f_s = 26$  MHz and  $N_{FFT} = 256$ .

This methodology is intended to be performed over a large variety of devices. Therefore, signal design must be carefully handled in order to avoid typical impairments that occur along the transmission chain. Examples from this are LO leakage, I/Q imbalance, etc. Since the methodology is based on the DFT, we impose several constraints:

**Constraint 1.** *Exponentials' frequencies must be lined up with DFT sampling, i.e.  $k_i = \frac{\omega_i N_{FFT}}{2\pi}$ , in order to make them orthogonal. That is,*

$$S[k] = \begin{cases} A_i e^{j\phi_i}, & \text{if } k = k_i \\ 0, & \text{otherwise.} \end{cases} \quad (4.4)$$

**Constraint 2.** *To ensure an equispaced channel excitation, the same separation among exponentials  $\Delta\omega_i = \text{constant}$  is chosen. In terms of used DFT bins spacing,  $\Delta k_i$ , this can be summarized as*

$$\Delta k_i = \text{constant} \quad \forall i. \quad (4.5)$$

**Constraint 3.** *In order to avoid the presence of the LO leakage, we impose*

$$S[0] = 0. \quad (4.6)$$

The phase and amplitude imbalance existing in the I/Q modulator besides I/Q branches imbalances introduced by filtering, amplifications and D/A and A/D conversions are considered as an effect called I/Q imbalance. This impairment has been presented in Chapter 3 Section 3.3.

**Constraint 4.** *A simple solution in order to avoid the impact of the crosstalk, when dealing with symmetrical exponentials, due to I/Q imbalance, is shifting the whole spectrum one DFT bin around the RF frequency in such a way that*

$$S[k] \neq 0 \Leftrightarrow S[-k] = 0. \quad (4.7)$$

It is obvious that, according to Constraints 1 to 4, the separation between used DFT bins must be an integer value fulfilling

$$\Delta k_i \in \left[ 3, \frac{N_{FFT} - 1}{M} \right]. \quad (4.8)$$

Furthermore, these constraints and other parameters such as the desired bandwidth to be measured,  $B$ , and the frequency resolution,  $\Delta f$ , determine the number of exponentials,  $M$ , and frequencies,  $f_i$ , to be chosen. As a drawback, this kind of multifrequency signals also leads to a large peak-to-average power ratio (PAPR) so, aiming at its reduction, the search of the optimal phases,  $\phi_i$ , must be performed.

**Number of exponentials ( $M$ ) and frequencies ( $f_i$ ) calculation** Two key design parameters of a frequency-domain channel measurement system are the bandwidth of interest,  $B$ , and the frequency resolution,  $\Delta f$ . Furthermore, other common limitations that come up from hardware are a predefined set of sampling frequencies,  $f_s$ , and a limited processing power (i.e. maximum affordable length of DFT),  $N_{FFT}$ .

Subsequently, algorithm 4.1, that calculates  $M$  and  $f_i$  considering  $B$ ,  $\Delta f$ ,  $f_s$  and  $N_{FFT}$  as input parameters, is described. This algorithm strictly fulfills the hard constraints imposed in Subsection 4.3.1 while trying to fit the soft constraints pointed out as input parameters.

**Input:**  $B, \Delta f, f_s, N_{FFT}$   
**Output:**  $M, \{f_i\}$

$$M = \left\lfloor \frac{B}{\Delta f} \right\rfloor$$

$$\Delta k_{min} = 3, \quad \Delta k_{max} = \left\lfloor \frac{N_{FFT}}{M} \right\rfloor$$

$$\Delta k' = \arg \min_{\Delta k_{min} \leq \Delta k \leq \Delta k_{max}} \left| \frac{\Delta k}{N_{FFT}} \cdot f_s - \Delta f \right|$$

**for**  $i = -\left\lfloor \frac{M}{2} \right\rfloor$  **to**  $\left\lfloor \frac{M}{2} - 1 \right\rfloor$  **do**

$$k_i = 1 + \Delta k'$$

$$f_i = k_i \frac{f_s}{N_{FFT}}$$

**end**

**Algorithm 4.1:** Developed procedure to obtain the number of exponentials,  $M$ , and their frequencies,  $f_i$ .

**Phases ( $\phi_i$ ) calculation** The choice of the proper signal phases tries to avoid an inefficient use of the dynamic range of the electronic devices due to a high PAPR. Power peaks derived from phase alignments may cause nonlinear effects <sup>1</sup> giving rise to intermodulation products

<sup>1</sup>It is important to differentiate between the nonlinear effects that affect the envelope of the signal, derived from e.g. the power amplifier (PA), up/down conversion, etc., from the ones that affect the I and Q of the signal, starting out in ADCs and DACs when saturation exists.

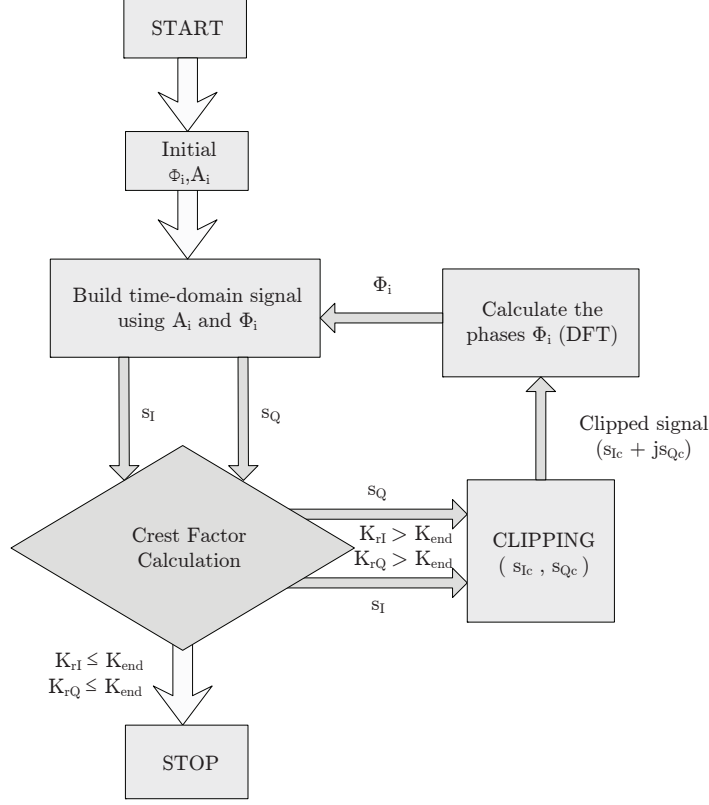


**Figure 4.6:** Block diagram of the phase optimization procedure and crest factor correction.

that can distort other exponentials. Low PAPR signals are distinguished by a flat time domain envelope.

This phase optimization is carried out by modifying a minimization algorithm [der Ouderaa et al., 1988] that relies on a mixture on clipping and phasing strategies. The goal of this modification is simultaneously minimizing the crest factor (square root of PAPR) of  $s[n]$  real and imaginary parts.

Therefore, considering the discrete signal  $s[n] = s_I[n] + js_Q[n]$  of length  $N$  and denoting as  $s_{Ipp}$  and  $s_{Qpp}$  the peak-to-peak amplitude of real and imaginary part respectively, we have the following definition for the real and imaginary crest factor

$$K_{rI} = \frac{s_{Ipp}/2}{2\sqrt{\frac{1}{N}\sum_{n=0}^{N-1} s_I[n]^2}} \quad K_{rQ} = \frac{s_{Qpp}/2}{2\sqrt{\frac{1}{N}\sum_{n=0}^{N-1} s_Q[n]^2}}. \quad (4.9)$$

Several closed-form expressions have been proposed to obtain the suboptimal phases for multifrequency signals. Newman phases [Boyd, 1986] will serve us as a starting point on our phase optimization procedure, which is depicted in Figure 4.6. The assigned initial phases and amplitudes to the  $i$ -th complex exponential (for both real and imaginary parts) are

$$\phi_i = \pi \cdot \frac{(i-1)^2}{M} \quad 1 \leq i \leq M. \quad (4.10)$$

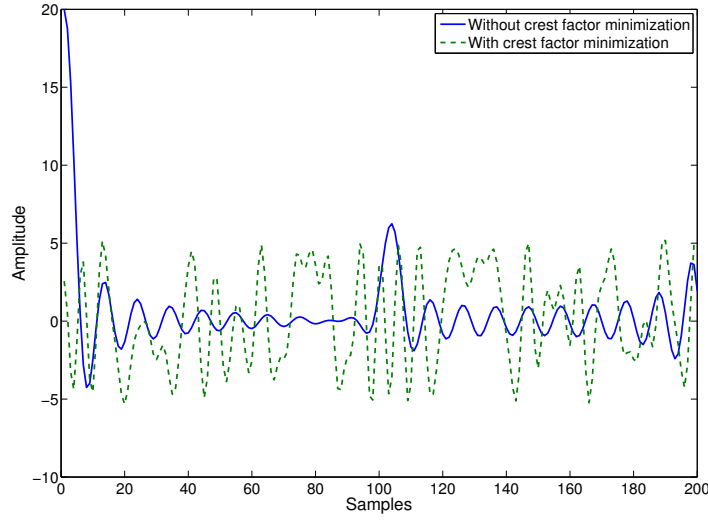


**Figure 4.7:** Comparison of the transmitted signal envelope before and after crest factor correction.

First, the time domain signal  $s[n]$  is built with the initial amplitudes and the Newman phases. Then, the crest factor calculation is performed. The real ( $s_I$ ) and imaginary ( $s_Q$ ) components are clipped ( $s_{I_c}$  and  $s_{Q_c}$  respectively) in the time domain to cut off the peaks. Subsequently they are combined and the DFT is performed to obtain the new phases,  $\phi_i$ , and amplitudes,  $A_i$ . This procedure is cyclically repeated until both real and imaginary crest factors are lower than a threshold ( $K_{r_I} < K_{end}$  &  $K_{r_Q} < K_{end}$ ). With few iterations, a quasi-optimal solution (a multifrequency signal with peak envelope around  $\sqrt{M}$ ) is obtained for signals with the same amplitude (peak envelope =  $M$ ). This fact is noticeable in Figure 4.7, where  $M = 20$ ,  $f_s = 26$  MHz and  $N_{FFT} = 256$ .

#### 4.3.2 Signal processing at the receiver side. IWPA algorithm

After generating the signal at the TX, we must prepare the receiver in order to acquire it through the receive antennas and estimate its amplitude, frequency and phase using the IWPA algorithm.

This algorithm is a high-accuracy non-parametric frequency estimation method based on the FFT. It is able to provide accurate frequency estimates even when the signals are not well separated in frequency (even less than  $1/T$ , where  $T$  is the observation time of the signal). At first it was intended for estimating the signal peaks obtained from the vibration analysis in rotative machines [Santamaría et al., 2000]. Here, it allows the amplitude, frequency and phase estimation of the received signals. Moreover, it has been modified in order to deal with complex exponentials instead of sinusoids. This method is able to reduce both the short- and long-range spectral leakage.

Since we do not intend to perform a physical synchronization by means of auxiliary cables or additional hardware (i.e. GPS disciplined oscillators), the signal processing at the receiver side must handle this issue in order to ensure a proper synchronization.

The received signals, according to Figure 4.4, can be expressed as

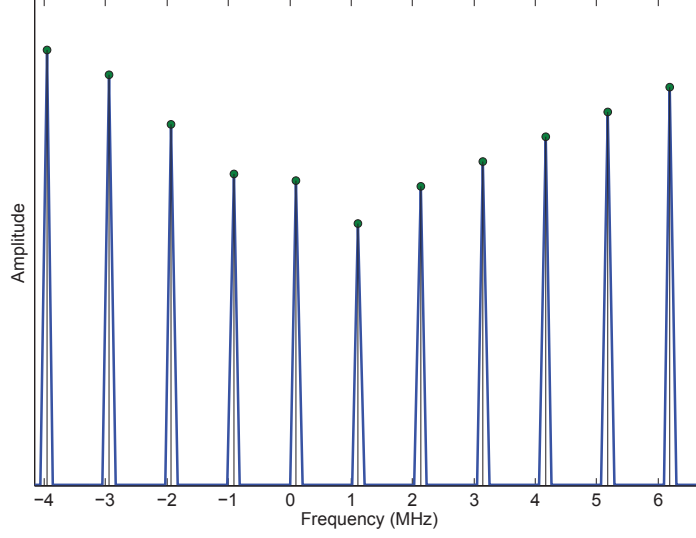


**Figure 4.8:** Received signal and IWPA estimation (zoomed area).

$$r[n] = \sum_{i=1}^N A'_i \cdot e^{j(\omega'_i n + \phi'_i)} + w[n], \quad (4.11)$$

where  $\omega'_i$  are the frequencies of the received signals,  $\phi'_i$  are the phases,  $A'_i$  are the amplitudes, and  $w[n]$  is Gaussian white noise.

First, the FFT is performed to obtain the spectrum of  $r[n]$ . The frequency of the received complex exponentials,  $\hat{f}'_i$ , is estimated as the frequency corresponding to the largest FFT output coefficient magnitude (coarse estimation) and a frequency interpolation of these results (fine estimation). Subsequently, a new complex exponential  $v[n]$  is generated

$$v[n] = e^{j\hat{\omega}'_i n}, \quad (4.12)$$

where  $\hat{\omega}'_i = 2\pi\hat{f}'_i/f_s$ . By means of the matched filter

$$\hat{h} = \frac{1}{N} \sum_{n=1}^{N_{fft}} v^*[n] \cdot r[n], \quad (4.13)$$

the amplitude  $\hat{A}'_i = |\hat{h}|$  and phase  $\hat{\phi}'_i = \arg(\hat{h})$  are estimated (see Figure 4.8). Once an exponential is detected, its contribution is subtracted from the initial spectrum and the procedure starts again. A key point of the IWPA method is that each time a new frequency is estimated, all previously computed frequencies, amplitudes and phases are reestimated.

From the quotient among the exponentials' complex values,  $\hat{A}'_i e^{j\hat{\phi}'_i}$ , and the transmitted ones,  $A_i e^{j\phi_i}$ , the frequency response of the channel,  $H(f_i)$ , is estimated. It is important to notice the advantages that this frequency estimation offers dealing with frequency offsets. These issues derive from a LO mismatch between TX and RX. The IWPA, since it is able to detect the higher received peaks, is able to correctly detect exponentials as well as to calculate the frequency offset. The use of this algorithm gets rid of developing any synchronization step between TX and RX equipment, causing lower equipment costs and more flexibility and simplicity at the time of carrying out field measurements.

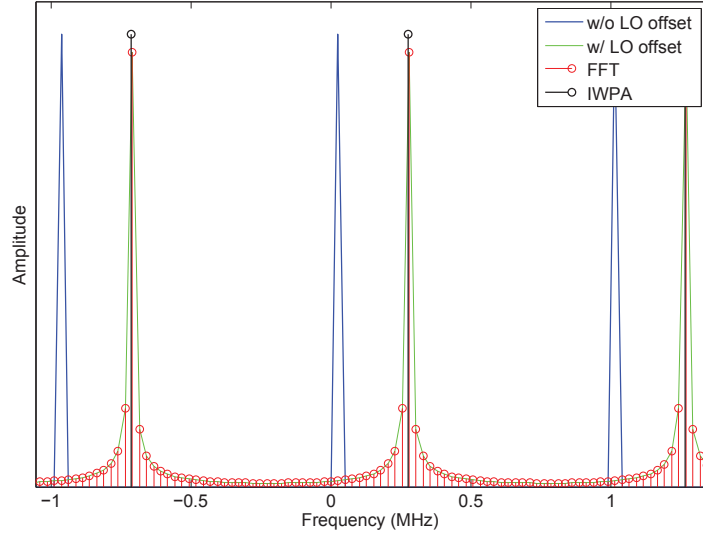


**Figure 4.9:** IWPA performance against LO offset.

As seen in Chapter 3, any transmission/reception using an RF front-end is troubled by impairments such as I/Q imbalance, that can be corrected using the constraints and calibration; and carrier frequency offset (CFO), which can be solved using auxiliary cables or using the IWPA algorithm. The CFO is simulated in order to check and compare the behavior of two frequency estimation algorithms: the proposed IWPA and the simple FFT.

A possible cause of error can be provoked by the LO offset or by doppler, the latter due to motion. We have tested our methodology against this impairment. In Figure 4.9 we analyze both FFT and IWPA performance against LO offset, realizing that IWPA outperforms FFT since it more precisely estimates each complex exponential. Concretely, IWPA is able to recover the original amplitude of the complex exponentials in any case. For these results we consider  $M = 20$ ,  $f_s = 26$  MHz and  $N_{FFT} = 1024$ . It is important to point out that, as the  $N_{FFT}$  value decreases, the performance of the FFT gets worse.

## 4.4 Extension to MIMO channels

Once the methodology for measuring SIMO channels has been described, the next step involves dealing with a MIMO scheme. To that end, we follow the same procedure described in Section 4.3 as many times as the number of TX antennas. A switching in time algorithm is proposed for multiplexing the transmissions along with a transmitter identification technique to correctly label them.

### 4.4.1 Multiplexing technique

This procedure is based on the idea of sequential sounding, following a semi-switched strategy. An orthogonal transmission must be carried out in order to identify each TX antenna at the RX nodes. Regarding this issue two schemes are studied: a frequency-orthogonal transmission technique and a time-orthogonal transmission technique [Molina-Garcia-Pardo et al., 2008]. The former involves that each TX antenna uses its own orthogonal set of frequencies to transmit the probe signal. The latter alternates the transmission of  $s[n]$  and zeros in or-

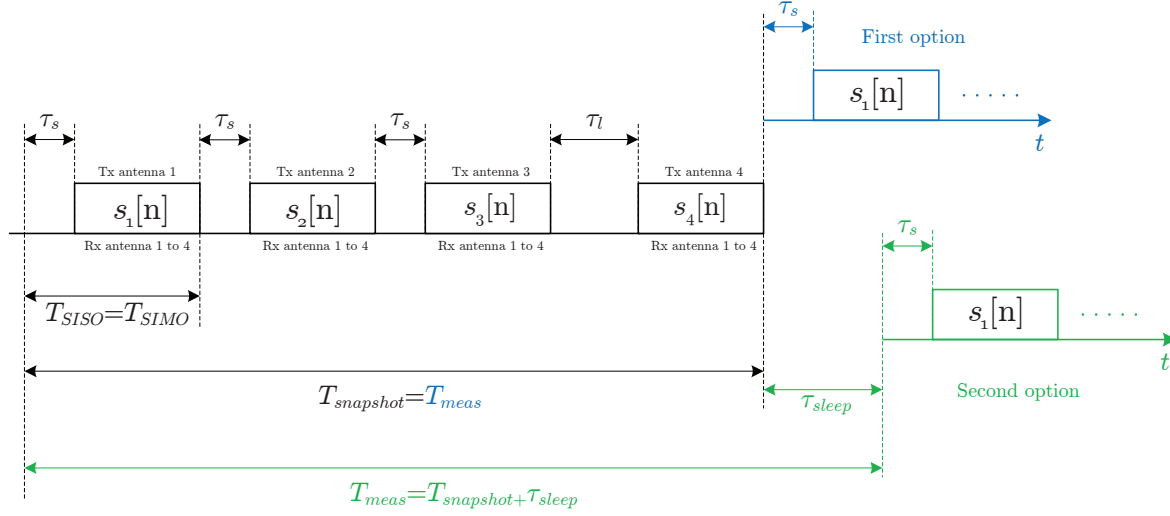


**Figure 4.10:** Time diagram representing the transmission/reception scheme for our  $4 \times 4$  antenna configuration.

der to produce orthogonal transmissions in time. The time-orthogonal alternative is finally developed due to its simplicity.

Figure 4.10 represents the transmission diagram of our semi-switched scheme for a  $4 \times 4$  antenna configuration. The transmitted signal through antenna 1 is denoted as  $s_1[n]$ , the transmitted through antenna 2 denoted as  $s_2[n]$ , etc. The fact of utilizing parallel receivers provokes that the necessary time for measuring a SISO channel coincides with the time necessary to measure a SIMO channel,  $T_{\text{SISO}} = T_{\text{SIMO}}$ . The overall time required to estimate the MIMO channel is denoted as  $T_{\text{snapshot}}$ .

This idea is the base for the TX identification procedure (see 4.4.2). The guard intervals,  $\tau_s$  and  $\tau_l$ , are the key point to solve this issue.

Our system is able to transmit the sequence depicted in Figure 4.10 one after another (MIMO channel snapshots estimated consecutively) which means that the time among measurements,  $T_{\text{meas}}$ , is the same as the duration of the snapshot,  $T_{\text{meas}} = T_{\text{snapshot}}$ . It is also possible to introduce 'no transmission' gaps among sequences,  $T_{\text{sleep}}$ , which means that the measurement time will be  $T_{\text{meas}} = T_{\text{snapshot}} + T_{\text{sleep}}$ .  $T_{\text{sleep}}$  is a time interval defined by the user (e.g. any pause or sleep time). This interval allows changing the measurement time, thus affecting Doppler performance, etc.

#### 4.4.2 Transmitter identification

As stated at the beginning of this section, the second objective of the extension to MIMO channels is to identify the signals at the receiver that correspond to the adequate TX. To this end, we insert different guard intervals among the transmissions in a way that we can, by means of an energy detector, identify one of the transmitters (the one with the largest guard interval).

Concretely, being  $n_T$  the number of transmit antennas, the strategy carried out to identify each one is based on prepending  $n_T$  small guard intervals  $\tau_s$  before each antenna transmission, being the last one  $\tau_l > \tau_s$  (see Figure 4.10).

At the receiver we must ensure the presence of  $n_T$  complete signal blocks in the received signal  $r[n]$ , as shown in Figure 4.11.



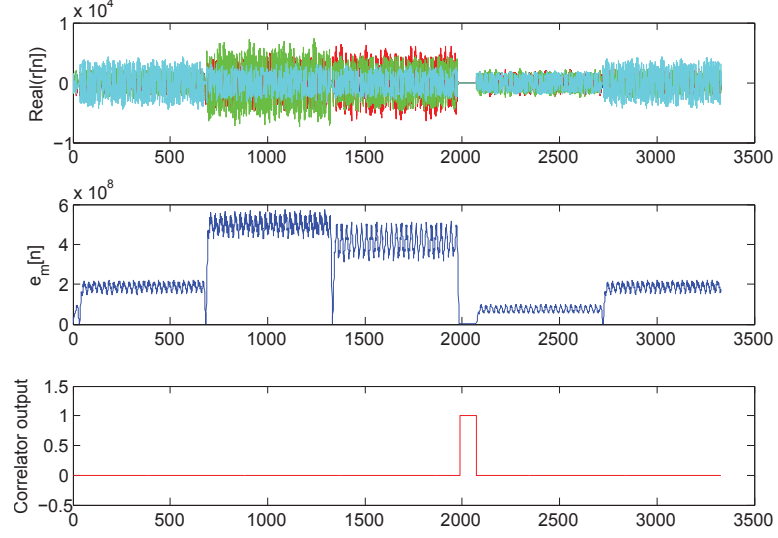


**Figure 4.11:** Transmitter identification: a) Received signal, b) Energy signal, c) Correlator output.

The energy signal,  $e[n]$ , is built from the sum of the energy of each received signal  $r_i[n]$  by the  $n_R$  receive antennas

$$e[n] = \sum_{i=1}^{n_R} |r_i[n]|^2. \quad (4.14)$$

To detect the energy, the signal  $e[n]$  is fed into a moving average (MA) filter of  $L_m$  equal coefficients.

$$e_m[n] = e[n] * h_m[n] \quad \text{where} \quad h_m = \begin{cases} 1 & 0 \leq n \leq L_m - 1 \\ 0 & \text{otherwise} \end{cases} \quad (4.15)$$

We can now locate the center of the largest guard interval by correlating the energy with a pulse of length  $\tau_l$ . Once we have identified it, knowing the transmission order, we can correctly label the transmissions as depicted in Figure 4.12, and apply  $n_T$  times the SIMO methodology described in Section 4.3. It is marked in Figure 4.12 with stars the start of the signal blocks which are obtained with the identification method. As explained previously, between TX3 and TX4 the signal level is lower than among the other TX blocks.

## 4.5 Implementation in GTAS MIMO testbed

Once we have described the methodology in Section 4.4, and the hardware in which it has been implemented (see details in Chapter 3), we address the setup and the measurement procedure for measuring a  $4 \times 4$  MIMO channel using our testbed. As stated previously, this methodology can be implemented in any system that consists of BB boards with DPUs and RF capabilities. In this case, we present the necessary steps and particularities of running it in our MIMO testbed. Subsequently, in order to illustrate the proposed methodology performance, a measurement campaign is carried out in an indoor environment. Once the MIMO channel frequency response,  $\mathbf{H}(f)$ , is obtained, a set of parameters can be extracted.

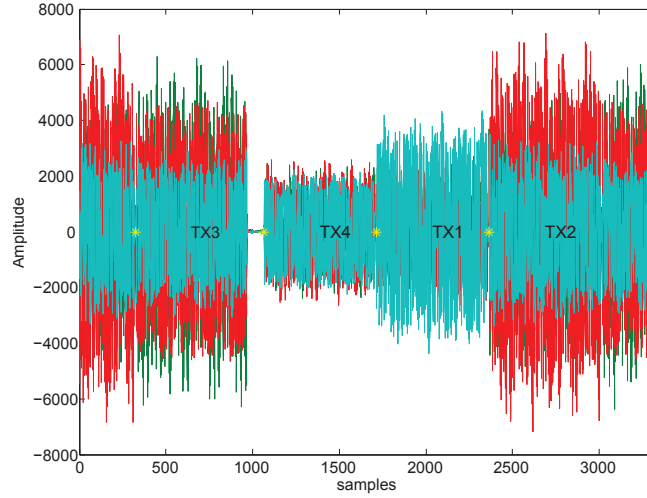


Figure 4.12: Transmitter labeling.

#### 4.5.1 Description of Measurement Setup

Figure 4.13 presents the testbed block diagram of two of the nodes of the GTAS MIMO testbed. Although the MIMO channel can be measured from one node to several (multiuser scenario), in this section we present the results using one node as the TX and another one as the RX. We must point out that only one board per node is used; the TX uses its DAC board and the receiver its ADC board.

We first generate in Matlab the signal at the TX and then, after the signal conditioning steps presented in Section 4.3.1, we transmit the signals through the four transmit antennas. Before transmission we must perform a necessary calibration in order to compensate the responses of the transmit branches (see Section 4.5.2).

Logically, the implementation of the methodology in a MIMO testbed is constrained by the limitations that it imposes. These limitations are:

- Number of TX and RX antennas limited to 4, although it is extendable to 8.
- Maximum 20 MHz bandwidth in BB.
- Sampling frequencies of 52 MHz and 104 MHz, even though interpolation and decimation are feasible (as outlined in Chapter 3).
- Carrier frequency among the ranges  $f_c \in [2.4, 2.5] \cup [4.9, 5.875]$  GHz.
- Size of the FFT,  $N_{FFT}$ , constrained by the available memory.

The TX uses the VHS-DAC board to playback the signals. The FPGA of this board is programmed in such a way that it uses a sampling frequency of 26 MHz (with interpolation by a factor of 2 within the FPGA), being able to playback the signals through 8 channels (I and Q of the 4 transceivers). The RX uses the VHS-ADC board to acquire the signals at a rate of 26 MHz (with decimation by a factor of 2 within the FPGA).

#### 4.5.2 System calibration

An essential part for the proper behavior of the methodology, once we aim at its implementation, is to determine an efficient calibration process. To separate the actual channel response from circuitry effects, a back to back system calibration procedure must be performed by

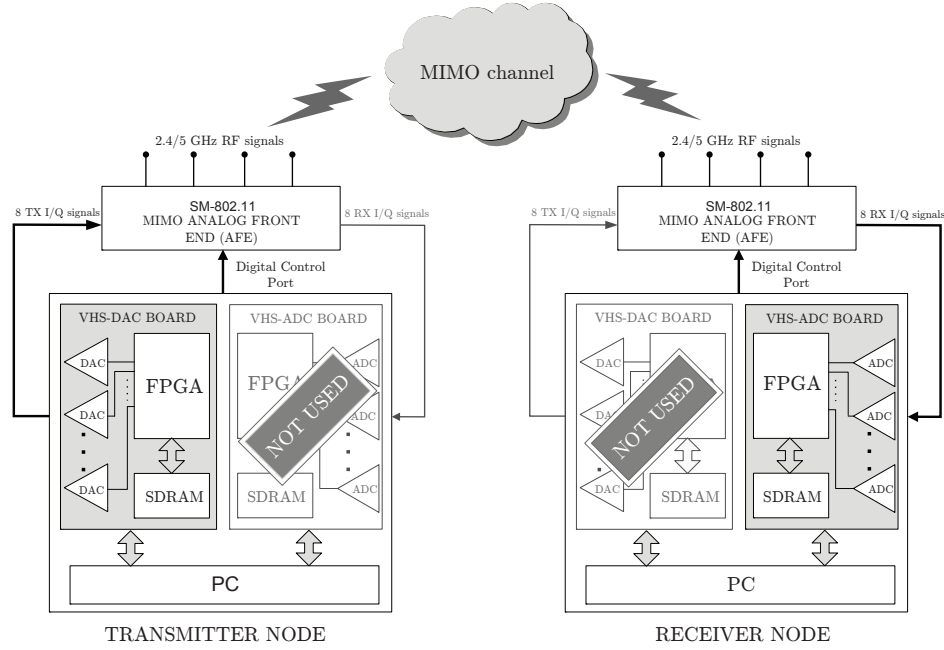


**Figure 4.13:** Block diagram of the  $4 \times 4$  MIMO testbed. Transmitter node (left) only using DAC board and receiver node (right) only using ADC board.

means of a cable connecting in pairs every TX and RX antenna. This aims at ensuring that the TX and the RX frequency response are removed from the measured data.

First, our objective is to realize how the impairments of the TX and RX chain affected the measurements. To that end, as an example, the transmit antenna 1 of the TX node is connected using a cable to a spectrum analyzer. Subsequently, we transmit  $M = 20$  complex exponentials with a flat spectrum (low PAPR). The frequency response is represented at the spectrum analyzer and gives an idea of the frequency response of the transmit chain (RF circuitry, BB filters, DAC, etc.) for the TX antenna 1. Figure 4.14 shows the setup and the resulting complex exponential in the spectrum network analyzer for this initial test.

### Back to back calibration

The previous measurements show that a back to back calibration is mandatory. This can not be carried out with an spectrum analyzer since the phase also plays a role. So, we connect each TX transceiver to each RX transceiver using auxiliary cables (for a total of 16 SISO combinations). Then, we transmit the low PAPR signal (fulfilling the constraints) and we estimate the frequencies, phases and amplitudes of the received signals using the IWPA algorithm. Hence, the obtained 16 frequency responses correspond to the frequency response of the 16 TX and RX chains, respectively.

In summary, the procedure is as follows:

- Generate in Matlab complex exponentials with low PAPR, which frequency response is  $\mathbf{X}(f)$ .
- Transmit through cables towards the receiver.
- Estimate at the receiver, using the IWPA, the amplitudes, phases and frequencies of the received exponentials. We get the receive frequency response,  $\mathbf{Y}(f)$ .

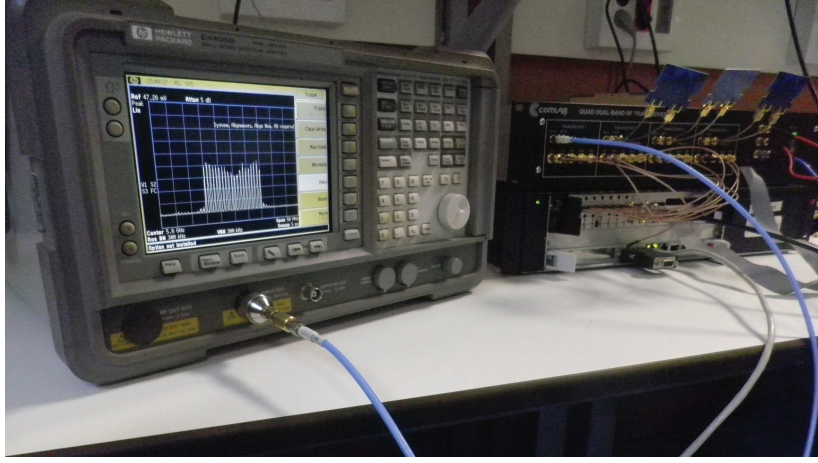


**Figure 4.14:** Setup for compensating the hardware.

- Calculate the actual physical channel between the TX and the RX as

$$\mathbf{H}_{cal}(f) = \frac{\mathbf{Y}(f)}{\mathbf{X}(f)} \quad (4.16)$$

### Preparation for measurements

After back to back calibration, we need to know how to procedure if we want to carry out channel measurements. The next steps need to be followed:

- Generate complex exponentials in Matlab fulfilling the constraints outlined in Section 4.3.1. Their frequency response is  $\mathbf{X}(f)$ .
- Transmit these signals through the MIMO channel and acquire them at the receiver.
- Perform the IWPA algorithm to obtain the frequency response of the receive signals,  $\mathbf{Y}(f)$ .
- The true channel frequency response is obtained using

$$\mathbf{H}_0(f) = \frac{\mathbf{Y}(f)}{\mathbf{X}(f)\mathbf{H}_{cal}(f)} \quad (4.17)$$

### 4.5.3 System validation

This subsection aims at analyzing the optimal operation range of the methodology when it is implemented in our GTAS MIMO testbed. Figure 4.15 represents the setup for carrying out this validation between transmit antenna 1 and receive antenna 1. This must be done for the rest of the combinations. Each TX/RX antenna combination is connected by means of a cable and a 35 dB attenuator. This value is selected to avoid ADCs saturation for a transmit power of 0 dBm, and with maximum low noise amplifier (LNA) gain at the receiver and a VGA mid-range value.

As an example of the range that we can cover with this testbed, we calculate in free space according to Friis formula for a loss exponent of 2, the propagation losses,  $L(\text{dB})$ , as

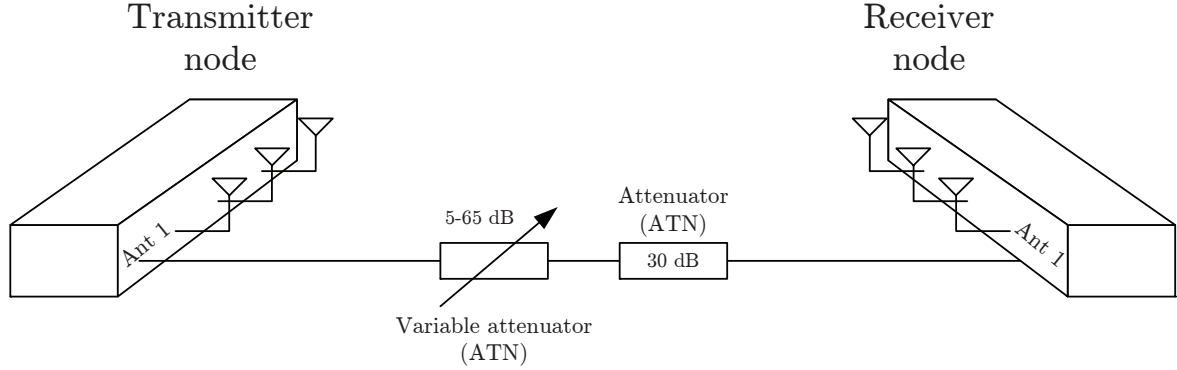


**Figure 4.15:** Precision measurement setup.

$$L(\text{dB}) = 20 \cdot \log(d(\text{Km})) + 20 \cdot \log(f(\text{MHz})) + 32.5 \quad (4.18)$$

where  $d$  represents the distance in kilometers and  $f$  the carrier frequency in  $\text{MHz}$ . For an attenuation of 35 dB, the separation distance for transmitter and receiver is calculated as

$$d = 10^{\frac{L(\text{dB}) - 20 \cdot \log_{10}(f(\text{MHz})) - 32.5}{20}} \approx 25 \text{ cm}. \quad (4.19)$$

### Precision

We consider an attenuation of 35 dB as the mean value returned by 1000 executions of the IWPA algorithm when transmitting a power of  $-7 \text{ dBm}$  (minimum power). The uncertainty with a 95% confidence level for that mean is 0.37 dB. Regarding the FFT algorithm, these values are 36.71 dB and 0.74 dB respectively. The linear estimated amplitude of the data is assumed to be Gaussian distributed. These same results are obtained when TX and RX are placed 1, 5 and 10 meters apart.

Following along the same lines, relating attenuation to distances to evaluate system precision, we vary the attenuation from 35 to 105 dB (in steps of 10 dB) which approximately results in distances from 25 cm to 800 m. This experiment allows to compare the precision of both algorithms, FFT-based frequency estimation and IWPA, under different SNR conditions. Also, this evaluation is useful for determining their optimal operating ranges.

When simulating a wireless channel with cables and attenuators, the achievable isolation between TX and RX will often limit the calibration precision at high attenuation values. This is due to the fact that power reaching the receiver through spurious radiation might dominate over the attenuated power transmitted by the cables, when the attenuation is large enough. In this case, this aspect is verified and the separation among nodes as well as the careful shielding measurements ensures no spurious radiation, hence the precision is not affected.

The experiment results are depicted in Figure 4.16. As can be seen, when transmitting with a power of  $-7 \text{ dBm}$ , uncertainty noticeably grows up beyond 75 dB, being equivalent to 25 meters of separation. That means that the optimal operation range covers from 35 dB and 75 dB of attenuation. Increasing the transmit power shifts both curves to the right which enlarges the operating range the same quantity (e.g. additional 16 dB, from 35 dB to 91 dB, can be obtained by changing the transmitted power from  $-7$  to  $9.6 \text{ dBm}$ ). This last value ensures avoiding the presence of nonlinearities. In summary, the overall range in meters varies

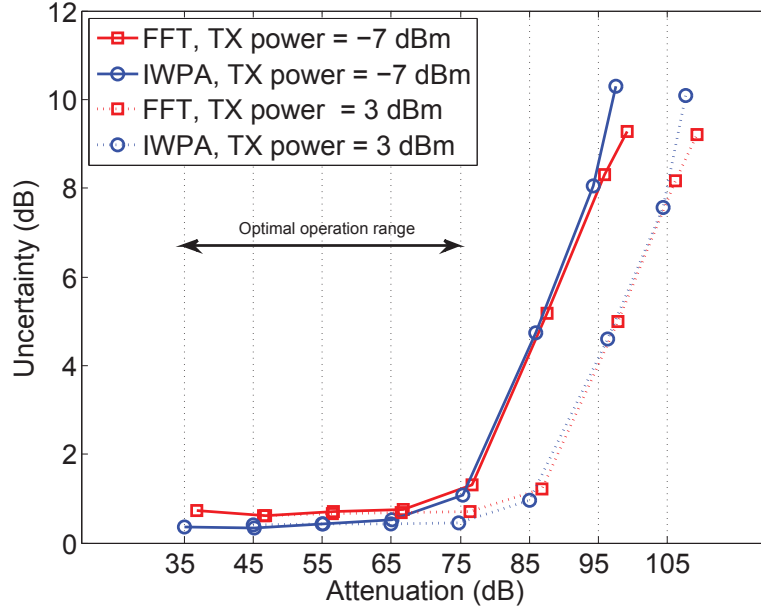


**Figure 4.16:** Precision and operating range of the estimation methods used at the receiver: FFT and IWPA.

from 0.25 m to 250 m. Figure 4.16 also justifies the use of IWPA since it outperforms FFT in terms of uncertainty within the optimal operation range, as stated previously.

### Accuracy

In order to show how realistic the system behaves, i.e. we want to compare the real channel with the one measured with our system, we should compare it with any commercial measurement equipment. We validate the proper behavior of our measurement system considering a wired SISO scheme. The additional instrumentation to perform the validation involves an Agilent N3383A programmable network analyzer (PNA) with a frequency range from 300 kHz to 9 GHz and a passive filter. We consider a bandwidth of 20 MHz.

First, we calibrate both systems; our measurement system carrying out a back-to-back calibration using a cable, and the PNA using the same cable along with the calibration kit. Then, we connect a passive filter to the PNA ports and we measure its  $S_{21}$  (forward transmission) parameter sweeping the frequency from 5 to 5.6 GHz. This parameter is depicted in Figure 4.17.

We choose a 20 MHz representative window of the  $S_{21}$ . This window is centered at  $f_{RF} = 5.328$  GHz. The measure consists of 6401 points with 10 KHz separation. We connect the filter using the same cables from the transmit node to the receive node of our measurement system and we run our methodology. Subsequently, at the same RF frequency, we measure the filter response with our system. The results from both measurement setups are depicted in Figure 4.18, showing that the proposed measurement system accurately reflects reality. Since the measurement systems are calibrated, the vertical axis represents the attenuation (in dB) introduced by the filter.

Another figure of merit to evaluate the accuracy of our methodology is to estimate the SNR in the channel measures as the average ratio of the received power from the transmitted signal versus the noise in the system. This parameter is deterministic and quantifies the

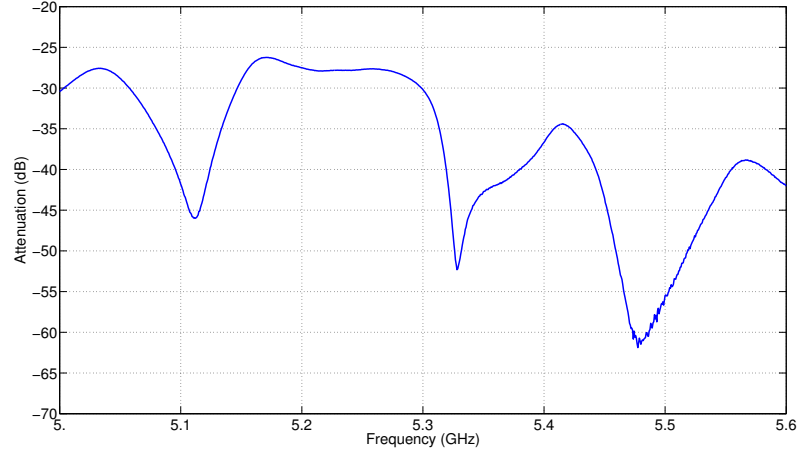


**Figure 4.17:** Frequency response of the bandpass filter.

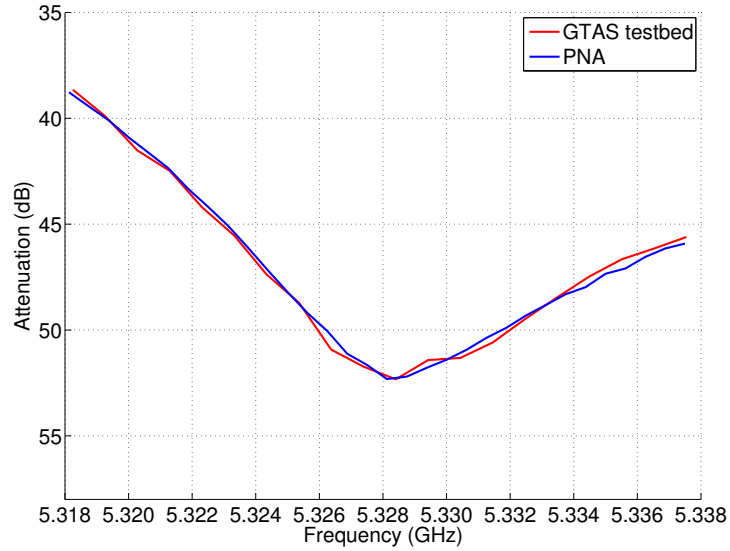


**Figure 4.18:** Comparison of the  $S_{21}$  parameter using our technique and the results from the PNA.

quality of the channel. The noise figure of the receiver and the received signal level at each antenna are the main parameters that determine the value of the SNR.

We depict in Figure 4.19 100 measures of the actual physical channel,  $\mathbf{H}_0$ , obtained in our lab. These channel realizations are measured along 90 seconds.

To illustrate the performance of the channel measurement methodology, we present in Table 4.1 the estimated signal-to-noise ratio (SNR) of the channel measures in Figure 4.19. Due to the precise calibration, we then take for granted that the center point of each cloud is the actual value of the channel. Therefore, the SNR (in dB) is calculated as the inverse of the variance of these group of points.

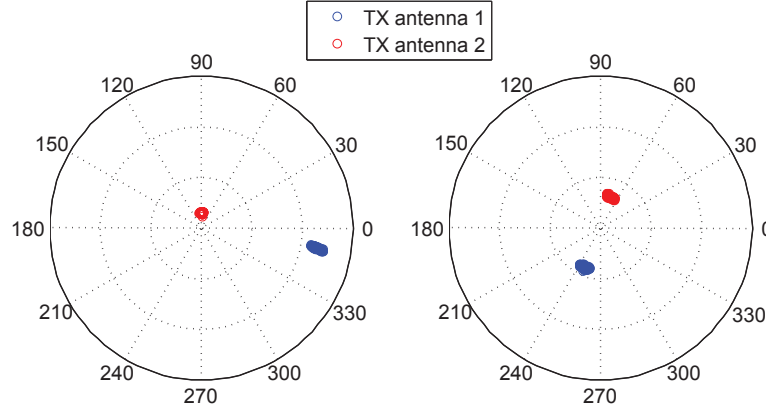


**Figure 4.19:** MIMO  $2 \times 2$  channel measures. Left: Receive antenna 1, right: Receive antenna 2.

	$h_{11}$	$h_{21}$	$h_{12}$	$h_{22}$
SNR (dB)	28.8073	22.3865	22.5993	21.7302

**Table 4.1:** Performance results: measurement of  $\mathbf{H}_0$ .

The obtained values confirm the great performance of the methodology. We assume that the noise figure at the different RX antennas is the same, as well as the estimation error in all cases. Therefore, the highest SNR values correspond to the channels with highest amplitude.

## 4.6 Comparison with other channel sounders

A performance comparison among different channel sounding schemes and the one we are referring in this dissertation is presented in Table 5.2. As can be expected, these sounders outperform ours by achieving a higher measured bandwidth (better time resolution), a better frequency resolution and higher storage capacity. However, the use of a MIMO testbed to implement the proposed methodology involves a cheaper solution besides reducing the complexity since synchronization between nodes is not needed. For more details regarding parameter calculations see Appendix A.

## 4.7 Experimental results

Once the measurement system is perfectly characterized and calibrated, we are ready to use the GTAS MIMO testbed along with the presented methodology to measure wideband MIMO channels.

A series of measurements are carried out with different purposes. On one hand, low-mobility scenarios are considered as the straightforward way to present an example of channel measures. On the other hand we make use of the concept *nomadic* which refers to a series of low-mobility measurements carried out in different positions within a local area. This kind

<sup>4</sup>Results of Doppler bandwidth ( $D_B$ ) have been obtained using the expression:  $D_B = \frac{K}{T_{SISO} \cdot n_T \cdot n_R}$  for fully-switched configurations and  $D_B = \frac{K}{T_{SISO} \cdot n_T}$  for semi-switched configurations, where  $K = 1$ .



	GTAS	HUT	MEDAV RUSK	Durham
Frequency RF (GHz)	2.4, 5	2.145, 5.3	1.8-2.5, 5-6	1.9, 2.1
Maximum antenna matrix ( $n_R \times n_T$ )	4x4	32x32	8x8	8x8
Multiplexing scheme	Semi-switched	Switched	Switched	Semi-switched
Excitation signal	Multitone CW	PRNS	Multitone CW	<i>chirp</i>
Synchronization	Not needed	Rubidium	Rubidium	Rubidium
SISO measurement time $T_{SISO}$ ( $\mu s$ )	24.6	8.5	6.4	78
Doppler 4 Bandwidth (Hz)	10163	115	2441	1602
Maximum scatterer velocity (Km/h)	45	57.9	60	56.84
Bandwidth de (MHz)	20	100	120	300
Time resolution (ns)	50	10	8.3	3.33

**Table 4.2:** Comparison of channel sounders: the one we are proposing in this paper (GTAS), the one developed at Helsinki University of Technology (HUT) [Kivinen et al., 1999a], the MEDAV RUSK [RUSK, 2012] and the one developed at Durham University (DURHAM) [Salous et al., 2005].

of measurements will allow us to spatially average the measurements, which is quite useful to obtain certain channel characteristics.

For performing all these measurements, we consider a 5.33 GHz carrier frequency and  $B = 20$  MHz bandwidth. The frequency separation between two consecutive exponentials is  $\Delta f \approx 1$  MHz and we consider a  $f_s = 26$  MHz sampling frequency and  $N_{FFT} = 256$  DFT points. In fact, the procedure described in Subsection 4.3.1 outputs  $M = 20$  exponentials separated  $\Delta f' \approx 1.015$  MHz. That means that the covered bandwidth extends from  $-9.95$  to  $9.34$  MHz around the carrier frequency.

#### 4.7.1 Description of Measurements Scenarios

Figure 4.20 shows the layout of the measurement site in the GTAS lab at the University of Cantabria. The laboratory is furnished with office equipments: tables, cabinets, PCs and seats. Three scenarios are analyzed keeping fixed the receiver (RX in Figure 4.20). The transmitter is placed in three locations. In the first one, TX 1 in Figure 4.20), the transmitter is placed 3.5 meters away from the receiver, with a clear line-of-sight (LOS) between them. In the second one, the transmitter (TX 2 in Figure 4.20) is located further away from the receiver ( $\approx 12$  meters) avoiding a clear LOS. In the third experiment, the transmitter (TX 3

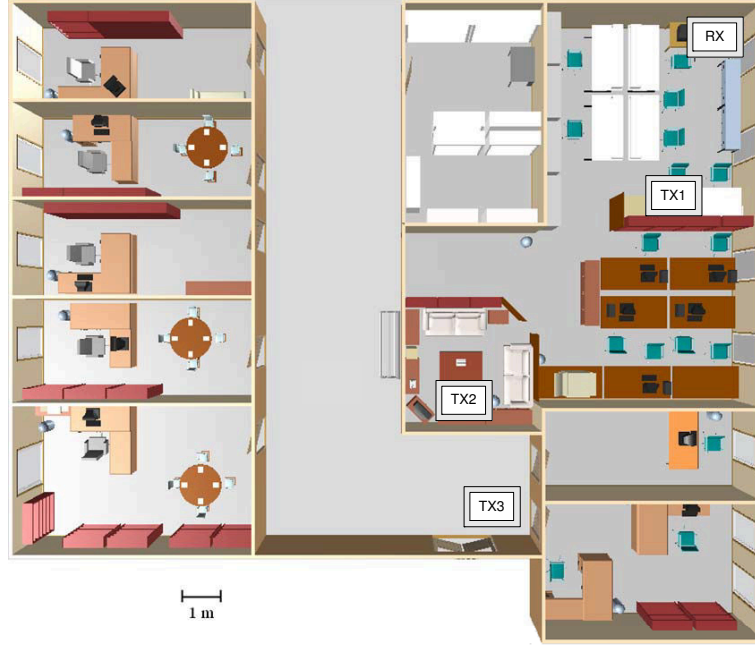


**Figure 4.20:** Node locations of the different experiments conducted at the laboratory of the Advanced Signal Processing Group (GTAS).

in Figure 4.20) is placed out of the lab in the middle of the corridor. The transmitted power ranges from  $-7$  dBm to  $9.6$  dBm depending on the transmitter location.

As briefly explained previously, two different environments are considered, depending on the mobility. In a low mobility environment the transmitter is kept fixed at each location during each experiment. In the second environment, measures are taken by moving the transmitter within a small local area (e.g.  $900 \text{ cm}^2$ ) among experiments but stood still during them, so, no Doppler effect exists due to movement. This is usually referred to as a nomadic scenario, whose aim is to obtain a statistical analysis by averaging the obtained measures in space. Therefore, we can carry out, e.g. a correlation study as well as obtaining the wideband parameters.

#### 4.7.2 Low-mobility measurements

Low mobility measurements are carried out to study the time variability of the channel at the different transmitter node locations. It is important to point out that neither people nor scatterers are hanging around within the lab when conducting the measurement campaign. As an example, the MIMO channel frequency response at position 1 is depicted in Figure 4.21, considering  $T_{meas} = 100 \text{ ms}$  and  $\tau_{sleep} \approx T_{meas} - n_T \cdot T_{SISO} = 100 \text{ ms} - 4 \cdot 24.6 \text{ us} = 99.9 \text{ ms}$ , hence the 11 curves representing each SISO channel.

As can be seen, these 11 curves are almost perfectly overlapping and cannot be individually resolved in the presented graphs. Therefore, we can state that in our lab, the MIMO channel can be considered time-invariant when the environment is static.

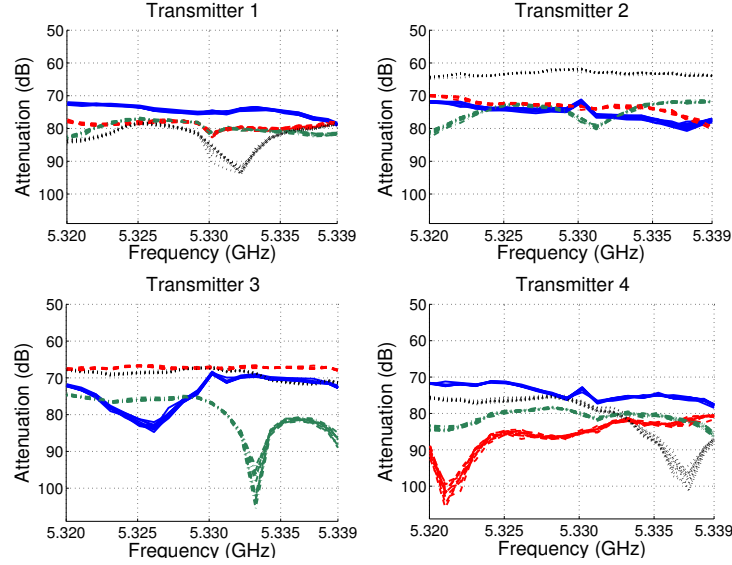


**Figure 4.21:** MIMO channel frequency response measured at position 1 (see Figure 4.20) in a low mobility environment. 11 curves for each SISO channel are represented.

### 4.7.3 Nomadic measurements

Stochastic channel characterization has great implication on wireless communication system design. Therefore, we carry out several MIMO channel measurement campaigns in a nomadic scenario, using the proposed multifrequency methodology. From these results we expect to obtain parameters derived from the statistic characterization that offers this kind of scenario. TX and RX nodes are placed at locations TX2 and RX according to Figure 4.20. For all the experiments, we cover a 20 MHz bandwidth (20 exponentials are used) at the frequency of 5.6 GHz.

#### MIMO channel histograms

Figure 4.22 shows the histogram representing the absolute value of MIMO channel. These results come from 10000 realizations obtained with the RX in different positions. As expected, the histogram follows a Rayleigh distribution. This is because of, although node separation is relatively low, there not exist a predominant direct ray.

#### Wideband parameters estimation

To obtain wideband MIMO channel parameters, we conduct a series of measurements according to the transmit and receive node locations. Let us consider a nomadic environment in order to obtain wideband parameters: coherence bandwidth,  $B_c$ , and delay spread,  $\sigma_\tau$ . The three transmitter locations are considered to make the wideband parameters comparisons by varying certain parameters such as transmitting and receiving node separation, object reflections, LOS/NLOS conditions, etc.

In a general manner, from  $\mathbf{H}$  we can obtain the normalized frequency autocorrelation function,  $\mathbf{R}_h$ , according to 2.21, as

$$\mathbf{R}_h(\Delta f) = E [H(f) H^*(f - \Delta f)]. \quad (4.20)$$

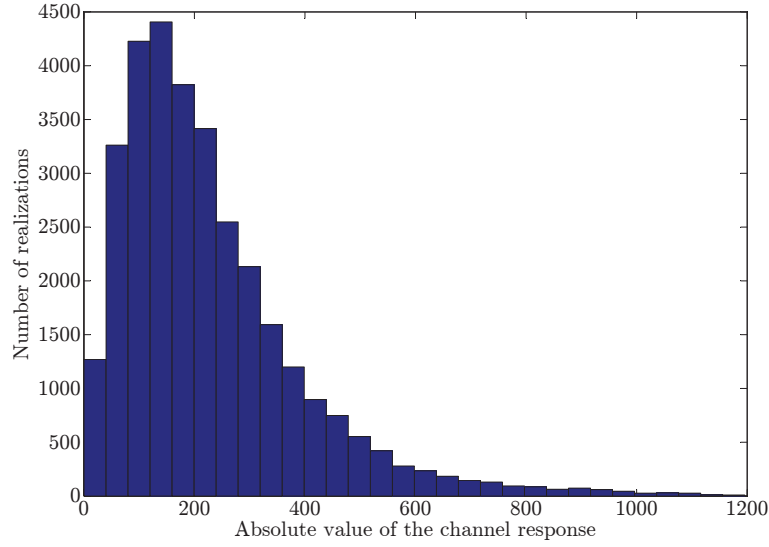


**Figure 4.22:** Histogram that represents the absolute value of the channel response.

Then, from  $R_h$  we can graphically obtain  $B_c$  as depicted in Figure 4.23 considering that  $B_c$  equals the frequency difference where normalized autocorrelation value is 0.5. The rule of thumb to obtain the root mean square (RMS) delay spread in this case is given by [Durgin, 2002]

$$\sigma_\tau = \frac{0.2}{B_c}. \quad (4.21)$$

In Table 5.3, a summary of the obtained wideband parameters in a nomadic environment is shown. The coherence bandwidth and delay spreads are obtained by averaging the results of up to 1000 snapshots and all the 16 SISO channels. As was expected, and according to these averaged results, the coherence bandwidth is observed to decrease as the transmitter moves away with respect to the receiver. However, the decrease trend is not monotonically since the coherence bandwidth is highly fluctuating due to multipath.

Transmitter Position	Coherence bandwidth (MHz)	Delay spread (ns)
TX1	9.185	22.736
TX2	8.275	26.207
TX3	7.796	28.165

**Table 4.3:** Wideband parameters.

Finally, these results are compared with those obtained with others extracted from related publications in indoor environments [Medbo et al., 1999], confirming their validity.

### MIMAX antenna tests

The measures provided by the proposed methodology are also used for calculating the correlation in different antenna array configurations for the MIMAX [Óscar Gago et al., 2009].

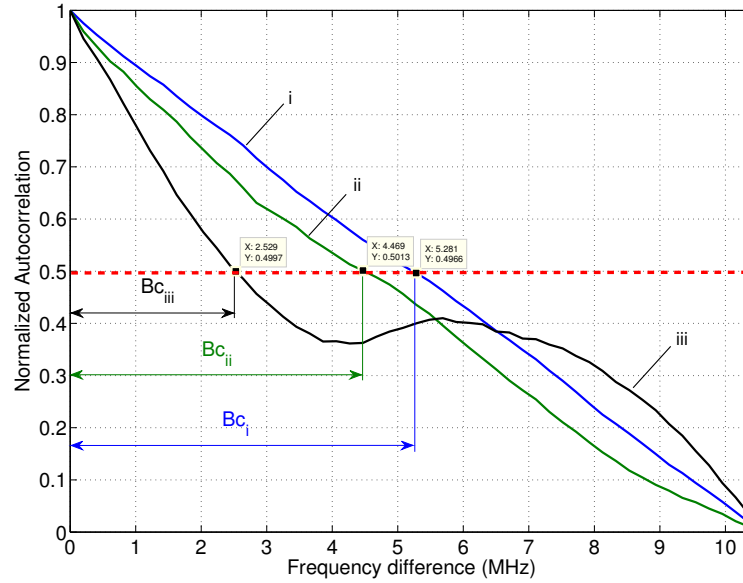


**Figure 4.23:** Example of coherence bandwidth calculation from the normalized autocorrelation function for different channels: i) non frequency-selective channel, ii) intermediate channel, iii) frequency-selective channel.

These antenna arrays, used both at TX and RX, consist of four elements constituting a  $4 \times 4$  MIMO system. The arrays are located in a plastic frame, which allows positioning the elements in different configurations for the four form factors. The correlation is investigated in arrays with a laptop form factor ( $25 \text{ cm} \times 35 \text{ cm}$ ) and PCMCIA form factor ( $60 \text{ mm} \times 54 \text{ mm}$ ). The selected radiating element for making these tests is the Vivaldi MIMAX radiating element working in the 5 GHz band. More details are presented in [Óscar Gago et al., 2009]. As an example, the antenna configuration for the laptop form factor is depicted in Figure 4.24.

The distance between the TX and the RX is variable; the RX is fixed and the TX is placed in position *TX2*. The TX is moved randomly over a grid of  $1 \times 1 \text{ m}$  along 100 positions (see Figure 4.25). An average of these 100 realizations is carried out for each SISO channel (16 channels) for laptop and PCMCIA form factors (ideally, the signal level should be similar).

Considering 100 realizations of channel measurements, and four antennas in each side we have the 4-dimensional channel matrix,  $\mathbf{H}_0$ , with dimensions: number of realizations, number of exponentials, number of TX antennas and number of RX antennas.

For each TX antenna  $i$  and subcarrier, the correlation coefficient is obtained by means of the Matlab function *corrcoef*, which calculates, for any RX antenna  $a$  and antenna  $b$ , the following expression

$$\rho_R^i = \frac{\mathbf{C}(a, b)^i}{\sqrt{\mathbf{C}(a, a)^i \mathbf{C}(b, b)^i}}, \quad (4.22)$$

where  $\rho_R^i$  is the receive correlation coefficient between antenna  $a$  and antenna  $b$ , being  $\mathbf{C}(a, b)$  the covariance matrix. This calculation is also known as the sample covariance matrix. In this case, instead of using correlation matrices, as described in Section 2.2.1, covariance matrices play a role. For calculating the correlation coefficient between each pair of RX antennas (for

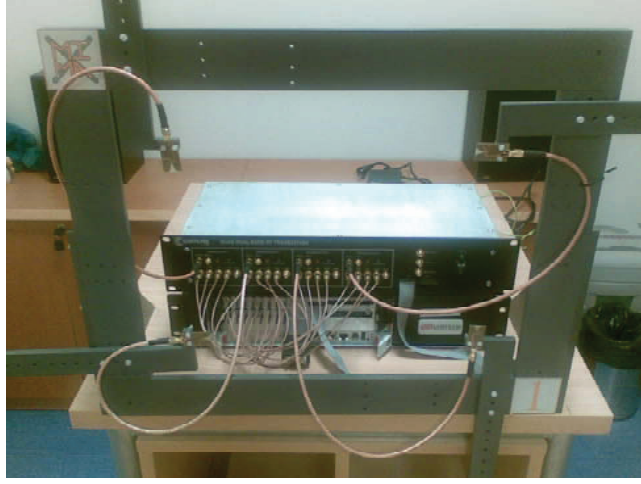


**Figure 4.24:** Laptop antenna form factor.

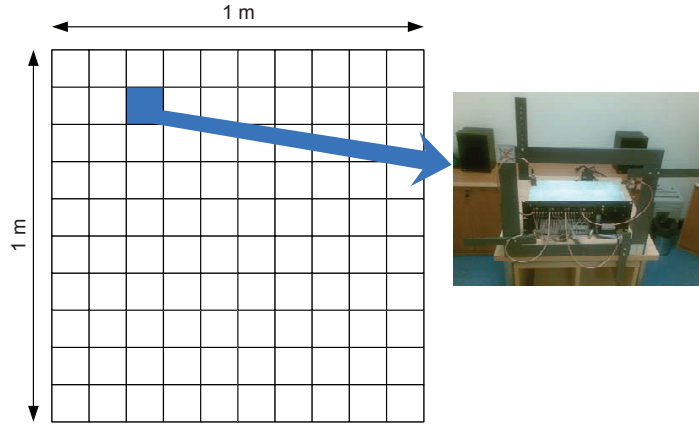


**Figure 4.25:** Measurement grid for the two array configurations.

a given TX antenna), the input argument of the function is a matrix with rows corresponding to the number of realizations and columns to the number of RX antennas. Table 4.4 shows the modulus of the maximum and the mean correlation coefficient obtained in each form factor configuration. It is important to point out that the correlation coefficient includes both the correlation of the channel plus the correlation among the antennas.

In both configurations, the mean correlation is low because polarization diversity is applied. However, higher correlation coefficients are obtained for the PCMCIA form factor, in which the elements are closer to each other. Finally, the MIMAX project considered a laptop form factor configuration.

## 4.8 Verification of the MIMAX channel estimation procedure

One of the first objectives of this methodology after verifying its proper behavior is to validate the MIMAX channel estimation methodology presented in Section 3.9.3. To that end we measure the MIMO channel with both strategies with the aim (hope) of obtaining the same results.

Form factor	Maximum correlation coefficient	Mean correlation coefficient
Laptop	0.2711	0.0331
PCMCIA	0.6299	0.0782

**Table 4.4:** Correlation coefficients (in modulus) of the different form factor configurations.

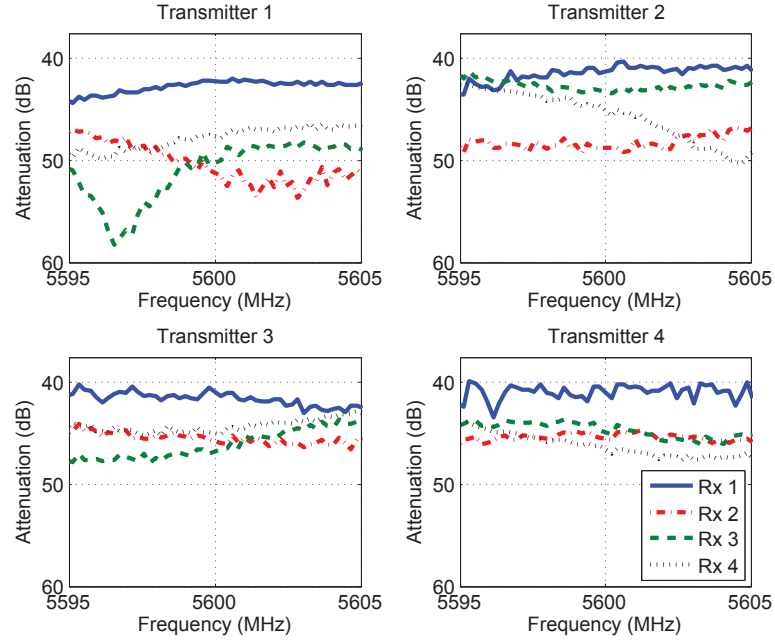


**Figure 4.26:** MIMAX  $4 \times 4$  channel estimation results.

The measurement setup is as follows. We place the transmit node in TX1 and the receive node in the RX position, according to Figure 4.20. We consider a bandwidth of 10 MHz, since MIMAX utilizes less bandwidth than the methodology proposed in this Chapter.

We first perform one channel snapshot of the  $4 \times 4$  MIMO channel with the MIMAX methodology given place to the results depicted in Figure 4.26. Then, we set a time difference between both measurements of 5 min. After this time, we run the methodology based on multi-frequency signals, which results are shown in Figure 4.27.

As can be seen, both methodologies obtain practically the same results. In favor of the multifrequency methodology, it is important to stand out that it avoids the presence of intercarrier interference (ICI), a difficult task to resolve with the MIMAX methodology.

## 4.9 Success stories

After outlining the methodology, describing its implementation on the GTAS MIMO testbed and presenting some results, it is also of high importance to make known the different uses that this methodology has had so far. It has been used within the GTAS group and in other research groups. Within this dissertation, it has been of high importance and sets the basis for Chapter 5.

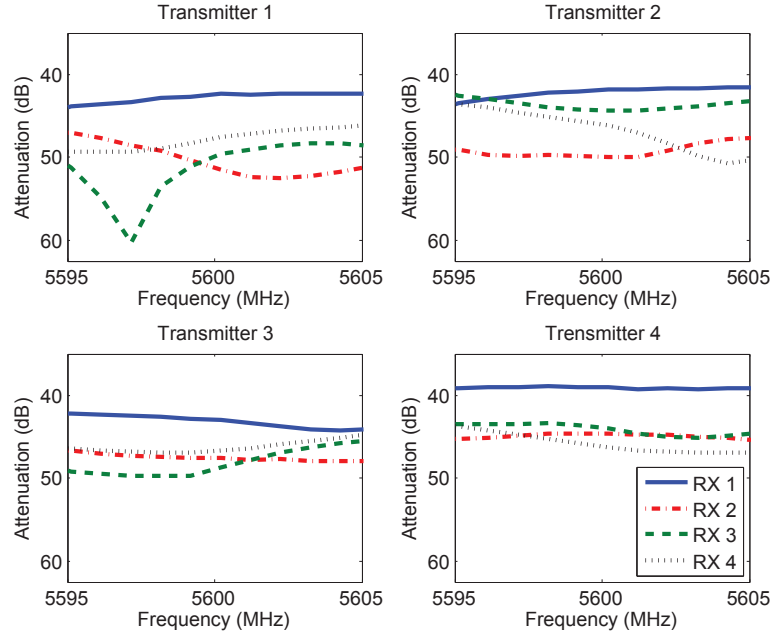


**Figure 4.27:** Multifrequency  $4 \times 4$  channel estimation results.

First of all, we highlight the availability of the software to carry out channel measurements under GTAS web page. Through the following link, the methods that allow measuring the wideband MIMO channel can be downloaded

[http://www.gtas.unican.es/testbed/downloads/remote\\_MIMO\\_Channel\\_Characterization.zip](http://www.gtas.unican.es/testbed/downloads/remote_MIMO_Channel_Characterization.zip)

Its use provides a simple way to measure the frequency response of the MIMO channel in indoor and even outdoor scenarios. Also, a GUI is created (see Figure 4.28) to easily configure the basic parameters and extract the resulting measures.

Moreover, Lyrtech (now Nutaq) released in the webpage this methodology, as an example of how to measure the MIMO channel using their equipment.

<http://nutaq.com/en/products/view/+nutaq-vhs-adc#Literature>

Apart from this, several publications have either made use of the methodology or have considered measures using the testbed as real channel measures.

- In [Céspedes et al., 2013], the authors use the GTAS MIMO testbed along with this methodology to measure the MIMO channel for testing the performance of Block Diagonalization.
- In [Pérez-Cruz et al., 2013], the authors track frequency-selective and time-varying channels, which measures have been obtained with the proposed methodology.

## 4.10 Conclusions

We have presented in Chapter 4 the design and implementation of a flexible broadband MIMO channel measurement methodology. It involves sending complex exponentials for estimating the MIMO channel over a certain bandwidth, which can be arbitrarily chosen as



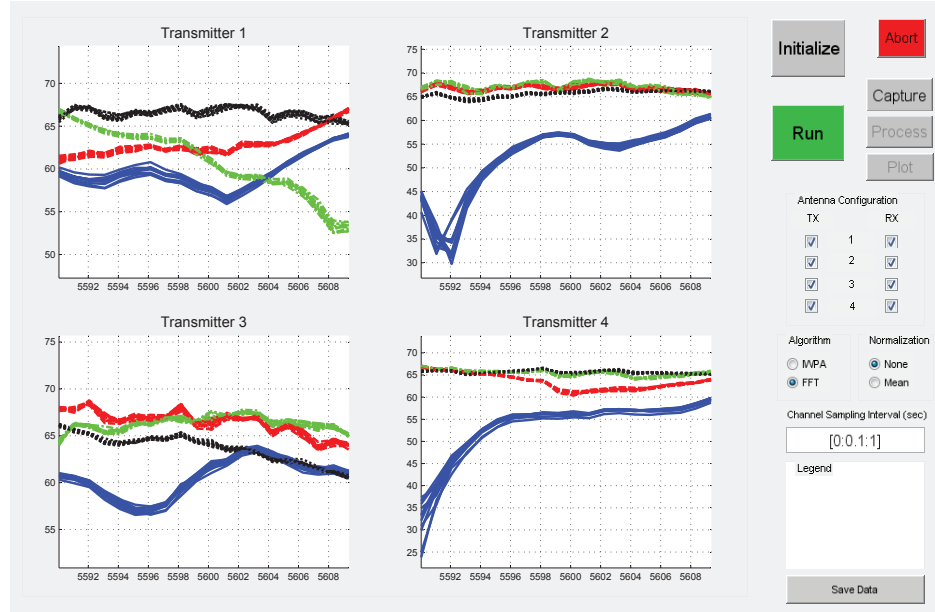


**Figure 4.28:** Frequency Domain channel estimation MATLAB GUI.

well as the separation between exponentials. Logically, the bandwidth and separation among exponentials are limited by the hardware in which it is implemented. These exponentials are transmitted through the actual MIMO channel and are acquired at the receive side. Here, the amplitude, frequency and phase of the received exponentials are estimated using a high-accuracy non-parametric frequency estimation method based on the FFT, denoted as IWPA. Unlike other channel characterization systems, it is able to be implemented in any transmit/receive hardware without the need of neither additional synchronization circuitry nor real-time processing. In this case it is implemented and verified using the GTAS MIMO testbed with successful results, although is by far not comparable in terms of performance to dedicated equipment. However, it results a low-cost tool for accurately obtain MIMO channel measures that faithfully represent the actual channel conditions. The resulting MIMO channel matrices can be stored and used in link level simulations of communications systems in order to obtain results that are representative of real-world situations. Moreover, we have validated the measurement technique by means of commercial equipment. Many measurement campaigns have been carried out and valuable parameters have been obtained for different publications and research goals. From the obtained results, we can corroborate the assumptions that came up when measuring the MIMO channel with the methodology developed for the MIMAX project. When facing up with indoor MIMO channels, e.g. in a research laboratory, we realize that the channel measures are time invariant till there exist any movement, whether exist people hanging around or scatterers. One of the main conclusions of this chapter is that, in static indoor environments, the channel remains constant; which gives an idea of its high temporal coherence.



# 5

Chapter

## Testbed-based MIMO channel emulation

Real-world over-the-air (OTA) characterization and testing is an essential part of the certification testing of wireless devices. This assessment, including the actual interaction of the antennas, radio frequency (RF) front ends and baseband (BB) processing elements, is the best way to understand the performance as experienced by the user. As multiple-input multiple-output (MIMO) advantages rise from the characteristics of the propagation environment, having the control over them is of great importance for MIMO systems testing. Channel emulation is meant to bring some of this ability to wireless research since it offers repeatability and reliability to realistic fading conditions.

As revealed in Chapter 4, the MIMO channel often encountered in indoor research laboratories can be considered time-invariant when the environment is static. This fact imposes a huge restriction when assessing MIMO systems, hence the need of varying this MIMO channel in a controlled and repeatable way.

The current context, along with the previous use of the time-varying beamforming scheme presented in Chapter 3, motivated us to design a solution for testing devices under test (DUTs), with controlled time-variant channel conditions using channel emulation. In a preliminary stage this channel must be estimated by the GTAS MIMO testbed, e.g. using the methodology proposed in Chapter 4; including the DUT. Then, during the testing stage, the signals at the transmitter (TX) are linearly combined in order to emulate the desired MIMO channel. This operation can be easily performed at the TX BB processor. The DUT(s) can be at the TX and/or at the receiver (RX). The DUT can be also a complete RX able to estimate the channel.

The proposed method is also well suited to test MIMO specific algorithms (space-time coding, spatial multiplexing, etc.), that are usually implemented in the BB processors. The proposed method emulates BB equivalent channel responses so, unlike reverberation chambers, it cannot emulate separately the effects of the multipath propagation scenario, antennas, or other embedded elements.

We consider two types of channel emulation: deterministic and stochastic. In the first case the goal is to emulate a given channel realization (or a given sequence of channel realizations). We show closed-form expressions for the coefficients of the linear combination as functions of the actual channel in the laboratory and of the channel to emulate. In stochastic channel emulation, the objective is just to emulate a channel as a stochastic process with desired statistics (mean, spatial autocovariance, etc), regardless the channel realizations. The stochastic em-

ulation is motivated by the fact that, the field programmable gate arrays (FPGA) or digital signal processors (DSP) of the TX testbeds can efficiently generate realizations of multiple independent and identically distributed (i.i.d.) random variables. Adequate linear combinations of such variables can be used to generate the coefficients for the channel emulation with desired statistics.

This solution does not pretend to compete with commercial channel emulators, which costs are unaffordable. Each time, more laboratories are provided with MIMO testbeds or multiantenna transmit/receive equipment. These are used to assess algorithms, BB processors, and RF chains. This testing in selected channel conditions can be carried out with a commercial channel emulator in a straightforward manner, but requires a huge expense and does not often offer OTA capabilities. The proposed solution offers a flexible and low-cost OTA testing methodology able to run on a conventional MIMO testbed without the need of additional equipment.

In this chapter, the design steps of the proposed Testbed-based MIMO Channel Emulation (TBMCE) solution are presented, as well as its implementation and subsequent verification over the GTAS MIMO testbed. The proposed methodology provides a convenient, thorough approach for testing wireless communications equipment by emulating different characteristics of RF mobile communication channels.

This chapter is organized as follows: Section 5.1 reviews the concept of channel emulation and enumerates the different techniques and equipment to emulate MIMO channels. In Section 5.2 we introduce the idea of MIMO channel emulation using a conventional testbed. Section 5.3 describes the steps to emulate MIMO channel realizations. In Section 5.4 we present the theoretical formulation for statistical MIMO channel emulation with certain spatial correlation. As an example we emulate correlated channels of well-known channel distributions: Rayleigh and Rician. In Section 5.5 we focus on the temporal variations and temporal correlation when emulating realizations of the MIMO channel using the proposed solution. Section 5.6 discusses and justifies the decision not to consider receive linear processing. The implementation aspects and the integration within the GTAS MIMO testbed are put forward in Section 5.7. In Section 5.8 we verify the proper emulation of MIMO channel realizations with our MIMO testbed. Section 5.9 shows the results when emulating MISO channels in the testbed with Rician distribution along with spatial and temporal correlation. Once we presented our solution, in Section 5.10, we make a comparison between this solution and the other OTA solutions presented in Section 5.1. Finally, in Section 5.12, the main conclusions are resumed.

## 5.1 MIMO channel emulation review

There exist two main challenges in testing MIMO devices. First, to specify the channel conditions, including noise, interference, etc., in which the performance is to be evaluated. Then, to physically create that environment and test the device. Usually, the channel emulation concept involves recreating desired propagation characteristics, whether they are indoor or outdoor, within a testing lab. In this section we distinguish between two philosophies for performing channel emulation: *conducted testing* and *OTA emulation*. Figure 5.1 outlines this classification along with the corresponding solutions.

In the *conducted testing* philosophy, radio transmitters (TX) and receivers (RX) are directly connected using RF cables. Therefore, they offer controlled and repeatable testing. Its main disadvantage is that they bypass the DUT antenna to provide direct access to the

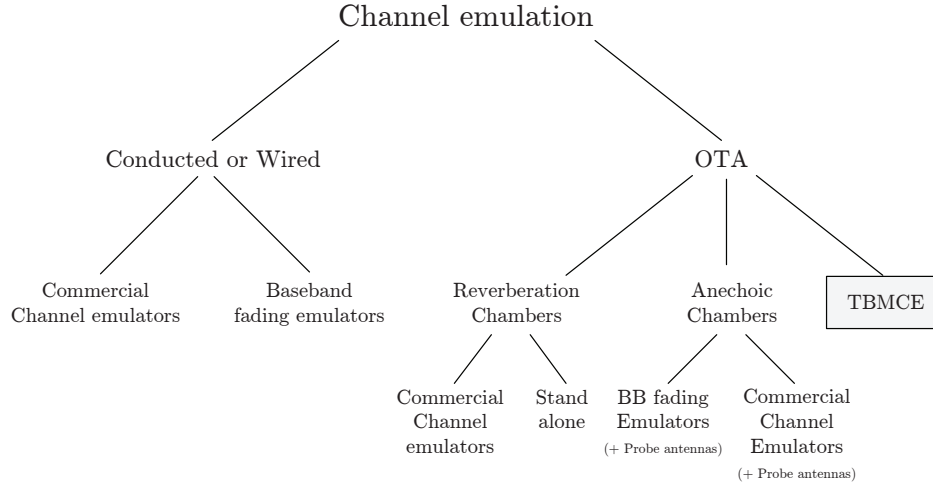


**Figure 5.1:** Solutions for MIMO channel emulation.

transceiver, which results a handicap to perform full TX/RX testing. From this, it is easy to realize how conducted testing results no longer represent the radiated performance of the device in a real network.

The *OTA testing* solutions have the advantage of complete MIMO systems testing. The major challenge for the test of MIMO OTA solutions is how to emulate an RF environment which accurately reflects the performance of the DUT in wireless propagation environments. A primary goal of OTA testing is to determine radio performance of the DUT with the actual antenna patterns, orientation and antenna spacing, that is why traditional OTA measurements perform simultaneous evaluation of the entire RF signal chain. A number of MIMO OTA test solutions are being proposed in the wireless industry [Kyosti et al., 2010], enabling device testing in a fully repeatable and realistic wireless network environment.

MIMO channel emulation solutions are often focused on the achievement of different goals:

- Test MIMO algorithms and debug errors.
- Optimize the performance of existing/future WiFi devices in MIMO environments.
- Perform competitive performance benchmarks.
- Test interoperability between MIMO implementations from multiple vendors.

In this Chapter, we present a testbed-based MIMO channel emulation (TBMCE) solution that can be classified as an OTA solution. Once we describe its features through the following sections, in Section 5.10 we compare it to other OTA solutions to emulate MIMO channels.

### 5.1.1 Conducted (or wired) testing solutions

The traditional method for testing TX and RX performance involves connecting emulators with cables to the TX and the RX DUT respectively. This solution clearly bypasses the DUT antennas and has no relevance as OTA testing. The main solutions based on conducted testing are commercial channel emulators and baseband fading emulators.

#### Commercial channel emulators

Commercial channel emulators [Spirent, 2013, Azimuth, 2012, Agilent, 2012] reproduce the behavior of any RF channel, providing realistic emulation of real-world RF environments.

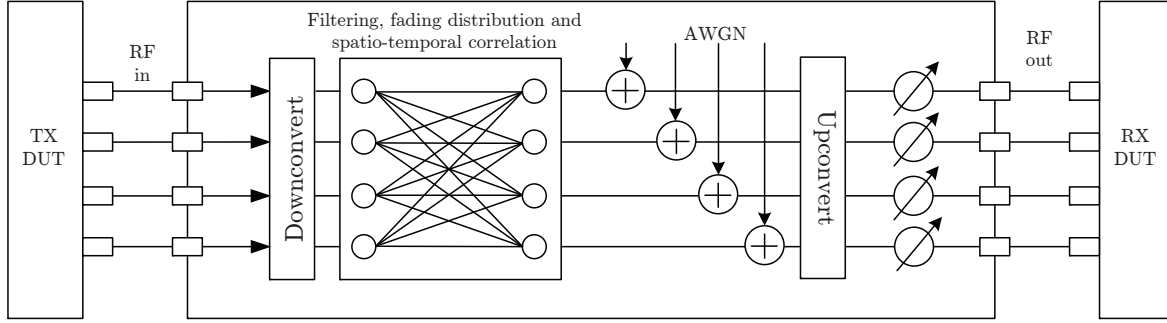


**Figure 5.2:** Block diagram of a typical commercial  $4 \times 4$  channel emulator.

They are generally stand-alone units and work great for most applications but they are very expensive. Their conducted testing nature prevents the tests from 'leaking' and possibly causing interference. Most of the commercial channel emulators are bi-directional, with independent forward and reverse paths to account for products that are tuned in each direction. Although most of them are based on conducted testing, some have introduced OTA testing among their features [Elektrobit F8, 2013].

These emulators are capable of recreating multipath and MIMO antenna correlations in a real-time digital signal processing engine, for dynamic and statistically reliable channel emulation with endless repeat times. As an example, the block diagram of the forward path of a typical commercial channel emulator is depicted in Figure 5.2. The TX is connected via RF cables to the RF input ports. The transmit RF signals are then downconverted to BB within the emulator. These signals are impaired by injecting delay, amplitude variation, and other perturbations that can rely on certain spatial and temporal characteristics. Also, noise and programmable attenuation can be introduced as well. Each path, represented as a line, is a finite impulse response (FIR) structure emulating reflections and clusters in the channel. All these steps make up the channel emulation process. Then the impaired signals are upconverted to RF and the RF outputs are connected by cables to the RX.

Channel emulators can be characterized by two fundamental features: the number of channels and the number of taps. The number of channels is the product of the TX and RX inputs and outputs, respectively. Each channel must be subjected to different statistic impairments to emulate obstacles and reflections that would be present in real-world environments. The number of taps dictates how much control the user has over signal delay, fading, etc. Generally, more taps are desired because they allow greater control over the channel. The impairments are introduced by the channel emulator tap settings. Of course, there exist other important characteristics that define the performance of commercial channel emulators, such as the RF frequency range and bandwidth.

These emulators are usually general-purposed but there are some that allow evaluating a specific technology, like Azimuth's 400WB MIMO Channel Emulator (for IEEE 802.11n and Mobile WiMAX MIMO systems) or Agilent's N5106A PXB MIMO Receiver Test (with built-in Long-term Evolution (LTE) and Mobile Worldwide Interoperability for Microwave Access (WiMAX) channels). The following lines give a short overview of MIMO channel emulators available on the market nowadays.

- The PropSim C8 [Kolu and Jamsa, 2002] from Elektrobit Ltd. features up to 8 channels with up to 24 taps. Channel models must be precalculated and uploaded to the simulator. Elektrobit also provides tools to analyze and preprocess channel sounder

measurements for the PropSim C8. The RF frequency ranges from 350 MHz to 6 GHz and the maximum RF bandwidth is 70 MHz. A new release, the PropSim F8 OTA MIMO channel emulator [Elektrobit F8, 2013], features up to 8 channels with up to 24 taps per channel. Its RF frequency ranges from 220 MHz to 6 GHz and the maximum RF bandwidth is 125 MHz. Finally, the PropSim FS8, features up to 8 channels with up to 48 taps. Its RF frequency ranges from 30 MHz to 2.7 GHz, and the maximum RF bandwidth is 40 MHz. It provides a channel modeling tool for MIMO OTA testing.

- The ARC SmartSim [Kaltenberger et al., 2005], from the Austrian Research Centers GmbH. ARC can simulate up to 64 channels with up to 36 taps each. It implements the COST-259 geometry-based stochastic channel model. Moreover, user-defined channel models can be generated in advance and played back. It has an RF frontend with a frequency range from 450 MHz to 6 GHz and a 40 MHz bandwidth.
- The ACE MX MIMO channel emulator from Azimuth [Azimuth Systems, 2006] is designed for bi-directional simulation of  $4 \times 4$  MIMO systems (with up to 64 channels available in a scalable configuration) with up to 18 taps. The simulator features built-in IEEE 802.11n channel models. The input RF frequency is scalable from 2400 to 2500 MHz and 4900 to 5845 MHz, and the bandwidth is 40 MHz. There exist a new version, the ACE MX2, but its performance is not yet known.
- The VR5 HD Spatial Channel Emulator from Spirent [Spirent VR5HD, 2013] features up to  $8 \times 4$  MIMO channels with up to 24 taps per digital channel. It allows MIMO OTA testing and supports a RF frequency range from 400 MHz to 6 GHz and a bandwidth up to 100 MHz.

In summary, this option is powerful, is perfectly calibrated and characterized, and flexible up to its specifications. On the other hand, acquiring a commercial channel emulator involves a great expense ( $\approx 300$  K), which usually is the main reason why small research groups opt for different tools to emulate the MIMO channel. Commercial channel emulators are commonly used jointly with anechoic and reverberation chambers to perform OTA testing. These setups are presented in Section 5.1.2.

### Baseband fading emulators

Apart from commercial products, several authors have described how they built their own channel emulators. A highly effective and cheaper MIMO emulation solution would be one that emulates the channel within the BB of a TX. The BB signals are altered to emulate the properties of an equivalent time varying radio channel.

Among the available technologies, microcontrollers and DSPs are not valid due to processing and real-time constraints, while application-specific integrated circuits (ASICs) are discarded since their development time is too high for a prototype (although they offer better performance). Thus, the choices could be reduced to complex programmable logic devices (CPLDs) and FPGAs. CPLDs can execute tasks at a faster rate, but FPGAs can deal with more complex designs and they own specific resources (such as counters or arithmetic operator blocks), that are more adequate for implementing a channel emulator. Due to the facts mentioned, FPGAs are probably the most popular hardware technology for developing channel emulators [Nasr and Daneshrad, 2009].

One of the main problems when implementing MIMO channel emulators within an FPGA is that they usually require large designs, since people include the whole filtering process, impairments, correlation schemes, etc., into the FPGA. Therefore, it is desirable to optimize the use of resources in order to fit the design into the FPGA. Although most of the studied channel emulators are able to implement the whole system into only one FPGA, there exist examples that distribute computing among different FPGAs [Hwang et al., 2007, Mehlfuhrer et al., 2005, Dung et al., 2006].

### 5.1.2 OTA solutions

In order to understand the end-to-end reception performance of a MIMO TX or RX, OTA testing is needed [Rumney et al., 2012]. Due to the complexity of multiple antenna setups, a flexible and fast accurate testing solution becomes a major asset in the antenna design cycle and final product verification. The whole emulation system allows testing at once all critical parts of the mobile terminal design: antennas, RF front end, BB processing, etc., without using artificial cabling in the test setup.

#### Anechoic chambers

An anechoic chamber (AC) is a room designed to completely absorb reflections of either sound or electromagnetic waves. It systematically eliminates multipath reflections, which leads to a unique multipath component according to the theoretical channel background presented in Chapter 2. This fact keeps the environment controlled but, in order to test MIMO devices, the effects of multipath must be added back to the measurement system. It has been a unique reference environment for testing of systems for use in line-of-sight (LOS) environments.

They are usually combined with a commercial channel emulator (see Figure 5.3) or even with a BB fading emulator. These solutions provide multipath fading channel generators capable of controlling the multipath delays, Doppler spreads and correlation. Also, as depicted in Figure 5.3, they are usually connected to arrays of probe antennas. The positioning of these antennas create the spatial environment. Each antenna emulates a multipath component, being faded by a channel emulator to provide the temporal characteristics.

In [Rumney et al., 2012], the authors propose five schemes for OTA testing using probe antennas. This is a powerful approach, but in order to achieve arbitrary channel model flexibility large number of probes are required, with the expense it involves.

Also, there exist some publications that use BB fading emulators (instead of commercial channel emulators) for OTA testing of MIMO devices [Kosako et al., 2011, Karasawa et al., 2012].

#### Reverberation chambers

An electromagnetic reverberation chamber (RC) is an electrically large, highly conductive closed cavity or chamber used to perform electromagnetic measurements on electronic equipment. They represent reliable and repeatable test facilities for the testing of wireless communications devices. Unlike ACs, within RCs the spatial richness is provided by relying on the natural reflections within the chamber. In an ideal RC, the Rayleigh fading is naturally obtained by using stirrers (e.g. a stirrer is a large metal plate box which plays a role as a scatterer of radio waves), that oscillate to provide a spatial field, which over long periods of time approaches an isotropic field. Also, another stirring method is carried out using turntables (see Figure 5.4). At any observation point within the chamber, the field will vary as



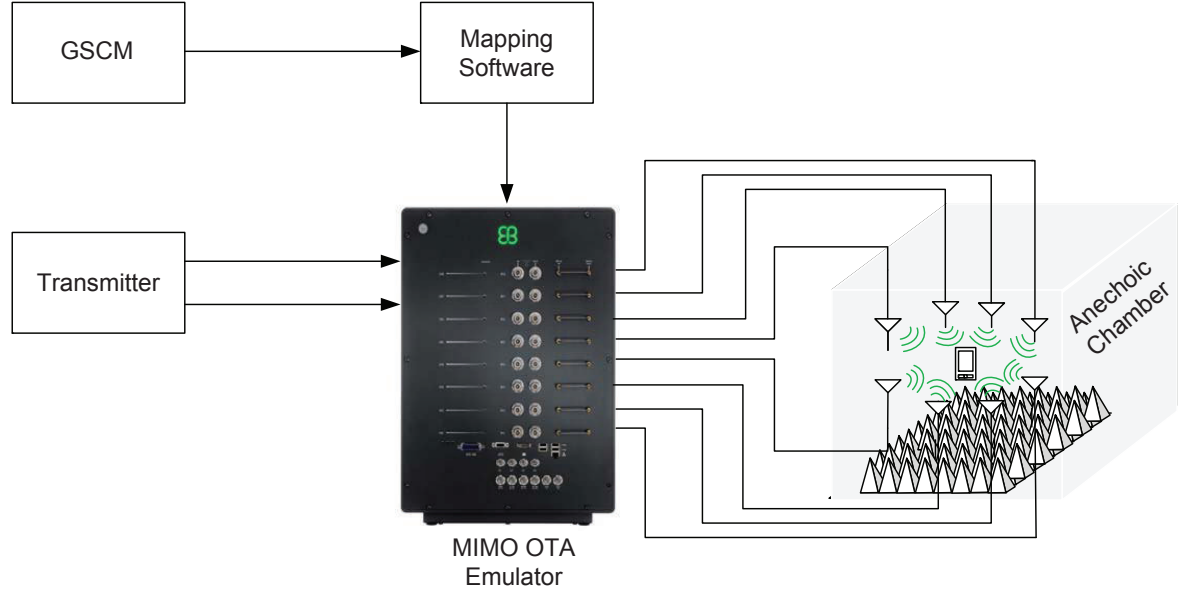


**Figure 5.3:** Anechoic chamber method for MIMO OTA testing.

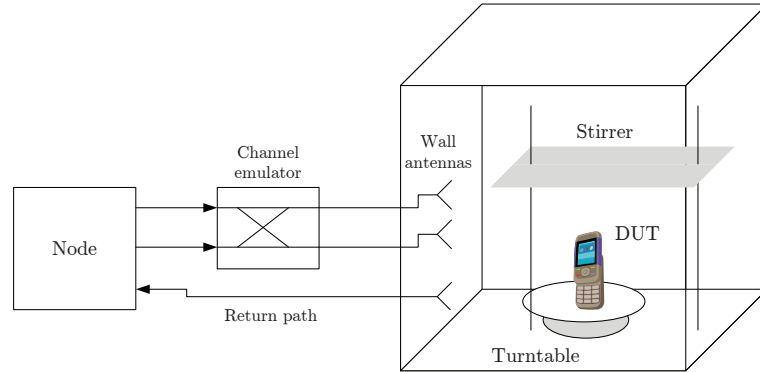


**Figure 5.4:** Test bench configuration using channel emulator and reverberation chamber for a  $2 \times 2$  MIMO configuration.

the different elements (stirrers and turntables) change the boundary conditions. However, a practical RC that uses mechanical stirring does not automatically provide such a perfect scenario. Therefore, in addition to the stirred component there might be an unstirred component too. In order to model Rician fading, we need to recreate this channel by controlling the K-factor in the chamber, which might involve hardware changes.

To perform channel emulation they can work either stand alone, as presented in [Sanchez-Heredia et al., 2011], or combined with a channel emulator [García-Fernández et al., 2011, Chen et al., 2009]. This setup is depicted in Figure 5.4.

In this measurement system, signals from the emulator arrive at the DUT via the wall antennas in the reverberation chamber. At this time, the system activates the stirrers and the turntable on which the DUT rests and performs switching among the wall antennas so as to reproduce a Rayleigh fading environment having a statistically three-dimensional uniform distribution in the vicinity of the DUT.

As occurs with ACs, the combined solution RC and commercial channel emulator enables true OTA testing of devices located within the chamber. The emulator is added to the downlink prior to launching the signals into the chamber. This allows the temporal aspects of the desired channel to be controlled. They suffer from very limited capability to vary the fading environment, and so can only provide very limited evaluation of the terminal. Their main drawback is that the emulated scenario is limited to the chamber volume and they require additional equipment to carry out the emulation.

As in the AC case, the expense that entails acquiring a RC along with a commercial channel emulator is out of our reach. The time and frequency domain characteristics can readily be accounted for in practical measurement situations for both ACs and RCs by using a channel emulator on the transmitting side of the measurement setup. The main advantage of the RC versus the AC is that it is smaller and cheaper, and that the measurements take shorter time. The disadvantage is that radiation patterns can not be obtained.

## 5.2 MIMO channel emulation using a conventional testbed

The GTAS group has a conventional MIMO testbed in the laboratory, which has been described in Chapter 3. In this chapter we propose a methodology that allows narrowband OTA MIMO testing using channel emulation using the GTAS MIMO testbed solely. The methodology relies on MIMO channel emulation to perform this OTA testing. Other options to emulate OTA MIMO channels were discarded since they would involve high additional costs.

Node mobility and, consequently, the time-varying nature of fading, are two key ingredients that must be taken into account in order to conduct realistic experiments. Static scenarios are often found within indoor laboratories, which have a large coherence time (the order of seconds). This fact was verified from several measurement campaigns carried out with the methodology presented in Chapter 4.

Taking this premise as our starting-point, one can imagine a research lab with a TX and RX node in certain positions with neither people nor objects moving in the surroundings. In this case, the channel between the nodes is time-invariant. As stated in Chapter 4, we consider nomadic channels to obtain channel realizations. In a nomadic scenario, channel measurements are taken within a small local area changing the position of the TX (or the RX, or both) between consecutive measurements, keeping fixed both TX and RX nodes while measuring the channel. This kind of experiments requires a person in charge of moving one of the nodes (or both) between measurements. Moreover, if instead of the nodes, the position of the antennas can be changed. There exist positioning tables that can move the TX/RX antennas along their axis. These two options get channel variations but, in the first case, these channel variations lack of controllability and repeatability, besides being time consuming. The second option allows controlled and repeatable channel variations, but results quite expensive due to the high cost of these positioning tables. Therefore, we ruled out both ideas for controlling the channel variations.

With the experience gained in the MIMAX project, from the implementation of the beamforming scheme in BB, we realized that the use of time-varying beamforming to induce those channel fluctuations [Viswanath et al., 2002] could fit our needs. Then, we thought about retrieving the MIMAX digital beamforming scheme described in Section 3.9 which, in a real-time basis, linearly combines the incoming BB signals by a certain set of weight coefficients. Moreover, this scheme could be implemented in our GTAS MIMO testbed.

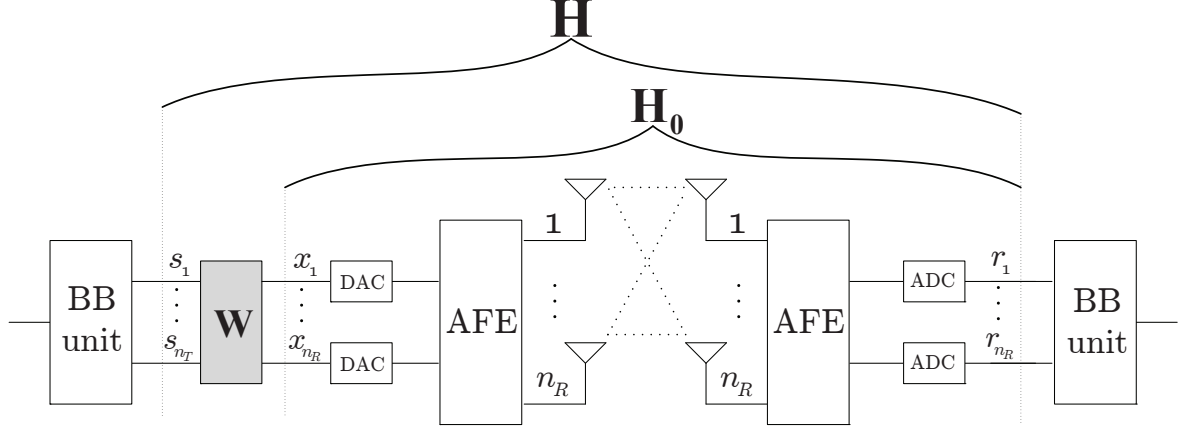


**Figure 5.5:** Proposed scheme using linear signal processing at the TX. AFE denotes the analog front-end, BB denotes baseband and the DACs and ADCs are the digital-to-analog and the analog-to-digital converters, respectively.

The new challenge involves selecting the weights that must be applied. Where to apply them, their adequate values and, how fast they need to be applied, are some of the main requirements that must be defined. The theoretical background for calculating the necessary weights is presented in this chapter.

Figure 5.5 presents the diagram of the channel emulation scheme. The following sections detail the procedure to calculate the weights along with the description of the final implementation in our GTAS MIMO testbed and its particularities.

As it was mentioned, the DUTs can be at the TX and/or at the RX. The DUT could be even a complete RX. The only requirement is that the BB processor of the RX must be able to estimate  $\mathbf{H}_0$ , which is assumed constant during the process. The BB equivalent channel includes not only the effects of the multipath propagation scenario but also the antennas and the AFEs at TX and RX.

Then, in the second stage, we combine the BB signals at the TX to emulate the desired baseband equivalent channel  $\mathbf{H}$ . Note that the effects of the multipath propagation scenario, antennas, and AFEs remain the same as in the first stage.

The following two sections describe two problems derived from the proposed solution. They focus on two different objectives but they are based on the same idea: the combination of the TX antennas and the use of the actual physical channel and the target channel to calculate the necessary weights. Then, narrowband MIMO channel realizations could be emulated.

### 5.3 Emulation of channel realizations

In this section, our aim is to introduce the theoretical analysis for calculating the required weights to emulate a certain channel realization. These channel realizations can be imported from previous channel measurement campaigns or channel models (e.g. WINNER [WINNER II, 2006]), whatever they are their characteristics: indoor or outdoor environments, etc. The weights are calculated from the actual physical channel,  $\mathbf{H}_0$ , and the channel to emulate,  $\mathbf{H}$ .  $\mathbf{H}_0$  is assumed to be previously estimated by using the techniques presented in Chapters 3 and 4, and is assumed static.

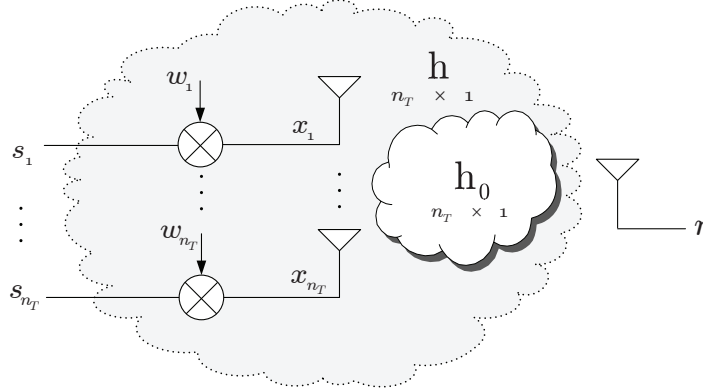


**Figure 5.6:** Proposed MISO scheme using transmit beamforming.

The straightforward solution is to multiply each transmit signal by a complex weight, as occurs in beamforming. This is useful for emulating multiple-input single-output (MISO) channels. All the considered signals and channel responses are discrete BB equivalent representations.

### 5.3.1 Emulation of MISO channel realizations

Our aim is to emulate a MISO channel with  $n_T$  transmit antennas. To that end, we use a MISO testbed, also with  $n_T$  transmit antennas. Figure 5.6 depicts the proposed MISO channel emulation scheme. Let  $\mathbf{s} \in \mathbb{C}^{n_T \times 1}$  denote the transmit signal vector,  $\mathbf{h}_0 \in \mathbb{C}^{n_T \times 1}$  the physical channel vector between the testbed nodes, and  $\mathbf{h} \in \mathbb{C}^{n_T \times 1}$  the  $n_T \times 1$  MISO channel we want to emulate, which includes the linear processing scheme (in this case we can call it beamforming, which is a special case) and the physical MISO channel.

The transmit signal vector,  $\mathbf{s}$ , is element-wise multiplied by a complex transmit weight vector,  $\mathbf{w} \in \mathbb{C}^{n_T \times 1}$ , resulting in the signal vector  $\mathbf{x} \in \mathbb{C}^{n_T \times 1}$ ,

$$\mathbf{x} = \text{diag}(\mathbf{w}) \mathbf{s}. \quad (5.1)$$

In absence of noise, the output signal at the RX,  $r$ , can be expressed as

$$r = \mathbf{x}^T \mathbf{h}_0 = (\text{diag}(\mathbf{w}) \mathbf{s})^T \mathbf{h}_0 = \mathbf{s}^T \text{diag}(\mathbf{w}) \mathbf{h}_0 = \mathbf{s}^T \mathbf{h}, \quad (5.2)$$

being

$$\mathbf{h} = \text{diag}(\mathbf{w}) \mathbf{h}_0 = \text{diag}(\mathbf{h}_0) \mathbf{w}. \quad (5.3)$$

Then, the required weight vector to emulate the desired channel,  $\mathbf{h}$ , can be calculated as

$$\mathbf{w} = (\text{diag}(\mathbf{h}_0))^{-1} \mathbf{h} \quad (5.4)$$

So far, we have emulated one channel realization. To emulate a given set of channel realizations,  $\mathbf{h}[n]$ , we will obtain the corresponding sequences of weights,  $\mathbf{w}[n]$ , from (5.4), assuming  $\mathbf{h}_0$  is time-invariant. Otherwise we should estimate  $\mathbf{h}_0$  whenever it changes, and recalculate the adequate weights.

In summary, if we have in our lab a TX with  $n_T$  antennas and a RX with one antenna, it is possible to emulate any channel,  $\mathbf{h}$ , between the TX and the RX. To that end, we simply include a beamforming stage within the TX which apply a weight vector given by (5.4).

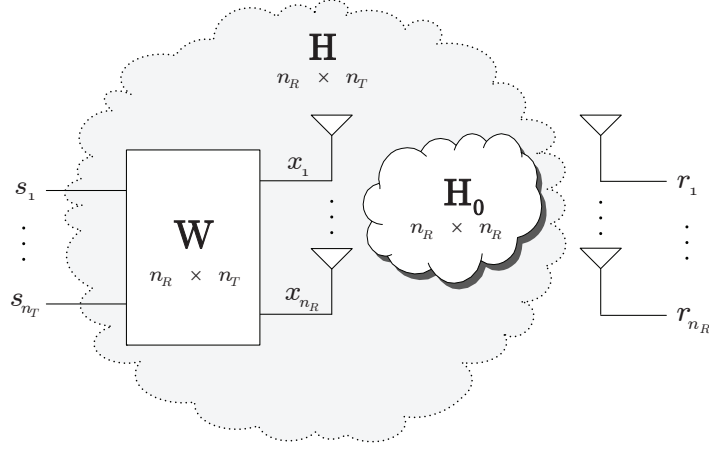


**Figure 5.7:** Proposed MIMO scheme using transmit linear processing.

Previously, we must estimate the channel between both testbed nodes,  $\mathbf{h}_0$ . It can be carried out with the methodology proposed in Chapter 4.

In (5.4) we assume that  $\text{diag}(\mathbf{h}_0)$  is invertible, that is, all entries of  $\mathbf{h}_0$  are distinct from zero. Otherwise  $\text{diag}(\mathbf{h}_0)$  is not invertible. In that case, a straightforward solution will be to change the position of the TX or the RX.

### 5.3.2 Emulation of MIMO channel realizations

Figure 5.7 depicts the proposed scheme for MIMO channel emulation. This scheme aims at emulating a equivalent MIMO channel,  $\mathbf{H} \in \mathbb{C}^{n_R \times n_T}$ , with  $n_T$  inputs and  $n_R$  outputs. It requires a  $n_R \times n_R$  MIMO testbed. Let  $\mathbf{H}_0 \in \mathbb{C}^{n_R \times n_R}$  be the actual channel,  $\mathbf{r} \in \mathbb{C}^{n_R \times 1}$  the received signal vector, and  $\mathbf{W} \in \mathbb{C}^{n_R \times n_T}$  the weight matrix.

The transmit signal vector,  $\mathbf{s}$ , is multiplied by this matrix, resulting in the signal vector  $\mathbf{x} \in \mathbb{C}^{n_R \times 1}$ ,

$$\mathbf{x} = \mathbf{W}\mathbf{s}. \quad (5.5)$$

The receive signal vector will be

$$\mathbf{r} = \mathbf{H}_0\mathbf{x} = \mathbf{H}_0\mathbf{W}\mathbf{s} = \mathbf{H}\mathbf{s}. \quad (5.6)$$

Therefore, the scheme depicted in Figure 5.7 emulates a  $n_R \times n_T$  MIMO channel with channel response given by

$$\mathbf{H} = \mathbf{H}_0\mathbf{W}. \quad (5.7)$$

Then, the required weight matrix to emulate the desired channel,  $\mathbf{H}$ , will be

$$\mathbf{W} = (\mathbf{H}_0)^{-1} \mathbf{H}, \quad (5.8)$$

where we assume that  $\mathbf{H}_0$  has been previously estimated using the methodology proposed in Chapter 4.

In (5.8) we assume that  $\mathbf{H}_0$  is invertible. The laboratory is typically an indoor rich multipath environment, so it is unlikely that  $\mathbf{H}_0$  is ill-conditioned. In spite of this, if it was ill-conditioned, the straightforward solution would be changing the position of the TX or the RX before carrying out the measurements, so that changing the actual channel.

As for the MISO case, to emulate a given set of channel realizations,  $\mathbf{H}[n]$ , we will obtain the corresponding sequences of weights,  $\mathbf{W}[n]$ , from (5.8), assuming  $\mathbf{H}_0$  is time-invariant. Otherwise, we should estimate  $\mathbf{H}_0$  whenever it changes and recalculate the weighting matrix,  $\mathbf{W}$ .

Note that in (5.8), by inverting  $\mathbf{H}_0$ , we are compensating the effect of all the elements that influences the actual baseband channel  $\mathbf{H}_0$ , including the antennas. This allow us to emulate any baseband channel  $\mathbf{H}$  with the weights  $\mathbf{W}$ , regardless the antennas at TX and RX.

The performance of different DUT RX with different antennas can be compared. For each DUT RX there will be a different BB equivalent channel  $\mathbf{H}_0$  (because the antennas and AFEs are different) but, using (5.8), we will select the weights  $\mathbf{W}$  for each receiver so all operate under identical equivalent baseband channel  $\mathbf{H}$ .

Note that for MISO channel emulation,  $n_R = 1$ , we only need a SISO testbed, which is simpler than the solution given in Section 5.3.1. On the other hand, to emulate a SIMO scheme we still need a  $n_R \times n_R$  MIMO testbed.

## 5.4 Emulation of spatial correlation

Now, the channel to emulate,  $\mathbf{H}$ , is a random process with a given distribution and spatial covariance. Using our scheme, the statistics of  $\mathbf{H}$  can be emulated by using a random weights matrix,  $\mathbf{W}$ , with adequate distribution and spatial covariance. In the following lines we will derive the statistical properties of  $\mathbf{W}$  as function of the required statistics for  $\mathbf{H}$ , assuming that  $\mathbf{H}_0$  is time-invariant (deterministic) during the emulation process. We distinguish two cases regarding the mean of  $\mathbf{H}$ : emulation of MIMO channels with zero-mean and with arbitrary mean.

In practice, there exist the possibility of efficiently generate i.i.d Gaussian realizations, in real time, within an FPGA or DSP. This possibility is often available as synthesizable blocks in software as System Generator [Sysgen, 2012]. In this section we present a method to emulate spatially correlated MIMO channels from i.i.d. realizations, regardless the fading distribution. Then, as example, we show how to emulate spatially correlated Rician and Rayleigh channels. We first start with the MISO case to then generalize to MIMO.

### 5.4.1 Emulation of MISO channels

We refer again to the MISO scheme depicted in Figure 5.6. From (5.4), the distribution of  $\mathbf{w}$  is determined by the distribution of  $\mathbf{h}$ .

#### Emulation of channels with zero-mean

Let suppose we want to emulate a channel  $\mathbf{h}$  with zero-mean distribution, i.e.  $E[\mathbf{h}] = \mathbf{0}$ , and correlation matrix  $\mathbf{R}$ .

From (5.3), it must be fulfilled that  $E[\mathbf{w}] = \mathbf{0}$ . Regarding the correlation matrix, considering (5.3)

$$\mathbf{R} = E[\mathbf{h}\mathbf{h}^H] = E[\text{diag}(\mathbf{h}_0) \mathbf{w}\mathbf{w}^H \text{diag}(\mathbf{h}_0)^H] = \text{diag}(\mathbf{h}_0) \mathbf{R}_w \text{diag}(\mathbf{h}_0)^H \quad (5.9)$$

where  $\mathbf{R}_w$  is the correlation matrix of  $\mathbf{w}$ .

Therefore, to obtain the desired correlation matrix  $\mathbf{R}$ , the weight vector must have the following correlation matrix

$$\mathbf{R}_w = [\text{diag}(\mathbf{h}_0)]^{-1} \mathbf{R} [\text{diag}(\mathbf{h}_0)^H]^{-1}. \quad (5.10)$$

The aforementioned is valid for any distribution of the elements of  $\mathbf{h}$  with zero mean. As example, to emulate a Rayleigh channel with correlation matrix  $\mathbf{R}$ , we generate realizations of the weight vector according to

$$\mathbf{w} = \mathbf{R}_w^{1/2} \cdot \mathbf{w}_w, \quad (5.11)$$

where  $\mathbf{w}_w \sim \mathcal{CN}(\mathbf{0}, \mathbf{I}_{n_T})$  and  $\mathbf{R}_w$  is given by (5.10).

#### Emulation of channels with arbitrary mean

Let suppose we want to emulate a channel  $\mathbf{h}$  with mean  $E[\mathbf{h}] = \boldsymbol{\mu} \neq \mathbf{0}$ , and covariance matrix  $\mathbf{C}$ . From (5.3),

$$\boldsymbol{\mu} = \text{diag}(\mathbf{h}_0) \boldsymbol{\mu}_w, \quad (5.12)$$

where  $\boldsymbol{\mu}_w = E[\mathbf{w}]$ . Then, it must be fulfilled

$$\boldsymbol{\mu}_w = [\text{diag}(\mathbf{h}_0)]^{-1} \boldsymbol{\mu}. \quad (5.13)$$

Let  $\mathbf{h} = \boldsymbol{\mu} + \tilde{\mathbf{h}}$  and  $\mathbf{w} = \boldsymbol{\mu}_w + \tilde{\mathbf{w}}$ , where  $\tilde{\mathbf{h}} = \text{diag}(\mathbf{h}_0) \tilde{\mathbf{w}}$ , and  $\tilde{\mathbf{h}}$  and  $\tilde{\mathbf{w}}$  are zero-mean.

By definition, the covariance matrices of  $\mathbf{h}$  and  $\mathbf{w}$  are  $\mathbf{C} = E[\tilde{\mathbf{h}}\tilde{\mathbf{h}}^T]$  and  $\mathbf{C}_w = E[\tilde{\mathbf{w}}\tilde{\mathbf{w}}^T]$ , respectively; which are the correlation matrices of  $\tilde{\mathbf{h}}$  and  $\tilde{\mathbf{w}}$ , respectively.

Applying (5.9) for  $\tilde{\mathbf{h}}$  and  $\tilde{\mathbf{w}}$ ,

$$\mathbf{C} = \text{diag}(\mathbf{h}_0) \mathbf{C}_w \text{diag}(\mathbf{h}_0)^H. \quad (5.14)$$

Then, to emulate a channel with covariance matrix  $\mathbf{C}$ ,  $\mathbf{w}$  must have a covariance matrix given by

$$\mathbf{C}_w = [\text{diag}(\mathbf{h}_0)]^{-1} \mathbf{C} [\text{diag}(\mathbf{h}_0)^H]^{-1} \quad (5.15)$$

The aforementioned is valid for any distribution of the elements of  $\mathbf{h}$  (or  $\tilde{\mathbf{h}}$ ). As example, to emulate a Rician channel with mean  $\boldsymbol{\mu}$  and covariance matrix  $\mathbf{C}$ , we will generate realizations of  $\mathbf{w}$  according to

$$\mathbf{w} = \boldsymbol{\mu}_w + \mathbf{C}_w^{1/2} \mathbf{w}_w, \quad (5.16)$$

where  $\boldsymbol{\mu}_w$  is given by (5.13) and  $\mathbf{C}_w$  is given by (5.15).

#### 5.4.2 Emulation of MIMO channels

Now, let us consider the scheme in Figure 5.7 and equations (5.7) and (5.8). The distribution of the elements of  $\mathbf{W}$  will be determined by the distribution of  $\mathbf{H}$ .

### Emulation of channels with zero-mean

Let suppose we want to emulate a MIMO channel  $\mathbf{H}$  with zero mean  $E[\mathbf{H}] = \mathbf{0}$  and correlation matrix  $\mathbf{R}$ .

Then, from (5.7), it must be fulfilled that  $E[\mathbf{W}] = \mathbf{0}$ . Also  $\text{vec}(\mathbf{H}) = \text{vec}(\mathbf{H}_0 \mathbf{W}) = (\mathbf{I}_{n_T} \otimes \mathbf{H}_0) \text{vec}(\mathbf{W})$ , where  $\otimes$  denotes the Kronecker product. Then, the correlation matrix of  $\mathbf{H}$  will be

$$\mathbf{R} = E[\text{vec}(\mathbf{H})\text{vec}(\mathbf{H})^H] = (\mathbf{I}_{n_T} \otimes \mathbf{H}_0) \mathbf{R}_W (\mathbf{I}_{n_T} \otimes \mathbf{H}_0)^H, \quad (5.17)$$

where  $\mathbf{R}_W = [\text{vec}(\mathbf{W})\text{vec}(\mathbf{W})^H]$  is the correlation matrix of  $\mathbf{W}$ . Then, the weights correlation matrix,  $\mathbf{R}_W$ , is obtained from the correlation matrix,  $\mathbf{R}$ , as

$$\mathbf{R}_W = (\mathbf{I}_{n_T} \otimes \mathbf{H}_0^{-1}) \mathbf{R} (\mathbf{I}_{n_T} \otimes (\mathbf{H}_0^{-1})^H), \quad (5.18)$$

where it is assumed that  $\mathbf{H}_0$  is invertible. The aforementioned is valid for any distribution of the elements of  $\mathbf{H}$  with zero mean.

As example, to emulate a Rayleigh channel with correlation matrix  $\mathbf{R}$ , we generate realizations of the matrix  $\mathbf{W}$  according to

$$\text{vec}(\mathbf{W}) = \mathbf{R}_W^{1/2} \text{vec}(\mathbf{W}_W), \quad (5.19)$$

where  $\mathbf{R}_W$  is given by (5.18) and  $\text{vec}(\mathbf{W}_W) \sim \mathcal{CN}(\mathbf{0}, \mathbf{I}_{n_R n_T})$ .

### Emulation of channels with arbitrary mean

Let suppose we want to emulate a MIMO channel  $\mathbf{H}$  with mean  $E[\mathbf{H}] = \mathbf{M} \neq \mathbf{0}$  and covariance matrix  $\mathbf{C}$ .

From (5.7) we have that  $\mathbf{M} = E[\mathbf{H}] = \mathbf{H}_0 \mathbf{M}_W$ , where  $\mathbf{M}_W = E[\mathbf{W}] \neq \mathbf{0}$ .

Then, the mean of  $\mathbf{W}$  must be

$$\mathbf{M}_W = \mathbf{H}_0^{-1} \mathbf{M} \quad (5.20)$$

Let  $\mathbf{H} = \mathbf{M} + \tilde{\mathbf{H}}$  and  $\mathbf{W} = \mathbf{M}_W + \tilde{\mathbf{W}}$ , where  $\tilde{\mathbf{H}} = \mathbf{H}_0 \tilde{\mathbf{W}}$ , being  $\tilde{\mathbf{H}}$  and  $\tilde{\mathbf{W}}$  zero-mean.

The covariance matrices of  $\mathbf{H}$  and  $\mathbf{W}$  are the correlation matrices of  $\tilde{\mathbf{H}}$  and  $\tilde{\mathbf{W}}$ ;  $\mathbf{C} = E[\text{vec}(\tilde{\mathbf{H}})\text{vec}(\tilde{\mathbf{H}})^H]$  and  $\mathbf{C}_W = E[\text{vec}(\tilde{\mathbf{W}})\text{vec}(\tilde{\mathbf{W}})^H]$ , respectively.

Then, from (5.17)

$$\mathbf{C} = (\mathbf{I}_{n_T} \otimes \mathbf{H}_0) \mathbf{C}_W (\mathbf{I}_{n_T} \otimes \mathbf{H}_0^H). \quad (5.21)$$

The covariance matrix of  $\mathbf{W}$ ,  $\mathbf{C}_W$ , can be obtained from the covariance matrix of  $\mathbf{H}$ ,  $\mathbf{C}$ , as follows

$$\mathbf{C}_W = (\mathbf{I}_{n_T} \otimes \mathbf{H}_0^{-1}) \mathbf{C} (\mathbf{I}_{n_T} \otimes (\mathbf{H}_0^{-1})^H). \quad (5.22)$$

The aforementioned is valid independently of the distribution of the elements of  $\mathbf{H}$  (or  $\tilde{\mathbf{H}}$ ). As example, to emulate a Rician channel with mean  $\mathbf{M}$  and covariance matrix  $\mathbf{C}$ , we generate realizations of  $\mathbf{W}$  according to

$$\text{vec}(\mathbf{W}) = \text{vec}(\mathbf{M}_W) + \mathbf{C}_W^{1/2} \text{vec}(\mathbf{W}_W), \quad (5.23)$$

where  $\mathbf{M}_W$  and  $\mathbf{C}_W$  are given by (5.20) and (5.22) respectively.



### 5.4.3 Emulation of MIMO channels based on dual-polarized antennas

The use of dual-polarized antennas at the TX and RX leads to a  $2 \times 2$  MIMO channel. The diagonal elements of the channel matrix correspond to transmission and reception on the same polarization, while off-diagonal elements correspond to transmission and reception on orthogonal polarization. Assuming Rayleigh fading, the channel is usually modeled approximately as follows [Paulraj et al., 2008], [Coldrey, 2008], [Neubauer and Eggers, 1999]

$$\text{vec}(\mathbf{H}) = \text{vec}(\mathbf{X}) \odot (\mathbf{R}^{1/2} \text{vec}(\mathbf{H}_w)), \quad \mathbf{H}_w \sim \mathcal{CN}(\mathbf{0}, \mathbf{I}) \quad (5.24)$$

where  $\odot$  stands for the Hadamard product,  $\mathbf{R}$  is now the so-called polarization correlation matrix (usually it is approximated in terms of the transmit and receive polarization correlation matrices:  $\mathbf{R} = \mathbf{R}_t^T \otimes \mathbf{R}_r$ ), and  $\mathbf{X}$  is the polarization leakage matrix given by

$$\mathbf{X} = \begin{bmatrix} \sqrt{1-\alpha} & \sqrt{\alpha} \\ \sqrt{\alpha} & \sqrt{1-\alpha} \end{bmatrix}, \quad (5.25)$$

where  $\alpha$  is a parameter which depends on the cross-polarization discrimination (XPD) of the antennas and of the cross polarization coupling (XPC) of the propagation environment, often collectively referred to as XPD.

In order to emulate a Rayleigh channel with given polarization correlation matrix,  $\mathbf{R}$ , and polarization leakage matrix,  $\mathbf{X}$ , one simply should use the weights vector  $\mathbf{W}'$  given by

$$\mathbf{W}' = \mathbf{X} \odot \mathbf{W}, \quad (5.26)$$

where  $\mathbf{W}$  is obtained from (5.18) and (5.19) as a function of  $\mathbf{R}$ . Now, the emulated channel will be

$$\mathbf{H} = \mathbf{H}_0 \mathbf{W}' = \mathbf{X} \odot \mathbf{H}_0 \mathbf{W}, \quad (5.27)$$

Then,

$$\text{vec}(\mathbf{H}) = \text{vec}(\mathbf{X}) \odot (\mathbf{I}_{n_T} \otimes \mathbf{H}_0) \text{vec}(\mathbf{W}). \quad (5.28)$$

Considering (5.17) and (5.19),

$$\text{vec}(\mathbf{H}) = \text{vec}(\mathbf{X}) \odot (\mathbf{I}_{n_T} \otimes \mathbf{H}_0) \mathbf{R}_W^{1/2} \text{vec}(\mathbf{W}_W) \quad (5.29)$$

$$= \text{vec}(\mathbf{X}) \odot \mathbf{R}^{1/2} \text{vec}(\mathbf{W}_W), \quad (5.30)$$

which is exactly the model in (5.24).

## 5.5 Emulation of time-varying MIMO channels

Focusing on the general MIMO case, to emulate a given set of channel realizations,  $\mathbf{H}[n]$ , we will obtain the corresponding sequences of weights,  $\mathbf{W}[n]$ , from (5.8), assuming  $\mathbf{H}_0$  is time-invariant. Otherwise we should estimate  $\mathbf{H}_0$  whenever it changes and recalculate the adequate weights.

At this point one can consider two different issues regarding temporal analysis:

1. How fast the channel changes from one realization to another, which in turn, determine the speed at which weights are applied.
2. The temporal correlation among realizations.

The whole system is able to work in two modes, each suited to different requirements.

Channel variations in indoor environments often rely on the common *block-fading* assumption. In this first mode, the system emulates a block-fading channel. During each channel state (block) the signals are transmitted with fixed weights and the equivalent channel remains constant within a block. Then, the weights change according to the following realizations. To emulate a *block-fading* channel, the user is able to change the weights from time to time and, as a result, the time among channel realizations is determined by user decisions and the delays related to weight uploading and application. This fact is thoroughly studied in Section 5.7.

The second operation mode considers a sample-based weight application, hence the possibility of emulating high demand variability environments. In this case, the weight realizations obtained from 5.8 and the transmit signals, are stored in the synchronous dynamic random-access memory (SDRAM) and are applied in a sample by sample manner. In a sample-based weight delivering, the sampling frequency of the transmitter determines the time resolution at which the channel realizations are applied. The limitation is that the data must be pre-stored in memory, which is finite.

Regarding temporal correlation, we can distinguish between two different analysis, depending on the technique utilized for channel emulation.

- If MIMO channel realizations are imported from a model or from previous channel measurements, the temporal correlation is implied within the realizations to be emulated.
- In the case that we do not have previous measurements or realizations from channel models, the option is to generate MIMO channel realizations and introduce temporal correlation. To that end we must use temporal correlation models, e.g. autor-regressive (AR) [Baddour and Beaulieu, 2005], Markov [Tan and Beaulieu, 2000], Jakes [Jakes, 1994] and Lee [Lee, 1982], are examples. One of the main parameters to be introduced within the model is the maximum Doppler frequency,  $f_D$ . Then, we generate the realizations according to the chosen model, hence these realizations will present temporal correlation. Finally, the calculated weights to be applied will intrinsically have temporal correlation.

## 5.6 Why not apply the linear processing at the receive side?

The proposed scheme relies on a linear combination of the signals at the transmitter to emulate the channel. One might think to do the same for the receiver, as depicted in Figure 5.8. The RX processing produces an artificial noise unbalance among the RX inputs. The following lines describe this fact.

The transmit signal vector,  $\mathbf{s}$ , is multiplied by the transmit weight matrix,  $\mathbf{W}_T$ , resulting in the signal vector  $\mathbf{x}$

$$\mathbf{x} = \mathbf{W}_T \mathbf{s}, \quad (5.31)$$

where  $\mathbf{W}_T$  is the combination matrix at the TX. The signal before the processing at the receiver,  $\mathbf{y}$ , will be

$$\mathbf{y} = \mathbf{H}_0 \mathbf{W}_T \mathbf{s} + \mathbf{n}_0. \quad (5.32)$$

After processing, the received signal vector,  $\mathbf{r}$ , will be

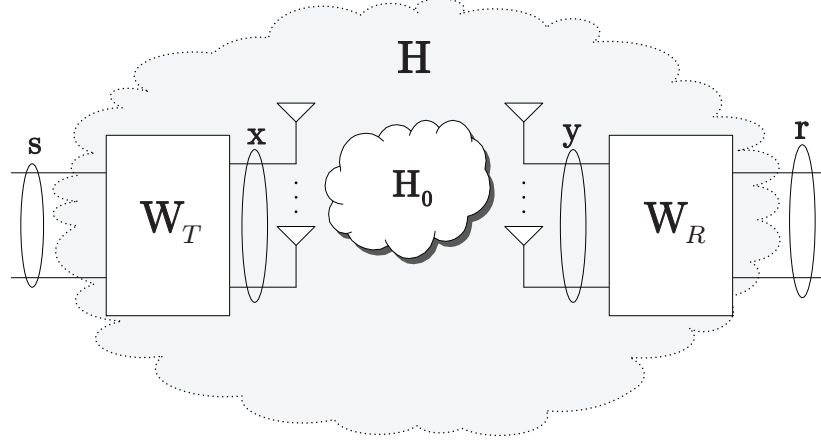


**Figure 5.8:** Scheme using linear processing at both sides.

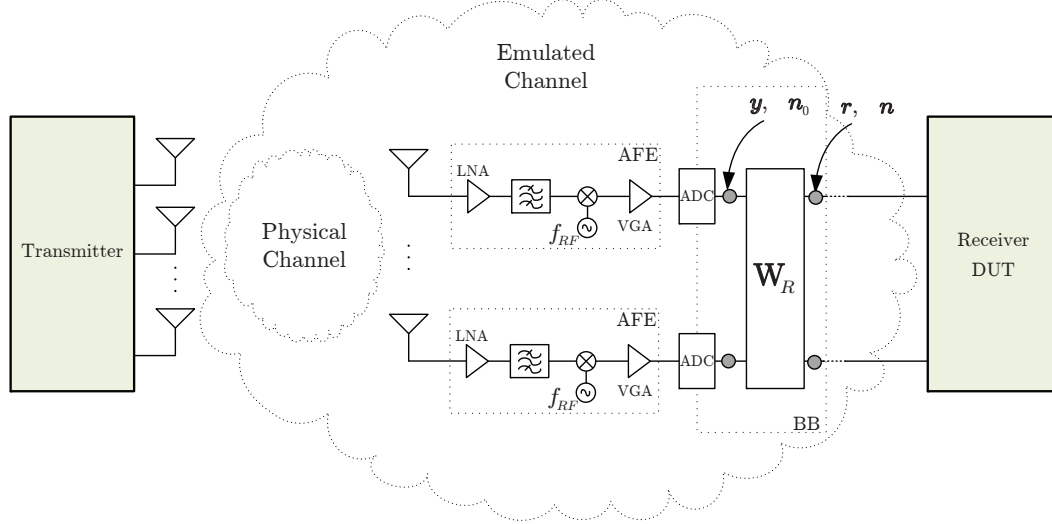


**Figure 5.9:** Scheme with receive processing.

$$\mathbf{r} = \mathbf{W}_R \mathbf{H}_0 \mathbf{W}_T \mathbf{s} + \mathbf{W}_R \mathbf{n}_0 = \mathbf{H} \mathbf{s} + \mathbf{n} \quad (5.33)$$

where  $\mathbf{H} = \mathbf{W}_R \mathbf{H}_0 \mathbf{W}_T$  is the equivalent MIMO channel,  $\mathbf{W}_R$  is the combination matrix at the RX, and  $\mathbf{n} = \mathbf{W}_R \mathbf{n}_0$  is the equivalent noise vector. In general,  $\mathbf{W}_R$  introduces spatially colored noise on  $\mathbf{r}$ . If  $\mathbf{n}_0$  is spatially white Gaussian,  $\mathbf{n}_0 \sim \mathcal{CN}(\mathbf{0}, \sigma^2 \mathbf{I}) \Rightarrow \mathbf{n} \sim \mathcal{CN}(\mathbf{0}, \sigma^2 \mathbf{W}_R \mathbf{W}_R^H)$ .

Moreover, when emulating a certain MIMO channel with the proposed method (see Figure 5.9), the signal strength at the antenna input will be different to that of the conventional receiver depicted in Figure 5.10. This is due to the different channels that the receiver faces in each case. The same occurs at all the receive stages: low noise amplifier (LNA), downconverter, variable gain amplifier (VGA), automatic gain control (AGC), etc. This fact prevents the use of this setup when we are also interested in the behavior and performance of the AFE of the RX DUT.

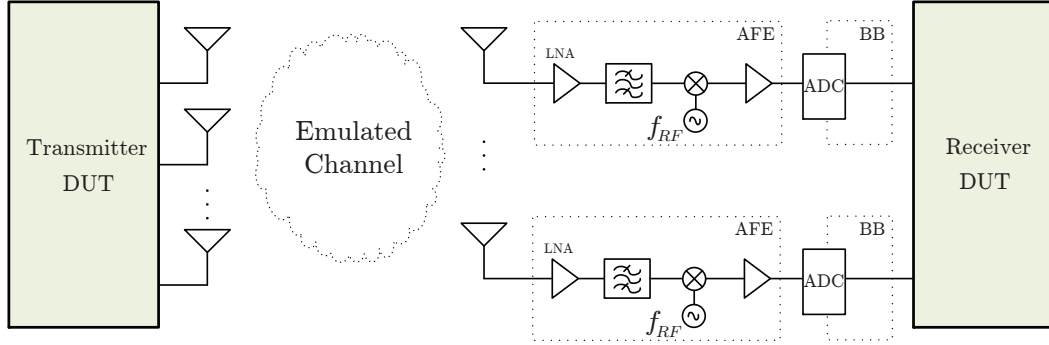


**Figure 5.10:** Conventional receiver.

All of these reasons justify the use of only transmit processing to emulate MIMO channels. Moreover, holding all the processing at the transmit side has great benefits from a practical point of view:

1. The only changes are in the TX of the testbed.
2. The receiver does not require changes. So, the testing of any RX under the emulated channel is straightforward.

## 5.7 Implementation and measurement setup

In Section 5.6, we gave reasons that support including the processing scheme for weight application only at the TX side. The first step regarding implementation leads us to decide where to fit it. The aim of OTA testing forced us to include the implementation within the TX DUT. Therefore, the weights can be applied in two possible domains: RF or BB.

The spatial signal processing at the RF front-end would require extra hardware, e.g. phase and amplitude shifters or vector modulators, that are not included in a conventional MIMO testbed setup. Hence, this hardware must be designed and built within the RF part. Its use involves many drawbacks such as impairments or difficulties in order to cover the whole in-phase and quadrature (I/Q) weight vector space. Moreover it requires a thorough calibration process.

The second option is more suitable given the available hardware and its implementation is easier. Since we want to apply the weights in a real-time context, we decided to implement the *weighting scheme* within the FPGA of the transmit DUT. This solution avoids the need of extra hardware and is of our interest since it runs in BB, which involves a more flexible implementation.

The requirements for the hardware implementation of the proposed MIMO OTA testing method are:

- A TX and a RX with adequate number of antennas, according to Sections 5.2), 5.4 and 5.3.
- A weighting block at the TX where the baseband signals,  $\mathbf{s}$ , are linearly combined according to the adequate weights,  $\mathbf{W}$ .
- Channel estimation capability at the RX baseband processor.

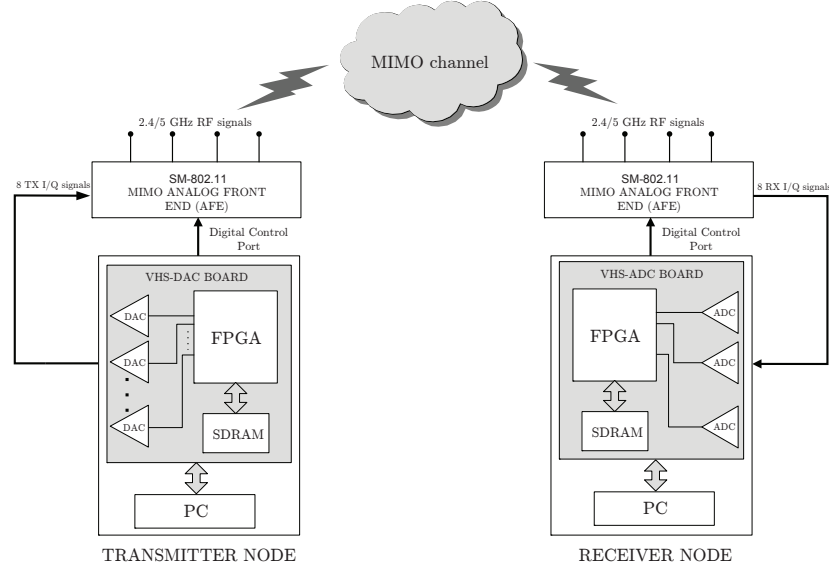


**Figure 5.11:** Block diagram two of the nodes of the  $4 \times 4$  MIMO testbed. (Left) Transmitter. (Right) Receiver.

The DUTs can be any part of the TX and/or RX (antennas, elements of the analog front-ends (AFEs), MIMO algorithms implemented at the BB processors, etc.). The DUT can be also the complete RX, provided that its BB processor is able to estimate the equivalent baseband channel,  $\mathbf{H}_0$ .

### 5.7.1 Implementation setup

Figure 5.11 presents the configuration of two of the GTAS testbed nodes, one acting as the TX and the other as the RX. The *weighting scheme* has been implemented on the transmit FPGA making use of Simulink and using the blocks provided by System Generator [Sysgen, 2012], as in Chapter 3. Finally we obtain the *bitstream* to be loaded on the FPGA. The scheme was built in this manner and gave rise to a low complexity block called *Weighting Block* which has been fitted into the FPGA of the TX node. This block is able to apply weights for both MISO and MIMO schemes.

The procedure is as follows: the transmit signals are multiplied by the required weights, calculated from an estimation of the actual physical channel,  $\mathbf{H}_0$ , and the desired channel to be emulated  $\mathbf{H}$ . These signals are transmitted through the air for, subsequently, being received by the testbed RX. In summary, the received signals have gone through an equivalent channel determined by  $\mathbf{H}_0$  and the weights.

As stated in previous sections, the emulation methodology requires previous channel estimation of the actual channel,  $\mathbf{H}_0$ , in order to emulate the desired channel,  $\mathbf{H}$ . Typically, the initial estimation of  $\mathbf{H}_0$ , assumed constant during the experiment, is performed by the RX BB processor; otherwise, it can be carried out as described in Chapter 4.

### 5.7.2 Weighting block

Figure 5.12 depicts an example of the *Weighting Block* implementation in Simulink. More specifically, it represents a MISO  $4 \times 1$  scheme that is in charge of applying the weights

The diagram illustrates the architecture of an 8-channel beamforming system. It starts with Baseband I/Q input signals entering an FPGAs SDRAM Playback1 block. This block outputs eight channels (data\_ch1 to data\_ch8) to a series of up-sampling blocks (Up Sample1 to Up Sample9). These signals then pass through a series of registers (Register1 to Register4) and delay blocks (z^-1) before entering a Weighting Block. The Weighting Block contains four parallel processing paths, each with a multiplier (xof), a delay block (z^-1), and a convert block. The outputs of these paths are then fed into four DACs (DAC1 to DAC4) to produce Baseband I/Q output signals. A Run signal is also provided to the DACs.

The weights are defined within the range  $[-1, 1]$  to ensure that if they are fixed to the maximum value, the I/Q signals are not affected by saturation that can occur at the *Weighting Block* or at the DACs. Therefore, the transmit weight vector has one bit for the sign and 15 bits for the decimal part, which allow great resolution. If a higher dynamic range is desired, there exist a control that allows varying the transmit power amplifier (PA) gain at the AFE.

We now link the implementation point of view of the weights with the theoretical analysis. The distribution of the weights is determined by the distribution of the realizations. As an example, when emulating Rayleigh channel realizations some of the weight values are close to zero. Since the transmit signals can take values between  $-2^{13}$  to  $2^{13} - 1$  (14 bit resolution), their multiplication by the weights result in a low level signal transmitted through the air.

Resources	Virtex II XC2V3000-4 FF1152
Slice flif plops	16%
Slice LUT's	21%
Occupied slices	33%

**Table 5.1:** FPGA resources utilization.

This signal will be hardly acquired by the RX DUT, hence the emulation is not performed correctly. To solve this issue, once the weights are calculated, they must be scaled within the range  $[-1, 1]$  to increase the dynamic range of the signal and then receive it properly.

Moreover, the low value of the resulting weights can affect the energy detector used for identifying the transmitters presented in Chapter 4, leading to an wrong behavior. This fact would provoke synchronization errors as well as an incorrect transmitter identification. To solve this issue, pseudo-noise (PN) sequences have been prepended to the probing signals which are used to measure the channel. Then, the received signals are correlated with the PN sequence to properly recover these probing signals.

The proposed MIMO channel emulation methodology makes use of the methodology for measuring the MIMO channel described in Chapter 4. Basically, the only difference among both implementations is the inclusion of the *Weighting block*. Fixing the weights value to one involves bypassing the *Weighting block*, thus giving the possibility to use the same implementation for both measuring and emulating the MIMO channel.

The *Weighting block* implementation on the FPGA involves the utilization of FPGA resources, since new functionalities have been included within the custom logic. Table 5.1 shows the resources occupied by the *Weighting block* when implemented in a Xilinx Virtex II XC2V3000-4 FF1152 FPGA.

### 5.7.3 Weights application

We have stated in Section 5.5 that a *block fading* assumption is considered. Once described the implementation of the *Weighting block* we are able to determine how fast the weights can be applied for the required channel variations.

Weights are loaded into FPGA registers and, each time we want to apply them, a Matlab command for their application is executed. It is the user who decides when the weight realizations are applied. The function sets to high level the run signal and the weights multiply the BB input signals at the complex multipliers. In summary, weight application entails a certain delay from the moment that we execute the function till the weights are applied. We can now refer to Section 3.5.2 to realize the different steps that such a high-level function involves. The time required since the weight application command is executed to the real application of the corresponding weights will determine the maximum speed at we can change the weights, i.e. how fast the channel varies. This time is around 35 ms, which results enough to represent typical mobility in indoor scenarios.

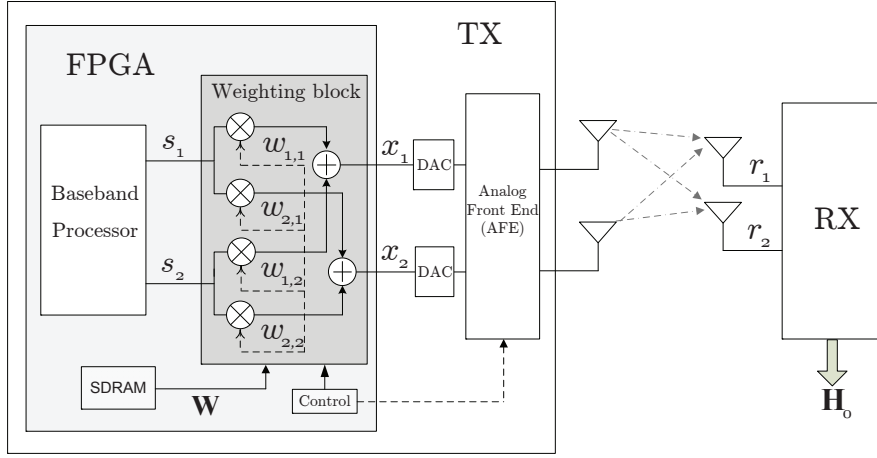


**Figure 5.13:** Implementation diagram for emulating a  $2 \times 2$  MIMO channel.

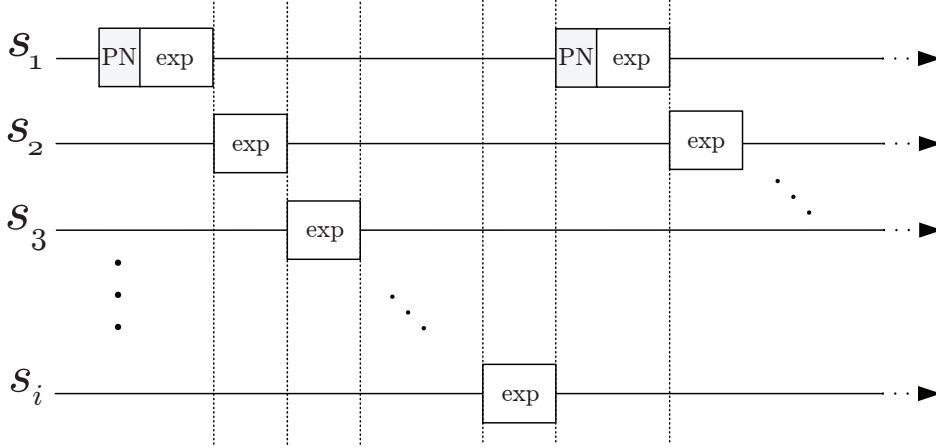


**Figure 5.14:** Diagram representing how to create the transmit signals.

## 5.8 Validation of the emulation of MIMO channel realizations

In this section, following the methodology described in Section 5.3.2, we present results regarding the emulation of a  $2 \times 2$  MIMO channel, operating at 5.6 GHz. To emulate such channel we require two nodes of the GTAS MIMO testbed, as outlined in Section 5.7. The TX and the RX nodes use 2 transmit and 2 receive antennas, respectively. Figure 5.13 depicts the TX/RX diagram for carrying out the  $2 \times 2$  channel emulation.

Figure 5.14 depicts the BB I/Q input signals used in for a general TX scheme; in the present case we just consider two TX signals. The complex transmit signals associated to each antenna are denoted as  $s_i$ . They consist of PN sequences, complex exponential signals (*exp*), and zeros. As explained in Section 5.7, PN sequences are prepended to the signal with higher level (in this case, corresponding to Antenna 1) to facilitate the synchronization scheme. The complex exponentials serve as probing signals as occurred in Chapter 4, for obtaining the actual channel,  $\mathbf{H}_0$ , as well as the emulated channel,  $\mathbf{H}$ . The signal transmission is multiplexed in time as we considered in Chapter 4. These sequences are cyclically repeated in time so the TX node is transmitting the same sequence continuously.



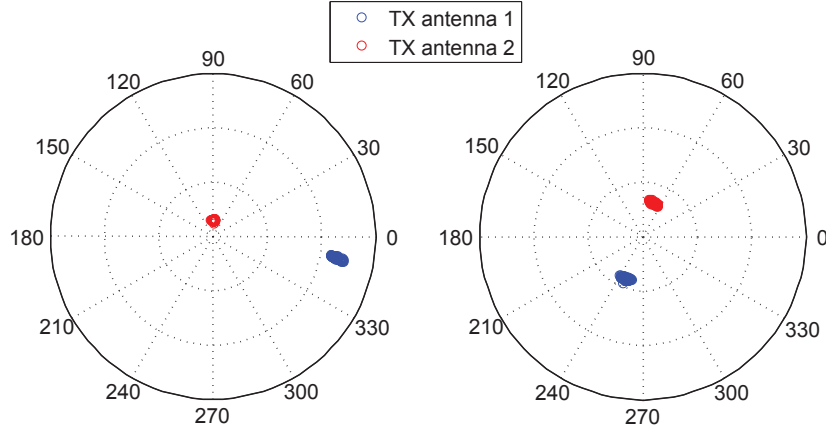


**Figure 5.15:** MIMO  $2 \times 2$  initial channel measures. Left: Receive antenna 1, right: Receive antenna 2

The transmit and receive testbed nodes are placed in *TX1* and *RX* positions respectively according to Figure 4.20, being the TX placed 3.5 meters away from the RX. We use a TX power of 1 dBm.

Our aim is to emulate 200 Rayleigh i.i.d. channel realizations,  $\mathbf{H}[n]$ ,  $n = 1, \dots, 200$ . For the sake of clarity, just 20 are depicted (circle marks) in Figure 5.16. The following lines describe the emulation procedure:

1. Firstly, the physical  $2 \times 2$  channel,  $\mathbf{H}_0$ , is measured using the method described in Chapter 4. Figure 5.15 shows a polar plot with the 100 realizations of  $\mathbf{H}_0$ . These measurements are obtained along 90 seconds, showing the lack of variability of the channel in the lab.
2. Using (5.8), we calculate the corresponding sequence of weight matrices,  $\mathbf{W}[n]$ .
3. We generate the transmit signals according to Figure 5.14. They are multiplexed in time so that we easily identify the TX at the RX side.
4. The transmit signals are multiplied within the FPGA by the sequence of weight matrices. The weights realizations are fed to the *Weighting Block* along with the BB I/Q signals, and the actual emulated channel,  $\mathbf{H}_e[n]$ , was measured using again the methodology presented in Chapter 4. These resulting channel realizations are also compared in Figure 5.16 with the desired channel realizations. As can be seen, our emulator closely matches the desired realizations.

The performance of the communication systems is determined by the quality, e.g. signal-to-noise ratio (SNR), of the BB signals at the receiver. Our testing/emulation method show us the impact of the DUTs in such signals under any (controlled) equivalent baseband MIMO channel. Obviously, the emulation performance depends on both the precision of the channel measurement procedure and on the testbed. To illustrate the performance of the channel measurement methodology, we present in Table 5.2 the SNR of the measurements obtained in Figure 5.15, where

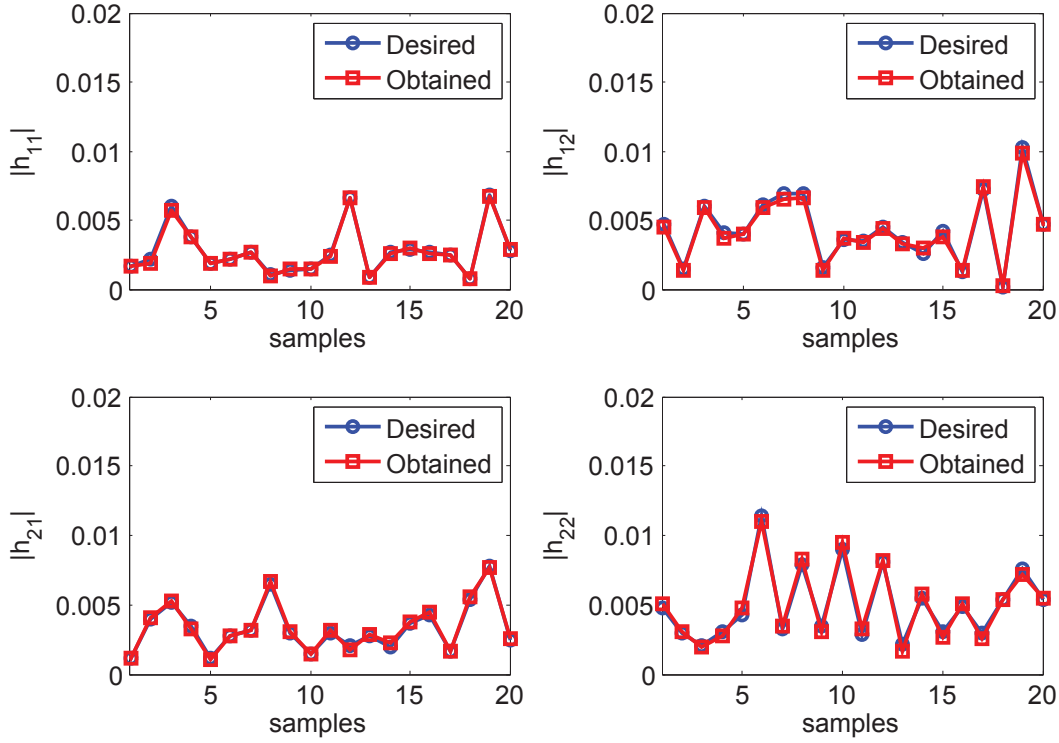


**Figure 5.16:** Comparison between the desired and the actual emulated channel.

	$h_{11}^0$	$h_{21}^0$	$h_{12}^0$	$h_{22}^0$
SNR (dB)	28.8073	22.3865	22.5993	21.7302

**Table 5.2:** Performance results: measurement of  $\mathbf{H}_0$ .

$$SNR = \frac{E\left(\left|h_{i,j}^0\right|^2\right)}{\text{var}\left(h_{i,j}^0\right)}, \quad (5.34)$$

being  $h_{i,j}^0$  the corresponding entry of  $\mathbf{H}_0$ .

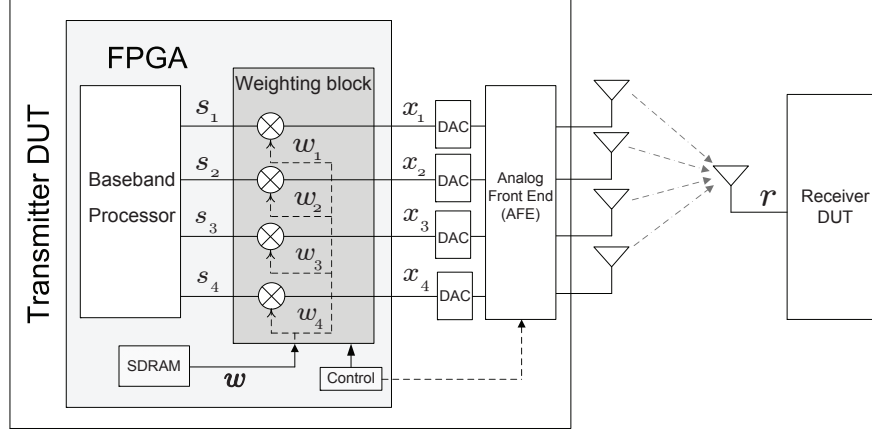
The obtained values reveal a good performance, which can also be deduced from the "error clouds" in Figure 5.15.

In Table 5.3 we present the performance of the whole channel emulation methodology. Now, the SNR is calculated from the whole channel realizations as the ratio of the desired signal power and the variance of the error between the desired and the obtained realizations.

$$SNR = \frac{E\left(\left|h_{i,j}\right|^2\right)}{\text{var}\left(\left|h_{i,j} - h_{i,j}^e\right|\right)}, \quad (5.35)$$

being  $h_{i,j}$  and  $h_{i,j}^e$  the corresponding entries of  $\mathbf{H}$  and  $\mathbf{H}_e$ , respectively. Comparing the SNR results with those in Table 5.2 we can conclude that the emulation errors are mainly due to

	$h_{11}$	$h_{21}$	$h_{12}$	$h_{22}$
SNR (dB)	31.2819	21.9089	22.7801	18.7281

**Table 5.3:** Performance results: emulation of  $\mathbf{H}[n]$ .**Figure 5.17:** MISO implementation scheme.

the channel measurement procedure, so that the channel emulation methodology does not introduce significant errors.

## 5.9 Validation of statistical channel emulation

In this section we evaluate the emulation methodology described in Section 5.4.1. In particular, we emulate a Rician  $4 \times 1$  MISO channel. The testbed has  $n_T = 4$  and  $n_R = 1$  transmit and receive antennas respectively, using a uniform linear antenna array at the TX at a carrier frequency of 5.6 GHz. Here, we present the results obtained when using our MIMO testbed.

Figure 5.17 depicts the data transmission diagram for emulating a  $4 \times 1$  MISO channel. We maintain the same TX and RX locations and the transmit power, as in Figure 4.20. Once again, we refer to Figure 5.14 to generate our four TX signals, in this case  $i = 4$ .

Let assume we desire to emulate a Rician fading channel with the following mean

$$|\boldsymbol{\mu}| = \begin{bmatrix} 0.5500 \\ 0.8803 \\ 0.8944 \\ 0.6708 \end{bmatrix} \quad \arg(\boldsymbol{\mu}) = \begin{bmatrix} 14.8969 \\ 7.1620 \\ 11.4592 \\ 46.9825 \end{bmatrix}$$

and the following spatial covariance matrix

$$|\mathbf{C}| = \begin{bmatrix} 0.0605 & 0 & 0.0583 & 0 \\ 0 & 0.1550 & 0.1360 & 0 \\ 0.0583 & 0.1360 & 0.1600 & 0 \\ 0 & 0 & 0 & 0.0900 \end{bmatrix} \quad (5.36)$$

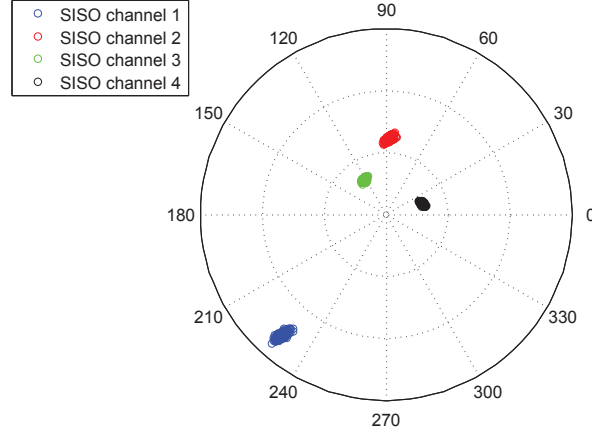


**Figure 5.18:** MISO initial channel estimation resulting time-invariant channels.

$$\arg(\mathbf{C}) = \begin{bmatrix} 0 & 0 & -59.0362 & 0 \\ 0 & 0 & 36.0274 & 0 \\ 59.0362 & -36.0274 & 0 & 0 \\ 0 & 0 & 0 & 0 \end{bmatrix}.$$

The following lines describe the emulation procedure:

1. Making use of the channel measurement methodology presented in Chapter 4, we measure the physical channel,  $\mathbf{h}_0$ . We repeat these measurements 1000 times to prove the lack of variability of the channel (see Figure 5.18). The last channel measurement was carried out 10 minutes later than the first one. The measured channel is

$$|\mathbf{h}_0| = \begin{bmatrix} 5.0750 \\ 2.4195 \\ 1.2912 \\ 1.2102 \end{bmatrix} \quad \arg(\mathbf{h}_0) = \begin{bmatrix} -128.6567 \\ 89.4564 \\ 123.9377 \\ 18.2808 \end{bmatrix}.$$

These channel measurements will serve us as starting point for the implementation results.

2. The transmit signals, generated according to Figure 5.14, are fed to the complex multipliers as well as the weights obtained from (5.16). As in the previous case, this solution gets rid of prepending the small guard intervals (as we did in Chapter 4) but prepending a PN sequence to the best SISO channel in terms of received power, known in advance from the MIMO channel estimation that has to be done to obtain  $\mathbf{h}_0$  (SISO channel 1 in Figure 5.18).
3. Using (5.16) we calculate the weights realizations,  $\mathbf{w}[n]$ , to generate  $N = 1000$  Rician channel realizations,  $\mathbf{h}[n]$ , according to  $\boldsymbol{\mu}$  and  $\mathbf{C}$ .
4. We transmit the signals  $\mathbf{s}_i[n]$  multiplied by the weight vector,  $\mathbf{w}[n]$  and we obtain  $N$  estimates of the equivalent channel,  $\tilde{\mathbf{h}}[n]$ .
5. From  $\tilde{\mathbf{h}}[n]$  we calculate the sample estimates of  $\boldsymbol{\mu}$  and  $\mathbf{C}$ :

$$\hat{\boldsymbol{\mu}} = \frac{1}{N} \sum_{n=1}^N \hat{\mathbf{h}}[n] \quad (5.37)$$

$$\hat{\mathbf{C}} = \frac{1}{N} \sum_{n=1}^N \left( \hat{\mathbf{h}}[n] - \hat{\boldsymbol{\mu}} \right) \left( \hat{\mathbf{h}}[n] - \hat{\boldsymbol{\mu}} \right)^H \quad (5.38)$$

$$|\hat{\mathbf{C}}| = \begin{bmatrix} 0.0829 & 0.0084 & 0.0530 & 0.0104 \\ 0.0084 & 0.1726 & 0.1399 & 0.0134 \\ 0.0530 & 0.1399 & 0.1600 & 0.0049 \\ 0.0104 & 0.0134 & 0.0049 & 0.0949 \end{bmatrix} \quad (5.39)$$

$$\arg(\hat{\mathbf{C}}) = \begin{bmatrix} 0 & 0.9116 & -47.6868 & -47.8626 \\ -0.9116 & 0 & 31.1895 & -76.9322 \\ 47.6868 & -31.1895 & 0 & -61.5086 \\ 47.8626 & 76.9322 & 61.5086 & 0 \end{bmatrix},$$

and the estimated mean is

$$|\hat{\boldsymbol{\mu}}| = \begin{bmatrix} 0.5580 \\ 0.8979 \\ 0.8647 \\ 0.6622 \end{bmatrix} \quad \arg(\hat{\boldsymbol{\mu}}) = \begin{bmatrix} 16.2647 \\ 5.4304 \\ 9.1129 \\ 45.5734 \end{bmatrix}. \quad (5.40)$$

By comparing (5.39) and (5.36), we realize that the measurement results do not match very well with the simulated ones. Noise impairments and channel estimation errors, affect to the channel emulation procedure, but the main reason of the gap between measured and simulated covariance is the low number of realizations used to estimate the covariance matrix. To verify this fact, we took those 1000 weights realizations,  $\mathbf{w}[n]$  and we calculate with (5.3), the emulated channel,  $\mathbf{h}[n]$ .

6. Finally, we obtain the sample estimate of the covariance matrix making use of (5.38)

$$|\hat{\mathbf{C}}| = \begin{bmatrix} 0.0805 & 0.0054 & 0.0536 & 0.0090 \\ 0.0054 & 0.1613 & 0.1369 & 0.0103 \\ 0.0536 & 0.1369 & 0.1600 & 0.0037 \\ 0.0090 & 0.0103 & 0.0037 & 0.0953 \end{bmatrix} \quad (5.41)$$

$$\arg(\hat{\mathbf{C}}) = \begin{bmatrix} 0 & -27.47 & -55.4035 & -48.6718 \\ 27.4713 & 0 & 36.0939 & -105.7887 \\ 55.4035 & -36.0939 & 0 & -80.2164 \\ 48.6718 & 105.7887 & 80.2164 & 0 \end{bmatrix}.$$

and the sample mean estimation

$$|\hat{\boldsymbol{\mu}}| = \begin{bmatrix} 0.5589 \\ 0.9105 \\ 0.8995 \\ 0.6738 \end{bmatrix} \quad \arg(\hat{\boldsymbol{\mu}}) = \begin{bmatrix} 16.3674 \\ 4.8773 \\ 9.2676 \\ 45.5806 \end{bmatrix}. \quad (5.42)$$

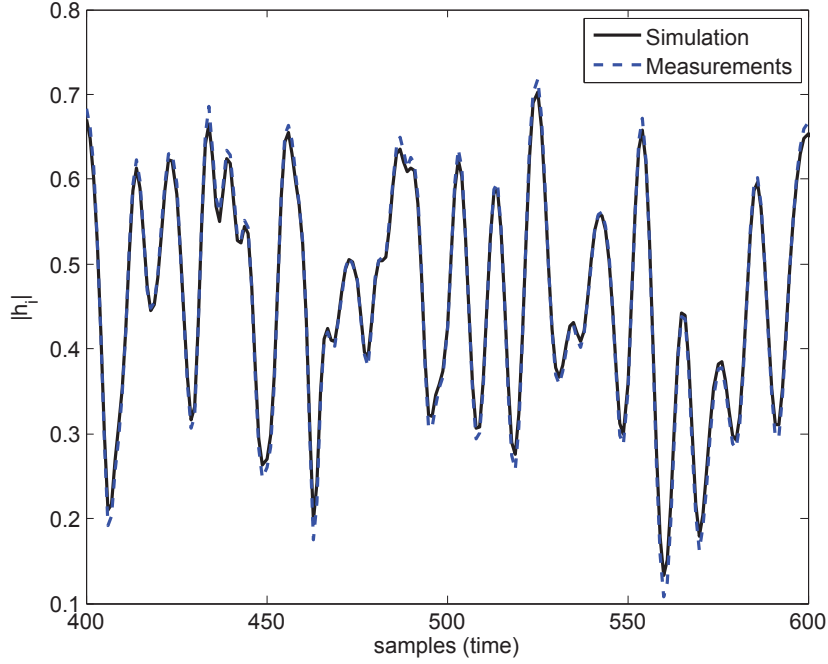


**Figure 5.19:** Temporal evolution comparison.

As can be seen, regarding covariance matrix, (5.39) and (5.41) match very well; as well as the mean, (5.40) and (5.42).

The last results involves checking the temporal correlation and comparing it with both simulation and empirical results. We consider again the  $4 \times 1$  MISO scheme. Now, the Rician channel realizations,  $\mathbf{h}[n]$ , have been generated according to one time-correlated Rayleigh fading channel model. Concretely, the Lee model [Lee, 1982] has been used, which introduces temporal correlation according to a doppler frequency,  $f_D$ . Now, we assume that the channel is spatially uncorrelated.

1. We obtain  $N$  correlated realizations of  $\mathbf{h}[n]$  using the Lee model with  $f_D = 0.1$  Hz.
2. We measure the physical channel,  $\mathbf{h}_0$ , with the testbed.
3. From the  $N$  realizations of  $\mathbf{h}[n]$  we calculate the weight vectors,  $\mathbf{w}[n]$ , using (5.16).
4. We transmit the signals  $\mathbf{s}_i[n]$  multiplied by the corresponding weights and we estimate the equivalent channel,  $\tilde{\mathbf{h}}[n]$ .

Figure 5.19 compare the amplitudes of 200 out of 1000 realizations of the first component of  $\mathbf{h}[n]$  and  $\tilde{\mathbf{h}}[n]$ . The same behavior is also observed for other realizations and components of  $\mathbf{h}[n]$  and  $\tilde{\mathbf{h}}[n]$ .

## 5.10 Comparison between TBMCE and other OTA emulation methods

In this section, we aim at comparing the existing MIMO OTA emulation solutions against our TBMCE solution. There exist different ways to test the OTA performance of MIMO devices. Each of them has its own advantages and drawbacks. This section aim at comparing them according the following features.

	RC	AC + emulator	RC + emulator	TBMCE
Performance	✗	✓	✓	✗
Flexibility	✗	✗	✓	✓
Cost	✓	✗	✗	✓
TX/RX testing	✗/ ✗	✓/ ✓	✓/ ✓	✗/ ✓
Mpath Scenario	✓	✓	✓	✗
Scalability	✗	✗	✗	✓
Portability	✗	✗	✗	✓

**Table 5.4:** Features of TBMCE OTA emulation solutions.

1. **Flexibility:** Capability to emulate any MIMO channel realization.
2. **Cost:** Hardware equipment cost.
3. **Complexity:** software complexity, implementation resources.
4. **Testing capabilities:** if the emulation solution offers the possibility of testing the TX or the RX from the antenna towards BB.
5. **Multipath scenario emulation:** possibility of emulating a multipath propagation scenario (e.g. angular distribution of scatters) separately from the effects of the antennas and AFEs.
6. **Scalability:** whether the number of transmit or receive antennas can be extended. If there exist hardware limitations.
7. **Portability:** if the solutions are stand alone or they depend from other devices, e.g. for generating the transmit signal.
8. **Emulation time:** the time that takes emulating the MIMO channel.

Table 5.4 shows the OTA emulation solutions analyzed in this dissertation and whether or not they meet the previous requirements. As can be seen, our proposal achieves almost all the requirements.

Obviously, TBMCE can not be compared in terms of performance with the OTA solutions that use a commercial channel emulator and a chamber. Commercial channel emulators are built for this purpose and each time are provided with more powerful testing capabilities. Our suggestion is that, if a conventional MIMO testbed is available in the laboratory, we recommend the implementation of the TBMCE solution on it, so that allowing the emulation of MIMO channels.

TBMCE, as detailed in Section 5.3, it is able to emulate any channel realization by simply selecting the appropriate weights. Otherwise, in RCs without an emulator and in ACs it is impossible to get any channel realization, even with additional equipment, e.g. stirrers, etc. it will be unfeasible.

Actually, for testing DUTs using channel emulation we do not need such equipment; these solutions would involve a huge expense that might not be affordable for small research groups. Although, for example, the reverberation chambers are cheaper than the anechoic chambers, the solution will still require a commercial channel emulator or a BB fading emulator to emulate any set of MIMO channel realizations. The implementation of TBMCE does not add any

cost to the available hardware. The fading generation, spatial and temporal characteristics are generated in BB within the TX, which avoids the extra upconversion and downconversion that a commercial channel emulator performs. Also, a point in its favor is that the RX does not need modifications, which simplifies the solution.

The main drawback of the TBMCE solution is that it does not offer TX testing capabilities. The fact that all the processing is performed at the TX and it can not be tested by itself, makes the TX testing unfeasible. Solutions based on channel emulators might offer OTA TX testing capabilities, but they will need additional chambers to provide this functionality.

Also, another downside of the method is that, since we work with equivalent BB channels, it cannot emulate a multipath propagation scenario (e.g. angular distribution of scatters) separately from the effects of the antennas and AFE's.

Regarding portability, TBMCE uses the testbed for generating the signals and transmitting them through the air to perform channel emulation. In short, only the testbed is required for the steps that involve MIMO OTA testing. The other solutions will require additional hardware like signal generators, a testbed, etc. to generate the transmit signals to be fed into the channel emulator and, subsequently, to the RC or AC.

Another point of discussion is how to keep the environment static, as the anechoic chambers features. In our case, we take advantage of the low mobility of the MIMO channel in indoor environments to consider them as controlled scenarios.

There exist, however, certain similarities concerning the implementation of TBMCE that could be compared to other proposals. Our solution follows the same principle used by BB fading emulators, in such a way that the transmit signals are generated within the TX and then altered in BB. As an example, a MIMO frequency-based wideband channel emulator is proposed in [Nasr and Daneshrad, 2009]. This scheme is quite similar to ours since it accepts channel measurements to be loaded and reproduces them as well. It is also based on weighting the transmit signals to emulate the MIMO channel. However, the TX and RX DUT are integrated on the same hardware, hence it does not belong to the OTA emulation solutions. We are not constrained to provide only the I/Q signals, but upconverting them to RF in order to perform OTA emulation.

One can think that adding a AFE along with the antennas to a solution that provides the I/Q signal, would represent our solution. TBMCE goes beyond in its goals and in its targets. When implementing this solution over a MIMO testbed, there exist some requirements that we provide, which make the difference between our proposal and others:

- **Synchronization:** TBMCE is based on the TX/RX scheme proposed in Chapter 4, using complex exponentials for synchronization. In this Chapter, the validation of the results is carried out by transmitting complex exponentials. However, in the case that, for example, a commercial RX device acts as the RX DUT, the transmitted signals from our TX would not be exponentials but others compatible to the RX DUT communication rules. So, the synchronization could be performed as well.
- **Know the actual MIMO channel:** There is a need to measure the MIMO channel in advance. This fact justifies using the methodology presented in Chapter 4. The propagation environment is one in particular depending on the position of the TX and RX node and might change, so we need to measure it at that time. In the case that the RX testbed node is a commercial RX, it must provide the channel measures.



## 5.11 Successful stories

Finally, we briefly highlight the successful stories that the implementation of the TBMCE has given rise.

- In [Vásquez et al., 2012], the authors generate time-variant channels by emulating them using time-varying beamforming.
- In [Pérez-Cruz et al., 2013], the authors track frequency-selective and time-varying channels, which measures have been obtained with the proposed methodology.

## 5.12 Conclusions

In this chapter, a simple and flexible solution for the OTA emulation of narrowband MIMO systems using a MIMO testbed has been proposed.

- The emulation solution requires measuring the MIMO channel in advance. This channel is assumed invariant during the emulation process.
- The solution is flexible in the sense that it can emulate any channel realization by properly choosing the weights of the linear combination.
- The emulation can be carried out only using the MIMO testbed. We just simply need to add an additional linear processing within the transmitter.
- We also provide real-world measurements to prove the feasibility and correctness of its implementation on the GTAS MIMO testbed with excellent results.
- To emulate a  $n_R \times n_T$  MIMO channel, we need a testbed with  $n_R \times n_R$  antennas. So, for a MISO case we just need a SISO testbed.
- The solution allows testing complete MIMO receivers, without the need of modifications.
- The DUTs could be at the TX and/or at the RX. The DUT can be also a complete RX provided that the BB processor at the RX is able to estimate the equivalent baseband channel.
- The scheme is well suited to test MIMO specific algorithms (space-time coding, spatial multiplexing, etc.), that are usually implemented in TX and RX baseband processors.
- It offers a more flexible and cheaper solution compared to the current OTA emulation techniques, typically based on commercial channel emulators, anechoic and reverberation chambers.



# 6

Chapter

## Conclusions and Future Lines

In this work, a series of methodologies for measuring and emulating the MIMO channel are presented. They have been implemented within the GTAS MIMO testbed in a simple and effective way. With this aim, the testbed has been provided with a web interface based on webservices which allows making the most of its functionalities and performance, allowing these implementations and other forthcoming ones.

### 6.1 Conclusions

In Chapter 3, we have described the main features of MIMO wireless testbeds, focusing on the one available in the GTAS group. As the main activity in this first part, the GTAS MIMO testbed has been provided with an interface based on webservices that facilitates its control and the implementation of MIMO techniques and algorithms. The interface is versatile, efficient and secure. This webservice is accessible from almost every software application like Matlab, web applications or even desktop applications. The whole system forms a great academic solution but also turns on a powerful wireless research tool. The availability of three testbed nodes along with the remote handling capabilities open the door to carry out more complex experiments as multiuser schemes, cooperative communications, etc. Also, as an example, a MIMO channel estimation methodology under MIMAX project based on time-varying beamforming is described. Its implementation within our MIMO testbed led to MIMO channel measurements that proved that the indoor MIMO channel is static when the environment is stationary. This supposed one of the first challenges after the testbed and the interface to control it were ready. The experience gained working in this project was of paramount importance for the next chapters of this dissertation.

We have presented in Chapter 4 the design and implementation of a flexible broadband MIMO channel measurement methodology. It is based on sending multifrequency signals within a certain bandwidth, being really flexible since the separation between exponentials can be chosen arbitrarily as well as the desired bandwidth. These parameters are limited by the hardware in which it is implemented. The estimation algorithm used at the receiver side (IWPA) has been modified to deal with complex exponentials and avoids the need of synchronizing transmitter and receiver. This methodology can be implemented in any hardware made up of radiofrequency (RF) modules and digital processing units (DPUs). In this case it has been implemented and verified using the GTAS MIMO testbed with successful results, although is by far not comparable in terms of performance to dedicated equipment. However, it results a low-cost tool for accurately obtain MIMO channel measures that faithfully repre-

sent the actual channel conditions. Many measurement campaigns have been carried out and valuable parameters have been obtained for different publications and research goals. One of the main conclusions of this chapter is that, in static indoor environments, the channel remains constant; which gives an idea of its high temporal coherence. Therefore, realistic channel conditions are difficult to reproduce given the nature of such indoor propagation environments. This deterministic nature of these scenarios, far from being a disadvantage, has motivated the design and implementation of a simple channel emulation methodology, that will be described in Chapter 5.

Finally, in Chapter 5, we have proposed a simple and flexible solution for the OTA emulation of narrowband MIMO systems using a MIMO testbed. In this dissertation, as well as in the previous chapter, the GTAS MIMO testbed has been utilized to implement this solution. In this case, it is based on linear combinations of the transmit signals to emulate the MIMO channel. The coefficients of the linear combinations are complex weights which are obtained from measuring the MIMO channel in advance. This channel is assumed invariant during the emulation process. The solution is flexible in the sense that it can emulate any channel realization by properly choosing the weights of the linear combination which, in terms of implementation, just simply requires adding an additional linear processing within the transmitter. To prove the feasibility and correctness of its implementation on the GTAS MIMO testbed we have provided real-world measurements with excellent results. The solution allows testing complete MIMO receivers, without the need of modifications. It offers a more flexible and cheaper solution compared to the current OTA emulation techniques, typically based on commercial channel emulators, anechoic and reverberation chambers.

## 6.2 Future lines

The theoretical and practical work that arises from this dissertation, can lead to different interpretations and points of view when deciding which future lines are to be followed. In our opinion, the most important future direction would be to improve our MIMO channel emulation scheme in a way that wideband emulation can be performed. Below, the key steps to follow this direction are explained. In addition, we

### 6.2.1 Wideband MIMO channel emulation

In Chapter 5, we have described the procedure for emulating narrowband MIMO channels. As stated in that chapter, a linear combination of the transmit signals is performed in order to emulate a desired channel.

As presented in Chapter 2, the wireless channel consists of several multipath components (MPCs), each with its amplitude and delay. With the methodology proposed in Chapter 4 we can measure wideband MIMO channels, i.e. we are able to extract each channel component, with its associated gain and delay. If we consider this BB discrete-time model of the channel, the transfer function is evaluated only over the bandwidth of the channel. This can be represented as a complex-coefficient FIR filter. The number of MPCs depends on the longest delay and the sample time. In our case, for our emulation methodology we only choose one of these MPCs, so we simplify the wideband channel to a channel with just one MPC (narrowband channel).

Thus, for emulating the narrowband channel we just consider the actual MIMO channel,  $\mathbf{H}_0$ , with one entry for each antenna combination. Therefore, the coefficients of the

linear combination are just complex numbers, each multiplying the corresponding channel coefficient.

For wideband emulation we need a set of weights corresponding to each entry of the MIMO channel (in this case, each entry represents several coefficients since we consider a wideband channel). Therefore, wideband emulation can be realized if, instead of complex weights and complex multipliers, we multiply the entries of the MIMO channel by a filter of length  $i$ , being  $i$  the number of MPCs to be considered.

In the literature, there exist several books for designing filters [Jackson, 1989, Antoniou, 1993], that could serve as an initial point to design such model for emulating wideband channels. It is of high importance to carefully quantize the filter coefficients from floating-point to fixed-point, since this step can perturb the implemented frequency response from its intended response.

### 6.2.2 Scope of application

The proposed methodologies (implementations) can be also be applied to different research topics. This dissertation can contribute to improve the development and verification of current theoretical research that is being carried out in GTAS. Some of its staff are investigating on Interference Alignment (IA), relay channels and cognitive radio. Below we briefly describe the potential applications in these areas:

- Regarding IA, some outstanding publications have been addressed in the last few years. At present, these theoretical achievements are being evaluated in our lab using the GTAS MIMO testbed in combination with the MIMO testbed of the University of La Coruña [García-Naya et al., 2011]. As a main contribution for this research, the Testbed-based MIMO Channel Emulation (TBMCE) results quite useful when assessing these algorithms under controlled channels, with the possibility of making the conditions repeatable. This would be a great improvement since it is desirable to maintain the environment as much stable as possible for evaluating the performance of these techniques.
- Also, our tools turn out to be of high importance when implemented in the cheaper and open source Universal Software Radio Peripheral (USRP) [Vásquez et al., 2012] hardware, which have been briefly described in Chapter 3. The possibility of knowing the actual channel, along with the capability of emulating it, give us the chance of carrying out a huge amount of experiments. For example, this would bring along heterogeneous experiments with both USRP and Nutaq equipment (or other different manufactures), aiming at the design of MIMO multiple-access channels (MAC) as well as broadcast channels (BC), under controlled conditions.

### 6.2.3 Straightforward improvements

Finally, as straightforward extensions of this dissertation, we point out several ideas that would provide the different implementations with more flexibility.

- In Chapter 4 the back-to-back calibration has been carried out for a certain RF frequency. Therefore, an open issue is to cover other central frequencies and bandwidths (of course depending on the hardware in which it is implemented).

- In Chapter 5, we have put forward closed forms for calculating the necessary weights to emulate Ricean and Rayleigh channels. However, other expressions can be found for emulating other kind of distributions, such as Nakagami, Weibull, etc.

## MIMO channel measurement features (Section 4.6)

In this chapter, the performance parameters of the multifrequency methodology for measuring multiple-input multiple-output (MIMO) channels are put forward. Note that the values are obtained when this methodology is implemented in the GTAS MIMO testbed, which means that the performance results are constrained by the hardware in which it is implemented.

First of all, it is important to point out that our methodology is based on a semi-switched configuration (switching in time at transmission and parallel reception). Figure A.1 represents the semi-switched scheme for a  $4 \times 4$  configuration. Since we use parallel receivers, the time employed to perform a single-input single-output (SISO) measurement,  $T_{SISO}$ , matches up with the time employed to perform a single-input multiple-output (SIMO) measurement,  $T_{SIMO}$ . The total time for a MIMO measurement is denoted as  $T_{snapshot}$ , where  $\tau_s$  and  $\tau_l$  are the spaces among transmissions that allows transmitter identification.

Our system is able to transmit the sequence depicted in Figure 4.10 one after another (MIMO channel snapshots estimated consecutively) which means that the time among measurements,  $T_{meas}$ , is the same as the duration of the snapshot,  $T_{meas} = T_{snapshot}$ . It is also possible to introduce "no transmission" gaps among sequences,  $\tau_{sleep}$ , which means that the measurement time will be  $T_{meas} = T_{snapshot} + \tau_{sleep}$ .  $\tau_{sleep}$  is a time interval defined by the user (e.g. any pause or sleep time).

The parameters that can be tuned in this scheme are:

- The number of samples of each  $s_i[n]$ . In our case, we consider 640.
- The sampling frequency. In our case,  $f_s = 26$  MHz

### A.1 SISO measurement time

The SISO measurement time is obtained as the quotient of the number of samples of the signals and the sampling frequency, i.e.

$$T_{SISO} = T_{SIMO} = \frac{640}{26 \exp(-6)} = 24.6 \mu s \quad (\text{A.1})$$

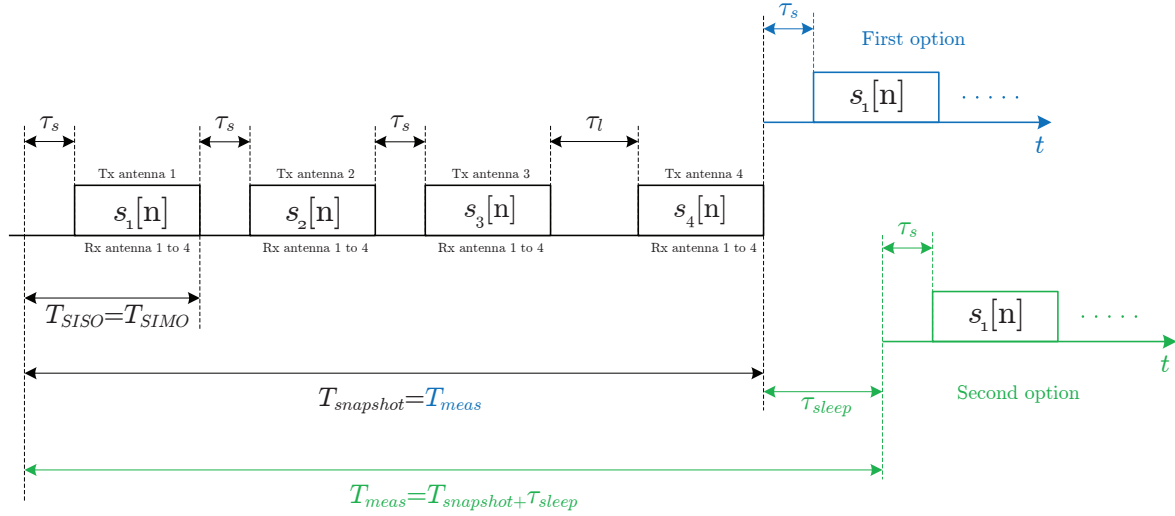


**Figure A.1:** Time diagram representing the transmission/reception scheme for our  $4 \times 4$  antenna configuration.

## A.2 Doppler Calculation

We try to measure the time varying nature of the channel by estimating the time that a snapshot takes. The resolution in  $t$  will give us the maximum Doppler. This is, how fast can be variation in  $t$  of our MIMO channel. So, we can express the Doppler bandwidth in a general way as the inverse of the measurement time interval  $T_{meas}$ .

$$D_{BW} = \frac{K}{T_{meas}} \quad (A.2)$$

where  $K$  is usually a factor of value  $K = 1$ . For a fully-switched configuration, (A.2) can be expressed as

$$D_{BW} = \frac{K}{T_{snapshot} + \tau_{sleep}} = \frac{K}{T_{SISO} \cdot n_T \cdot n_R + \tau_{sleep}} \quad (A.3)$$

where  $T_{SISO}$  is the SISO measurement time (equal in this case to  $T_{SIMO}$ ) and  $n_T$  is the number of transmit antennas and  $n_R$  is the number of receive antennas. Since we are dealing with a semi-switched configuration, the Doppler bandwidth can be expressed as

$$D_{BW} = \frac{K}{T_{snapshot} + \tau_{sleep}} = \frac{K}{T_{SISO} \cdot n_T + \tau_{sleep}} \quad (A.4)$$

where  $T_{SISO}$  is the SISO channel measurement time (equal in this case to  $T_{SIMO}$ ) and  $n_T$  is the number of transmit antennas.

We have presented in the current manuscript on Table I that the  $T_{SISO} = T_{SIMO} = 24.6 \mu s$ . Figure 6 in the current manuscript presents 11 MIMO channel snapshots (the curves are overlapped since there was no moving objects in the environment and the nodes were kept fixed). The sleep time,  $\tau_{sleep}$ , in this case will be

$$\tau_{sleep} \approx 100 \text{ ms} - (24.6 \mu s \cdot 4) \approx 99.9 \text{ ms} \quad (A.5)$$

If we set  $\tau_{sleep} = 0$  our Doppler bandwidth will be



$$D_{BW} = \frac{K}{T_{SIMO} \cdot n_T + 0} = 10163 \text{ Hz} \quad (\text{A.6})$$

In summary, we can control the duration of the sleep time,  $\tau_{sleep}$ , among snapshots but the results presented in Table 5.2 compare the best Doppler bandwidth capabilities of each testbed taking into account the different antenna schemes ( $n_R \times n_T$ ), i.e., assuming that  $\tau_{sleep} = 0$ .

### A.3 Maximum scatterer velocity

We define the maximum Doppler bandwidth as

$$D_{BW_{max}} = \frac{\nu_{max} f_c T_s}{c} \quad (\text{A.7})$$

where  $\nu_{max}$  is the maximum supported user velocity,  $f_c$  is the carrier frequency,  $T_s$  is the symbol duration and  $c$  stands for the speed of light. In our case we assume that  $T_s = 1$  since we are dealing with complex exponentials. Therefore, the maximum supported velocity will be

$$\nu_{max} = \frac{D_{BW_{max}} f_c}{c} = \frac{10163 \cdot 3 \exp(8)}{5.6 \exp(9)} = 1960 \text{ Km/h} \quad (\text{A.8})$$



# Appendix **B**

## Publications

### B.1 Publications derived from the dissertation

These Dissertation has given place to the following publications:

#### B.1.1 Journal publications

1. J. Gutiérrez, Ó. González, J. Pérez, D. Ramírez, L. Vielva, J. Ibáñez and I. Santamaría. “Frequency-domain methodology for measuring MIMO channels using a generic test bed”. *IEEE Transactions on Instrumentation and Measurement*, vol.60, no.3, pp.827-838, March 2011.
2. J. Gutiérrez, J. Ibáñez and J. Pérez. “MIMO OTA Testing Based on Transmit Signal Processing”. *Hindawi International Journal of Antennas and Propagation (Special Issue on Antenna Measurement Systems and Antenna Technology for Next Wireless Generation (NEXT))*, vol. 2013, June 2013.

#### B.1.2 International Conferences

3. J. Gutiérrez, J. Ibáñez and J. Pérez. “Beamforming-based emulation of spatial and temporal correlated MISO channels”. *International Symposium on Signals, Systems and Electronics (ISSSE 2012)*, Potsdam, Germany, October 2012.
4. J. Gutiérrez, J. Ibáñez and J. Pérez. “Spatial correlation beamforming scheme for MISO channel emulation”. *International Symposium on Wireless Communication Systems (ISWCS 2012)*, Paris, France, August 2012.
5. Ó. González, J. Gutiérrez, J. Ibáñez, L. Vielva y R. Eickhoff. “Experimental evaluation of an RF-MIMO transceiver for 802.11a WLAN”. *Future Network and Mobile Summit 2010*, Florence, Italy, June 2010.
6. L. Vielva, J. Vía, J. Gutiérrez, Ó. González, J. Ibáñez y I. Santamaría. “Building a Web Platform for Learning Advanced Digital Communications using a MIMO Testbed”. *IEEE International Conference on Acoustics, Speech and Signal Processing (ICASSP 2010)*, Dallas, USA, March 2010.

## B.2 Other Publications

During this Dissertation, we have been working also in other research fields, not related to the topic:

### B.2.1 International Conferences

7. M. Morales, J. Gutiérrez and A. G. Armada. “Achievable Throughput with Block Diagonalization on OFDM Indoor Demonstrator”. *European Signal Processing Conference (EUSIPCO 2013)*, Marrakech, Morocco, September 2013.
8. J. Gutiérrez, A. Habib and M. Rupp. “Selection Schemes for Orthogonal Tripole Antennas”. *European Conference on Antennas and Propagation (EUCAP 2013)*, Gothenburg, Sweden, April 2013.
9. J. Gutiérrez, A. Habib and M. Rupp. “Indoor measurements by dual tripole antennas”. *Loughborough Antennas & Propagation Conference (LAPC 2012)*, Loughborough, UK, November 2012.
10. J. Manco Vásquez, J. Gutiérrez, J. Pérez, J. Ibáñez and I. Santamaría. “Experimental Evaluation of Multiantenna Spectrum Sensing Detectors using a Cognitive Radio Testbed”. *International Symposium on Signals, Systems and Electronics (ISSSE)*, Potsdam, Germany, September 2012.
11. J. Pérez, J. Gutiérrez y L. Vielva. “Performance Analysis of Transmit Antenna Selection in Broadcast MISO Channels”, *IEEE International Symposium on Broadband Multimedia Systems and Broadcasting*, Bilbao, Spain, May 2009.

# List of Figures

1.1	Evaluating MIMO radio communication. . . . .	4
1.2	General methodology followed during thesis and type of result from each step. . . . .	6
2.1	Multipath components . . . . .	10
2.2	Fading channel manifestations. . . . .	11
2.3	An example of the discrete channel impulse response for a 5-path radio channel. . . . .	12
2.4	Multipath propagation causing fading in time, frequency and space. . . . .	15
2.5	Stochastic definition of coherence parameters . . . . .	16
2.6	Baseband equivalent MIMO channel . . . . .	19
3.1	MIMO testbed hardware components . . . . .	26
3.2	Block diagram of a Lyrtech node. . . . .	30
3.3	Lyrtech BB boards . . . . .	31
3.4	Quad Dual-Band AFE from Lyrtech, Inc. . . . .	32
3.5	Zero-IF AFE architecture based on MAX2829 chip (Comlab). . . . .	33
3.6	I/Q modulator imbalance. . . . .	34
3.7	Block diagram of a Lyrtech node. . . . .	35
3.8	VHS control utility General Controls tab . . . . .	36
3.9	Communication path between host CPU application and AFE . . . . .	37
3.10	Lyrtech node control possibilities. . . . .	38
3.11	Block diagram of two of the nodes of the $4 \times 4$ GTAS MIMO testbed. . . . .	39
3.12	Block diagram approach of the FPGA interfaces . . . . .	40
3.13	New interface within the Lyrtech node. . . . .	41
3.14	First interface architecture, based on PNET . . . . .	42
3.15	Architecture of the web platform. . . . .	43
3.16	MIMO network scenarios. . . . .	44
3.17	Multi-user testbed capabilities . . . . .	44
3.18	Final interface architecture . . . . .	45
3.19	FPGA interfaces and custom logic. . . . .	49
3.20	Typical MBDK FPGA model. . . . .	53
3.21	System Generator block dialog box for the VHS-ADC/DAC. . . . .	54
3.22	Simulink scheme. . . . .	55
3.23	MIMAX BB processor architecture . . . . .	58
3.24	Spatial MIMO beamforming. . . . .	59
3.25	Analog antenna combining in RF . . . . .	59
3.26	BB weight application. . . . .	60
3.27	MIMAX training frame. . . . .	60
3.28	Weight values for a $4 \times 4$ MIMAX training frame. . . . .	61
3.29	MIMAX channel measuring procedure. . . . .	61

3.30	LS MIMAX $4 \times 4$ channel estimation results. . . . .	62
4.1	Vector Network Analyzer (VNA). . . . .	65
4.2	Fully-switched scheme. . . . .	68
4.3	Semi-switched scheme. . . . .	68
4.4	Measurement scheme for SIMO channels. . . . .	69
4.5	Example of exponential signals spectra, $M = 20$ . . . . .	70
4.6	Block diagram of the phase optimization procedure and crest factor correction. . . . .	72
4.7	Transmitted signal envelope before and after crest factor correction . . . . .	73
4.8	Received signal and IWPA estimation (zoomed area). . . . .	74
4.9	IWPA performance against LO offset. . . . .	75
4.10	TX/RX time diagram for our $4 \times 4$ antenna configuration. . . . .	76
4.11	Transmitter identification . . . . .	77
4.12	Transmitter labeling. . . . .	77
4.13	Block diagram of the $4 \times 4$ MIMO testbed . . . . .	78
4.14	Setup for compensating the hardware. . . . .	79
4.15	Precision measurement setup. . . . .	81
4.16	Precision and operating range of the FFT and IWPA methods . . . . .	81
4.17	Frequency response of the bandpass filter. . . . .	82
4.18	$S_{21}$ parameter comparison . . . . .	83
4.19	MIMO $2 \times 2$ channel measures . . . . .	84
4.20	Node locations of the different experiments . . . . .	86
4.21	MIMO channel frequency response . . . . .	87
4.22	Histogram that represents the absolute value of the channel response. . . . .	88
4.23	Example of coherence bandwidth calculation . . . . .	89
4.24	Antenna form factors . . . . .	90
4.25	Measurement grid . . . . .	90
4.26	MIMAX $4 \times 4$ channel estimation results. . . . .	91
4.27	Multifrequency $4 \times 4$ channel estimation results. . . . .	92
4.28	Frequency Domain channel estimation MATLAB GUI. . . . .	93
5.1	Solutions for MIMO channel emulation. . . . .	97
5.2	Block diagram of a typical commercial $4 \times 4$ channel emulator. . . . .	98
5.3	Anechoic chamber method for MIMO OTA testing. . . . .	100
5.4	Test bench configuration: RC and channel emulator . . . . .	101
5.5	Proposed scheme using linear signal processing at the TX. . . . .	103
5.6	Proposed MISO scheme using transmit beamforming. . . . .	104
5.7	Proposed MIMO scheme using transmit linear processing. . . . .	105
5.8	Scheme using linear processing at both sides. . . . .	110
5.9	Scheme with receive processing. . . . .	111
5.10	Conventional receiver. . . . .	112
5.11	Block diagram of two of the nodes of the $4 \times 4$ MIMO test bed . . . . .	113
5.12	Weighting block implementation. . . . .	114
5.13	Implementation diagram for emulating a $2 \times 2$ MIMO channel. . . . .	116
5.14	Diagram representing how to create the transmit signals. . . . .	116
5.15	MIMO $2 \times 2$ initial channel measures . . . . .	117
5.16	Comparison between the desired and the actual emulated channel. . . . .	118
5.17	MISO implementation scheme. . . . .	119

---

5.18 MISO initial channel estimation . . . . .	120
5.19 Temporal evolution comparison. . . . .	122
A.1 MIMO $4 \times 4$ timing diagram. . . . .	132





# List of Tables

2.1	Relevant autocorrelation-spectrum relationships. . . . .	16
4.1	Performance results: measurement of $\mathbf{H}_0$ . . . . .	83
4.2	Comparison of channel sounders . . . . .	85
4.3	Wideband parameters. . . . .	88
4.4	Correlation coefficients (in modulus) of the different form factor configurations. . . . .	91
5.1	FPGA resources utilization. . . . .	115
5.2	Performance results: measurement of $\mathbf{H}_0$ . . . . .	117
5.3	Performance results: emulation of $\mathbf{H}[n]$ . . . . .	118
5.4	Features of TBMCE OTA emulation solutions. . . . .	123



# List of Algorithms

4.1	Procedure to obtain the number of exponentials and their frequencies . . . . .	71
-----	--	----



# Bibliography

- [3GPP, 2013] 3GPP. “The Mobile Broadband Standard”. <http://www.3gpp.org/>, 2013. [Online; accessed 12-January-2013].
- [Adjoudani et al., 2003] A. Adjoudani, E. Beck, A. Burg, G. Djuknic, T. Gvoth, D. Haessig, S. Manji, M. Milbrodt, M. Rupp, D. Samardzija, A. Siegel, I. Sizer, T., C. Tran, S. Walker, S. Wilkus, and P. Wolniansky. “Prototype experience for MIMO BLAST over third-generation wireless system”. *IEEE Journal on Selected Areas in Communications*, volume 21, n<sup>o</sup> 3, pages 440–451, 2003.
- [Agilent, 2012] Agilent. “Agilent Technologies”. <http://www.home.agilent.com>, 2012. [Online; accessed 13-December-2012].
- [Almers et al., 2007] P. Almers, E. Bonek, A. Burr, N. Czink, M. Debbah, V. Degli-Esposti, H. Hofstetter, P. Kyösti, D. Laurenson, G. Matz, A. F. Molisch, C. Oestges, and H. Özcelik. “Survey of channel and radio propagation models for wireless MIMO systems”. *EURASIP Journal on Wireless Communications and Networking*, volume 2007, n<sup>o</sup> 1, 2007.
- [Antoniou, 1993] A. Antoniou. *Digital Filters, Analysis, Design and Applications*. McGraw-Hill, 1993.
- [Aschbacher et al., 2004] E. Aschbacher, S. Caban, C. Mehlfürer, G. Maier, and M. Rupp. “Design of a Flexible and Scalable 4 x 4 MIMO Testbed”. *11th Digital Signal Processing Workshop*, pages 178–181, 2004.
- [Azami et al., 2008] F. Azami, A. Ghorssi, H. Hemesi, A. Mohammadi, and A. Abdipour. “Design and implementation of a flexible 4x4 mimo testbed”. In *Telecommunications, 2008. IST 2008. International Symposium on*, pages 268 –272. 2008.
- [Azimuth, 2012] Azimuth. “Azimuth Systems”. <http://www.azimuthsystems.com>, 2012. [Online; accessed 13-December-2012].
- [Azimuth Systems, 2006] I. Azimuth Systems. “Ace”. <http://www.azimuthsystems.com/wp-content/uploads/PB-ACEMX-20110928.pdf>, 2006.
- [Baddour and Beaulieu, 2005] K. Baddour and N. Beaulieu. “Autoregressive modeling for fading channel simulation”. *IEEE Transactions on Wireless Communications*, volume 4, n<sup>o</sup> 4, pages 1650 – 1662, 2005.
- [Baum et al., 2000] D. Baum, D. Gore, R. Nabar, S. Panchanathan, K. Hari, V. Erceg, and A. Paulraj. “Measurement and Characterization of Broadband MIMO Fixed Wireless Channels at 2.5 GHz”. In *Personal Wireless Communications, 2000 IEEE International Conference on*, pages 203–206. 2000.

- [Bialkowski et al., 2007] K. Bialkowski, A. Postula, A. Abbosh, and M. Bialkowski. “2x2 MIMO Testbed for Dual 2.4GHz/5GHz Band”. In *Electromagnetics in Advanced Applications, 2007. ICEAA 2007. International Conference on*, pages 1–4. 2007.
- [Borkowski et al., 2006] D. Borkowski, L. Brühl, C. Degen, et al. “Saba: A testbed for a real-time mimo system”. *EURASIP Journal on Applied Signal Processing*, 2006.
- [Boyd, 1986] S. Boyd. “Multitone signals with low crest factor”. *IEEE Trans. on Circuits and Systems*, volume CAS-33, n<sup>o</sup> 10, pages 1018–1022, 1986.
- [Bultitude, 1987] R. Bultitude. “Measurement, characterization and modeling of indoor 800/900 MHz radio channels for digital communications”. *IEEE Communications Magazine*, volume 25, n<sup>o</sup> 6, pages 5–12, 1987.
- [Bultitude et al., 1988] R. Bultitude, S. Mahmoud, and W. Sullivan. “A comparison of indoor radio propagation characteristics at 910 MHz and 1.75 GHz”. In *WESCANEX 88: 'Digital Communications Conference Proceedings'*, pages 161–168. 1988.
- [Burg and Rupp, 2004] A. Burg and M. Rupp. *EURASIP Book on SMART Antennas*, chapter Demonstrators and Testbeds. Hindawi Publishing Corporation, 2004.
- [Caban et al., 2006] S. Caban, C. Mehlführer, R. Langwieser, A. L. Scholtz, and M. Rupp. “Vienna MIMO testbed”. *EURASIP Journal on Applied Signal Processing, special issue on Implementation Aspects and Testbeds for MIMO systems*, 2006.
- [Céspedes et al., 2013] M. M. Céspedes, J. Gutiérrez, and A. G. Armada. “Achievable throughput with Block Diagonalization on OFDM indoor demonstrator”. In *submitted to IEEE International Conference on Communications (ICC 2013)*. 2013.
- [Chen et al., 2009] X. Chen, P.-S. Kildal, C. Orlenius, and J. Carlsson. “Channel Sounding of Loaded Reverberation Chamber for Over-the-Air Testing of Wireless Devices: Coherence Bandwidth Versus Average Mode Bandwidth and Delay Spread”. *IEEE Antennas and Wireless Propagation Letters*, volume 8, pages 678–681, 2009.
- [Chiurtu et al., 2005] N. Chiurtu, L. Gasser, P. Roud, and B. Rimoldi. “Software-defined radio implementation of multiple antenna systems using low-density parity-check codes”. In *Wireless Communications and Networking Conference, 2005 IEEE*, volume 1, pages 527–531 Vol. 1. 2005.
- [Chung et al., 2005] H. K. Chung, N. Vloeberghs, H. K. Kwon, S. J. Lee, and K. C. Lee. “MIMO Channel Sounder Implementation and Effects of Sounder Impairment on Statistics of Multipath Delay Spread”. In *Vehicular Technology Conference*, volume 1, pages 349–353. 2005.
- [Coldrey, 2008] M. Coldrey. “Modeling and capacity of polarized MIMO channels”. In *Proc. IEEE Vehicular Technology Conference, VTC Spring.*, pages 440–444. Marina Bay, Singapore, 2008.
- [Comlab, 2013] Comlab. “Comlab Telecommunications Inc.”. [http://www.comlab.com/\\_home](http://www.comlab.com/_home), 2013. [Online; accessed 09-February-2013].
- [Correia, 2006] L. M. Correia. *Mobile Broadband Multimedia Networks Techniques, Models and Tools for 4G*. Academic Press, 2006.

- [der Ouderaa et al., 1988] E. V. der Ouderaa, J. Schoukens, and J. Renneboog. “Peak factor minimization using a time-frequency domain swapping algorithm”. *IEEE Trans. Instrum. Meas.*, pages 145–147, 1988.
- [Dowle et al., 2006] J. Dowle, S. Kuo, K. Mehrotra, and I. McLoughlin. “An FPGA-Based MIMO and Space-Time Processing Platform”. *EURASIP Journal on Advances in Signal Processing*, volume 2006, n<sup>o</sup> 1, page 034653, 2006.
- [Dung et al., 2006] D. N. Dung, K. Sakaguchi, S. Suyama, R. Nagareda, J. Takada, H. Suzuki, K. Araki, S. Arata, K. Kaiga, S. Manabe, T. Yamaguchi, and K. Miwa. “Implementation and evaluation of 4x4 mimo fading simulator considering antenna characteristics”. In *First International Conference on Communications and Electronics (ICCE '06)*, pages 472 –477. 2006.
- [Durgin, 2002] G. Durgin. *Space-time wireless channels*. Prentice Hall Press, Upper Saddle River, NJ, USA, first edition, 2002.
- [Eickhoff et al., 2008] R. Eickhoff, F. Ellinger, U. Mayer, M. Wickert, I. Santamaría, R. Kraemer, L. González, P. Sperandio, and T. Theodosiou. “MIMAX: Exploiting the maximum performance and minimum system costs of wireless MIMO systems”. In *17th ICT Mobile and Wireless Summit*. Sweden, 2008.
- [Elektrobit F8, 2013] Elektrobit F8. “Elektrobit F8 MIMO OTA channel emulator”. [http://www.elektrobit.com/what\\_we\\_deliver/wireless/offering/mimo\\_ota](http://www.elektrobit.com/what_we_deliver/wireless/offering/mimo_ota), 2013.
- [Ettus, 2013] Ettus. “Ettus Research LLC”. <http://www.ettus.com>, 2013. [Online; accessed 12-January-2013].
- [Foschini, 1996] G. J. Foschini. “Layered space-time architecture for wireless communication in a fading environment when using multi-element antennas”. *Bell Labs Technical Journal*, volume 1, n<sup>o</sup> 2, pages 41–59, 1996.
- [García-Fernández et al., 2011] M. García-Fernández, J. Sánchez-Heredia, A. Martínez-González, D. Sánchez-Hernández, and J. Valenzuela-Valdés. “Advances in Mode-Stirred Reverberation Chambers for Wireless Communication Performance Evaluation”. *IEEE Communications Magazine*, volume 49, n<sup>o</sup> 7, pages 140 –147, 2011.
- [Garcia-Naya et al., 2007] J. Garcia-Naya, T. Fernandez-Carames, H. Perez-Iglesias, M. Gonzalez-Lopez, L. Castedo, D. Ramirez, I. Santamaria, J. Perez, J. Via, and J. Torres-Royo. “Performance of STBC transmissions with real data”. In *16th IST Mobile and Wireless Communications Summit*, pages 1 –5. 2007.
- [García-Naya et al., 2011] J. A. García-Naya, L. Castedo, Ó. González, D. Ramírez, and I. Santamaría. “Experimental Evaluation of Interference Alignment Under Imperfect Channel State Information”. In *19th European Signal Processing Conference (EUSIPCO 2011)*. Barcelona, Spain, 2011.
- [García-Naya et al., 2010] J. A. García-Naya, P. M. Castro, M. González-López, and A. Dapena. “Testbed-assisted learning for digital communications courses”. *Computer Applications in Engineering Education*, pages n/a–n/a, 2010.

- [Garrett et al., 2004] D. Garrett, G. Woodward, L. Davis, G. Knagge, and C. Nicol. “A 28.8 Mb/s 4E4 MIMO 3G high-speed downlink packet access receiver with normalized least mean square equalization”. *Proceedings of IEEE International Solid-State Circuits Conference (ISSCC 2004)*, volume 1, pages 420–536, 2004.
- [GE, 2013] GE. “GE Fanuc”. <http://www.gefanucembedded.com>, 2013. [Online; accessed 12-January-2013].
- [GNU Radio, 2012] GNU Radio. “GNU Radio”. <http://www.gnuradio.org>, 2012. [Online; accessed 02-January-2013].
- [Hashemi, 1993a] H. Hashemi. “Impulse response modeling of indoor radio propagation channels”. *IEEE Journal on Selected Areas in Communications*, volume 11, n<sup>o</sup> 7, pages 967–978, 1993.
- [Hashemi, 1993b] H. Hashemi. “The indoor propagation channel”. In *Proceedings of the IEEE*, volume 81, pages 1804–1824. 1993.
- [Howard and Pahlavan, 1990] S. J. Howard and K. Pahlavan. “Measurement and analysis of the indoor radio channel in the frequency domain”. *IEEE Transactions on Instrumentation and Measurement*, volume 39, n<sup>o</sup> 5, pages 751–755, 1990.
- [HUNT, 2012] HUNT. “Hunt Engineering”. <http://hunteng.co.uk>, 2012. [Online; accessed 20-December-2012].
- [Hwang et al., 2007] J.-K. Hwang, K.-H. Lin, J.-D. Li, and J.-H. Deng. “Fast FPGA prototyping of a multipath fading channel emulator via high-level design”. In *International Symposium on Communications and Information Technologies (ISCIT '07)*, pages 168–171. 2007.
- [i. Fábregas et al., 2006] A. G. i. Fábregas, M. Guillaud, D. T. M. Slock, et al. “A MIMO-OFDM Testbed for Wireless Local Area Networks”. *EURASIP Journal on Applied Signal Processing*, volume 2006, 2006.
- [IEEE, 2006] IEEE. “Amendment 2: Physical and Medium Access Control Layers for Combined Fixed and Mobile Operation in Licensed Bands and Corrigendum 1”. Technical report, IEEE Standard for Local and Metropolitan Area Networks Part 16: Air Interface for Fixed and Mobile Broadband Wireless Access Systems, 2006.
- [IEEE, 2013] IEEE. “Wireless LAN Medium Access Control (MAC) and Physical Layer (PHY) specifications”. <http://standards.ieee.org/about/get/802/802.11.html>, 2013. [Online; accessed 12-December-2013].
- [IEEE 802.16, 2004] IEEE 802.16. “IEEE Standard for Local and Metropolitan Area Networks Part 16: Air Interface for Fixed Broadband Wireless Access Systems”. Technical report, IEEE, 2004.
- [Innovative, 2013] Innovative. “Innovative Integration”. <http://www.innovative-dsp.com>, 2013. [Online; accessed 12-January-2013].
- [Jackson, 1989] L. B. Jackson. *Digital Filters and Signal Processing*. Kluwer Academic Publishers, 1989.



- [Jagannatham and Erceg, 2004] A. Jagannatham and V. Erceg. “MIMO indoor WLAN channel measurements and parameter modeling at 5.25 GHz”. In *IEEE 60th Vehicular Technology Conference (VTC2004-Fall)*, volume 1, pages 106 – 110 Vol. 1. 2004.
- [Jakes, 1994] W. C. Jakes. *Microwave Mobile Communications*. Wiley-IEEE Press, 1994.
- [Kaiser et al., 2004] T. Kaiser, A. Wilzeck, M. Berentsen, and M. Rupp. “Prototyping for mimo systems - an overview”. 2004.
- [Kaltenberger et al., 2005] F. Kaltenberger, G. Steinböck, R. Kloibhofer, R. Lieger, and G. Humer. “A multi-band development platform for rapid prototyping of MIMO systems”. In *Proc. ITG Workshop on Smart Antennas*. Duisburg, 2005.
- [Karasawa et al., 2012] Y. Karasawa, Y. Gunawan, S. Pasisngi, K. Nakada, and A. Kosako. “Development of a MIMO-OTA System with Simplified Configuration”. *Journal of the Korean Institute of Electromagnetic Engineering and Science*, volume 12, n<sup>o</sup> 1, pages 77–84, 2012.
- [Kemp and Bryant, 2004] A. H. Kemp and E. B. Bryant. “Channel Sounding of Industrial Sites in the 2.4 GHz ISM band”. *Wireless Personal Communications*, volume 31, n<sup>o</sup> 3-4, pages 235–248, 2004.
- [Kermoal et al., 2000] J. Kermoal, L. Schumacher, P. Mogensen, and K. Pedersen. “Experimental investigation of correlation properties of MIMO radio channels for indoor picocell scenarios”. In *52nd Vehicular Technology Conference (IEEE VTS-Fall VTC)*, volume 1, pages 14 –21 vol.1. 2000.
- [Kermoal et al., 2002] J. Kermoal, L. Schumacher, K. Pedersen, P. Mogensen, and F. Frederiksen. “A stochastic MIMO radio channel model with experimental validation”. *IEEE Journal on Selected Areas in Communications*, volume 20, n<sup>o</sup> 6, pages 1211 – 1226, 2002.
- [Keshavarzian et al., 2007] A. Keshavarzian, E. Uysal-Biyikoglu, D. Lal, and K. Chintalapudi. “From Experience with Indoor Wireless Networks: A Link Quality Metric that Captures Channel Memory”. *IEEE Communications Letters*, volume 11, n<sup>o</sup> 9, pages 729–731, 2007.
- [Kivinen et al., 1999a] J. Kivinen, T. Korhonen, P. Aikio, R. Gruber, P. Vainikainen, and S.-G. Haggman. “Wideband radio channel measurement system at 2 ghz”. *Instrumentation and Measurement, IEEE Transactions on*, volume 48, n<sup>o</sup> 1, pages 39 –44, 1999.
- [Kivinen et al., 1999b] J. Kivinen, T. O. Korhonen, P. Aikio, R. Gruber, and P. Vainikainen. “Wideband Radio Channel Measurement System at 2 GHz”. *IEEE Transactions on Instrumentations and Measurement*, volume 48, pages 39–44, 1999.
- [Kivinen et al., 2001] J. Kivinen, X. Zhao, and P. Vainikainen. “Empirical Characterization of Wideband Indoor Radio Channel at 5.3 GHz”. *IEEE Transactions on Antennas and Propagation*, volume 49, n<sup>o</sup> 8, pages 1192–1203, 2001.
- [Kolu and Jamsa, 2002] J. Kolu and T. Jamsa. “A real-time simulator for MIMO radio channels”. In *Proc. 5th Intl. Symposium on Wireless Personal Multimedia Communications*, volume 2, pages 568–572. 2002.

- [Kosako et al., 2011] A. Kosako, M. Shinozawa, and Y. Karasawa. “Simplified configuration of fading emulator system for MIMO-OTA testing”. In *2nd International Conference on Wireless Communication, Vehicular Technology, Information Theory and Aerospace Electronic Systems Technology (Wireless VITAE)*, pages 1 –5. 2011.
- [Kyosti et al., 2010] P. Kyosti, J.-P. Nuutinen, and T. Jamsa. “MIMO OTA test concept with experimental and simulated verification”. In *Proceedings of the Fourth European Conference on Antennas and Propagation (EuCAP 2010)*, pages 1 –5. 2010.
- [Kyritsi et al., 2003] P. Kyritsi, D. Cox, R. Valenzuela, and P. Wolniansky. “Correlation analysis based on MIMO channel measurements in an indoor environment”. *IEEE Journal on Selected Areas in Communications*, volume 21, n<sup>o</sup> 5, pages 713 – 720, 2003.
- [Lafon and Mitra, 2007] Y. Lafon and N. Mitra. “SOAP version 1.2 part 0: Primer (second edition)”. Technical report, W3C, 2007.
- [Lang et al., 2004] S. Lang, M. Rao, and B. Daneshrad. “Design and development of a 5.25 GHz software defined wireless OFDM communication platform”. *IEEE Communications Magazine*, volume 42, n<sup>o</sup> 6, pages S6–12, 2004.
- [Lee, 1982] W. C. Y. Lee. *Mobile Communications Engineering*. Mc, 1982.
- [Maharaj et al., 2005] B. Maharaj, L. Linde, J. Wallace, and M. Jensen. “A cost-effective wideband MIMO channel sounder and initial co-located 2.4 GHz and 5.2 GHz measurements”. In *IEEE International Conference on Acoustics, Speech, and Signal Processing (ICASSP '05)*, volume 3, pages iii/981–iii/984 Vol. 3. 2005.
- [Maharaj et al., 2008] B. T. Maharaj, J. W. Wallace, M. A. Jensen, and L. P. Linde. “A Low Cost Open-Hardware Wideband Multiple-Input Multiple-Output (MIMO) Wireless Channel Sounder”. *IEEE Transactions on Instrumentation and Measurement*, volume 57, pages 2283–2289, 2008.
- [Malik, 2008] W. Malik. “Spatial correlation in ultrawideband channels”. *IEEE Transactions on Wireless Communications*, volume 7, n<sup>o</sup> 2, pages 604 –610, 2008.
- [MAX2828/MAX2829, 2013] MAX2828/MAX2829. “Maxim Integrated Products”. <http://datasheets.maximintegrated.com/en/ds/MAX2828-MAX2829.pdf>, 2013.
- [Medbo et al., 1999] J. Medbo, H. Hallenberg, and J.-E. Berg. “Propagation characteristics at 5 GHz in typical radio-LAN scenarios”. In *IEEE 49th Vehicular Technology Conference*, volume 1, pages 185 –189. 1999.
- [Mehlführer et al., 2006] C. Mehlführer, S. Caban, R. Langwieser, L. W. Mayer, and A. L. Scholtz. “Testbeds and rapid prototyping in wireless system design”. *EURASIP Newsletter*, volume 17, pages 32–50, 2006.
- [Mehlführer et al., 2005] C. Mehlführer, M. Rupp, F. Kaltenberger, and G. Humer. “A scalable rapid prototyping system for real-time MIMO OFDM transmissions”. In *The 2nd IEE/EURASIP Conference on DSP enabled Radio*, page 7 pp. 2005.
- [MIMAX, 2008] MIMAX. “MIMAX: Advanced MIMO systems for maximum reliability and performance”. <http://www.ict-mimax.eu>, 2008.

- [Molina-Garcia-Pardo et al., 2008] J.-M. Molina-Garcia-Pardo, J.-V. Rodriguez, and L. Juan-Llacer. “MIMO Channel Sounder Based on Two Network Analyzers”. *IEEE Transactions on Instrumentation and Measurement*, volume 57, n<sup>o</sup> 9, pages 2052–2058, 2008.
- [Morawski et al., 2003] R. Morawski, T. Le-Ngoc, and O. Naeem. “Wireless and wireline MIMO testbed”. In *Canadian Conference on Electrical and Computer Engineering (CCECE 2003)*, volume 3, pages 1913 – 1916 vol.3. 2003.
- [Murphy et al., 2003] P. Murphy, F. Lou, A. Sabharwal, and J. Frantz. “An FPGA based rapid prototyping platform for MIMO systems”. In *Conference Record of the Thirty-Seventh Asilomar Conference on Signals, Systems and Computers*, volume 1, pages 900–904 Vol.1. 2003.
- [Nasr and Daneshrad, 2009] O. A. Nasr and B. Daneshrad. “Design and FPGA implementation an accurate real time 3x4 MIMO channel emulator”. In *Proceedings of the 43rd Asilomar conference on Signals, systems and computers*, Asilomar’09, pages 764–768. IEEE Press, Piscataway, NJ, USA, 2009.
- [National Instruments, 2012] National Instruments. “National instruments corporation website”. <http://www.ni.com>, 2012. [Online; accessed 13-December-2012].
- [Naya, 2010] J. A. G. Naya. *Testbed Design for Wireless Communications Systems Assessment*. PhD Thesis, Universidade Da Coruña, 2010.
- [Neubauer and Eggers, 1999] T. Neubauer and P. Eggers. “Simultaneous characterization of polarization matrix components in pico cells”. In *Proc. IEEE Vehicular Technology Conference, VTC*, pages 1361–1365. Amsterdam, The Netherlands, 1999.
- [Nieto et al., 2006] X. Nieto, L. Ventura, and A. Mollfulleda. “Gedomis: a broadband wireless mimo-ofdm testbed, design and implementation”. In *Testbeds and Research Infrastructures for the Development of Networks and Communities, 2006. TRIDENTCOM 2006. 2nd International Conference on*, pages 10 pp.–. 2006.
- [Nutaq, 2012] Nutaq. “Nutaq - DSP & FPGA solutions supplier”. <http://nutaq.com/>, 2012. [Online; accessed 4-November-2012].
- [Papoulis and Pillai, 2002] A. Papoulis and S. Pillai. *Probability, Random Variables and Stochastic Processes*. Mc Graw Hill, 2002.
- [Parsons, 2000] J. D. Parsons. *The Mobile Radio Propagation Channel*. Wiley, 2000.
- [Paulraj et al., 2008] A. Paulraj, R. Nabar, and D. Gore. *Introduction to Space-Time Wireless Communications*. Cambridge University Press, New York, NY, USA, 1st edition, 2008.
- [Peigang et al., 2004] J. Peigang, W. Shaobo, and L. Huajia. “An Effective Solution of Wireless Channel Sounder and Its Channel Modeling Application”. In *Vehicular Technology Conference*, volume 1, pages 249–253 Vol.1. 2004.
- [Pentek, 2013] Pentek. “Pentek Inc.”. <http://www.pentek.com>, 2013.

- [Pérez-Cruz et al., 2013] F. Pérez-Cruz, S. V. Vaerenbergh, J. J. Murillo-Fuentes, M. Lázaro-Gredilla, and I. Santamaría. “Gaussian Processes for Nonlinear Signal Processing”. *Special Issue on Advances in Kernel-based Learning for Signal Processing*, 2013.
- [Ramírez et al., 2008] D. Ramírez, I. Santamaría, J. Pérez, J. Vía, J. A. García-Naya, T. M. Fernández-Caramés, H. Pérez-Iglesias, M. G. López, L. Castedo, and J. M. Torres-Royo. “A comparative study of STBC transmissions at 2.4 GHz over indoor channels using a 2 x 2 MIMO testbed”. *Wireless Communications and Mobile Computing*, volume 8, n<sup>o</sup> 9, pages 1149–1164, 2008.
- [Rao et al., 2004] R. Rao, W. Zhu, S. Lang, C. Oberli, D. Browne, J. Bhatia, J.-F. Frigon, J. Wang, P. Gupta, H. Lee, D. Liu, S. Wong, M. Fitz, B. Daneshrad, and O. Takeshita. “Multi-antenna testbeds for research and education in wireless communications”. *Communications Magazine, IEEE*, volume 42, n<sup>o</sup> 12, pages 72 – 81, 2004.
- [Rappaport, 2001] T. Rappaport. *Wireless Communications: Principles and Practice*. Prentice Hall PTR, Upper Saddle River, NJ, USA, 2nd edition, 2001.
- [Rumney et al., 2012] M. Rumney, R. Pirkel, M. H. Landmann, and D. A. Sanchez-Hernandez. “MIMO Over-The-Air Research, Development, and Testing”. *International Journal of Antennas and Propagation*, volume 2012, 2012.
- [RUSK, 2012] RUSK. “RUSK MIMO Channel Sounder”. <http://www.channelsounder.de>, 2012. [Online; accessed 11-December-2012].
- [Sakaguchi et al., 2002] K. Sakaguchi, J. Takada, and K. Araki. “A Novel Architecture for MIMO Spatio-Temporal Channel Sounder”. *IEICE Trans. Electron.*, volume E85-C, n<sup>o</sup> 3, pages 436–441, 2002.
- [Salous et al., 2005] S. Salous, P. Filippidis, R. Lewenz, I. Hawkins, N. Razavi-Ghods, and M. Abdallah. “Parallel receiver channel sounder for spatial and MIMO characterisation of the mobile radio channel”. *IEEE Proceedings Communications*, volume 152, n<sup>o</sup> 6, pages 912–918, 2005.
- [Salous and Razavi-Ghods, 2004] S. Salous and N. Razavi-Ghods. “Semi-Sequential MIMO Channel Measurements in Indoor Environments”. Gothenburg, Sweden. COAT 273 TD(04) 079, 2004.
- [Sanchez-Heredia et al., 2011] J. Sanchez-Heredia, J. Valenzuela-Valdes, A. Martinez-Gonzalez, and D. Sanchez-Hernandez. “Emulation of MIMO Rician-Fading Environments With Mode-Stirred Reverberation Chambers”. *IEEE Transactions on Antennas and Propagation*, volume 59, n<sup>o</sup> 2, pages 654 –660, 2011.
- [Santamaría et al., 2000] I. Santamaría, C. Pantaleón, and J. Ibáñez. “A comparative study of high-accuracy frequency estimation methods”. *Mechanical Systems and Signal Processing*, volume 14, n<sup>o</sup> 5, pages 819–834, 2000.
- [Óscar Gago et al., 2009] Óscar Gago, S. Ruiz, and L. González. “Design of Antenna Array”. Technical report, TTI, 2009.
- [Schenk, 2008] T. Schenk. *RF imperfections in High-Rate Wireless Systems*. Springer, 2008.

- [Sklar, 1997] B. Sklar. “Rayleigh fading channels in mobile digital communication systems .I. Characterization”. *IEEE Communications Magazine*, volume 35, n<sup>o</sup> 7, pages 90 –100, 1997.
- [Skycross, 2013] Skycross. “Skycross antennas”. <http://www.skycross.com/>, 2013. [Online; accessed 02-December-2012].
- [Smith, 2004] P. Smith. “Little known Characteristics of Phase Noise”. Application Note AN-741, Analog Devices, 2004.
- [Spirent, 2013] Spirent. “Spirent Communications”. <http://www.spirent.com>, 2013. [Online; accessed 12-January-2013].
- [Spirent VR5HD, 2013] Spirent VR5HD. “VR5 HD Spatial Channel Emulator”. <http://www.spirent.com>, 2013. [Online; accessed 12-January-2013].
- [Sundance, 2013] Sundance. “Sundance Multiprocessor”. <http://www.sundance.com>, 2013. [Online; accessed 12-January-2013].
- [Svantesson and Wallace, 2002] T. Svantesson and J. Wallace. “Statistical characterization of the indoor MIMO channel based on LOS/NLOS measurements”. In *Conference Record of the Thirty-Sixth Asilomar Conference on Signals, Systems and Computers, 2002.*, volume 2, pages 1354 –1358 vol.2. 2002.
- [Sysgen, 2012] Sysgen. “System Generator for DSP”. <http://www.xilinx.com/tools/sysgen.htm>, 2012. [Online; accessed 5-December-2012].
- [Takada et al., 2001] J. Takada, K. Sakaguchi, and K. Araki. “Development of High Resolution MIMO Channel Sounder for the Advanced Modeling of Wireless Channels”. In *Asia-Pacific Microwave Conference (APMC)*, volume 2, pages 563–568 vol.2. 2001.
- [Tan and Beaulieu, 2000] C. Tan and N. Beaulieu. “On first-order Markov modeling for the Rayleigh fading channel”. *IEEE Transactions on Communications*, volume 48, n<sup>o</sup> 12, pages 2032 –2040, 2000.
- [Thoma et al., 2000] R. Thoma, D. Hampicke, A. Richter, G. Sommerkorn, A. Schneider, U. Trautwein, and W. Wirnitzer. “Identification of time-variant directional mobile radio channels”. *IEEE Transactions on Instrumentation and Measurement*, volume 49, n<sup>o</sup> 2, pages 357–364, 2000.
- [Thomä et al., 2005] R. S. Thomä, M. Landmann, A. Richter, and U. Trautwein. “Multidimensional high-resolution channel sounding measurement”. In *Smart Antennas State of the Art*, volume 3, pages 241–270. T. Kaiser and A. Bourdoux and H. Boche and J. R. Fonollosa and J. B. Andersen, Hindawi Publishing Corporation, 2005.
- [Tse and Viswanath, 2005] D. Tse and P. Viswanath. *Fundamentals of Wireless Communications*. Cambridge University Press, 2005.
- [Tubbax et al., 2004] J. Tubbax, B. Côme, L. V. der Perre, S. Donnay, M. Moonen, and H. D. Man. “Compensation of transmitter IQ imbalance for OFDM systems”. In *Proc. IEEE Int. Conf Acoust., Speech and Signal Process. (ICASSP)*. 2004.

- [Vásquez et al., 2012] J. M. Vásquez, J. Gutiérrez, J. Pérez, J. Ibáñez, and I. Santamaría. “Experimental Evaluation of Multiantenna Spectrum Sensing Detectors using a Cognitive Radio Testbed”. In *International Symposium on Signals, Systems and Electronics (ISSSE)*. 2012.
- [Via et al., 2010] J. Via, I. Santamaria, V. Elvira, and R. Eickhoff. “A General Criterion for Analog Tx-Rx Beamforming Under OFDM Transmissions”. *IEEE Transactions on Signal Processing*, volume 58, n<sup>o</sup> 4, pages 2155 –2167, 2010.
- [Vielva et al., 2010] L. Vielva, J. Vía, J. Gutiérrez, O. González, J. Ibáñez, and I. Santamaría. “Building a web platform for learning advanced digital communications using a MIMO testbed”. *IEEE Int. Conf. on Acoust., Speech, and Signal Processing (ICASSP 2010)*, 2010.
- [Viswanath et al., 2002] P. Viswanath, D. Tse, and R. Laroia. “Opportunistic beamforming using dumb antennas”. *IEEE Trans. on Information Theory*, volume 48, n<sup>o</sup> 6, pages 1277–1294, 2002.
- [Wallace et al., 2004] J. Wallace, B. Jeffs, and M. Jensen. “A real-time multiple antenna element testbed for MIMO algorithm development and assessment”. In *Antennas and Propagation Society International Symposium, 2004. IEEE*, volume 2, pages 1716 – 1719 Vol.2. 2004.
- [Wallace et al., 2003] J. Wallace, M. Jensen, A. Swindlehurst, and B. Jeffs. “Experimental characterization of the MIMO wireless channel: data acquisition and analysis”. *IEEE Transactions on Wireless Communications*, volume 2, n<sup>o</sup> 2, pages 335 – 343, 2003.
- [Weichselberger et al., 2006] W. Weichselberger, M. Herdin, H. Ozelik, and E. Bonek. “A stochastic mimo channel model with joint correlation of both link ends”. *Wireless Communications, IEEE Transactions on*, volume 5, n<sup>o</sup> 1, pages 90 – 100, 2006.
- [Weijun Zhu, 2005] M. F. Weijun Zhu, David Browne. “An Open Access Wideband Multi-Antenna Wireless Testbed with Remote Control Capability”. *tridentcom*, pages 72–81, 2005.
- [Wilzeck et al., 2006] A. Wilzeck, M. El-Hadidy, Q. Cai, M. Amelingmeyer, and T. Kaiser. “MIMO prototyping test-bed with off-the-shelf plug-in RF hardware”. In *IEEE Workshop on Smart Antennas*. Ulm, Germany, 2006.
- [WINNER, 2006] WINNER. <https://www.ist-winner.org>, 2006.
- [WINNER II, 2006] WINNER II. “WINNER II Interim Channel Models”. [http://www.ist-winner.org/phase\\_2\\_model.html](http://www.ist-winner.org/phase_2_model.html), 2006.
- [Wirnitzer et al., 2001] W. Wirnitzer, D. Bruckner, R. Thoma, G. Sommerkorn, and D. Hampicke. “Broadband vector channel sounder for MIMO channel measurement”. In *MIMO: Communications Systems from Concept to Implementations (Ref. No. 2001/175), IEE Seminar on*, pages 17/1–17/4. 2001.
- [Wolniansky et al., 1998] P. W. Wolniansky, G. J. Foschini, G. D. Golden, and R. A. Valenzuela. “V-Blast: an architecture for realizing very high data rates over the rich-scattering wireless channel”. *Proceedings of International Symposium on Signals, Systems, and Electronics (ISSSE Š98)*, pages 295–300, 1998.

- [Won et al., 2003] S. H. Won, D.-S. Lyu, and H. J. Park. “Physical layer implementation and evaluation of multiple input multiple output - orthogonal frequency division multiplexing (MIMO-OFDM) system”. *Proceedings of International Conference on Communication Technology (ICCT Š03)*, volume 2, pages 1348–1352, 2003.